



**Politecnico  
di Torino**

# **POLITECNICO DI TORINO**

**Master's Degree in Energetic and Nuclear Engineering**

**Master Thesis**

## **Experimental and modelling investigation on degradation of the low temperature electrolyser through Electrochemical Impedance Spectroscopy**

**Supervisor**

prof. Massimo SANTARELLI

**Candidate**

Laura GENNARO

**Co-supervisor**

Mohsen MANSOURKIAEI

March 2022





---

# Abstract

The threat of climate change with its catastrophic impacts on the natural environment and human health and wellbeing became more evident in the last decades. While the world is facing the Covid-19 pandemic, climate change is still present and it will have devastating consequences if climate actions will be postponed due to the urgent health crisis. To fulfil climate pledges of COP21, renewed in the recently COP26, a transition to decarbonized economy and energy sector is of fundamental importance. Hydrogen technologies to produce low-carbon hydrogen- principally fossil fuels coupled with CCUS and water electrolysis -have a key role in the challenging energy transition to carbon-free economy and energy sectors. Green hydrogen or electrolytic hydrogen- produced from RES through electrolysis process- is considered the best energy carrier to store energy coming from renewable and intermittent power sources. Electrolysis using renewable energy sources is the cleanest way to produce high purity hydrogen with low carbon footprint. There are mostly three types of water electrolysis technologies: alkaline, polymer electrolyte membrane (PEM) and solid oxide electrolyser cells (SOECs). PEM electrolyzers are becoming dominant in projects since they can provide hydrogen at high pressure and they could also benefit from technological advancement of PEM fuel cells. The market penetration of PEM electrolyzers depends on innovation, fundamental to costs reduction and performance and durability enhancement as well.

The objective of the present work is to investigate the performance of a single PEM electrolytic cell by carrying out electrochemical impedance spectroscopy measurements coupled with polarization curves. Electrochemical impedance spectroscopy is a powerful non-destructive method to individuate the origins of the several polarization processes (activation, ohmic and diffusion losses) affecting the cell performance. In combination with other characterization methods such as polarization curves, it allows to discern among the several phenomena on the basis of the different relaxation times of each single process and furthermore it helps to quantify their impact on the efficiency and durability of the MEA.

The methodology for the system's characterization is based on two steps, the experimental procedure and the model development. In the first step several tests under different operating conditions are performed. Accordingly, the main variables identified in potential, current density, temperature and pressure, which affect differently each process occurring within the cell, are varied. During operation at steady state condition, EIS tests are carried out and impedance data are collected. Prior to the second step, data quality check is needed to remove wild points, data affected by inductive effects of cables and noise. Then, the equivalent circuit model (ECM) is chosen to simulate the impedance spectra trying to minimize the deviation between experimental results and fitting. The electrochemical parameters (double layer capacitance, polarization resistance, ohmic resistance) are estimated by CNLS



---

analysis of the ECM model. To verify the validity of the results obtained from the impedance spectroscopy a comparison with the findings of the polarization curve is done.

The electrochemical characterization with polarization curves and EIS tests in potentiostatic and galvanostatic modes is performed on two MEAs having same features but different ageing conditions. Either characterization methods have been performed at different temperature, pressure, cathode configuration and mass flow rate. Moreover, degradation tests are carried out to quantify the effects of the different phenomena on the performance of both cells.

In conclusion, this work shows that electrochemical impedance spectroscopy side by side with polarization curves can provide useful information to individuate and quantify the contribution of the different processes affecting the performance of the electrolytic cell. Hence, it can help to find critical cell components that need to be improved in order to overcome performance and durability issue that currently create a barrier to the market penetration of this technology.

In future works, a fundamental aspect to account for is the ambiguity related to the equivalent circuit model used to simulate the experimental impedance spectrum. ECMs, generally chosen a priori, do not describe the physicochemical properties of the system, they simply reproduce the experimental data. Only a pre-knowledge of the system under study can guide on the choice of the ECM to get meaningful results. Therefore, other methods such as distribution of relaxation times (DRT), can assist to the identification of a proper number of circuit element avoiding problem of under- or over fitting as well as lack of correlation with the physics.

---

---

# Contents

|       |   |    |
|-------|---|----|
| 1     | List of Figures.....  | vi |
| 2     | Introduction.....   | 2  |
| 1.1   | Current situation in the global energy sector.....                | 4  |
| 1.2   | Hydrogen production by water electrolysis technologies.....       | 7  |
| 1.3   | Goals of the thesis .....   | 12 |
| 1.4   | Outline .....   | 13 |
| 3     | Fundamentals .....  | 14 |
| 2.1   | Working principle of PEM Water Electrolyser.....                  | 14 |
| 2.2   | Loss Mechanisms.....  | 17 |
| 2.3   | Electrochemical characterization: iV-Curve and EIS technique..... | 19 |
| 2.4   | EIS theory.....   | 22 |
| 2.4.1 | Basic background [28-29] .....                                    | 23 |
| 2.4.2 | Data validation [29-31] .....                                     | 25 |
| 2.4.3 | Equivalent Circuit Modelling .....                                | 29 |
| 2.4.4 | Data fitting [30, 36] .....                                       | 44 |
| 4     | Electrochemical characterization of PEMWE in literature.....      | 47 |
| 5     | Experimental .....  | 61 |
| 4.1   | Test bench description .....                                      | 61 |
| 4.2   | Cell components .....   | 65 |
| 4.3   | EIS measurements .....  | 66 |
| 4.3.1 | EIS test equipment and set-up .....                               | 66 |
| 4.3.2 | Measurement modes .....   | 69 |
| 4.3.3 | Test procedure.....   | 70 |
| 4.4   | Measurement Data Quality .....                                    | 76 |
| 4.5   | Cell measurement.....   | 78 |
| 6     | Modelling.....  | 80 |
| 5.1   | AC impedance spectra features.....                                | 80 |
| 5.2   | Data fitting procedure .....                                      | 85 |
| 5.2.1 | Qualitative analysis.....   | 85 |
| 5.2.2 | Parameters initial estimation .....                               | 85 |

---

|   |   |     |
|---|---|-----|
|   | 5.2.3 Model development and CNLS approximation .....  | 86  |
|   | 5.2.4 Final results.....  | 88  |
|   | 5.3 Ambiguities.....  | 89  |
| 7 | Results and discussion.....   | 92  |
|   | 6.1 Open cathode tests.....   | 92  |
|   | 6.1.1 Test Performed At 60°C, Imposed Gauge Pressure 0.5 bar, with 200 mL/min by needle valve with open cathode configuration .....                                       | 92  |
|   | 6.1.2 Test Performed At 60°C and 74°C, Imposed Gauge Pressure 0.5bar, with 10% by pump with open cathode configuration.....   | 95  |
|   | 6.1.3 Tests performed at T=79°C & T=71°C, with open cathode at different gauge pressure..   | 101 |
|   | Conclusion .....  | 106 |
|   | 6.2 Closed cathode tests.....   | 106 |
|   | 6.2.1 Tests performed at constant current density of 1 A/cm <sup>2</sup> with 60°C, 0.5 bar, closed cathode imposing different mass flow rate by recirculating pump ..... | 107 |
|   | 6.2.2 Test Performed At 60°C And 80°C With Closed Cathode, Imposed Gauge Pressure 0.5bar, 105% Mass Low Rate by Pump.....   | 112 |
|   | 6.2.3 Test Performed At 80°C With Closed Cathode, Imposed Gauge Pressure 0.5 bar, with different Mass Low Rates by Pump.....  | 116 |
|   | 6.2.4 Test performed at 80°C and 60°C, With Closed Cathode, Imposed Gauge Pressure 0.5bar, with 20% Mass Low Rates by Pump .....  | 121 |
|   | 6.2.5 Test Performed At 60°C, Imposed Gauge Pressure 0.5bar, with 10% Mass Low Rates by Pump With closed Cathode configuration .....                                      | 130 |
|   | Conclusion .....  | 134 |
|   | 6.3 Open vs Closed cathode tests.....   | 135 |
|   | 6.3.1 Tests performed at gauge pressure 1.4 bar, with open/closed cathode at different temperatures.....  | 135 |
|   | 6.3.2 Tests performed with open/closed cathode with different mass flow rates.....  | 140 |
|   | Conclusion .....  | 156 |
|   | 6.4 Degradation tests .....   | 157 |
|   | 6.4.1 Degradation test performed at 60°C and 80°C, 0.5bar, closed cathode, 10% mass flow rate, constant current density of 0.5 A/cm <sup>2</sup> .....                    | 157 |
|   | 6.4.2 Degradation test performed at 80°C, 0.5bar, closed cathode, 10% mass flow rate, constant current density of 1 A/cm <sup>2</sup> .....                               | 168 |
| 8 | Appendix-TABLES.....  | 176 |
| 9 | Bibliography.....   | 216 |

# List of Figures

|  |    |
|--|----|
| Figure 1 [1].....  | 2  |
| Figure 2 Change in electricity generation in 2020 and 2021 [7]. ....   | 5  |
| Figure 3 Global hydrogen demand by sector in the Net Zero Scenario, 2020-2030 (figure on the left); global hydrogen demand by production technology in the Net Zero Scenario, 2020-2030 (figure on the right) [9]..... | 6  |
| Figure 4 Global installed electrolysis capacity by region, 2015-2020 (figure on the left); global installed electrolysis capacity by technology, 2015-2020 (figure on the right) [9].....                              | 7  |
| Figure 5 Cost breakdown for a 1 MW PEM electrolyser [21].....  | 10 |
| Figure 6 Proposed activities to improve the performance of PEM electrolyzers [21].....   | 11 |
| Figure 7 Schematic representation of the PEM water electrolyser [24].....  | 15 |
| Figure 8 Experimental polarization curve of a PEM electrolyser [26].....   | 19 |
| Figure 9 Characteristic impedance spectrum [26]. ....  | 20 |
| Figure 10 General ECM to simulate the impedance spectrum of a PEMWE [23].....  | 21 |
| Figure 11 Nyquist and Bode plots under potentiostatic mode at 0V, with 60°C and 0.5bar, open cathode. ....   | 25 |
| Figure 12 Definition of the linearity domain for various values of the DC voltage. The amplitude $\Delta E$ of the perturbation signal must be in the white region at a given frequency. [29] .....                    | 26 |
| Figure 13 Impedance diagram of Resistance simulated in the frequency range $10^3 \div 10^{-3}$ Hz ( $R = 90 \text{ Ohm}, 200 \text{ Ohm}, 300 \text{ Ohm}, 400 \text{ Ohm}$ ) [28]. ....                               | 30 |
| Figure 14 Impedance diagram of Capacitance simulated in the frequency range $10^3 \div 10^{-3}$ Hz ( $C = 1\text{E-}3 \text{ F}$ ) [28]. ....  | 31 |
| Figure 15 Impedance diagram of Inductance simulated in the frequency range $10^3 \div 10^{-3}$ Hz ( $L = 1\text{E-}3 \text{ H}$ ) [28]. ....   | 32 |
| Figure 16 Impedance diagram of Warburg element simulated in the frequency range $10^3 \div 10^{-3}$ Hz ( $\sigma = 400 \text{ } \Omega / \text{s}^{1/2}$ ). ....   | 33 |
| Figure 17 Variation of impedance for diffusive systems: a semi-infinite diffusion; b reflective finite diffusion; c transmissive finite diffusion [27]. ....   | 34 |
| Figure 18 Impedance diagram for CPE simulated in the frequency range $10^3 \div 10^{-3}$ Hz at different values of $n$ ( $Q = 100$ ). ....   | 35 |
| Figure 19 Impedance diagram of Bounded Warburg element simulated in the frequency range $10^3 \div 10^{-3}$ Hz ( $\sigma = 0,01 \text{ } \Omega / \text{s}^{1/2}, R_0 = 100 \text{ } \Omega$ ).....                    | 36 |
| Figure 20 Impedance diagram of BCPE simulated in the frequency range $10^3 \div 10^{-3}$ Hz at different values of $R_0$ ( $A = 0,01$ ). ....  | 37 |
| Figure 21 Impedance diagram of Polarizable Electrode simulated in the frequency range $10^3 \div 10^{-3}$ Hz at different values of $R_{ct}$ ( $R_s = 100 \text{ Ohm}, C_{dl} = 1\text{E-}4 \text{ F}$ ) [28]. ....    | 38 |
| Figure 22.....   | 39 |

|  |    |
|--|----|
| Figure 23 Impedance diagram of Randles model at different values simulated in the frequency range $10^3 \div 10^{-3}$ Hz of $C_{dl}$ : 3E-4 F, 1E-3 F, 3E-3 F, 1E-2 F ( $R_0 = 100$ Ohm, $R_{ct} = 5000$ Ohm, $\sigma = 100$ ) [28].                                 | 41 |
| Figure 24 Impedance diagram of Bounded Randles model simulated in the frequency range $10^3 \div 10^{-3}$ Hz at different values of $R_0$ : 50 Ohm, 100 Ohm, 200 Ohm, 400 Ohm ( $R_0 = 20$ Ohm, $C_{dl} = 1E-4$ F, $R_{ct} = 50$ Ohm, $Q = 0.1$ , $n = 0.45$ ) [28]. | 42 |
| Figure 25 Impedance diagram of Voigt's model with three RC in series [28].   | 43 |
| Figure 26 (A) Cross section of a PEM water electrolysis cell; (B) equivalent electrical circuit [37].  | 47 |
| Figure 27 Protocol of measurements of the 8-cell 120 cm <sup>2</sup> stack: a) Input current density; b) Output stack potential. EIS was measured at the time steps T1, T2 and T3 of the protocol [44].  | 53 |
| Figure 28 E cell of all cells measured at 2 A/cm <sup>2</sup> after T1, T2 and T3 [44].  | 54 |
| Figure 29 Polarization curves of a PEM electrolyser single cell with and without MPL [45].   | 55 |
| Figure 30 Test Bench.  | 62 |
| Figure 31 Software interface.  | 63 |
| Figure 32 P&I electrochemical test bench.  | 64 |
| Figure 33 PEM water electrolyser placed inside the housing on the test bench.  | 65 |
| Figure 34 Schematic EIS measurement configuration [27].  | 66 |
| Figure 35 Input parameters and settings for the EIS instrument [23].   | 68 |
| Figure 36 Output parameters for the EIS measurement [23].  | 68 |
| Figure 37 Energy-Lab XM System.  | 70 |
| Figure 38 Schematic configuration of the connection between the cell and the device.   | 71 |
| Figure 39 Types of experiments in the XM-studio ECS software.  | 72 |
| Figure 40 Possible step types for Impedance Voltage Control and Impedance Current Control.   | 72 |
| Figure 41  | 73 |
| Figure 42 Hardware requirements and cell setup.  | 73 |
| Figure 43  | 74 |
| Figure 44 Impedance setup.   | 75 |
| Figure 45 Impedance spectrum with low noise and describing a time-invariant system.  | 77 |
| Figure 46 Impedance spectrum giving noisy residuals but still acceptable quality.  | 77 |
| Figure 47 Impedance spectrum with time-variant behaviour.  | 77 |
| Figure 48  | 81 |
| Figure 49  | 82 |
| Figure 50  | 82 |
| Figure 51  | 83 |
| Figure 52  | 83 |
| Figure 53  | 84 |
| Figure 54  | 85 |
| Figure 55  | 86 |
| Figure 56  | 86 |

|  |     |
|--|-----|
| Figure 57.....   | 87  |
| Figure 58.....   | 87  |
| Figure 59.....   | 88  |
| Figure 60.....   | 90  |
| Figure 61.....   | 91  |
| Figure 62 Nyquist plot under current control at 60°C 0.5bar open cathode 200mL/min. ....                                       | 93  |
| Figure 63 Nyquist plot under voltage control at 60°C 0.5bar open cathode 200mL/min. ....                                       | 94  |
| Figure 64 Trend of the parameters with galvanostatic mode. ....  | 95  |
| Figure 65 Trend of the parameters with potentiostatic mode. ....   | 95  |
| Figure 66 Nyquist plot under current control at 60°C 0.5bar open cathode 10%. ....   | 97  |
| Figure 67 Nyquist plot under voltage control at 60°C 0.5bar open cathode 10%. ....   | 97  |
| Figure 68 Nyquist plot under current control at 74°C 0.5bar open cathode 10%. ....   | 98  |
| Figure 69 Nyquist plot under voltage control at 74°C 0.5bar open cathode 10%. ....   | 98  |
| Figure 70 Parameters' trend obtained from potentiostatic test at 60°C.....   | 99  |
| Figure 71 Parameters' trend obtained from potentiostatic test at 74°C.....   | 99  |
| Figure 72 Parameters' trend obtained from galvanostatic test at 74°C. ....   | 99  |
| Figure 73 Comparison of the parameters gained from potentiostatic measurements<br>between 60°C and 74°C.....                   | 100 |
| Figure 74 Cell temperature measured during the test. ....  | 102 |
| Figure 75 Gauge pressure in the anode and cathode measured during the test. ....   | 102 |
| Figure 76 Nyquist plot under voltage control at 79°C open cathode at different gauge<br>pressures. ....                        | 103 |
| Figure 77 Nyquist plot under voltage control at 71°C open cathode at different gauge<br>pressures. ....                        | 103 |
| Figure 78 Nyquist plot under current control at 79°C open cathode at different gauge<br>pressures. ....                        | 104 |
| Figure 79 Nyquist plot under current control at 71°C open cathode at different gauge<br>pressures. ....                        | 104 |
| Figure 80 Trend of the ohmic resistance at 79°C and 71°C. ....   | 105 |
| Figure 81 Trend of charge transfer resistance and capacitance in the HF region at 79°C and<br>71°C. ....                       | 105 |
| Figure 82 Nyquist plot under voltage control at 60°C 0.5bar closed cathode at different<br>percentage of mass flow rates. .... | 108 |
| Figure 83 Nyquist plot under current control at 60°C 0.5bar closed cathode at different<br>percentage of mass flow rates. .... | 109 |
| Figure 84.....   | 110 |
| Figure 85 Trend of the voltage during the test. ....   | 110 |
| Figure 86 Trend of the pressures- anode, cathode, heater- during the test. ....  | 111 |
| Figure 87 Nyquist plot under current control at 0.5bar closed cathode with 105% at<br>different temperatures. ....             | 113 |
| Figure 88 Nyquist plot under voltage control at 0.5bar closed cathode with 105% at<br>different temperatures. ....             | 113 |

---

|  |     |
|--|-----|
| Figure 89.....   | 114 |
| Figure 90 Polarization curves at 60°C and 80°C. ....   | 115 |
| Figure 91 Nyquist plot under voltage control at 80°C 0.5bar closed cathode with different mass flow rates..... | 117 |
| Figure 92.....   | 117 |
| Figure 93 Nyquist plot under current control at 80°C 0.5bar closed cathode with different mass flow rates..... | 118 |
| Figure 94.....   | 118 |
| Figure 95.....   | 119 |
| Figure 96.....   | 119 |
| Figure 97.....   | 120 |
| Figure 98 Trend of pressure during potentiostatic and galvanostatic measurements.....                          | 122 |
| Figure 99 Nyquist plot under current control at 80°C 0.5bar closed cathode with 20% pump. ....                 | 122 |
| Figure 100 Zoom of Nyquist plot under current control at 80°C 0.5bar closed cathode with 20% pump.....         | 123 |
| Figure 101 Nyquist plot under voltage control at 80°C 0.5bar closed cathode with 20% pump. ....                | 123 |
| Figure 102 Zoom of Nyquist plot under voltage control at 80°C 0.5bar closed cathode with 20% pump.....         | 124 |
| Figure 103 Nyquist plot under voltage control at 60°C 0.5bar closed cathode with 20% pump. ....                | 124 |
| Figure 104 Zoom of Nyquist plot under voltage control at 60°C 0.5bar closed cathode with 20% pump.....         | 125 |
| Figure 105 Nyquist plot under current control at 60°C 0.5bar closed cathode with 20% pump. ....                | 125 |
| Figure 106 Zoom of Nyquist plot under current control at 60°C 0.5bar closed cathode with 20% pump.....         | 126 |
| Figure 107 Trend of the HF parameters at 60°C with 20%pump.....  | 127 |
| Figure 108 Trend of the HF parameters at 80°C with 20%pump. ....   | 128 |
| Figure 109.....  | 129 |
| Figure 110 Comparison between 80°C and 60°C of the HF parameters with 20%pump. ...                             | 129 |
| Figure 111 Nyquist plot under current control at 60°C 0.5bar closed cathode with 10% pump. ....                | 131 |
| Figure 112 Zoom of Nyquist plot under current control at 60°C 0.5bar closed cathode with 10% pump.....         | 131 |
| Figure 113 Nyquist plot under voltage control at 60°C 0.5bar closed cathode with 10% pump. ....                | 132 |
| Figure 114 Nyquist plot under voltage control at 60°C 0.5bar closed cathode with 10% pump. ....                | 132 |
| Figure 115 Trend of the HF parameters at 60°C and 10%pump.....   | 133 |
| Figure 116 Trend of cell temperature and gauge pressure in the anode and cathode.....                          | 135 |



---

|   |     |
|---|-----|
| Figure 117 Nyquist plot under voltage control at 1.4bar open cathode with different temperatures.....   | 136 |
| Figure 118 Nyquist plot under voltage control at 1.4bar closed cathode with different temperatures..... | 137 |
| Figure 119 Nyquist plot under current control at 1.4bar open cathode with different temperatures.....   | 138 |
| Figure 120 Nyquist plot under current control at 1.4bar closed cathode with different temperatures..... | 138 |
| Figure 121 Comparison between open and closed cathode of the HF parameters. ....                        | 139 |
| Figure 122 Nyquist plot under voltage control at 60°C- open vs closed cathode. ....                     | 142 |
| Figure 123 Nyquist plot under current control at 60°C- open vs closed cathode. ....                     | 143 |
| Figure 124 Nyquist plot under voltage control at 80°C- open vs closed cathode. ....                     | 144 |
| Figure 125 Nyquist plot under current control at 80°C- open vs closed cathode. ....                     | 145 |
| Figure 126 Polarization curves at 60°C- open vs closed cathode.....                                     | 146 |
| Figure 127 Polarization curves at 80°C- open vs closed cathode.....                                     | 147 |
| Figure 128 Nyquist plot under voltage control at 60°C- open vs closed cathode. ....                     | 148 |
| Figure 129 Nyquist plot under current control at 60°C- open vs closed cathode. ....                     | 149 |
| Figure 130 Nyquist plot under voltage control at 70°C- open vs closed cathode. ....                     | 150 |
| Figure 131 Nyquist plot under current control at 70°C- open vs closed cathode. ....                     | 151 |
| Figure 132 Nyquist plot under voltage control at 80°C- open vs closed cathode. ....                     | 152 |
| Figure 133 Nyquist plot under current control at 80°C- open vs closed cathode. ....                     | 153 |
| Figure 134 Polarization curves at 60°C- open vs closed cathode.....                                     | 154 |
| Figure 135 Polarization curves at 70°C- open vs closed cathode.....                                     | 155 |
| Figure 136 Polarization curves at 80°C- open vs closed cathode.....                                     | 156 |
| Figure 137 Voltage trend during the degradation test at 60°C.....                                       | 157 |
| Figure 138.....   | 158 |
| Figure 139.....   | 158 |
| Figure 140 All EIS measurements with potentiostatic mode. ....  | 159 |
| Figure 141 All EIS measurements with galvanostatic mode. ....   | 159 |
| Figure 142 EIS measurements with potentiostatic mode- removed invalid impedance spectra.....            | 160 |
| Figure 143 EIS measurements with galvanostatic mode- removed invalid impedance spectra.....             | 161 |
| Figure 144.....   | 162 |
| Figure 145.....   | 162 |
| Figure 146.....   | 163 |
| Figure 147 Voltage trend during the degradation test at 80°C.....                                       | 164 |
| Figure 148.....   | 164 |
| Figure 149.....   | 164 |
| Figure 150 EIS measurements with potentiostatic mode. ....  | 165 |
| Figure 151 All EIS measurements with galvanostatic mode. ....   | 165 |
| Figure 152.....   | 166 |

---

|                 |     |
|-----------------|-----|
| Figure 153..... | 167 |
| Figure 154..... | 167 |
| Figure 155..... | 168 |
| Figure 156..... | 170 |
| Figure 157..... | 170 |



---

# Introduction

The threat of climate change with its catastrophic impacts on the natural environment and human health and wellbeing became more evident in the last decades. While the world is facing the Covid-19 pandemic, climate change is still present and it will have devastating consequences if climate actions will be postponed due to the urgent health crisis after the long road to acknowledge its existence.

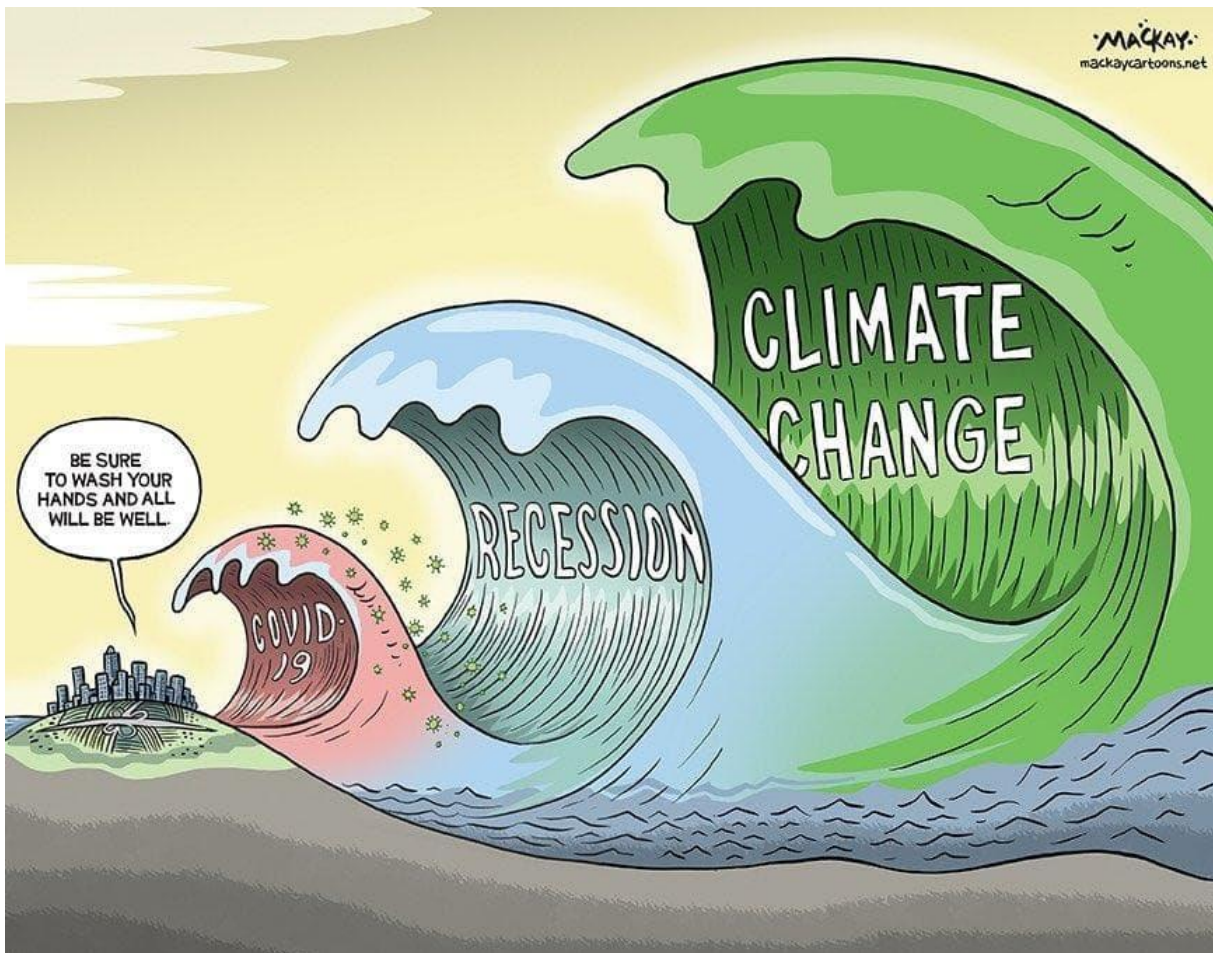


Figure 1 [1]

The efforts of the international community to reach a universal multilateral agreement on climate change recently became reality with the Paris Agreement. The Paris Agreement is the

---

first-ever universal, legally binding global climate change agreement, adopted at the Paris climate conference (COP21) in December 2015. It set out to keep the increase in global average temperature to well below 2°C above pre-industrial levels and pursue efforts to limit the increase to 1.5°C. To fulfil climate pledges, a transition to decarbonized economy and energy sector is of fundamental importance. Hence, governments-bound to their nationally determined contribution (NDC) defined in COP21 - developed strategies and policies based on emission reduction, efficiency improvement and renewables to achieve these goals. In this regard, the EU's initial nationally determined contribution under the Paris Agreement was the commitment to reduce greenhouse gas emissions by at least 40% by 2030 compared to 1990 [2]. European Union has a leadership role in fighting climate change, continuing to promote and implement ambitious environment, climate and energy policies across the world since it is necessary a global response to overcome a global threat as the climate change. In line with the Paris agreement the EU presented in 2019 the European Green Deal, a new growth strategy that aims to transform the EU into a fair and prosperous society, with a modern, resource-efficient and competitive economy where there are no net emissions of greenhouse gases in 2050 and where economic growth is decoupled from resource use [3]. Recently, the Commission adopted the communication 'Stepping up Europe's 2030 climate ambition – Investing in a climate-neutral future for the benefit of our people', commonly referred to as the 2030 EU climate target plan, in which it is proposed to raise the EU's ambition on reducing greenhouse gas emissions to at least 55% below 1990 levels by 2030 to reach climate neutrality by 2050 [4].

In the IEA's report Net Zero by 2050, the key pillars of decarbonisation of the global energy system over the next 30 years in the Net Zero Emissions by 2050 Scenario (NZE) are energy efficiency, behavioural changes, electrification, renewables, hydrogen and hydrogen-based fuels, bioenergy and CCUS [5].

Hydrogen technologies to produce low-carbon hydrogen- principally fossil fuels coupled with CCUS and water electrolysis -have a key role in the challenging energy transition to carbon-free economy and energy sectors. Green hydrogen or electrolytic hydrogen- produced from RES through electrolysis process- is considered the best energy carrier to store energy coming from renewable and intermittent power sources to avoid the RES curtailment. This concept goes under the name of Power-to-Hydrogen, assessing that once hydrogen is produced from low carbon electricity, a potentially large portfolio of uses is possible [6]. Hydrogen and hydrogen-based fuels use should fill the gaps where electricity cannot easily or economically replace fossil fuels and where limited sustainable bioenergy supplies cannot cope with demand [5]. Hence, it can replace conventional fuels in the oil refining sector, in industry, in the transport sector (aviation, ship) and in the electricity generation. In other words, electrolytic hydrogen may be used in a versatile way either as an energy carrier and energy storage medium.

---

This initial chapter aims to present the current condition of the global energy sector with more details on the electrolytic hydrogen production. Thereafter, a brief comparison of the electrolysis technologies is presented with more emphasis on PEM water electrolyzers. Finally, the goal of the thesis and its outlines are delineated.

## 1.1 Current situation in the global energy sector

The Covid 19 pandemic impacted toughly in 2020 on global economic output causing a consequent contraction of the global energy demand. Restrictions on movements, induced lockdowns, virus and its variations spreading all over the world, and uncertainties scarred economies determining the biggest decline since Second World II. Nevertheless, vaccine campaigns and expansive economic politics -such as Next generation EU in the European Union or American Rescue Plan in the USA- have led and still are leading to a slow recovery up to pre-Covid levels.

In the annual Global Energy Review by IEA [7] the latest statistical data and analysis for the 2020- year of the Covid-19 pandemic- and insights for the 2021 as well, about economic activity energy use and emissions are provided. In 2021 the global economic output is set to rebound by 6%, bringing the global GDP more than 2% higher than 2019 levels. Same for the global energy demand, with an expected increase by 4.6% principally driven by emerging markets and developing economies, bringing the demand 0.5% above 2019 projections, with a consequent probable rebound in CO<sub>2</sub> emissions. While the electricity demand is expected to increase by 4.5 % in 2021, over 1000TWh, five times greater than the decline in 2020. All fossil fuels demand is set to show an expected growth with respect to the drastic drop in 2020. Coal demand is expected to rise emissions of 5% (1500 Mt) in contrast to the 80% fall during the 2020, but still this remains 400 Mt below 2019 emission levels. As a matter of fact, it is mostly related to the rise in the coal demand for coal-fired generation principally concentrated in Asia whereas in the United States and the European Union this growth is anyway below pre-crisis levels. Moreover, CO<sub>2</sub> emissions could have ended up well above 2019 levels if the transport oil demand would have reached pre-crisis levels.

Despite the negative effects of pandemic on fossil fuels demand during 2020, renewables showed to be resilient with a demand increased by 3% in 2020, supported by new installed capacity, priority market access, and long-term contracts. As a result, the share of renewables in the electricity generation reached 29% in 2020 up from 27% in 2019 and it is expected to jump up to 30% in 2021. This large generation from renewables is expected to provide over half of the increase in the electricity supply in 2021.

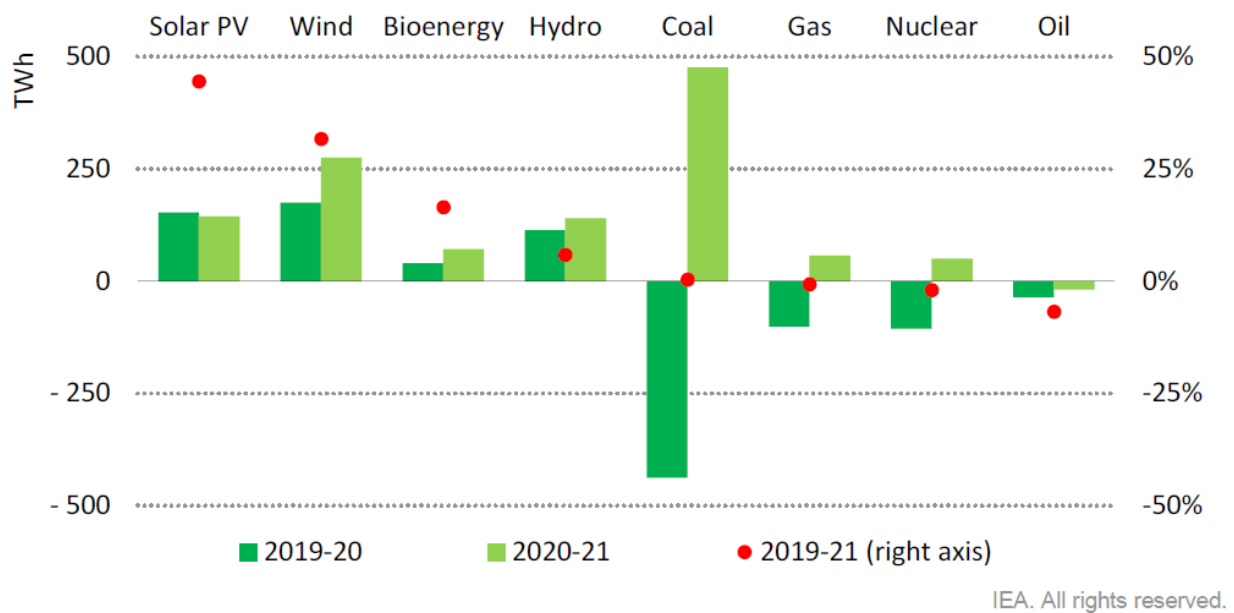


Figure 2 Change in electricity generation in 2020 and 2021 [7].

Hydrogen sector also stood up strenuously to the Covid-19 pandemic and further it was a momentum of growth for the low-carbon hydrogen technology (mainly fossil fuels coupled with CCUS and water electrolysis) [8].

Many governments announced strategies to develop hydrogen as a fundamental energy carrier for the global energy transition. In 2020 ten governments adopted hydrogen strategies: Canada, Chile, France, Germany, the Netherlands, Norway, Portugal, Russia, Spain and the European Union (France had already adopted a Plan for Deploying Hydrogen for the Energy Transition in 2018). As of September 2021, four more strategies had been adopted (by the Czech Republic, Colombia, Hungary and the United Kingdom) and Norway released a roadmap to complete its strategy adopted in 2020. In addition, Poland and Italy have released strategies for public consultation and more than 20 other countries have announced they are actively developing theirs [9].

During 2020 about 70 MW of electrolysis capacity was installed and two facilities producing hydrogen from fossil fuels with CCUS became operational [9]. These progresses, necessary although insufficient, are fundamental to reach the several ambitious targets individuated at the end of the COP26 (November 2021) of limiting global warming below 1.5°C, accelerating the elimination of coal and increasing the use of renewable energy sources in the energy mix, with the aim to mitigate the almost irreversible climate change [10, 11].

To date, hydrogen is mainly produced from fossil fuels, determining 900 Mt of CO<sub>2</sub> emissions per year and its demand, stood at 90 Mt in 2020, was almost all for refining and industrial uses.

Oil refining was the principal consumer of fossil-base hydrogen in 2020 and it is expected to remain so in the medium term as well. The substitution of blue hydrogen with the low carbon one is an opportunity to increase the demand of clean hydrogen with a consequent decrease of the CO<sub>2</sub> emissions. The European Union is following this road, with about 1.3 GW of electrolysis capacity (almost 230 kt of production capacity) under development in refineries having 2025 as deployment target [9]. In the industry sector hydrogen is used to produce ammonia, methanol and in the process of steelmaking; in 2020 the hydrogen demand was 51 Mt with only 0.3 Mt (20% more than in 2019) coming from clean hydrogen technologies (large-scale CCUS plants and small electrolytic units).

Anyway, more efforts are needed to stay within the roadmap tracked in the Net Zero Emission by 2050 Scenario, which foresees a low-carbon hydrogen demand of 5 Mt in refining and 21 Mt in the industries by 2030.

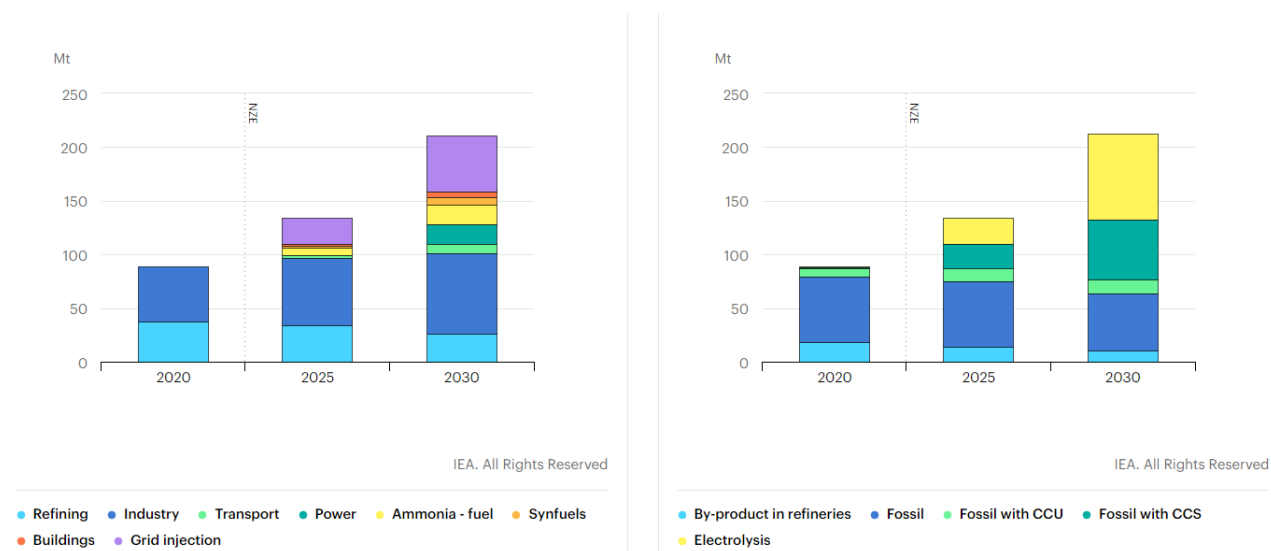


Figure 3 Global hydrogen demand by sector in the Net Zero Scenario, 2020-2030 (figure on the left); global hydrogen demand by production technology in the Net Zero Scenario, 2020-2030 (figure on the right) [9].

Currently, hydrogen production from electrolysis is 30 kt per year (0.03% of all hydrogen production) due to its high cost (USD 3-8/kg H<sub>2</sub>) compared with blue hydrogen (USD 0.5-1.7/kg H<sub>2</sub>). The total installed capacity of electrolyzers is 300 MW with an increment of 70 MW in 2020. Europe is very active with a dominant role in this sector, having 40% of the global installed capacity, thanks to policy support to the hydrogen strategies in countries like Germany, France and Spain. There is a high number of projects under development which could bring the total installed capacity around 1 GW (170 kt of hydrogen) in 2022.

Although this is significant, the target of 850 GW thus 80 Mt of electrolytic hydrogen prescribed in the Net Zero Emissions by 2050 Scenario seems a challenge to achieve by 2030 with the actual rate of growth [9].



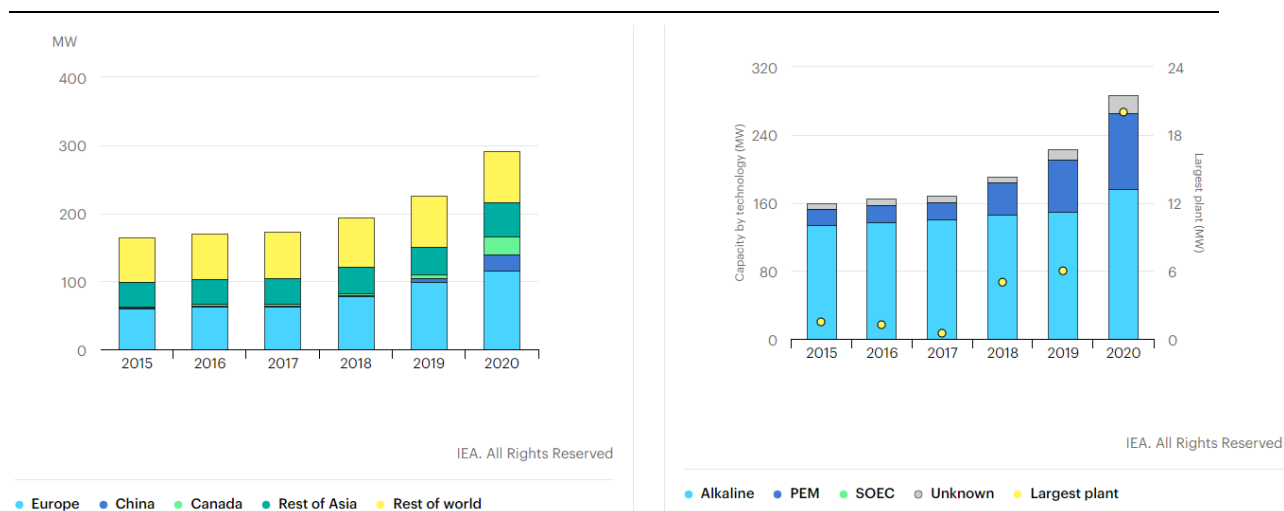


Figure 4 Global installed electrolysis capacity by region, 2015-2020 (figure on the left); global installed electrolysis capacity by technology, 2015-2020 (figure on the right) [9].

The barriers to make green hydrogen competitive are renewable power costs and electrolyzers cost. A steep fall of the electricity input will narrow the gap with blue hydrogen. Moreover, lower costs of the electrolyser technology will result in more possibilities to penetrate global market and make a step forward to the fulfilment of the climate pledges.

## 1.2 Hydrogen production by water electrolysis technologies

Electrolysis using renewable energy sources is the cleanest way to produce high purity hydrogen with low carbon footprint. In the electrolysis process water is split into hydrogen and oxygen through the application of electrical energy.

There are mostly three types of water electrolysis technologies: alkaline, polymer electrolyte membrane (PEM) and solid oxide electrolyser cells (SOECs). The first two are already commercial whereas SOECs are at the precommercial stage. Although alkaline electrolyzers are the most mature technology having also lower costs, PEM electrolyzers are becoming dominant in projects since they can provide hydrogen at high pressure and they could also benefit from technological advancement of PEM fuel cells [9]. A comprehensive comparison of the electrolysis technologies is provided in *Table 1.1* [12, 13].

| <b>Electrolysis process</b> | <b>Advantages</b>  | <b>Disadvantages</b>  |
|-----------------------------|--|---|
| Alkaline Electrolysis       | Well established technology; Non-noble catalysts; Low cost technology; Energy efficiency around 70-80%; Commercialized up to MW range  | Low current densities; Formation of carbonates on the electrode decrease the performance; Low purity gases; Low operation pressure (1-30bar); Low dynamic operation; Low partial load range |
| Solid Oxide Electrolysis    | High efficiency (90-100%); Non-noble catalysts; High working pressure  | Precommercial stage; Large system design; Low durability (brittle ceramics)   |
| PEM electrolysis            | High current densities; High voltage efficiency; Compact system design; Quick system response; Good partial load range; Greater hydrogen production rate; High purity gases (99.99%); Higher energy efficiency (80-90%); High dynamic operation; High operating pressure (30-60 bar) | High cost of components; Acid environment; Low durability   |

*Table 1.1 Advantages and disadvantages of water electrolysis technologies [12, 13].*

This thesis focuses on PEM water electrolyser so a brief description of the state of art will be addressed in the following part.

The essential components of the PEMWE are membrane electrode assembly (MEA), gas diffusion layers (GDLs) or porous transport layers (PTLs) or porous current collectors (PCCs), and bipolar plates (BP).

The MEA divides the cell into two half cells, anode and cathode, and it consists of a membrane with ionomer solution and electrocatalysts for each side. It is also called catalyst coated membrane (CCM) because of the method usually used for the fabrication. An electrocatalyst slurry- prepared by using appropriate amounts of electrocatalyst along with ionomer solution, isopropanol and water- is directly coated on the surface of the membrane and then hot pressed at 120°C [13]. Commonly, membranes are Perfluorosulfonic acid polymer membranes (PFSA) and typically the most used is Nafion (Dupont trademark) characterized by high durability, high proton conductivity and good mechanical stability. It is possible to choose among several thicknesses (Nafion 115,117 and 212) in order to gain a compromise between ASR, gas crossover and mechanical strength. The main drawback of PFSA is the reduced conductivity at temperature above 100°C due to the membrane dehydration [12,14]. Electrocatalysts made from elements belonging to the platinum group metal (PGM), enhance the charge transfer kinetics; the most used are palladium or platinum at the cathode and iridium or ruthenium oxides at the anode. These expensive noble materials are needed due to the harsh oxidative environment of the cell and their main characteristics are the particle size

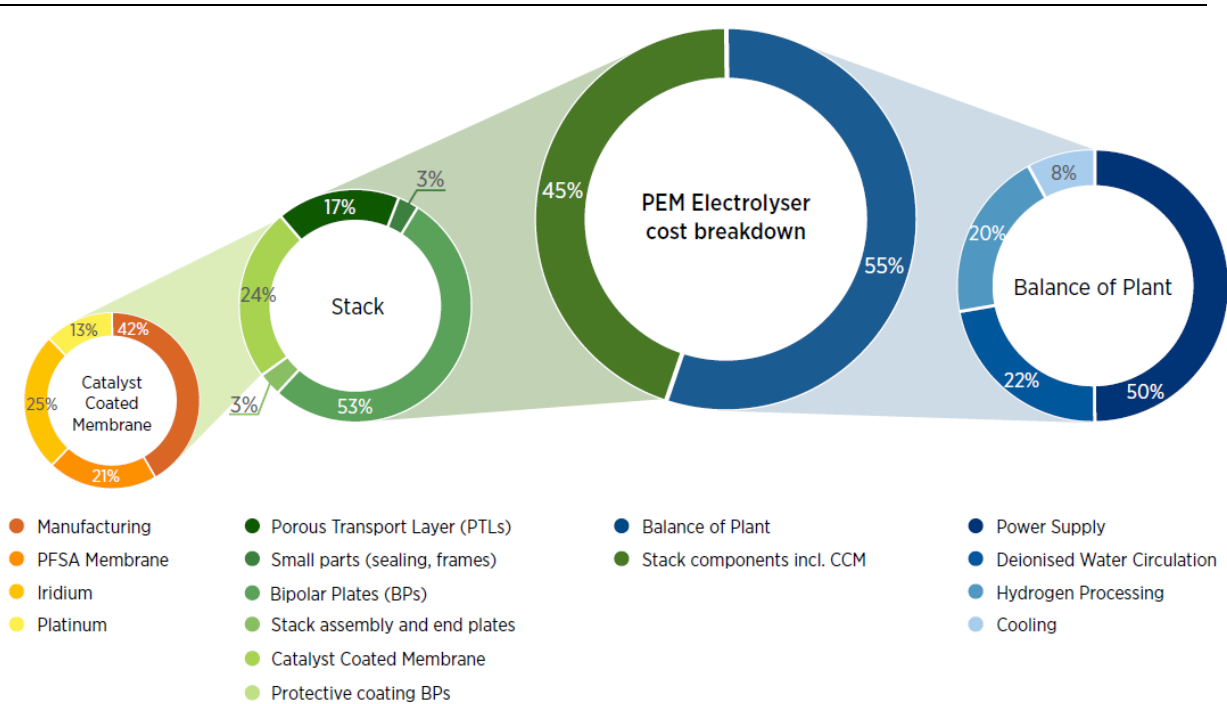
---

and the loading percentage. The cathode loads range from 0.5 to 1  $mg/cm^2$  [12] whereas the loadings for the anode catalyst layer range around 1-3  $mg/cm^2$  [15]. While for the cathode the catalyst loadings have dropped with time, conversely the anode catalysts loadings have not reduced as much. In these years many researchers have addressed this issue trying different catalyst loadings and materials for the anode to reduce costs and solve the corrosion limit of metals such as RuOx [13, 15-16].

Porous transport layers play a fundamental role in the diffusion processes within the cell since they enable the electronic flow from the bipolar plates to the electrodes and at the same time the supply of the reactant water to and the removal of oxygen and hydrogen from the catalytic sites of the electrodes. For these reasons its microstructure needs to be optimized with proper porosity and pore volumes [14]. They also must have corrosion resistance, mechanical stability and good electrical conductivity. Generally, the PTLs in the anodic compartment is more critical due to the coexistence of two counterflows (water reaching the electrode and oxygen away from the electrode) whereas at the cathode there are still two flows but both are co-linear, i.e. water and hydrogen away from the cathode [17-20]. In PEM water electrolysis PTLs are usually porous titanium plates; other types are titanium grids/meshes/felts, carbon current collector and stainless steel grids [12, 13].

Bipolar plates are made up titanium, stainless steel and graphite. Titanium BP have good performance (strength, high thermal conductivity, low permeability, low resistivity) but the anode side is subject to corrosion. Consequently, precious metal coatings are used to protect titanium bipolar plates with a further cost increase [12].

The costs breakdown for PEM electrolyzers is reported *Figure 5*. To date, the stack represents about 40-50% of the overall system costs. In particular, a significant contribution comes from the cost of porous transport layers (PTLs), bipolar plates (BPs) and catalyst coated membrane (CCM), principally linked to the highly expensive materials. Further on, from a balance of plant point of view, the power supply represents a relevant cost component. The market penetration of PEM electrolyzers depends on innovation, fundamental to costs reduction and performance and durability enhancement as well. Research is addressing this issue related to materials, trying to reduce catalyst loadings and titanium as well and, possibly, replacing these with less rare materials.



Note: The specific breakdown varies by manufacturer, application and location, but values in the figure represent an average.

Based on IRENA analysis.

Figure 5 Cost breakdown for a 1 MW PEM electrolyser [21].

To conclude, the figure below from Irena's report [21] gives a brief but concise summary of the activities to improve the performance of PEM electrolyzers, hence overcoming the barrier for the scaling up of the technology.

|  | CHALLENGE | BENEFIT |
|--|-----------|---------|
| 1. Mitigate membrane poisoning/deactivation by foreign elements from components and system                             | Easy      | Medium  |
| 2. Design, create, and integrate forms of recombination catalysts for gas permeation (crossover)                       | Easy      | Medium  |
| 3. Increase catalyst utilisation of anode and cathode catalysts  | Moderate  | High    |
| 4. Identify and reduce interface resistances from catalyst layer to PTLs   | Moderate  | Medium  |
| 5. Reduce the ohmic losses and gas permeation of PFSA membranes  | Difficult | High    |
| 6. Improve kinetics for oxygen evolution using iridium-free catalysts and maintain stability comparable to iridium SoA | Difficult | High    |
| 7. Eliminate mechanical degradation of catalyst layers (delamination, dissolution)                                     | Difficult | Medium  |
| 8. Create noble metal free protective layers for PTLs  | Difficult | High    |
| 9. Create titanium free PTLs   | Difficult | High    |

Based on IRENA analysis.

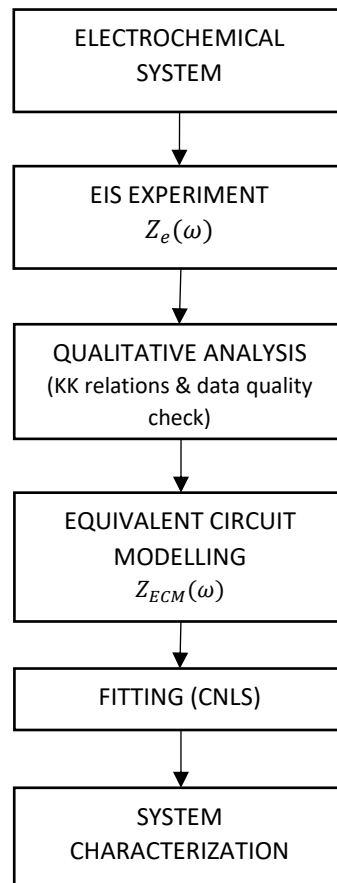
Figure 6 Proposed activities to improve the performance of PEM electrolyzers [21].

---

## 1.3 Goals of the thesis

Efficiency and durability issues are critical constraints that need a deep investigation. In this regard, the electrochemical impedance spectroscopy is a powerful non-destructive method to individuate the origins of the several polarization processes (activation, ohmic and diffusion losses) affecting the cell performance [22-23]. In combination with other characterization methods such as polarization curves, it allows to discern among the several phenomena on the basis of the different relaxation times of each single process and furthermore it helps to quantify their impact on the efficiency and durability of the MEA. The information of the electrolyser are contained in an implicit form in the impedance spectra. Hence, it is necessary to perform a multistep analysis. With a first qualitative analysis of the obtained impedance spectra is possible to provide an insight of ohmic resistance- associated with proton and electron conduction in the MEA, current collectors and bipolar plates- and polarization resistance due to electrode kinetics at the electrode/electrolyte interface and also, if present, to mass transport of water and gaseous products. Anyway, a further analysis of the impedance spectra is performed by complex non-linear least square (CNLS) approximation to a model function obtained by an equivalent circuit model used to fit the experimental data [23].

The objective of the present work is to investigate the performance of a single PEM electrolytic cell by carrying out electrochemical impedance spectroscopy measurements.



---

The methodology for the system's characterization depicted in the flow chart is based on two steps, the experimental procedure and the model development. In the first step several tests under different operating conditions are performed. Accordingly, the main variables identified in potential, current density, temperature and pressure, which affect differently each process occurring within the cell, are varied. During operation at steady state condition, EIS tests are carried out and data are collected. Prior to the second step, data quality check is needed to remove wild points, data affected by inductive effects of cables and noise. Then, the equivalent circuit model (ECM) is chosen to simulate the impedance spectra trying to minimize the deviation between experimental results and fitting. The electrochemical parameters (double layer capacitance, polarization resistance, ohmic resistance) are estimated by CNLS analysis of the ECM model. To verify the validity of the results obtained from the impedance spectroscopy a comparison with the findings of the polarization curve is done.

## 1.4 Outline

Here is presented a brief outline of what will follow in the next chapters.

In Chapter 2 is presented the basis of the theory beside this thesis, thus (i) working principle of PEMWE, (ii) loss mechanisms, (iii) electrochemical characterization, and (iv) electrochemical impedance spectroscopy theory. The latter wants to give a comprehensive view of a more extended argument which is impedance spectroscopy.

Chapter 3 presents the literature review mostly related to the modelling of the experimental data, whereas Chapter 4 describes the tests bench and the cell characteristics, the EIS instrumentation and setup, and finally the cell measurements.

Chapter 5 explains the modelling procedure to choose the equivalent circuit model and its correlated ambiguities.

In Chapter 6 the results obtained are presented and discussed.

Finally, the conclusion of the present work is given in the final chapter.

---

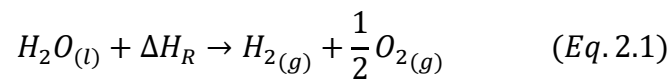
# Fundamentals

The first part of the chapter gives an insight of the working principle of a PEMWE cell. A brief discussion of the loss mechanisms occurring within the cell is carried out.

The second part provides a general overview to the electrochemical impedance spectroscopy (EIS) technique. After the short description of the basic theoretical background below EIS, data validation is presented. Thereafter, modelling of the experimental data through equivalent electrical circuit is discussed in detail. Finally, the parametrical identification approach to gain the fundamental parameters from the equivalent circuit model is carried out.

## 2.1 Working principle of PEM Water Electrolyser

PEM water electrolyzers are devices that perform water electrolysis, an electrochemical process in which hydrogen and oxygen are obtained by splitting water using electricity. At standard conditions ( $p = 1 \text{ atm}$ ,  $T = 25^\circ\text{C}$ ), the Gibbs free energy  $\Delta G_R^0$  of the overall reaction (Eq. 2.1) in the electrolyser is  $+236,483 \text{ kJ mol}^{-1}$  [14, 24].



The term  $\Delta H_R$  is the reaction enthalpy defined as the amount of energy required to break up the molecule to its components. Specifically, this amount of energy  $\Delta H_R [\text{J mol}^{-1}]$  consists of electrical work  $\Delta G [\text{J mol}^{-1}]$  and heat  $T \cdot \Delta S [\text{J mol}^{-1}]$ .

Figure 7 [24] shows the general working principle in PEMWE which uses as ionic conductor a polymer electrolyte membrane (or proton exchange membrane). The electrolyte consists of a thin, solid ion-conducting polymeric membrane, usually Perfluorosulfonic acid membrane (PFSA).



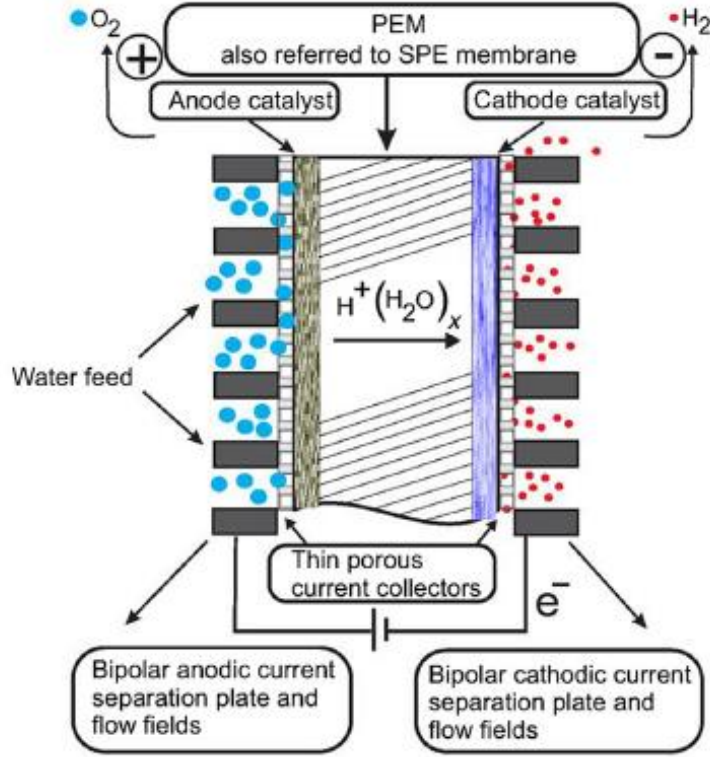
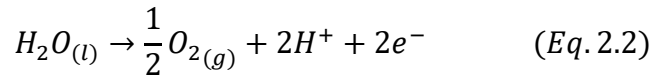


Figure 7 Schematic representation of the PEM water electrolyser [24].

An electrical DC power source is connected to the electrodes, the anode is the positive charged electrode whereas the cathode is the negatively charged electrode. Water is oxidized at the anode according to Eq. 2.2, the electrons pass through the external circuit and oxygen evolves as gas (oxygen evolution reaction, OER). Protons migrate through the acid electrolyte from the anode to the cathode and according to Eq. 2.3 they are reduced by the electrons from the external circuit to hydrogen gas (hydrogen evolution reaction, HER) [14].



Generally, two different cell voltages are used for the characterization of the water electrolysis reaction. Under reversible condition, the electrolysis process occurs if the potential difference at the electrodes is equal to the reversible cell voltage or Nernst voltage  $V_{rev}$ . The reversible cell voltage  $V_{rev}$  corresponds to the minimal electrical work needed to split water if a thermal

---

contribution of energy is present [14, 25]. It can be calculated by using the  $\Delta G$  at standard condition, the Faraday constant  $F$  and the amount of charges  $z$  (electrons) transferred during the reaction as in Eq. 2.4. This is also called open circuit voltage (OCV).

$$V_{rev}^0 = \frac{\Delta G^0}{zF} = 1.229 \text{ V} \quad (Eq. 2.4)$$

Nonetheless, without having an external source of heat the voltage required is higher than  $V_{rev}$  and it is called the thermoneutral voltage  $V_{th}$ . The thermoneutral voltage at standard state is calculated by Eq. 2.5.

$$V_{th}^0 = \frac{\Delta H_R^0}{zF} = 1.481 \text{ V} \quad (Eq. 2.5)$$

Therefore, the second definition considers the situation when the energy (electrical work plus heat) needs to be provided by the external DC power supply due to the lack of heat from the surroundings.

In other words, when the cell voltage is in the range between reversible cell voltage and thermoneutral voltage the electrolysis process can start but external heat is necessary to maintain the isothermicity. In case of absence of heat, this needs to be produced internally therefore the cell voltage must be higher than the thermoneutral voltage. In fact, for  $V > V_{th}$  current starts to flow and heat is produced within the cell by different internal irreversibility sources [25].

In general, the Nernst equation for reversible cell voltage of the water splitting process can be written as

$$V_{rev}(T, p) = V_{rev}^0 - \frac{RT}{2F} \ln \left( \frac{p_{H_2O}/p_{op}}{(p_{H_2}/p_{op}) \cdot (p_{O_2}/p_{op})^{\frac{1}{2}}} \right) \quad (Eq. 2.6)$$

with the reversible cell voltage at standard condition  $V_{rev}^0$ , the universal gas constant  $R$ , the Faraday constant  $F$ , the partial pressures at standard temperature in reference to the operation pressure  $p_{op}$  [14].

---

## 2.2 Loss Mechanisms

Due to several internal irreversible loss mechanisms, when the cell is loaded with electrical current, the actual cell voltage needs to be considerably higher with respect to the theoretical cell voltage of Eq. 2.4 and Eq. 2.5. In fact, above the reversible cell voltage current begins to flow across the cell but more power is necessary to overcome internal resistances which determine a dissipation of electricity in form of heat. Thereby, in the following section the different loss mechanisms will be briefly introduced [25].

Internal losses in a PEM water electrolyser are activation losses, ohmic losses and mass transfer losses. These can be further divided into two typologies: the faradaic and the non-faradaic processes.

The activation losses are faradaic and are ascribed to direct transfer of electrons between redox couples at the interface between the electrode and the electrolyte of the OER and the HER [14]. Sluggish kinetics of these reactions- measured with the rate of reaction, which provides the probability that the activation energy barrier can be overcome and thus that the reaction can occur- lead respectively to anodic overpotential and cathodic overpotential. The sum of these two provides the total activation overpotential, dominant at low current densities. Commonly, the Butler-Volmer equation (Eq. 2.7) is used to describe the influence of activation overpotential on current density.

$$i = i_0 \cdot \left\{ \exp\left(\frac{z\beta F\eta}{RT}\right) - \exp\left(-\frac{z(1-\beta)F\eta}{RT}\right) \right\} \quad (\text{Eq. 2.7})$$

where  $i_0$  is the exchange current density of anode/cathode,  $z$  the number of exchanged electrons,  $\beta$  the symmetry factor and  $\eta$  the activation overpotential of anode/cathode. From the Butler-Volmer equation is possible to obtain the expression for the activation losses (Eq. 2.8).

$$\eta_{act} = \frac{RT}{\alpha_{an}F} \sinh^{-1}\left(\frac{i}{2i_{0,an}}\right) + \frac{RT}{\alpha_{cath}F} \sinh^{-1}\left(\frac{i}{2i_{0,cath}}\right) \quad (\text{Eq. 2.8})$$

Where  $\alpha$  is the charge transfer coefficient function of the symmetry factor and of the number of electrons exchanged.

Since the charge-transfer kinetics of OER is significantly slower with respect to fast kinetics of HER, the anodic overvoltage is larger than the cathodic one, which can be considered negligible.

---

Conversely, ohmic losses and mass transfer losses are due to non-faradaic processes. Ohmic losses come from resistance to electron flow through the electrodes and the cell components and resistance to the flow of protons through the membrane [14]. The overall ohmic resistance is the sum of each individual ohmic contribution  $R_k$  and accordingly to Ohm's law, the ohmic overpotential increases linearly with the current density. These are dominant at mid current densities.

$$\eta_{ohm} = i \cdot \sum_k R_k = i \cdot R_{ohm} \quad (Eq. 2.9)$$

Generally, the ohmic losses arise mainly from the resistance describing the proton flow through the membrane. The most common material used for the membrane is PFSA membrane like Nafion. The proton conductivity  $\sigma_{mem}$  of Nafion is usually affected by temperature and therefore by membrane hydration as well.

Mass transport losses in water electrolyser are usually due to mass transport limitation across the current collectors and gas screening (or shielding) effects [25]. From these phenomena, respectively, derive two types of overvoltage-diffusion and bubble overvoltage. Diffusion overpotential arises when gas bubbles partially blocks the pores network of current collectors and thereby limiting the supply of reactant water to the active sites. Diffusion overpotential usually dominates at low current densities whereas at high current densities is predominant bubbles overpotential; the latter occurs when very large gas bubbles shield the electrochemical active area, reducing catalyst utilization [14]. The most critical aspect regarding mass transport is related to the anodic compartment. Whilst in the cathodic compartment both flows of liquid water and gaseous hydrogen are from the cathode to the cathodic bipolar plate, in the anodic compartment a two-phase flow coexists. In fact, at the anode contemporaneously liquid water goes inside the anode pores and gaseous oxygen flows in opposite direction, from the anode to the anodic bipolar plate.

Thereby, considering these irreversibility sources the actual cell voltage is the sum of the OCV plus all the overpotentials.

$$V_{cell} = V_{rev} + |\eta_{act}| + |\eta_{ohm}| + |\eta_{mass\ trans}| \quad (Eq. 2.10)$$

The cell voltage is generally represented in a current/voltage graph, the polarization curve.

## 2.3 Electrochemical characterization: iV-Curve and EIS technique

The polarization curve is the most used method for the characterization of PEM water electrolyser because it allows to estimate the effects of many parameters such as temperature, pressure, composition, relative humidity on the cell performance. In general, the polarization curve has three characteristic regions, as depicted in *Figure 8*, related to the major internal irreversibilities of the cell.

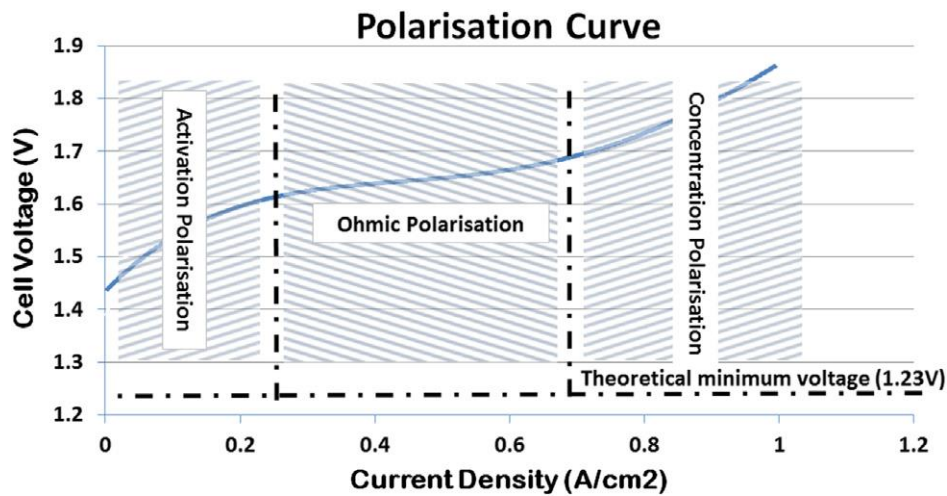


Figure 8 Experimental polarization curve of a PEM electrolyser [26]

The shape of the polarization curve is dictated by the several loss mechanisms aforementioned. At low current density, it assumes a logarithmic behaviour due to charge-transfer phenomena at the anode and the cathode; moreover, the anodic overvoltage is outweighed with respect to the cathodic one because the kinetics of the OER is lower than that of the HER. With increasing current densities, the shape becomes linear because activation losses are less relevant with respect to ohmic losses. Meanwhile, at high current densities the mass transfer processes are dominant giving to the cell voltage a non-linear behaviour. The polarization curve enables the identification of the overall loss of the cell making difficult to separate the different contributions of the loss mechanisms to the cell performance. In contrast to the I-V curves, the electrochemical impedance spectroscopy (EIS) is a very promising technique to analyse complex electrochemical systems like PEM water electrolyzers.

Electrochemical impedance spectroscopy (EIS) is a powerful and non-invasive in-situ diagnostic method for the characterization of electrochemical processes and devices. It is mainly used to study and evaluate the different phenomena in a separate way, taking

advantage from the fact that the polarization losses occurring within the cell exhibit different characteristic time constants and frequency response.

The measurement approach consists of applying a sinusoidal current (galvanostatic mode) or voltage (potentiostatic mode) of a certain amplitude and frequency superimposed on the normal operating DC current/voltage and measuring the amplitude and phase shift of the output voltage-in case of current control mode- or current when a voltage control mode is applied. This procedure is repeated for a discrete quantity of frequency values over kHz-mHz range, thereby generating a characteristic impedance spectrum. The impedance or the admittance (inverse of impedance), for galvanostatic and potentiostatic modes respectively, is obtained by the ratio between the response (output) and the perturbation (input) according to Eq. 2.11 and Eq. 2.12 [23].

$$Z(f) = \frac{U_{AC}(f)}{I_{AC}(f)} = |Z(f)| * e^{i\theta(f)} \quad (Eq. 2.11)$$

$$Y(f) = Z(f)^{-1} = \frac{I_{AC}(f)}{U_{AC}(f)} = |Z(f)|^{-1} * e^{-i\theta(f)} \quad (Eq. 2.12)$$

Generally, the impedance spectrum can be presented in Nyquist and Bode plots, which are representations of the impedance as a function of frequency. Nyquist plot- where imaginary part is plotted against the real part- consists of two or more (depressed) semicircles representing the different processes taking place in the WE cell such as charge transfer, electronic and ionic conduction, diffusion and transport processes [23]. In particular, it is possible to identify three domains as in the polarization curve.

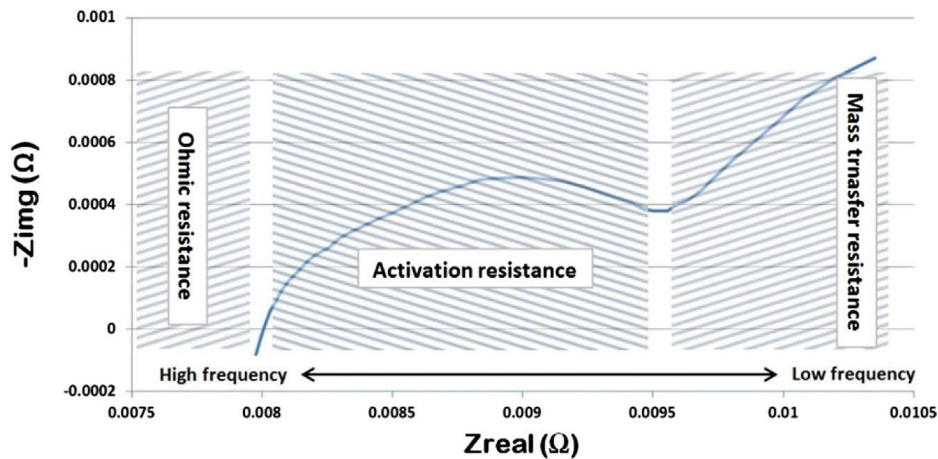


Figure 9 Characteristic impedance spectrum [26].

In the Bode graph each semicircle of the Nyquist representation- characterized by a specific time constant- is represented by a peak of the phase angle as function of frequency. When

semicircles merge, it means that processes have time constants with same order of magnitude and this, translated to the Bode plot, is graphically shown by merging peaks as well, but these are still pronounced and distinguishable even if merged. In these cases, the individuation and separation of the phenomena becomes challenging and troublesome.

The Nyquist plot is the most used graphical representation of the impedance data since from a visual inspection it allows to individuate some important features- high frequency, mid frequency and low frequency features- directly correlated to the main sources of losses in the cell. The high frequency intercept with the real axis corresponds to the sum of the internal ohmic resistances, including the electrolyte, active material, current collectors and electrical contacts. Hence, it gives an insight of the ohmic losses within the cell. The arcs appearing in the mid-frequency region- which can be more or less defined and usually it appears as two merged semicircles- are primarily due to the electrochemical processes occurring at the electrolyte/electrode interfaces inside the cell, which combine resistive and capacitive effects. These are OER at the anode and HER at the cathode, but mostly of the time the charge transfer reaction of the anode dominates due to its sluggish kinetics. Finally, the low-frequency range reflects mainly mass transport limitations in the active material of the cell electrodes.

It is important to point out that the impedance is defined for those systems that are compliant with the condition of causality, linearity and time-invariance. These are the conditions to get good impedances. Although PEM electrolyzers, and in general electrochemical systems, are non-linear, the condition of linearity can be achieved if the amplitude of the perturbing signal is small enough to determine a linear response from the system under study [23]. As a consequence, the impedance data obtained are numerically validated through the use of the Kramers-Kronig relations which describe the correlation between the real and imaginary parts of the impedance. More details will be discussed in the next sections.

The analysis of the impedance spectrum is made by fitting the experimental data with a suitable equivalent electrical circuit (EEC) model composed of a combination of resistances, capacitors, inductors, Warburg elements and constant phase elements. These impedance elements are connected in parallel and/or in series to closely simulate the impedance spectrum and thus for describing the different processes characterized by different time constant.

For PEM electrolyser a common ECM used for the fitting procedure is shown in the figure below.

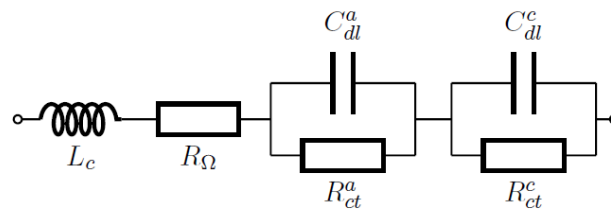


Figure 10 General ECM to simulate the impedance spectrum of a PEMWE [23].

---

The resistor  $R_{\Omega}$  in series with the inductor  $L_C$  represent the resistance of the electrolyte membrane and the inductance of cables/wires used in the test, respectively. Thereafter, the subsequent two impedance elements consist of an ideal capacitor  $C_{dl}$  in parallel with an ideal resistor  $R_{ct}$ . These parallel connections account for the electrode/electrolyte interface at the anode and the cathode; the capacitance represents the double layer charging at the electrode interface whereas the resistance, commonly called charge-transfer resistance, accounts for the effective resistance for the electrode reaction. More elaborate models substitute the capacitance with constant phase element (CPE) to simulate the fractal and porous nature of the electrodes and add a Warburg element to consider the diffusive processes occurring in both electrodes [23].

Finally, the unknown values of the ECM, such as  $R_{ct}$ ,  $R_{\Omega}$ ,  $CPE$ , are evaluated by a Non-linear Least Squares (CNLS) analysis. The CNLS-fit of the impedance data is carried out with commercially available software. It is an iterative process so once that good initial values of the parameters are estimated, the software will adjust them until the goodness of the fit is satisfactory. When the fit looks inappropriate, i.e. the simulation of the impedance spectrum results poorly close to the experimental data, the reason may be the wrong choice of the ECM or incorrect estimation of the initial values. Therefore, in these cases the procedure should be repeated [27].

## 2.4 EIS theory

The impedance spectroscopy technique is a powerful diagnostic method applied to electrochemical system for understanding and estimating its performance under different operating conditions. As the name mentions, it characterises the impedance of the system under investigation. Considering the analogy with electrical circuit, the impedance provides the measure of the opposition to current flow through the cell which derives from activation, ohmic and diffusion losses. Therefore, characterising impedance is an important task to characterise, control and enhance the cell behaviour.

The following section will describe the basic concepts of electrochemical impedance spectroscopy. The first part gives a brief description of the fundamental principles of EIS. Thereafter, data validation with Kramers-Kronig relations is discussed. The latter argument will focus on the modelling of the experimental impedance data and the parametrical identification with Complex Non-linear Least Squares analysis.



---

### 2.4.1 Basic background [28-29]

In the EIS experiment, the electrochemical system considered is perturbed with an input signal  $x(t)$  and the response is measured as an output signal  $y(t)$ . The conversion of the time domain input and output signals to gain a quantity, that is function of the frequency, is based on the *Transfer Function (TF) method* which involves the use of the Laplace Transforms. Under the hypotheses of steady-state system, Laplace transforms are replaced with simple Fourier Transforms. In this case, the TF takes the form of the ratio of the response to the input signal obtained in the frequency domain and moreover it describes entirely the properties of linear and steady-state systems [28].

In case of linear system, if  $x(t)$  is a sine wave input

$$x(t) = A\sin(\omega t) \quad (Eq. 2.13)$$

the response is also a sine wave

$$y(t) = B\sin(\omega t + \phi) \quad (Eq. 2.14)$$

From a theoretical point of view the perturbation signal can be of different nature- white noise, step, pulse, etc.- however the sinusoidal wave signal is considered the most appropriate for EIS technique [29].

The relation between the system and the response to a perturbing signal is quite complex in the time domain and generally it requires the solution of a system of differential equations. A very useful simplification of the mathematical procedure results from the use of Fourier transformation. Thereby, by applying the Fourier transforms the transfer function can be defined as reported in Eq. 2.15.

$$H(\omega) = |H(\omega)|e^{j\phi} \quad (Eq. 2.15)$$

Where  $|H(\omega)|$  and  $\phi$  are respectively the modulus and the phase shift of the transfer function.

If  $x(t)$  is a current and  $y(t)$  a voltage,  $H(\omega)$  is an impedance value  $Z(\omega)$ ; inversely, if  $x(t)$  is a voltage and  $y(t)$  a current, the transfer function is an admittance value  $Y(\omega) = Z(\omega)^{-1}$  [29]. As a consequence, in terms of electrical analogy, the transfer function in the frequency domain assumes a form similar to Ohm's law. As a matter of fact, this is true if the system obeys to the principles of linear time-invariant systems.

The impedance of an electrochemical system  $Z(\omega)$  is a complex number which can be represented either in polar coordinates or in Cartesian coordinates:

$$Z(\omega) = |Z|e^{j\phi} \quad (Eq. 2.16)$$

---


$$Z(\omega) = ReZ + jImZ \quad (Eq. 2.17)$$

Where  $ReZ$  and  $ImZ$  are the real part and the imaginary part of the impedance. The relationship between these quantities are:

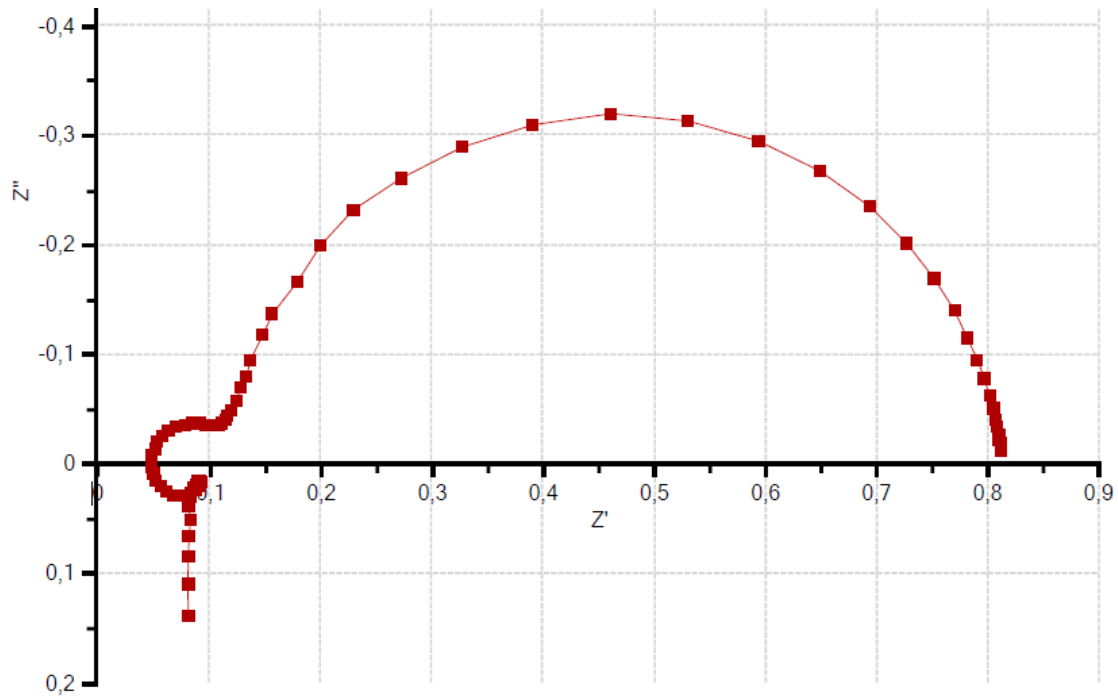
$$|Z|^2 = (ReZ)^2 + (ImZ)^2 \quad (Eq. 2.18)$$

$$\phi = \arctan \frac{ImZ}{ReZ} \quad (Eq. 2.19)$$

$$ReZ = |Z| \cos \phi \quad (Eq. 2.20)$$

$$ImZ = |Z| \sin \phi \quad (Eq. 2.21)$$

The graphical representation of the impedance spectrum can be done in Nyquist and Bode plots. In a Nyquist plot the x-axis represents the real part and the y-axis the imaginary part, thus the experimental data is characterized by  $ReZ$ ,  $ImZ$  and  $\omega$ . The Bode plots displays instead the frequency dependence of modulus and phase and usually is in logarithmic scale. Both plots start from high frequency impedance data to end with the low frequency ones.



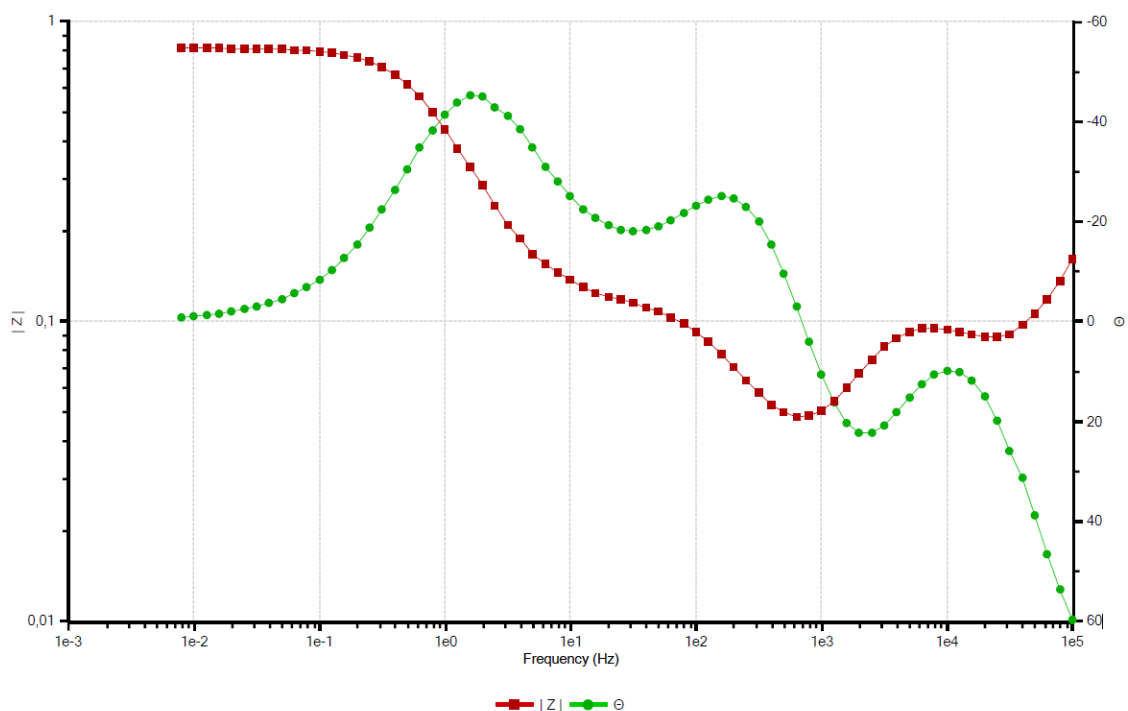


Figure 11 Nyquist and Bode plots under potentiostatic mode at 0V, with 60°C and 0.5bar, open cathode.

Electrochemical systems are complex systems where several elementary phenomena occur (transport, adsorption, diffusion, etc.) to end up with the charge transfer at the electrochemical interface. These processes determine the shape of the impedance spectrum.

An impediment to the application of the TF method arises from the assessment of non-linear behaviour in electrochemical systems, strictly linked to the laws which govern the kinetics of mass transport and those of the various electrochemical reactions, as well as the complex couplings between these elementary processes [29]. Moreover, real electrochemical systems behave as non- steady state systems with memory properties [28]. Therefore, the analysis of the impedance through the TF method requires that the system under investigation fulfils the conditions of *causality, linearity, stability, and finiteness*.

#### 2.4.2 Data validation [29-31]

The determination whether the obtained EIS data are good is fundamental to get a reliable and appropriate interpretation of the impedance data. In fact, EIS data should satisfy the main principles of linear time-invariant systems: linearity, causality, stability, and finiteness.

---

### Linearity

The condition of linearity is satisfied if the amplitude of the perturbation signal is small enough to approach quasi linear conditions for the response. The amplitude should be selected in the linearity domain, which depends on the values of the DC voltage.

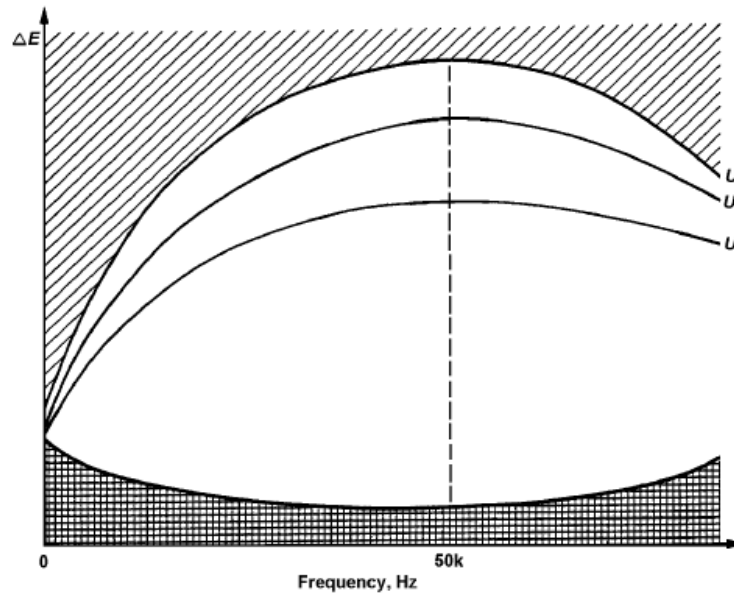


Figure 12 Definition of the linearity domain for various values of the DC voltage. The amplitude  $\Delta E$  of the perturbation signal must be in the white region at a given frequency. [29]

From the Figure 12 it is possible to assess that the maximum acceptable amplitude of the perturbation signal is smaller at low frequency than it is at high frequency. However, a constant amplitude perturbing signal is generally used over the whole frequency range [29]. Note that the low limit of the linearity range comes from the signal-to-noise (S/N) ratio acceptable by the measuring instrument whilst the high limit is determined by the generation of non-linear distortion. Too low perturbation amplitude will result in an unacceptable S/N ratio, so the response is buried in noise and its recognition becomes difficult. Thereby, it is necessary to consider trade-off between linearity and accuracy.

### Causality

The response of the system must be completely caused by the perturbing signal, thereby a causal system is not able to predict its future because its future is determined by the last event [30]. Measurement at high frequency are sensible to instrumentation artifacts concerning wires inductances and noise which affect the causality condition.

### Finiteness

This condition, also called boundedness, implies that real and imaginary parts of the impedance should take finite values over the entire frequency range. Moreover, the impedance must tend to a constant real value for  $\omega \rightarrow 0$  and  $\omega \rightarrow \infty$  [30].

---

### Stability

A system is considered stable if it returns to its original state after removal of the perturbation [30]. Moreover, it is required the steady-state condition, there is to say that the system should be independent from the moment of measurement (time invariant). However, completely stationary systems are difficult to achieve and in general non-stationary systems can be approximates to stationary by limiting the measurement time. Nonetheless, obtaining impedance data is time consuming, especially in low frequency range. Consequently, the stability is compromised and this condition is determined by the drift in the system with time which can be ascribed to changes in temperature, pressure, concentration and so on and so forth.

In order to check whether these aforementioned conditions are satisfied by the system, impedance data should be subjected to a numerical validation based on the Kramers-Kroning (KK) relations. In fact, if the results obtained from the transformations agree with the experimental data, then it is possible to state that the data are formally corrected and are Kramers-Kroning compliant [30-31].

The KK relations describe the correlation between the real and the imaginary parts of the impedance as shown in the following equations.

$$Z_{Im}(\omega) = Z''(\omega) = -\left(\frac{2\omega}{\pi}\right) \int_0^{\infty} \frac{Z_{Re}(x) - Z_{Re}(\omega)}{x^2 - \omega^2} dx \quad (Eq. 2.22)$$

$$Z_{Re}(\omega) = Z'(\omega) = Z_{re}(\infty) + \frac{2}{\pi} \int_0^{\infty} \frac{xZ_{Im}(x) - \omega Z_{Im}(\omega)}{x^2 - \omega^2} dx \quad (Eq. 2.23)$$

These equations show that if the real part of the impedance is known over the entire frequency range, its imaginary part is determined, and viceversa; when the imaginary part is given, the real part is completely determined up to the constant  $Z_{Re}(\infty)$ . In both cases, the degree of convergence between the measured values and the calculated one is an insight of the quality of the measurement [27]. When the measured real part and transformed imaginary part match, or the measured imaginary part match with the transformed real part, this means that data set is valid; instead, corrupted data set are found when neither of these two occurs and in this case invalid data should be rejected since are not suitable for further analysis. Usually, deviations between experimental and transformed data appear at low frequency due to the longer time to gain the data. In general, a criterion for the identification of a good fit comes from the deviation between measured and transformed data that should be below  $\pm 1\%$  [23].

The Kramers-Kronig relations are able to determine whether the impedance spectrum of a given system has been influenced by bias errors caused by instrumental artifacts or time-dependent phenomena. Nevertheless, their direct application is not used since the integration of the equations requires impedance spectra measured from 0 Hz to  $\infty$  Hz, which is experimentally impossible due to instrumental limitations or by noise attributable to instability of the electrode [31]. Various methods have been proposed. An approach to overcome this is based on the fact that if an appropriate ECM can be fitted to the experimental data, the data are assumed to be KK compliant. In other words, the equivalent circuit model satisfies the KK relations implicitly.

The equivalent electrical model used consists of a set of parallel RC circuits in series. This type of structure is called Voigt's structure where the resistors as well as the time constant of the ECM are fitted to a measured impedance spectrum by CNLS fitting. The impedance of the Voigt circuit is described as follows:

$$Z(\omega_k) = R_0 + \sum_{i=1}^n \frac{R_i}{1 + \omega_k^2 \tau_i^2} - j \sum_{i=1}^n \frac{\omega_k \tau_i R_i}{1 + \omega_k^2 \tau_i^2} \quad (\text{Eq. 2.24})$$

Using a sufficient number of such RC elements the CPE or Warburg elements can also be approximated. The main drawback of this method is the nonlinear nature of the fit problem, therefore good initial values have to be chosen, and also a proper selection of the weighting to be used for the regression is necessary. Although this approach allows to avoid the integration over an infinite frequency domain, in case of poor fit it is difficult to understand whether this condition is due to inconsistency of the data with KK relations or to the use of an inadequate model or to regression to a local rather than global minimum related to inappropriate initial guess [31].

A modified version of this method has been proposed by Boukamp [32]. The problem related to the nonlinearity of the fit is solved by only fitting the ohmic resistors and pre-setting the time-constants. Hence, the fit problem becomes linear. This method is generally referred as linear KK validity test. In this case, it is necessary to manually pre-set the number of RC-elements to be fitted generating possible situation of under- or over-fitting and therefore leading to ambiguities in the analysis of the obtained results. Schönleber et al. [33] have proposed a strategy on how to automatically choose the number of RC-elements to be fitted for any given impedance spectrum. A tool based on the linear KK test proposed in [32] and the automatic strategy for finding the appropriate number of RC-elements proposed in [33] is the *Lin-KK tool* [34], that will be used for impedance testing in this thesis.

---

### 2.4.3 Equivalent Circuit Modelling

The interpretation of impedance data requires the use of an appropriate model. The information are accumulated in the impedance function, which does not provide a direct measure of all physical phenomena taking place within the system, but it is more an information property that needs to be extracted through the construction of an appropriate working model [28].

In principle, modelling of experimental data may be divided into two types: measurement modelling and process modelling [30]. The measurement modelling models the impedance data experimentally obtained by using an exact mathematical model based on a plausible physical theory that predicts theoretical impedance (classical modelling) or by an equivalent electrical circuit which leads to equivalent impedance (structural modelling) [28]. In either these cases, classical or structural modelling, the model parameters are gained by a parametrical identification that foresees the use of statistical methods such as Newton-Marquard, CNLS, simplex, model reduction and others.

In general, the most used approach is Equivalent Circuit Modelling (ECM). The model should be carefully chosen to give the best possible match between the simulated impedance and the measured impedance of the system [27]. The equivalent circuit model (ECM) or equivalent electrical circuit (EEC) consists of impedance elements taken from electrical engineering like resistors, capacitors and inductors as well as specialized electrochemical elements that will be discuss below. A proper combination of the impedance elements describes each physical phenomenon taking place in the system and moreover it provides the shape of the impedance spectrum shown in the Nyquist plot.

As a matter of fact, it is necessary to pay attention that for a given set of impedance data it is possible to use different equivalent circuits and this may generate ambiguities. Hence, the choice of an adequate EEC needs the knowledge of the whole cell, including the behaviour of each element composing the cell and also the number of elements used should be small in order to avoid the lack of correlation between the impedance elements and the electrochemical processes [27]. Nevertheless, it is necessary to verify the validity of the model that has been constructed. As a rule of thumb, a model is valid when it can fit the impedance spectra obtained under a large variety of conditions.

#### *2.4.3.1 Modelling elements and their physical meaning [27-28]*

Equivalent electrical circuit is a combination of different elements, which are divided in two groups:

- *Lumped elements*: they are electrical elements and can describe only homogeneous systems. Resistors, capacitors and inductors belong to this category.

- 
- *Frequency dependent elements*: they are electrochemical elements, i.e. these are developed for the description of electrochemical processes.

### Lumped elements

#### a) Resistor

The impedance of a pure resistor, where  $R$  is the resistance [ $\Omega$ ], is characterized only by the real part:

$$Z_R(\omega) = R \quad (\text{Eq. 2.25})$$

In the Nyquist plot it appears as a single point in the real axis.

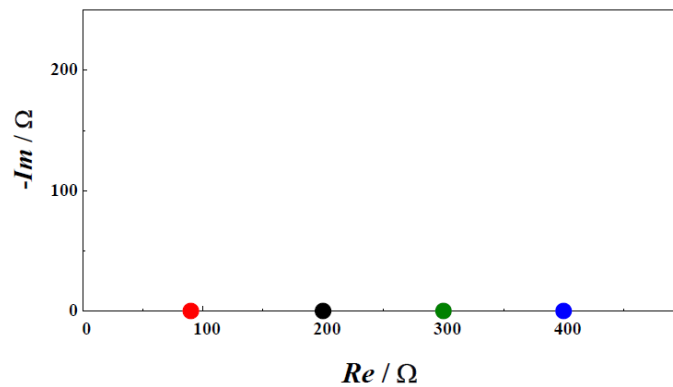


Figure 13 Impedance diagram of Resistance simulated in the frequency range  $10^3 \div 10^{-3}$  Hz ( $R = 90$  Ohm,  $200$  Ohm,  $300$  Ohm,  $400$  Ohm) [28].

In general, the resistance represents an internal opposition to the occurrence of a process within the system.

In PEM electrolyzers it is used to describe:

- Proton transport in the electrolytic membrane. It is known as *ionic or membrane resistance* and it is directly proportional to the electrolyte resistivity  $\rho$  [ $\Omega\text{cm}$ ] and the membrane thickness. The membrane resistance is affected positively by increasing value of temperature since the ionic conductivity  $\sigma = 1/\rho$ , reciprocal of the resistivity, is temperature dependent. Furthermore, lower value of the ionic resistance are provided by thinner membrane but in this case gas cross-over can occur.
- Movement of electrons in the metallic parts and conductors, such as current collectors and wires. Its name is *electronic resistance* and it is usually negligible in comparison with the membrane resistance.
- Electrons transfer at the electrode/electrolyte interface, named *charge-transfer resistance*. It is associated with the charge transfer mechanism for the electrode reactions. In other words, is the resistance that occurs when



electrons transfer at the electrode/electrolyte interface. It depends on the potential and temperature as well; an increase of the potential generally determines a decrease of the charge-transfer resistance [27] whereas higher temperature improves kinetics.

The sum of membrane resistance and electronic resistance is called ohmic resistance  $R_{\Omega}$  and it is obtained by the intercept of the HF feature with the real axis, whereas the overall resistance to electron crossing the interface at both anode and cathode is called polarization resistance  $R_p$  and it is gained by the difference between the intercept of low frequency feature and the intercept of high frequency feature. The total resistance corresponding to the differential resistance of the polarization curves is given by the intercept of the low frequency feature with the real axis, hence  $R_{\Omega} + R_p$ .

#### b) Capacitor

The impedance of a pure capacitor, where C is the capacitance [F], has only the imaginary part and its value is negative when C is positive.

$$Z_c(\omega) = \frac{1}{j\omega C} \quad (Eq. 2.26)$$

The behaviour of a pure capacitor is represented in the Nyquist diagram by a line parallel to the negative imaginary axis.

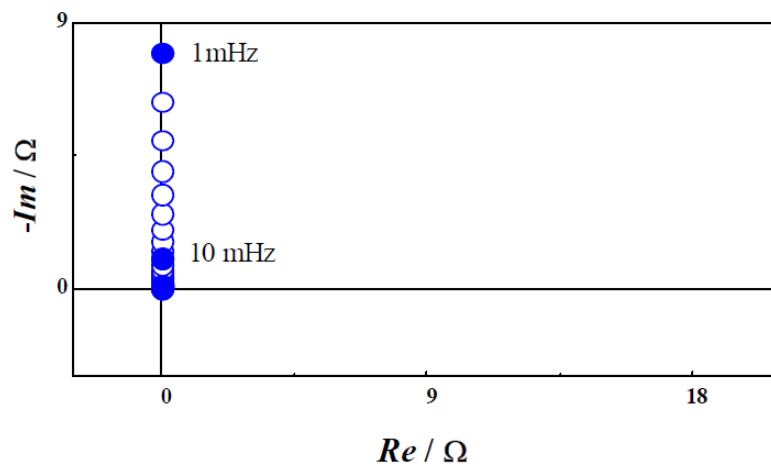


Figure 14 Impedance diagram of Capacitance simulated in the frequency range  $10^3 \div 10^{-3}$  Hz ( $C = 1E-3$  F) [28].

It is possible to distinguish between bulk capacitance which represents the electric charge stored between the electrodes, and double layer capacitance  $C_{dl}$ , arising from an electrical double layer formed at the interface between electrode and electrolyte [35].

c) Inductor

The impedance of a pure inductor, where  $L$  is the inductance [H], has only the imaginary part with positive values when  $L$  is positive.

$$Z_L(\omega) = j\omega L \quad (Eq. 2.27)$$

It is used to model the inductive behaviour of wires used for the test performance and its behaviour when considering a pure inductor is represented in the Nyquist diagram by a line parallel to the positive imaginary axis.

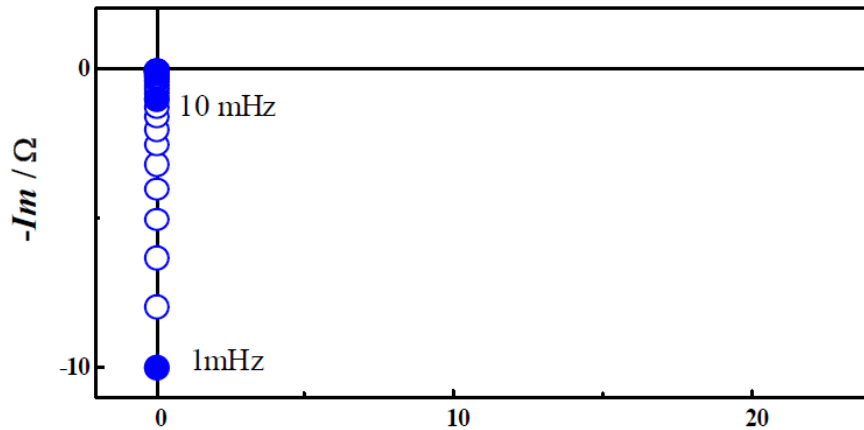


Figure 15 Impedance diagram of Inductance simulated in the frequency range  $10^3 \div 10^{-3}$  Hz ( $L = 1E-3$  H) [28].

### Frequency-dependent elements

a) Warburg element (W)

It is related to mass transfer in the electrochemical system. It describes *linear semi-infinite* diffusion. Its impedance is:

$$Z_w(\omega) = \sigma(i\omega)^{-\frac{1}{2}} \quad (Eq. 2.28)$$

Where  $\sigma$  is known as the Warburg parameter.

Real part and imaginary part of the impedance have same value thus in the Nyquist plot the Warburg impedance is represented by a line with 45° phase shift, and it is not dependent on frequency.

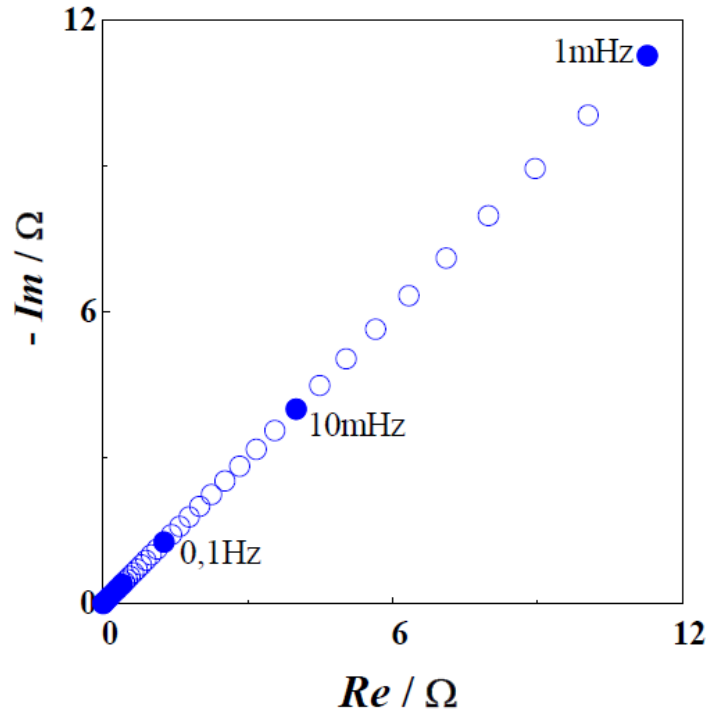


Figure 16 Impedance diagram of Warburg element simulated in the frequency range  $10^3 \div 10^{-3}$  Hz ( $\sigma = 400 \Omega / s^{1/2}$ ).

It is important to point out that in real systems diffusion is limited. Hence, a finite diffusion behaviour is generally present, which in the Nyquist plot is represented by a different shape with respect to the standard semi-infinite Warburg impedance. To consider finite diffusion two other type of equivalent circuit elements are used. These are the finite space Warburg (FSW) and finite length Warburg, sometimes called open and short Warburg elements respectively.

The finite space Warburg or open Warburg describes reflective finite diffusion. It tends towards capacitive behaviour at low frequency or in other words the impedance terminates in an open circuit, which corresponds to the reflection.

The finite length Warburg or short Warburg describes transmissive finite diffusion. It terminates in a large resistance at low frequency whether at high frequency the response is almost equal to that of the semi-infinite Warburg, i.e. it looks like a 45° line [27]. The short Warburg is also referred as bounded Warburg impedance and it will be discussed more in detail in the following paragraphs.

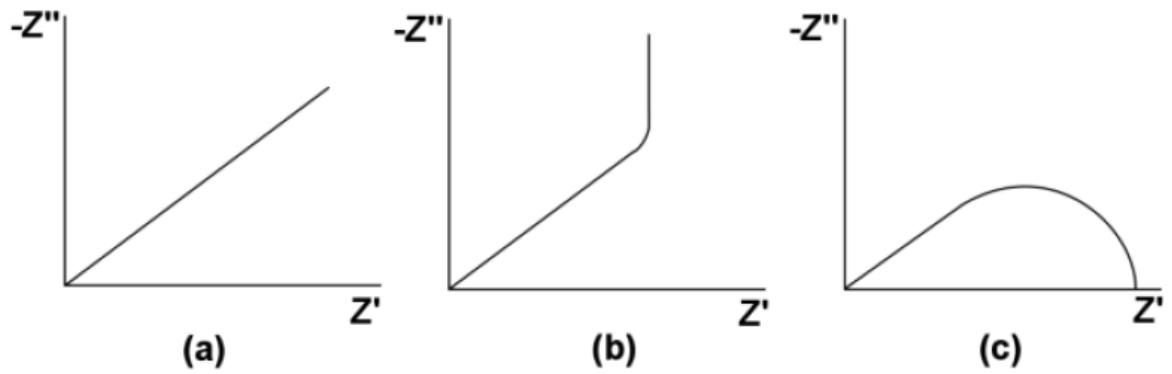


Figure 17 Variation of impedance for diffusive systems: a semi-infinite diffusion; b reflective finite diffusion; c transmissive finite diffusion [27].

#### b) Constant phase element (CPE)

It is a generalised element, it is used to consider the deviations of the double layer from ideal capacitive behaviours which are related to surface roughness and non-uniformly distributed properties of the irregular electrode surface, as well as varying thickness or composition, non-uniform current distribution. The impedance is described as:

$$Z_{CPE}(\omega) = Q^{-1}(i\omega)^{-n} \quad (Eq. 2.29)$$

where  $Q$  is a factor of proportionality and  $n$  is the CPE exponent which characterizes the phase shift. For integral values of  $n$  ( $n = 1, n = 0, n = -1$ ) the CPE represents C, R and L respectively. Instead, when  $n = 0.5$  it describes the Warburg impedance.

| <b>n</b> | <b>Physical meaning</b> | <b>parameter</b> | <b>units</b>                 |
|----------|-------------------------|------------------|------------------------------|
| 1        | capacitance             | $C$              | $F = \Omega^{-1}s$           |
| 0        | Resistance              | $R^{-1}$         | $\Omega^{-1}$                |
| -1       | Inductance              | $L^{-1}$         | $H^{-1} = \Omega^{-1}s^{-1}$ |
| 0.5      | Warburg element         | $\sigma^{-1}$    | $\Omega s^{-1/2}$            |

Table 2.1 Physical meaning of the parameter  $Q$  with different values of the exponent  $n$ .

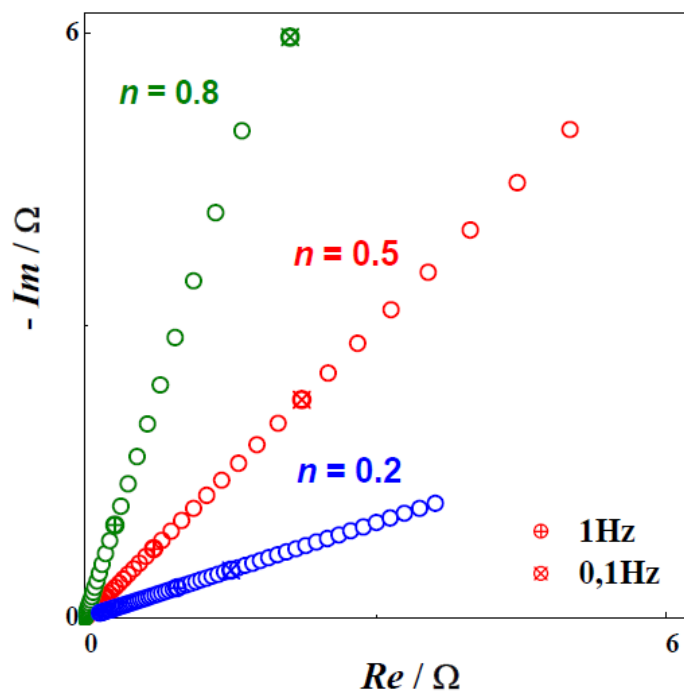


Figure 18 Impedance diagram for CPE simulated in the frequency range  $10^3 \div 10^{-3}$  Hz at different values of  $n$  ( $Q = 100$ ).

In the Nyquist plot, when a CPE is connected in parallel with  $R$ , it is represented by a semicircle with the centre located below the real axis, the so-called depressed semicircle.

### Bounded frequency-dependent elements

#### a) Bounded Warburg element (BW)

It describes linear diffusion in a homogeneous layer with *finite thickness*. It is also denoted as short Warburg element. Its impedance is written as

$$Z_{BW} = \sigma(i\omega)^{-1/2} \tanh\left(\frac{i\omega R_0^2}{\sigma^2}\right)^{1/2} \quad (Eq. 2.30)$$

Where  $\sigma$  and  $R_0$  are two independent structural parameters. It shows the behaviour of a Warburg element at  $\omega \rightarrow \infty$  and it tends to a finite value at  $\omega \rightarrow 0$ , therefore it is represented by a  $45^\circ$  line followed by a semicircle.

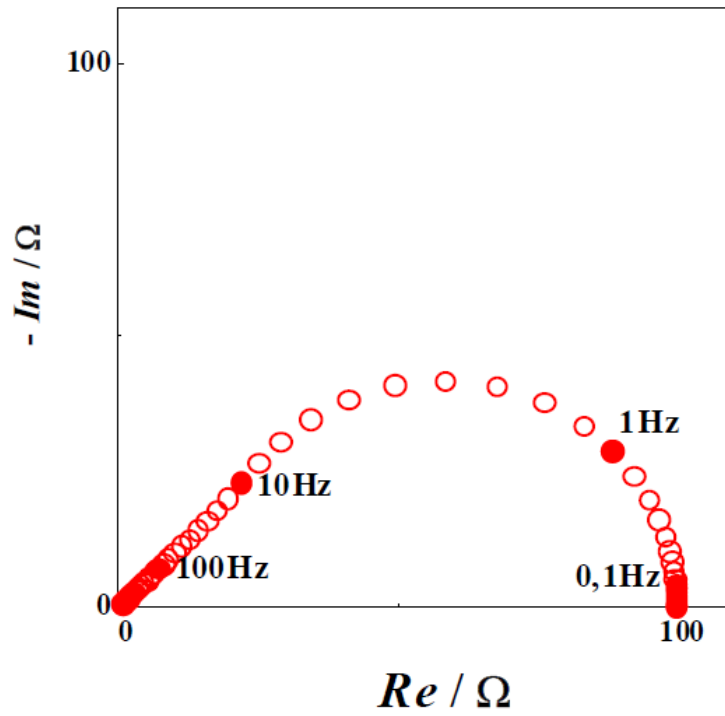


Figure 19 Impedance diagram of Bounded Warburg element simulated in the frequency range  $10^3 \div 10^{-3}$  Hz ( $\sigma = 0,01 \Omega/s^{1/2}$ ,  $R_0 = 100 \Omega$ ).

b) Bounded constant phase element (BCPE)

It represents the impedance of a bounded homogeneous layer with CPE behaviour. Its impedance is

$$Z_{BCPE} = Q^{-1}(i\omega)^{-n} \tanh(R_0 Q(i\omega)^n) \quad (Eq. 2.31)$$

where  $Q, R_0, n$  are structural parameters.

For  $n=0.5$  it corresponds to linear diffusion in a finite length (BW) and the parameter  $Q$  is related to the effective diffusion thickness and to the diffusion coefficient of the diffusing species. The diffusion resistance  $R_0$  is obtained by the intercept of the low frequency feature with the real axis at  $\omega \rightarrow 0$ .

To recap, the BCPE is the most generalised model for homogeneous layers, as it can represent BW as well as CPE with its transformations in R, C, L and W [28].

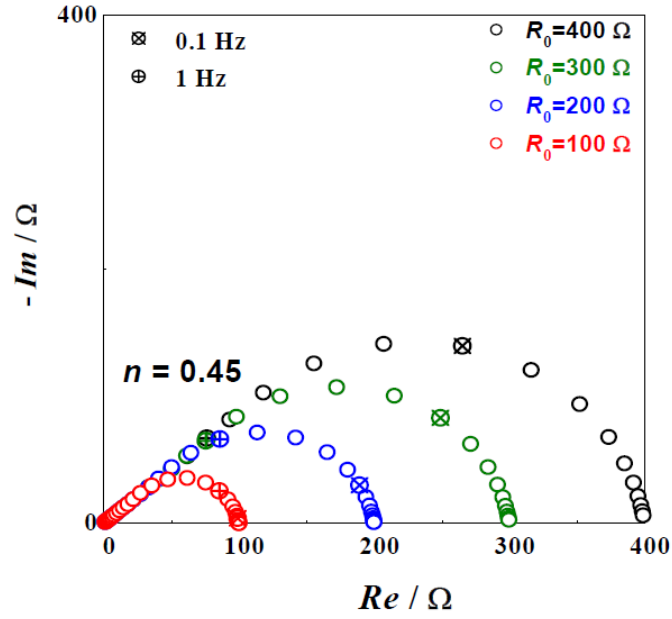


Figure 20 Impedance diagram of BCPE simulated in the frequency range  $10^3 \div 10^{-3}$  Hz at different values of  $R_0$  ( $A = 0,01$ ).

The table below summarizes the main impedance elements with their fundamental parameters.

| element     | name                   | parameter | units              |
|-------------|------------------------|-----------|--------------------|
| <b>R</b>    | Resistance             | $R$       | $\Omega$           |
| <b>C</b>    | Capacitance            | $C$       | $F = \Omega^{-1}s$ |
| <b>L</b>    | Inductance             | $L$       | $H = \Omega s$     |
| <b>W</b>    | Warburg element        | $\sigma$  | $\Omega s^{-1/2}$  |
| <b>BW</b>   | Bounded Warburg        | $\sigma$  | $\Omega s^{-1/2}$  |
|             |                        | $R_0$     | $\Omega$           |
| <b>CPE</b>  | Constant phase element | $Q$       | $\Omega^{-1}s^n$   |
|             |                        | $n$       | —                  |
| <b>BCPE</b> | Bounded CPE            | $Q$       | $\Omega^{-1}s^n$   |
|             |                        | $n$       | —                  |
|             |                        | $R_0$     | $\Omega$           |

Table 2.2 Description of the impedance elements.

### 2.4.3.2 Basic ECMs [27-28]

Here are presented the basic equivalent circuit models commonly used in electrochemical systems. They are the Randles model and the Voigt's model.

#### Randles model

Randles circuit represents the model of a polarizable electrode, in which a single electrochemical reaction occurs at the interface without diffusion limitations. It consists of an ohmic resistance in series with a parallel connection between a double layer capacitance and a charge transfer resistance.

The impedance diagram is an ideal semicircle as depicted in Fig.21. At high frequencies the measured impedance tends to  $R_\Omega$  while at very low frequency it tends to  $R_\Omega + R_{ct}$ . Therefore, the high frequency intercept is associated with the electrolyte resistance and the diameter of the semicircle is equal to the charge transfer resistance. The imaginary part of the impedance reaches a maximum value at a frequency denoted as characteristic frequency  $\omega_{max} = (R_{ct}C_{dl})^{-1} = \tau^{-1}$  where  $\tau = R_{ct}C_{dl}$  is the time constant.

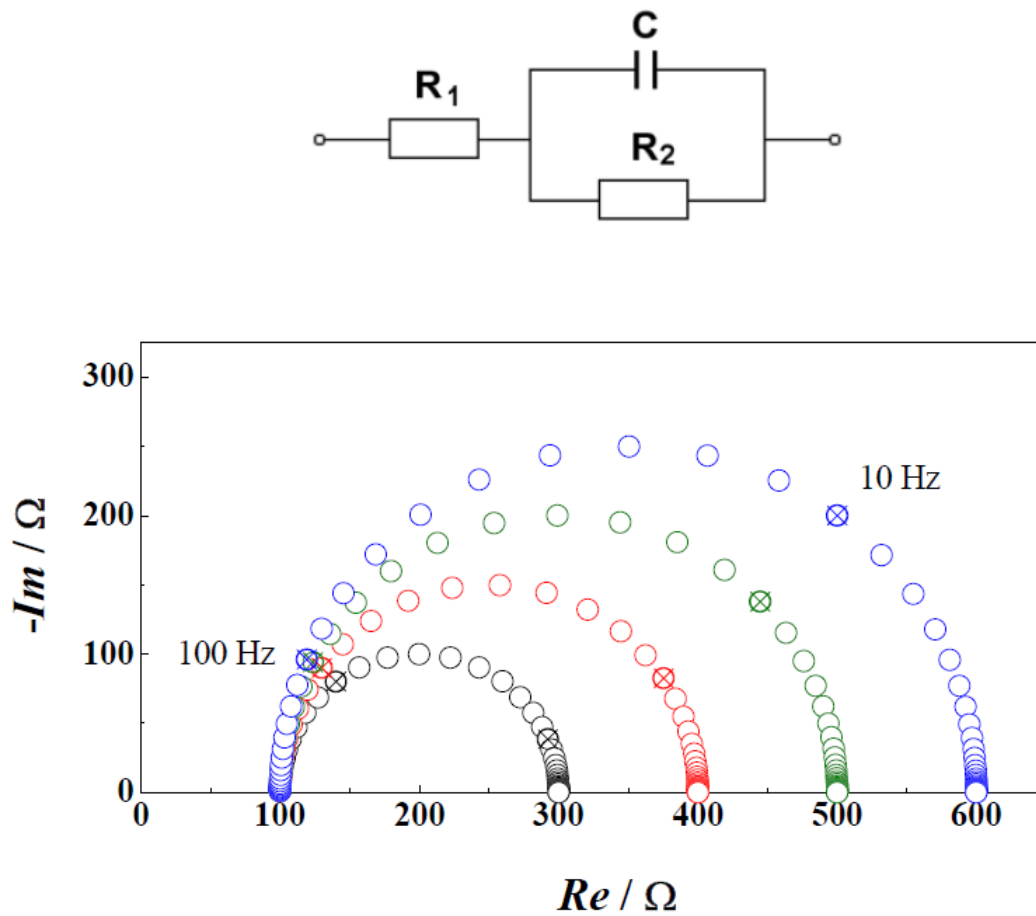


Figure 21 Impedance diagram of Polarizable Electrode simulated in the frequency range  $10^3 \div 10^{-3}$  Hz at different values of  $R_{ct}$  ( $R_s = 100$  Ohm,  $C_{dl} = 1E-4$  F) [28].



The total impedance is represented by the following equation:

$$Z(\omega) = R_{\Omega} + \frac{R_{ct}}{1 + \omega^2 \tau^2} - i \frac{\omega R_{ct} \tau}{1 + \omega^2 \tau^2} \quad (Eq. 2.32)$$

For an electrochemical reaction at open circuit voltage, the charge transfer resistance is given by

$$R_{ct} = \frac{RT}{nFi_0} \quad (Eq. 2.33)$$

where  $i_0$  is the exchange current,  $n$  the number of electrons transferred,  $F$  the Faraday constant. Since the exchange current depends on the rate of the reaction, which in turn is potential dependent, the value of the charge transfer resistance has the same dependence. Hence, a variation of  $R_{ct}$  with voltage determines a change of the semicircle diameter, of the time constant and thus of the characteristic frequency.

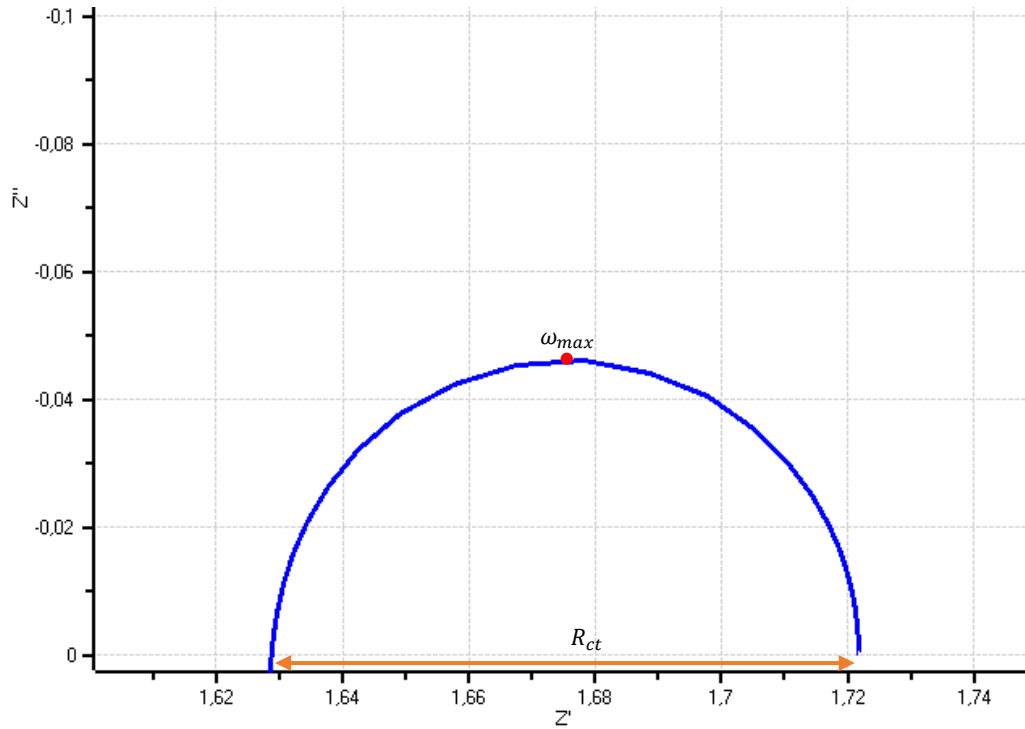


Figure 22

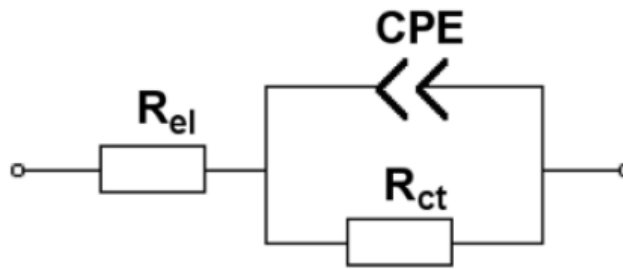
---

### Modified Randles circuit

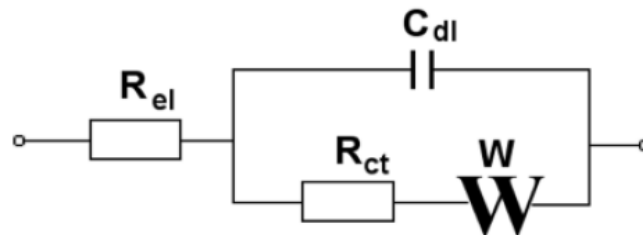
- 1) The Randles circuit is mostly used with the capacitance replaced by a CPE. In this case the graphical representation in the Nyquist plot is a depressed semicircle. As before, at high frequencies the impedance tends to  $R_\Omega$  while at very low frequency it tends to  $R_\Omega + R_{ct}$ ; the parameters of the CPE,  $n$  and  $Q$ , describe the deformation of the semicircle and its amplitude respectively.

The impedance expression becomes:

$$Z(\omega) = R_\Omega + \frac{R_{ct} + QR_{ct}^2\omega^n \cos\left(\frac{\pi}{2}n\right)}{1 + 2QR_{ct}\omega^n \cos\left(\frac{\pi}{2}n\right) + Q^2R_{ct}^2\omega^{2n}} - i \frac{QR_{ct}^2\omega^n \sin\left(\frac{\pi}{2}n\right)}{1 + 2QR_{ct}\omega^n \cos\left(\frac{\pi}{2}n\right) + Q^2R_{ct}^2\omega^{2n}} \quad (Eq. 2.34)$$



- 2) When polarization is controlled by the combination of kinetic and diffusion processes the circuit model changes, a Warburg element is added in series to the charge transfer resistance (because charge transfer resistance is influenced by diffusion to and from the electrode). In case of *linear semi-infinite diffusion*, the simple Warburg element is used and therefore the Nyquist plot has a semicircle and a 45° line in the lower frequency region.



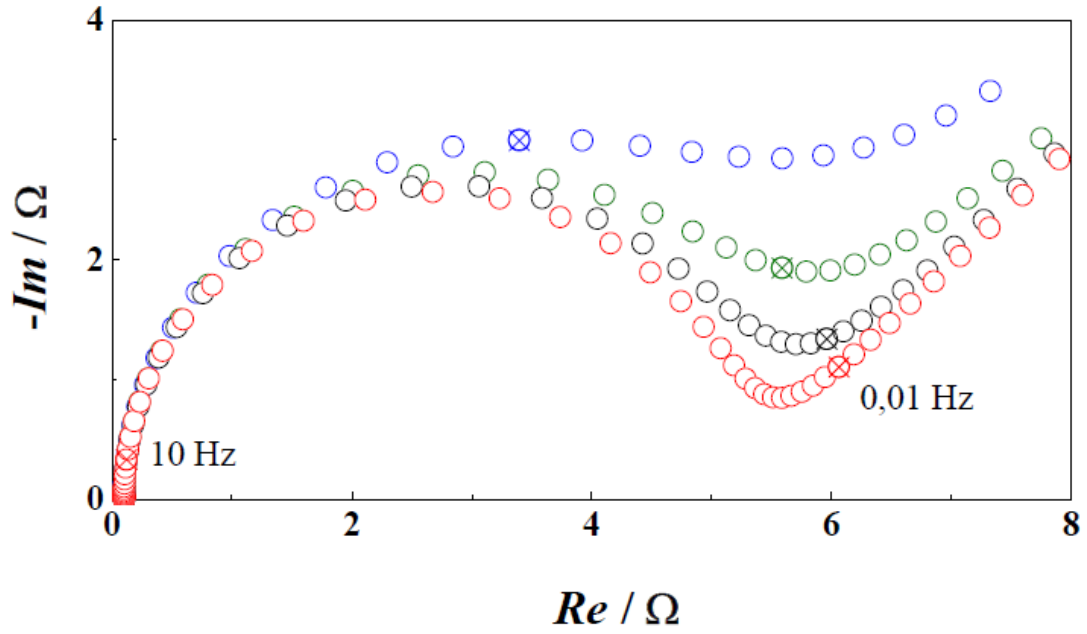
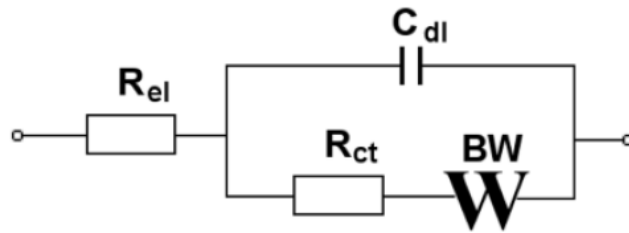


Figure 23 Impedance diagram of Randles model at different values simulated in the frequency range  $10^3 \div 10^{-3}$  Hz of  $C_{dl}$ : 3E-4 F, 1E-3 F, 3E-3 F, 1E-2 F ( $R_0 = 100$  Ohm,  $R_{ct} = 5000$  Ohm,  $\sigma = 100$ ) [28].

If linear but finite diffusion is present, the bounded Warburg element is used and the circuit is called bounded Randle circuit. The impedance diagram is characterized by a first semicircle and a  $45^\circ$  line followed by another semicircle. At high frequencies the impedance tends to  $R_\Omega$  while at very low frequency it tends to  $R_\Omega + R_{ct} + R_0$ .



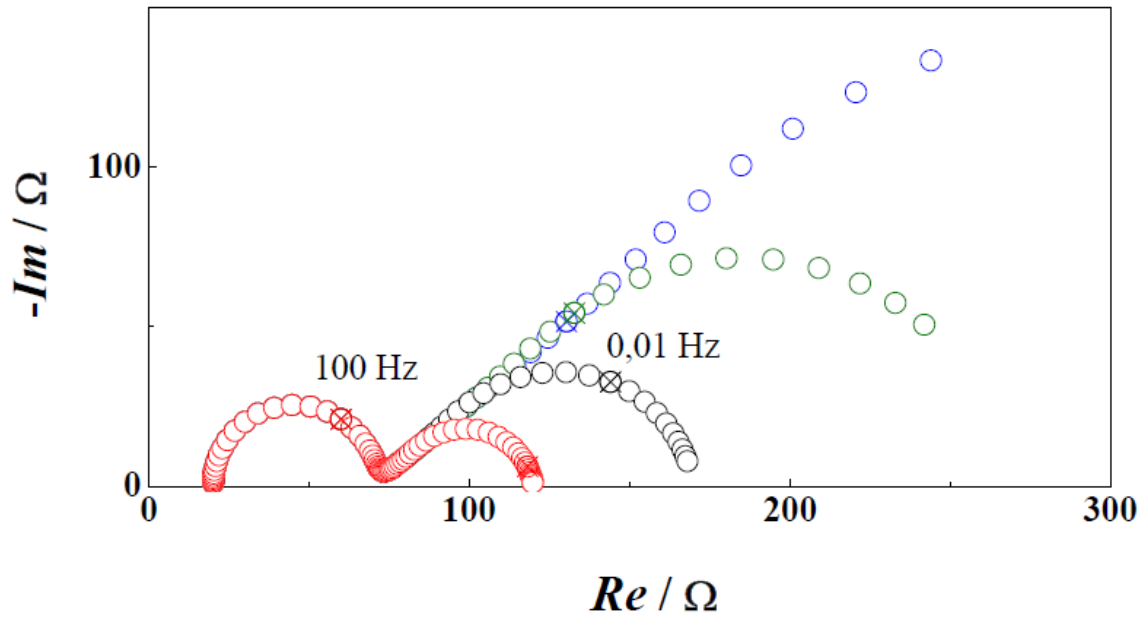


Figure 24 Impedance diagram of Bounded Randles model simulated in the frequency range  $10^3 \div 10^{-3}$  Hz at different values of  $R_0$ : 50 Ohm, 100 Ohm, 200 Ohm, 400 Ohm ( $R_0 = 20$  Ohm,  $C_{dl} = 1E-4$  F,  $R_{ct} = 50$  Ohm,  $Q = 0.1$ ,  $n = 0.45$ ) [28].

Another variation of these two circuits is possible by replacing the capacitance with a CPE; the Nyquist plot is unvaried with the only exception of the semicircles which become depressed.

### Voigt's model

The Voigt's model is mostly used to describe solid electrochemical systems, such as electrodes and electrolyte in fuel cells, or electrodes in battery. It consists of several RC circuits in series, each representing a process with a specific time constant  $\tau$ . Electrode/electrolyte interface in solid systems is challenging because the electrode reactions involves species coming from the electrode, the electrolyte and the gas phase. Hence, this three-phase boundary is described through the Voigt's model, where every semicircle has a physical meaning. In general, the first two are ascribed to the charge transport through the bulk phase and the grain boundaries of the electrolyte, whereas the third semicircle is due to the electrode response [28].

The total impedance for n RC circuit in series is calculated as

$$Z(\omega) = \sum_{k=1}^n Z_k(\omega) \quad (Eq. 2.35)$$

$$Z_k(\omega) = \frac{R_k}{1 + \omega^2 \tau_k^2} - i \frac{\omega R_k \tau_k}{1 + \omega^2 \tau_k^2} \quad (\text{Eq. 2.36})$$

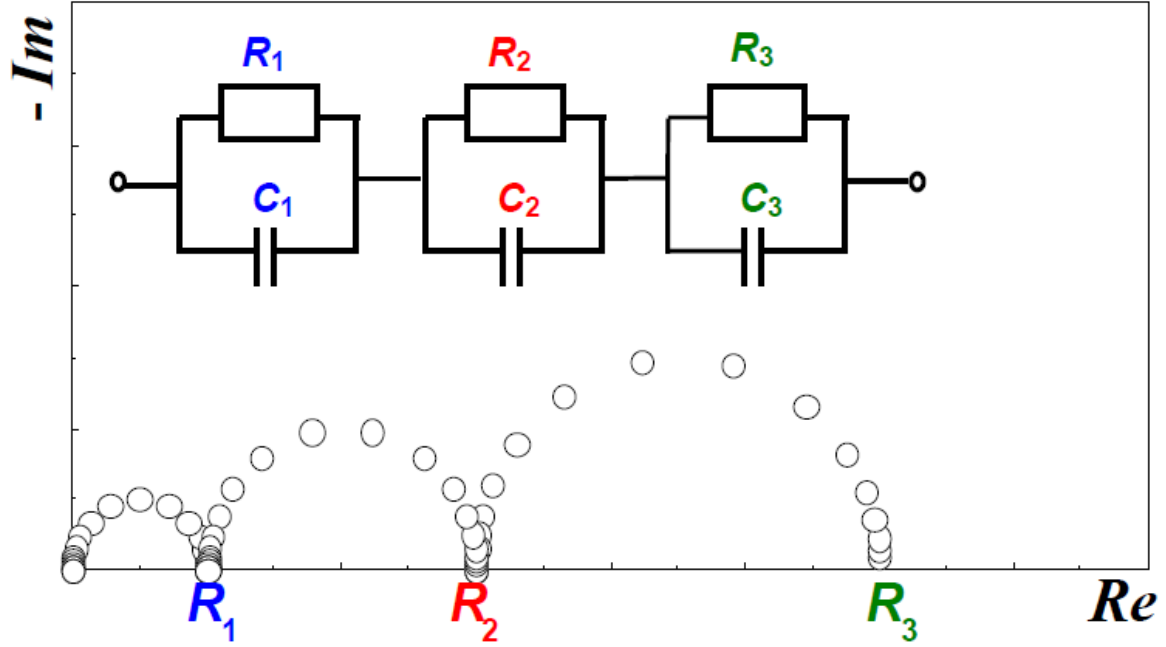


Figure 25 Impedance diagram of Voigt's model with three RC in series [28].

When using this model is advisable to see how many time constants are present in the Bode plot. In fact, it can happen that semicircles in the Nyquist plot may overlap because their time constants are very close. Therefore, an impedance spectrum characterized by two time constants can show in the Nyquist plot only one semicircle.

A modified Voigt's model is possible by replacing the capacitances with CPEs. The impedance diagram is a series of depressed semicircles.

---

#### 2.4.4 Data fitting [30, 36]

In order to evaluate the parameters of the model, the ECM is fitted to the measured impedance spectra by the Complex Non-linear Least Squares (CNLS) fitting algorithm. As a part of the statistical methods, it deals only with stochastic<sup>1</sup> (random) errors.

The purpose of the method is to find a set of parameters which minimize the objective function defined as:

$$S = \sum_{i=1}^n \left\{ w'_{i} [Z'_{i,ex} - Z'_{i,calc}]^2 + w''_{i} [Z''_{i,ex} - Z''_{i,calc}]^2 \right\} \quad (Eq. 2.37)$$

where  $w_{i,re}$ ,  $w_{i,im}$  are the statistical weights of the real and imaginary components of the impedance  $Z_i$ , respectively, and  $n$  denotes the number of frequencies in the experimental spectrum. The differences between the experimental impedance and the calculated one are the residuals of the two components of the impedance (real part  $Z'$  and imaginary part  $Z''$ ).

The method, based on the assumption that the distribution of error is normal (Gaussian), is iterative and nonlinear and moreover it requires an initial estimation of the model parameters. To gain a good fit the initial estimation of the parameters must be close as much as possible to the measured values. An inappropriate choice of these parameters may lead to error message from the software, for example “singular matrix”, or parameters with high error values. The latter case occurs usually when the algorithm finds a local minimum. In these cases, it is necessary to change the set of initial parameters with new estimated one.

When complicated circuits are used, it is recommended to fit just a part of the whole circuit. Thereby, the elements found are fixed and then additional elements are added as free parameters. Finally, all the parameters should be set as free and thus their final approximation can be gained [30]. Lots of software implement this method and they have similar procedures. The starting point is the initial value estimation for all the model parameters; then the software adjusts the parameters to get the fit. If the goodness of the fit is not satisfactory the process is repeated. Nonetheless, it is still possible to get a poor fit if the ECM is inadequate or the impedance data are affected by noise.

The goodness of the fit depends also on the statistical weight chosen for the evaluation of the parameters. In the following table are listed the possible choices. Since real and imaginary parts of the impedance change by several orders of magnitude when frequency changes, and the impedance is sensitive to low frequency, the unit weighting should never be used. Generally, modulus weighting and proportional weighting are recommended. These are based

---

<sup>1</sup> The stochastic or random error is intrinsic of each experiment whereas the bias error in the experiment arises from drift and instrumental artifacts [30]. In particular The stochastic errors in impedance measurements arise from an integration of time-domain signals that contain noise originating from the electrochemical cell and the instrumentation [31].

on an implicit assumption that the relative errors of  $Z'_{i,ex}$  and  $Z''_{i,ex}$  are proportional either to those quantities themselves or to  $|Z_i|$  [36].

| Method                 | Weighting  |
|------------------------|--|
| Statistical weighting  | $w_i' = \frac{1}{(\sigma_i')^2}$ and<br>$w_i'' = \frac{1}{(\sigma_i'')^2}$ |
| Unit weighting         | $w_i' = w_i'' = 1$   |
| Modulus weighting      | $w_i' = w_i'' = \frac{1}{ Z ^2}$   |
| Proportional weighting | $w_i' = \frac{1}{(Z_i')^2}$ and<br>$w_i'' = \frac{1}{(Z_i'')^2}$           |

Table 2.3 Statistical weighting methodologies.

The fitting of the model to the experimental data should provide  $\chi^2$  or  $\chi_v^2$  and the value of parameter with its standard deviation<sup>2</sup> (or confidence limit).

The minimal value of  $\chi^2$  (chi-square) provides a measure of the goodness of the fit of the model to the experimental data and it is defined as:

$$\chi^2 = \sum_{i=1}^n \left\{ \left[ \frac{Z'_{i,ex} - Z'_{i,calc}}{\sigma_i'} \right]^2 + \left[ \frac{Z''_{i,ex} - Z''_{i,calc}}{\sigma_i''} \right]^2 \right\} \quad (Eq. 2.38)$$

<sup>2</sup> The variance of a quantity  $x_k$ , sampled  $k=1 \dots n_x$  times, is given as  $\sigma_x^2 = \frac{1}{n_x-1} \sum_{k=1}^{n_x} (x_k - \mu_x)^2$  where  $\mu_x$  is the mean of the quantity  $x_k$ , while the standard deviation  $\sigma_x$  is given by the square root of the variance. The standard error  $s_x$  is the standard deviation scaled by square root of the sample size  $n_x$  [31].

---

The  $\chi_v^2$  does the same and it is expressed as

$$\chi_v^2 = \frac{\chi^2}{2n - p} \quad (\text{Eq. 2.39})$$

where  $p$  is the number of parameters of the fitted model. This value is more convenient than  $\chi^2$  for comparing the results of various fits. The smaller  $(2n - p)$  or the larger  $p$  at constant  $n$ , the larger is  $\chi_v^2$  [36]. This  $\chi_v^2$  should approach unity when the approximation of the standard deviations are correct.

When the standard deviation of the model parameters is excessively large, it means that the fitting to this parameter is poor. This suggests elimination of the given parameter from the model [36]. Moreover, the residuals should be small and uniformly distributed in the whole range of frequencies considered in the fitting.

To recap, the aim of the fitting of a model to the experimental impedance spectrum is to obtain the smallest  $\chi^2$ , and a set of model parameters with small standard deviations.



---

# Electrochemical characterization of PEMWE in literature

The following chapter presents a review of different studies related to the electrochemical characterisation of PEM water electrolysis cells.

Rozain and Millet reported in [37] the results obtained using a MEA consisting of PTFE-reinforced Nafion with unsupported iridium dioxide for the anode catalyst layer (loading  $1.5 \text{ mg/cm}^2$ ) and carbon-supported platinum for the cathode catalyst layer ( $0.5 \text{ mg/cm}^2$ ). They proposed the equivalent electrical circuit showed in *Figure 26 (B)*, which models:

- charge transfer interface with a parallel connection of the polarization (charge transfer) resistance and the constant phase element
- mass transport limitations with a diffusion impedance
- electron flow in the metallic components and ion flow in the membrane with ohmic resistances

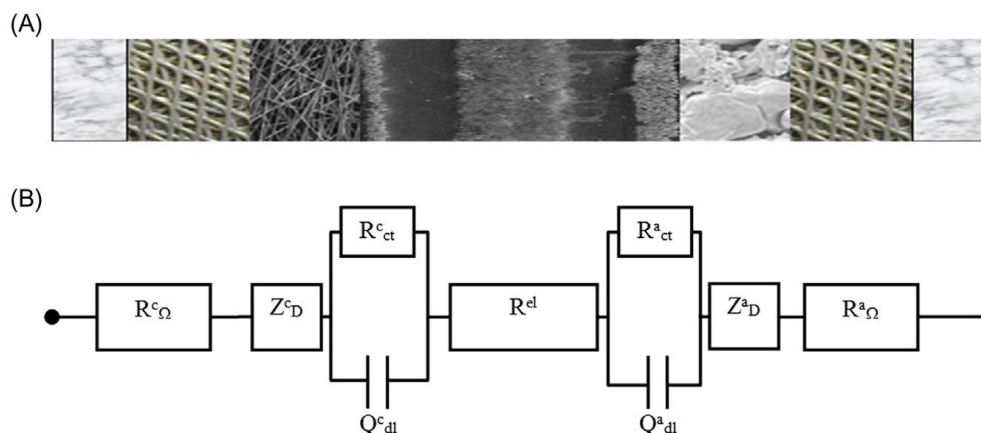


Figure 26 (A) Cross section of a PEM water electrolysis cell; (B) equivalent electrical circuit [37].

---

The different circuit components are:

$R_{\Omega}^c$  and  $R_{\Omega}^a$  [ $\Omega/cm^2$ ] are current non-dependent electronic resistances of electron-conducting metallic cell components, respectively, in the cathodic and anodic cell compartments.

$R^{el}$  [ $\Omega/cm^2$ ] is the current non-dependent ionic resistance of the membrane.

$R_{ct}^c$  [ $\Omega/cm^2$ ] is the current-dependant cathodic charge transfer (polarization) resistance associated with the HER.

$R_{ct}^a$  [ $\Omega/cm^2$ ] is the current-dependant anodic charge transfer (polarization) resistance associated with the OER.

$Q_{dl}^c$  [ $F/cm^2$ ] is the potential-dependant double layer capacitance associated with the cathode/electrolyte interface.

$Q_{dl}^a$  [ $F/cm^2$ ] is the potential-dependant double layer capacitance associated with the anode/electrolyte interface.

$Z_D^c$  [ $\Omega/cm^2$ ] is the current-dependant cathodic diffusion impedance due to  $H_2$  transport away from the cathode.

$Z_D^a$  [ $\Omega/cm^2$ ] is the current-dependant anodic diffusion impedance due to  $O_2$  transport away from the anode and/or to  $H_2O$  transport to the anode.

They performed the electrochemical characterization by measuring the polarization curve at 80°C and EIS impedance measurements at different DC voltage level (1.4-1.9V) and 80°C on a 23  $cm^2$  PEM electrolytic cell described before.

Impedance spectra obtained had an arc-shape; it is shown that the impedance associated with the HER is negligible and that the two time-constants observed on experimental impedance spectra can both be attributed to the OER. Since no mass transport limitations were evident, the EEC used to fit the results was simplified to a series connection of the ohmic resistance (taking into account both electronic resistances of anode and cathode plus the membrane resistance) and two (RQ) circuits:  $R_{\Omega} (R_{HF} Q_{HF}) (R_{LF} Q_{LF})$ . These elements modelled the single arc attributed to the anode by two semicircles. From the best fit, the polarization resistances at high and low frequency,  $R_{HF}$  and  $R_{LF}$ , were determined and they were plotted as a function of voltage and temperature. It is found that both polarization resistances decrease with increasing temperature and cell potential. It is shown that charge transfer processes were major cell impedance contributors at voltages up to 1.8-1.9 V whether for cell voltages larger than 1.8 – 1.9 V the impedance became mostly ohmic because  $R_{HF}$  and  $R_{LF}$  become negligible. This result was in accordance with the polarization curve results in which at high current densities they did not observe mass transport limitations and the current-voltage relationship was almost linear in shape, whereas at low current density the curve was controlled by charge transfer kinetics of anode and cathode.

Van der Merwe et al. [26] identified the losses of a PEM electrolyser by performing EIS measurements in galvanostatic mode. The impedance data recorded were fitted to an ECM consisting of an inductance and an ohmic resistance in series, in turn in series with the parallel between a constant phase element and the series of charge transfer resistance and Warburg

---

element. The Warburg element is used to model mass transfer effects in the cell. The results were verified through polarization curves and Tafel plots. Ohmic losses were individuated by changing only the membrane thickness and keeping unvaried electrocatalyst loadings. As expected, thinner membranes were characterized by lower ohmic resistance. This result is found in accordance with the trend of the polarization curves showing that thicker membrane had a steep slope, so higher ohmic resistance. Activation losses were identified by a change in temperature in the range between 60°C and 80°C. The charge transfer resistance- accounting for activation losses- decreased as temperature increased due to an improvement of kinetics. The effect of mass transport was determined by using two different GDLs and usually in the Nyquist plot is represented by a second semicircle or a 45° line after the first semicircle.

In another work, van der Merwe et al. [38] investigated through electrochemical impedance spectroscopy, current interruption and current mapping a PEM electrolyser of 25cm<sup>2</sup>, with MEA consisting of Nafion, 1mg IrO<sub>2</sub>/cm<sup>2</sup> on the anode and 0.3mg Pt/cm<sup>2</sup> on the cathode. Impedance measurements in galvanostatic mode performed at 0.1A/cm<sup>2</sup>, 0.5 A/cm<sup>2</sup>, 1 A/cm<sup>2</sup> showed that the ohmic resistance- the high frequency intercept with the real axis on the impedance plot- slightly increased whether the semicircle at intermediate frequencies related to the activation resistance decreased. Finally, mass transfer effect were evident with increasing current densities in the low frequency range. In particular, at 0.5A/cm<sup>2</sup> a small tail is observed indicating that a small amount of mass transfer is occurring; then mass transfer became dominated at 1A/cm<sup>2</sup>. This is seen by the combination of a semicircle and 45° line. The results obtained from EIS measurements were consistent with the CI results.

Dedigama et al. [39] examined using high-speed camera, thermal imaging and electrochemical impedance spectroscopy an optically transparent PEM electrolyser consisted of a 28cm<sup>2</sup> circular MEA with Nafion 117 and platinum catalyst layers on either side of it. Impedance spectra were obtained at different operating potentials, at different feed water flow rates and were fitted to an equivalent circuit consisting of an ohmic resistance in series with one or two circuit elements- made of a CPE in parallel with a charge transfer resistance. While the first parallel modelled the anode/electrolyte interface, the second is related to mass transfer effect if present in the impedance plot (second semicircle or 45° tail). It was observed that the flow changes from bubbly (many small bubbles) to slug (less but larger bubbles) flow at higher current densities. At high current density- changing the mass flow from low to high values- makes changing the flow from slug to bubbly, decreasing the performance of the electrolyser. This was in accordance with EIS measurements and polarization curves. Near OCV mass flow has little effect on EIS measurements whether at higher potential an increase of the mass flow has a negative effect (low frequency feature increased and internal resistance increased as well). Similar consideration can be done from the polarization curve, in which it was observed a slight decrease in voltage with decreasing flow rate. The main reason is that less heat is removed from the system, so activation overpotential decreased and ionic conductivity of the membrane increased leading to higher performance at lower flow rates. Hence at higher current densities it is better to decrease mass flow rate.

Elsøe et al. [40] investigated the performance of PEMEC at high current densities using EIS measurements in combination with CV, iV-curves and SEM. The PEM electrolyser had an active area of  $2.89\text{ cm}^2$  and it contained a Nafion 117 membrane, anode catalyst layer with  $0.3\text{ mg/cm}^2$   $\text{IrO}_x$  and cathode catalyst layer with  $0.5\text{ mg/cm}^2$  platinum supported on carbon. The anode side had a GDL made of two components, a titanium felt and an iridium metal with Nafion binder. The iridium metal is used only to ensure electrical contact between the catalyst layer and the titanium felt. Polarization curves were measured at 53, 61 and  $69^\circ\text{C}$  from  $0.050\text{ A/cm}^2$  to  $1\text{ A/cm}^2$  while EIS measurement were realized at 0.07, 0.35, 0.69 and  $1\text{ A/cm}^2$  at 53, 61 and  $69^\circ\text{C}$  in the frequency range 100 kHz–0.01 Hz with the alternating current (AC) amplitude of  $24.5\text{ mA/cm}^2$ . Higher performance was found at higher temperature due to lower ohmic resistance as confirmed by the EIS measurements at different temperature in which it was found a temperature dependent behaviour of the high frequency intercept with the real axis. Moreover, at fixed temperature, the shape of the spectrum changed with current density. At high current density the impedance spectra showed three arcs indicating three electrochemical processes, thus they used an equivalent circuit model consisting of a resistance-modelling the electrolyte resistance- in series with three R/CPE simulating these three arcs. They suggested that the high frequency arc independent on current density derived from current constrictions- ascribed to bad contact between Nafion and iridium oxide layer and iridium metal layer as supported by SEM- whereas the middle and low frequency features were determined by the interface between  $\text{IrO}_x$ /Nafion anode catalyst layer causing two capacitive impedances dependent on current density (mid frequency arc decreased while low frequency arc increased with increasing current density), but with total resistive impedance of the two processes constant at current densities from  $0.35\text{ A/cm}^2$ . These findings were consistent with results obtained from the polarization curves showing a linear behaviour from  $0.35\text{ A/cm}^2$ , meaning that ohmic losses are dominant from  $0.35\text{ A/cm}^2$ .

Rasten et al. [41] did studies on powders of iridium oxide ( $2\text{ mgIrO}_2/\text{cm}^2$ ) as anode catalyst in water electrolysis cells with SPE (active area  $5\text{ cm}^2$ ). The aim of their work was to develop a high performing water electrolysis cell with low loading of the noble metal oxide catalyst. The catalyst was annealed at different temperatures from  $450^\circ\text{C}$  to  $540^\circ\text{C}$  and then studied in an electrolytic cell using cyclic voltammetry, stationary i-V curves, and electrochemical impedance spectroscopy.

The electrochemical results showed that with increasing annealing temperature the electrical conductivity increased whereas the electrocatalytic activity (number of active sites available in the electrode, measured with the capacitance) deteriorated. This was evident in the EIS test performed at  $1.49\text{ V}$  with frequency range  $10\text{ kHz} - 10\text{ mHz}$  on samples with different annealing conditions. The ohmic resistance – including external circuit resistance, resistance of the electrodes and the electrolyte, and contact resistance- decreased up to a constant value with increasing annealing temperature, therefore the electrical conductivity improved. Instead, there was an increase of the diameter of the low frequency arc, which is a measure of the charge transfer resistance and thereby of the catalytic activity of the anode; the latter

case was determined by a decrease of the capacitance [ $\mu F/cm^2$ ] which is in turn due to a worsening of the electrocatalytic activity of the anode. These effects could be explained with the TEM (transmission electron microscopy). TEM revealed an increased crystallinity and size of the particles with increasing annealing temperature. In fact, the particle size growth determined a reduction of the active surface which consequently caused the capacitance reduction (C is a direct measure of the active surface). Meanwhile the higher electrical conductivity was probably related to the higher crystallinity. Furthermore, the impedance measurements performed in the voltage range between 1.54 – 1.61 V with annealed sample showed clearly the presence of two arcs identified in the Bode plot by two time constants. The time constant associated with the HF arc became more evident with increasing potential whereas that related to the LF range disappeared. The impedance spectra obtained were fitted with an  $R_\Omega(R_1Q_1)(R_{dl}Q_{dl})$  circuit where  $(R_1Q_1)$  circuit element was attributed by the literature to different phenomena. However, for the researchers it was more likely related to steps in the OER. Optimum annealing conditions were found at 490°C, where the total polarisation reaches a minimum in the high current density range ( $1 - 2 A/cm^2$ ), at the actual conditions. Very high performance of a total electrolysis cell can be obtained using a polymer electrolyte with iridium oxide catalyst for the oxygen electrode and platinum for the hydrogen electrode, using totally 2.5 mg of noble metal catalyst per  $cm^2$  MEA area [cit.40].

Rozain et al. [42] also studied the influence of iridium oxide loadings for OER on the overall performance of PEM water electrolyser with active area of  $25 cm^2$  using cyclic voltamperometry, electrochemical impedance spectroscopy and polarization curves. Electrochemical characterizations performed at 80°C and atmospheric pressure showed that there is a threshold loading value of  $0.5 \frac{mg}{cm^2} IrO_2$  above which the cell voltage does not depend on catalyst loading, i.e. an increment of the loadings does not produce a further decrease of the voltage. This because the positive effects generated by higher loadings (larger number of catalytic sites, better electronic conductivity through the catalyst layer and improved contact resistance between electrode and backing porous current collector) are counterbalanced by the worsening of the transport of protons through the catalyst layer, caused by the linear increase of the catalyst thickness with higher loadings. This, translated to the EIS results, means that the ohmic resistance (determined by the high frequency intercept with the real axis) measured at  $1 A/cm^2$  remains almost constant in the loadings range  $0.5 - 2.6 mg/cm^2 IrO_2$ , while the polarization resistance, taken as the difference between the extrapolated low frequency intercept and the high frequency intercept on the real axis, does not significantly change with  $IrO_2$  loadings. To conclude, below this threshold value the performance of the cell drops quickly and the anode tends to degrade rapidly. Hence a conductive support is needed to keep a good level of performance.

In another work Rozain et al. [43] deepened the influence of iridium oxide as anode catalyst layer in PEMWE by studying the applicability of micro-sized titanium particles as support of  $IrO_2$  particles in the low loading range ( $< 0.5 mg/cm^2 IrO_2$ ) in order to increase the electronic conductivity of the anodic catalytic layer. The electrochemical properties of the

---

*IrO<sub>2</sub>/Ti* catalyst were investigated in a 25 cm<sup>2</sup> PEM electrolytic cell with 50 wt.% *IrO<sub>2</sub>/Ti* anodes containing iridium oxide loading ranging from 0.1 to 0.7 mg/cm<sup>2</sup> through the application of CV, EIS and recording polarization curves at 80°C and atmospheric pressure. Regarding EIS measurements, the tests were carried out with DC current level between 0.04-2.00 A/cm<sup>2</sup> in the frequency range 10kHz – 200mHz. Experimental impedance spectra were fitted using a simple equivalent circuit (L+Rohm+R1//Q1+R2//Q2) where the high frequency equivalent circuit R1//Q1 is attributed to reactions occurring at the cathode, and the low frequency equivalent circuit R2//Q2 is attributed to anodic reactions.

The electrochemical investigation with EIS and i-V curves showed that for *IrO<sub>2</sub>* loadings below 0.25mg/cm<sup>2</sup> the addition of titanium particles to the catalyst layer improved the performance with respect to unsupported iridium oxide. This was valid whether they had same or different loadings. However, increasing the loadings when *IrO<sub>2</sub>/Ti* catalyst is used could caused increment of voltage, probably related to the thicker catalyst which introduces mass transport limitations. These results are interrelated with charge transfer kinetics and ohmic resistance of the catalyst layer. At low current density, the voltage drop due to the ohmic resistance of the cell is negligible whereas charge transfer effects are dominant; at high current density, charge transfer resistance are small and the voltage drop due to the internal cell resistance is predominant. Therefore, when *IrO<sub>2</sub>* loadings are below 0.25mg/cm<sup>2</sup>, titanium particles enhanced the electrocatalyst activity (more active sites) and ohmic losses because they favoured an intimate electrical contact between the catalyst layer and the current collector (hence improved electronic conductivity). Meanwhile, with higher loadings the addition of titanium particles determined a thicker catalyst layer which in turn caused the increase of the electronic resistance of the catalytic layer. However, the positive effect of titanium particles found an explanation in SEM and CV: meanwhile small particles are embedded within the catalyst layer, the bigger ones are found to protrude from it, penetrating inside the porosities of the current collector; this contributed to improve the electronic contact between the catalyst layer and the current collector, facilitating the electron transfer hence optimizing the number of active sites [cit. 43].

To evaluate the stability of *IrO<sub>2</sub>/Ti* catalyst- the titanium particles in the long-term can oxidize increasing the electrical resistance- they also performed two different ageing-tests. The durability test performed with a PEM electrolytic cell using IrO<sub>2</sub>/Ti as anode material demonstrated a good stability of the MEA over 1000 h of operation. Using such a low IrO<sub>2</sub> loading (0.1 mg cm<sup>-2</sup>IrO<sub>2</sub>), the degradation rate measured at 1 A cm<sup>-2</sup> was reduced from 180 μV h<sup>-1</sup> (measurement made on pure IrO<sub>2</sub> anode) down to only 20 μV h<sup>-1</sup> for the 50 wt.% IrO<sub>2</sub>/Ti anode [cit. 42]. A detailed analysis of the electrical properties of the PEM cells during these ageing tests revealed that three main different electrical factors contribute to the degradation of MEA performances: the purely ohmic resistance of the cell, the charge transfer resistance of the anode and the capacity measured at low frequency (this capacity is related to the electrochemically active surface area of the electrodes). The ohmic resistance during the operation at 60°C remained stable or slightly decreased (probably due to membrane thinning) while at 80°C both the ohmic resistance and the charge transfer resistance increased linearly with time. Their degradation was attributed to the oxidation of the titanium current

collectors and the resulting increase of the contact resistance between this material and the catalyst layer. The capacity measured at low frequency instead decreased quickly during the first hours of operation and then reached a constant value; this behaviour was attributed to the stress produced by oxygen nucleation within the porous catalyst layer, by bubbling and by erosion of the catalyst particles by water flowing [cit.43].

Lettenmeier et al. [44] did ageing tests on 8-cell stack having MEA from different suppliers operating up to  $4 \text{ A/cm}^2$  for more than 750h in a  $120 \text{ cm}^2$  PEM electrolyser stack. All MEAs had the same membrane Nafion 115 but different anode and cathode catalyst loadings.

The electrochemical characterization was performed recording i-V curves and EIS measurements with additional post-mortem analysis with SEM and AFM. EIS tests were executed at different current densities ( $0.025 - 0.35 \text{ A/cm}^2$ ) from 1kHz to 100mHz on each cell of the stack before and after the ageing tests. The EEC used to simulate the impedance data consisted of ohmic resistance in series with two  $R_{ct}/CPE$ . The element  $R_1$  represents the ohmic resistance while the two R/CPE elements model the features of HF and LF impedance spectra. The meaning of the two R/CPE circuits finds different possibilities in the literature. If the interpretation given in PEM fuel cell is considered, the HF arc is attributed to the HER at the cathode whereas the LF arc corresponds to the oxygen evolution reaction taking place at the anode. Another interpretation of other groups associates the HF arc with charge transfer processes combined with double layer effects of electrical and/or ionic conductive materials and oxides in the active layer [cit.44]. The latter is supported by Lettenmeier et al. due to the negligible dependence of the HF feature on current density and linear behaviour of the resistance. Polarization curves and impedance spectra were recorded before (T1) and after (T2) operating at  $2 \text{ A/cm}^2$  for ca. 500 h, and after 250 h at  $4 \text{ A/cm}^2$  (T3).

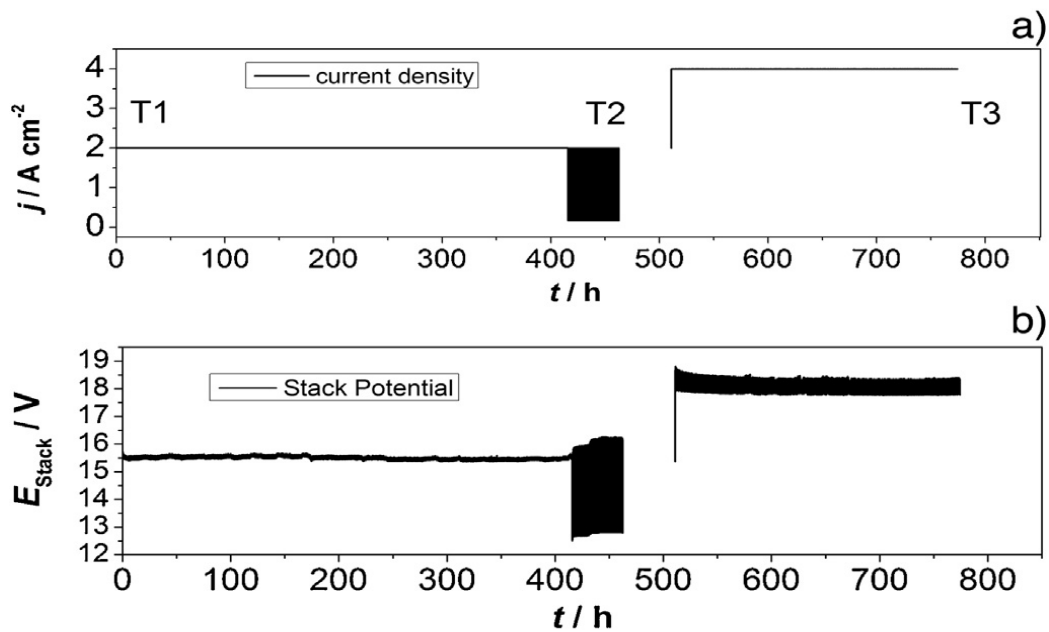


Figure 27 Protocol of measurements of the 8-cell  $120 \text{ cm}^2$  stack: a) Input current density; b) Output stack potential. EIS was measured at the time steps T1, T2 and T3 of the protocol [44].

For all MEAs it was found that the cell voltage decreased during the testing period. The picture below shows that for all MEAs the efficiency is improved because the voltage decreases over time.

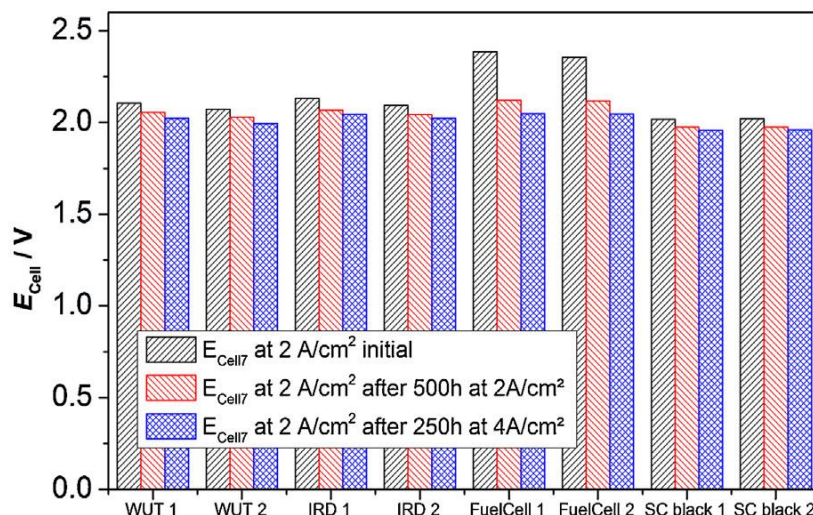


Figure 28  $E_{cell}$  of all cells measured at 2 A/cm<sup>2</sup> after T1, T2 and T3 [44].

From a deeper analysis of cell 7, it was found that the ohmic resistance decreased over time whereas the charge transfer resistance increased. The explanation of lower ohmic losses is related to the applied current density (the percentage of decrease increased with increasing operating time) and the increment of activation losses is ascribed to loss in the electrocatalytic properties supported by XPS measurements of DI water resin of the anodic water cycle. Concluding, current density and operation time had an impact on the performance of the PEM electrolyser. The operation at high current density reduced the ohmic drops but long-term operation caused a degradation of the anode. This is supported by post-mortem analysis of the MEAs (SEM and AFM) and water resin (XPS) which revealed a current dependent loss of ionomer and catalyst material in the anode [cit.44].

Lettenmeier et al. [45] worked on the development of a titanium MPL (macro-porous layer) produced by vacuum plasma spraying (VPS) on the current collector of PEM electrolysers. The aim of the macro-porous layer is to increase the contact surface with the catalyst while improving the water/gas management through a gradient of pore sizes [cit.]. They found that it enhances the efficiency when operating at high current density by reducing the contact resistance between anode catalyst layer and the current collector of around  $20 \text{ m}\Omega\text{cm}^{-2}$ , thus improving the activation losses and the reactant/product management. The electrochemical characterization (polarization curves and EIS tests) was performed on a  $25 \text{ cm}^2$  single PEM electrolyser cells- with a N115 membrane, Ir-based anode and Pt-based cathode- using the porous titanium disc as current collector with and without MPL at 85°C and



atmospheric pressure. EIS measurements were realized at different current densities between  $0.08 \text{ A/cm}^2$  and  $1.2 \text{ A/cm}^2$  in a frequency range of  $10\text{kHz} - 2\text{mHz}$ .

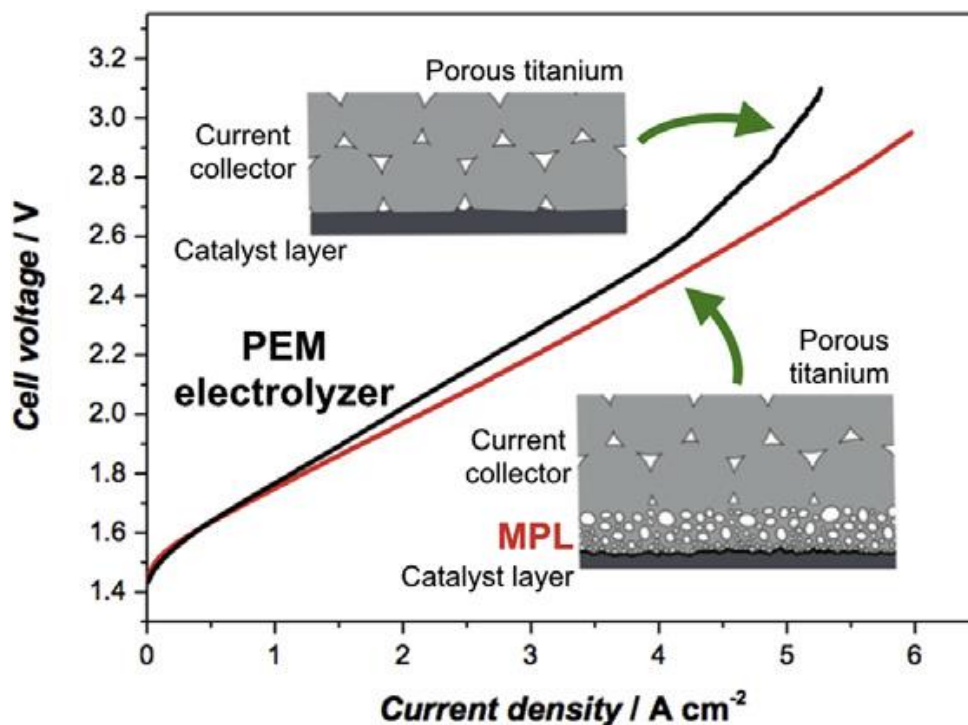


Figure 29 Polarization curves of a PEM electrolyzer single cell with and without MPL [45].

The EEC used to fit the experimental data consisted of a resistance  $R_1$ -associated to the interconnecting elements and membrane- in series with three  $R/CPE$  circuit elements modelling the three arcs appearing in the impedance spectra. The circuit element  $R_2/CPE2$  models the HF loop related to the interface between MPL and the catalyst layer/ionomer. Meanwhile  $R_3/CPE3$  and  $R_4/CPE4$  simulate respectively the OER and the mass transport limitation effects. A comparison between impedance spectra measured with and without MPL showed that at high current densities with MPL there is a decrease of  $R_1$  and  $R_2$ , thus of the HF loop, whereas the middle arc representing the kinetics of the oxygen evolution reaction is unvaried. The LF loop did not show a clear trend. Hence, the improvement obtained adding the MPL at high current density is confirmed by EIS results.

Siracusano et al. [46] studied the electrochemical behaviour of a sulfonated polysulfone membrane in a single PEM electrolyzer by linear sweep voltammetry, electrochemical impedance spectroscopy, chrono-amperometry and gas cross-over measurements. The results were compared to those obtained with a PEMWE based on a Nafion 115 reference membrane in order to assess the suitability of SPSf membranes for this application [cit.45].

---

Both SPSf membrane and Nafion 115 membrane were characterized by same active area of  $5\text{ cm}^2$  and same catalysts with same loadings of  $2.5\text{ mg IrO}_2/\text{cm}^2$  for the anode and  $0.4\text{ mgPt}/\text{cm}^2$  for the cathode. A comparison of the polarization curves for the electrolysis cells based on SPSf and Nafion 115 membranes at  $80^\circ\text{C}$  and atmospheric pressure showed that the cell equipped with Nafion 115 membrane had at 1.8V slightly higher performance (15%) than that of SPSf. This result is verified by EIS test in potentiostatic mode performed at 1.5V and  $80^\circ\text{C}$  and atmospheric pressure. Impedance spectra have been fitted with an equivalent circuit consisting of two (RQ) elements- representing HER and OER respectively- in series with the ohmic resistance  $R_s$  associated to the electrolyte. Both membranes had similar ohmic resistance, but Nafion membrane showed a lower polarization resistance probably due to a better electrode-membrane interface. This is reasonably related to the presence of Nafion ionomer dispersed in the catalytic layer of the electrodes, which makes the kinetics process faster because it extends the three-phase reaction zone. SPSf membrane is considered a valid alternative to Nafion 115 because, even if Nafion 115 has shown slightly better performance due to higher proton conductivity and improved electrode-membrane interface, their behaviour is comparable. Moreover, other tests such as chrono-amperometric and hydrogen cross-over tests demonstrated that SPSf has good stability and a lower permeability to gas cross-over with respect to Nafion 115, making this type of membrane very promising for the application in high pressure PEM electrolyzers [cit. 46].

Siracusano et al. [47] investigated in a PEM electrolyzer a composite Nafion-Sulfated Zirconia ( $\text{SZrO}_2$ ) membrane at different temperatures. Its performance was compared to a commercial Nafion 115 membrane of similar thickness. Both membranes were characterized by same active area of  $5\text{ cm}^2$  and same catalysts with same loadings of  $2.5\text{ mg IrO}_2/\text{cm}^2$  for the anode and  $0.4\text{ mgPt}/\text{cm}^2$  for the cathode. Nafion membranes decrease their proton conductivity at temperature above  $100^\circ\text{C}$ . Therefore, incorporation of sulfated zirconia has the aim to enhance its performance under thermal and water management point of view, as its use in fuel cells has demonstrated. In the polarization curves at  $80^\circ\text{C}$  and atmospheric pressure it is observed a slightly different trend between these two different membranes: at low current densities Nafion 115 showed better performance whether Nafion-Sulfated Zirconia performed better at high current densities. These results were consistent with the findings of the EIS test performed at 1.5V and  $80^\circ\text{C}$ . From impedance spectra it is found that ohmic resistance of the cell with the composite membrane had lower values (this explains better performance at high current densities where ohmic losses are dominant); instead, the polarization resistance for the cell with bare Nafion was characterized by lower values so better performance in the activation region of the polarization curve. The lower ohmic resistance for the composite membrane is ascribed to the higher humidification level gained with the addition of sulphated Zirconia, whether lower polarization resistance of bare Nafion is related to better catalyst-electrolyte interface. Further, electrochemical characterization at  $100^\circ\text{C}$  showed in general better performance of the Nafion-SZrO<sub>2</sub> membrane, essentially because sulfated Zirconia promoted higher hydration level determining a decrease of the ohmic resistance; instead, Nafion 115 showed some hydration constraints appearing in the

---

Nyquist plot as a linear slope at high frequencies. In conclusion, composite Nafion-SZrO<sub>2</sub> membrane showed better performance principally related to an increase of proton conductivity due to better hydration but it required enhancement of the catalyst-electrode interface affected by the formation of agglomerates which may reduce the adhesion of the catalytic layer on the composite membrane [cit.47].

Su et al. [48] investigated the feasibility of using the catalyst sprayed membrane under illumination (CSMUI) method to prepare low noble metal loading MEAs for PEM water electrolyser. The electrochemical and physical characterization of the MEAs was performed by I-V curves, electrochemical impedance spectroscopy (EIS) and scanning electron microscopy (SEM). It was found that MEA with noble metal loading (NML) of  $0.38 \text{ mg/cm}^2$  had lower ohmic resistance and negligible mass transport limitations. SEM and EIS measurements revealed that the MEA with low NML has very thin porous cathode and anode CLs that get intimate contact with the electrolyte membrane, which makes a reduced mass transport limitation and lower ohmic resistance of the MEA [cit. 47]. They also investigated the influence of the ionomer content in the anode catalyst layer using the MEA with low NML of  $0.38 \text{ mg/cm}^2$ , suggesting that the optimal Nafion content in the anode was 5wt.%. Finally, the durability test showed that MEA with low NML of  $0.38 \text{ mg/cm}^2$  and 5wt.% Nafion content exhibited good stability in water electrolysis and at a current of  $1 \text{ A/cm}^2$  its voltage remained at 1.60 V without significant degradation during the 122 h of testing [cit.48].

Siracusano et al. [49] studied the performance of a  $5 \text{ cm}^2$  PEM electrolysis cell through polarization curves and electrochemical impedance spectroscopy at different temperatures and catalyst loadings. The results from EIS measurements were obtained by fitting the experimental data to an ECM made of a series resistance- reflecting ohmic phenomena- and two RQ components associated to faradaic processes. The investigation of different cathode loadings consisted of polarization curves at  $80^\circ\text{C}$  coupled with EIS tests under voltage control at 1.5V. They observed that polarization curves, with constant anode loading but different cathode catalyst loading, overlap at all current densities, meaning that the cathode loading has no influence on the cell performance. Instead, its effect is visible on the Nyquist plots in which are evident two overlapping semicircles; the one appearing at high frequency is attributed to the cathode because as the cathode loading increases the resistance of the HF arc decreases considerably. On the other hand, the arc occurring at low frequency is attributed to the anode since it has a higher polarization resistance, which does not change with the cathode loading variation. Meanwhile, when the anode loadings is reduced, the polarization resistance at low frequency increases; this reflects in the polarization curves with an increase of voltage at low current densities, which in turn has an influence also at high current density. The study at different temperatures showed that the slope of the polarization curves increases as the temperature decreases. Also, it is observed that the anode benefits much more than membrane from the increase of temperature. Finally, they concluded with a 1000-h durability test carried out at  $3 \text{ A/cm}^2$ . The test showed a degradation rate of  $20 \mu\text{V/h}$  and the anode

---

was identified to contribute to the degradation behaviour since its polarization resistance showed a substantial increase.

Suermann et al. [50] proposed an approach to underline degradation mechanisms by using different electrochemical methods including polarization curves and EIS measurements. They suggested that there is an apparent degradation rate coming from the anode, which can be recovered by applying lower potential. Instead, real degradation is related to ohmic and mass transport overpotential occurring at higher current densities and for longer operating times. The degradation test, called constant current test, is performed at 60°C and ambient pressure at two different current densities, 1 A/cm<sup>2</sup> and 4 A/cm<sup>2</sup>. The CC test last for each constant current density 270 hours, and during the total measurement time electrochemical characterization- iV-curves, EIS measurements under galvanostatic mode, current interruption- is performed each 30 hours; hence, each 30h CC test has two electrochemical characterization, one at the start and the other at the end. The degradation rate is calculated taking the value obtained at the start of each 30h CC test phase. Another degradation rate is calculated using the end values. The degradation rate based on the start values are considered as the real degradation whereas those obtained with the end values include parts of apparent degradation. It is found that the degradation rate of the 4 A/cm<sup>2</sup> sample is higher than those of the 1 A/cm<sup>2</sup> sample with 10 μV/h. Moreover, degradation rate for the 1 A/cm<sup>2</sup> sample is mainly due to apparent degradation, hence to the activation overpotential. Concerning the 4 A/cm<sup>2</sup> sample the degradation rate is related to real degradation, thus to ohmic overpotential. These findings are consistent with the EIS results. While the ohmic resistance stays almost constant for the 1 A/cm<sup>2</sup> sample at least up to EIS current densities of about 1 A/cm<sup>2</sup>, an increase is measured for the 4 A/cm<sup>2</sup> sample. They suggested that the increasing HFR could be caused by cationic contamination of the membrane, dissolution and re-precipitation of the iridium within the membrane or rather by an increase in the interfacial contact resistances between the titanium PTL and the anode and/or the flow field [50]. The difference between the high frequency intercept and the low frequency intercept with the real axis shows a moderate increase for the 1 A/cm<sup>2</sup> whereas the increase is substantially significant for the 4 A/cm<sup>2</sup> sample. Therefore, it is verified that at 1 A/cm<sup>2</sup> the degradation concerns the anode, whereas it is attributed to the membrane at 4 A/cm<sup>2</sup>.

Aßmann et al. [51] proposed an accelerated stress test protocol for the evaluation of the PEMWE efficiency and durability. The aim of this type of test is to accelerate the degradation mechanisms by stressors such as high current density, dynamic operation, and shutdown modes. The first step is to individuate the main degradation mechanisms; these are the anode catalyst dissolution, membrane chemical decomposition, and formation of semiconducting oxides on the metal components [51]. Each of these mechanisms is sensible to a determine stressor. The high current density (>1 A/cm<sup>2</sup>) is the most dominant stressor; the use of EIS test confirms that the membrane shows degradation processes when higher current densities are applied. A visible reduction of the ohmic resistance is measured, which is linked to the thinning of the membrane. The latter is caused by a loss of ionomer in the anode catalyst layer. Another

---

cause of performance loss at constant current density is the formation of Ti oxides on the anode Ti-PTL [51]. Other stressors are dynamic operation and shutdown process. Both lead to the corrosion of Pt/C catalyst and to agglomeration of the Pt nanoparticles [51]. Generally, the degradation rate obtained during dynamic operation is lower compared to the degradation rate under constant operation. They suggested that the ASTs (accelerated stress tests) for PEMWE should include:

- nominal current density operation
- high current density operation, affecting the ionomer content in the anode catalyst layer and membrane, and the Ti-PTL.
- Load cycling, causing degradation of the cathode catalyst layer
- Shutdown process, having an impact on the cathode components.

They concluded that it is also necessary not only to individuate and understand the degradation mechanisms but also to establish a standardized PEMWE testing hardware for the development of ASTs and evaluation of cell components [51].

Alia et al. [52] evaluated the anode catalyst losses at low loading and intermittent operation. They observed higher durability losses at low catalyst loading. On the other hand, dynamic operation determined an acceleration of the anode degradation. It is noticed a decreasing of the kinetic performance and an increase of the polarization resistance, both linked to the thinning and deterioration of the anode catalyst layer. Hence, it is suggested that the electrolyzers' performance are affected by low catalyst loading and intermittent inputs like renewable source. As a consequence, there is the need of developing components and system controls able to limit these performance losses.

Rakousky et al. [53] investigated the durability of a PEM water electrolysis cell over 1000h at 80°C and 2 A/cm<sup>2</sup>. Before, during and after the measurement period EIS tests and polarization curves were recorded. They observed an average degradation rate of 194  $\mu V/h$  which accounts for both reversible and irreversible degradation. Using the results of EIS, it is seen an increase of the ohmic resistance from 131 to 157  $m\Omega cm^2$  corresponding to a voltage increase of 52 mV. From the evaluation of the polarization curves obtained during the long term test at 2 A/cm<sup>2</sup> it is found that of 159 mV increase, 17% (24 mV) is caused by the electrode degradation and the remaining 83% (129 mV) arises from the total resistance, which takes into account membrane resistance and contact resistances, including the electric resistance of the Ti-PTL. This rise of the total polarization has been assumed to derive from the oxidation of the Ti-PTL. This is experimentally validated using a second cell assembled using Pt-coated Ti-PTL, that determined a reduction of the degradation rate up to 12  $\mu V/h$  within a period of 380h.

Siracusano et al. [54] investigated a set of MEAs, already used for 3500-5700 h in a PEM electrolyser, through EIS measurements and physico-chemical techniques such as SEM, TEM and EDX (energy dispersive X-ray). The MEAs used had same basic components and active area (8 cm<sup>2</sup>) but they were prepared according to different hot-pressing procedures. All MEAs were

---

run at constant current of 1 A/cm<sup>2</sup> and 55°C and the degradation rate was 3.3  $\mu$ V/h. EIS measurements were gained at different current densities and at the end series resistance and polarization resistance are obtained. There was a progressive decrease of the polarization resistance with increasing applied current densities, according to the enhancement in reaction kinetics. However, with prolonged operation, at same current density it is observed an increase in the polarization resistance. On the other hand, the series resistance decreases, due to membrane thinning as assessed by SEM. TEM images of anode and cathode showed that there is an increase of particle size and agglomeration in both sides of the MEA. Moreover, EDX showed Ru dissolution and also the presence of Fe and Ti impurities in the anode, and a decrease of fluorine in the cathode. In conclusion, the main sources of degradation are listed: presence of impurities which affects ionic conductivity and membrane/ionomer degradation; Ru dissolution; Ti plate degradation, related to the release of fluoride species; decrease of ionomer content; membrane thinning and changes in the catalyst/membrane interface, which may affect hydrogen cross-over.

---

# Experimental

The main objective of this thesis is the characterization of a single PEM water electrolyser. The test station is located at HYSYLAB, a laboratory for testing electrochemical systems dealing with hydrogen at the Environment Park in Turin.



This section will discuss about the experimental part starting from (i) test bench description, (ii) cell components and (iii) EIS instrumentation and set up.

## 4.1 Test bench description

The test bench is designed and realized by the engineering company TECNODELTA S.r.l which provides services ranging from the design to the implementation of specialized systems and equipment for special fluids. The test bench is realized for the characterization of either a single electrolytic cell and a stack; moreover, it allows to perform experimental activities on electrolytic cells with temperature up to 150°C, and maximum operating pressure of 25bar.

The main components of the test bench are the external lines which deals with cooling water, nitrogen and compressed air, the water tank for demineralized water, the separation tanks, the cell itself and also volumetric pumps, valves and sensors.

There are principally three external lines: the nitrogen line to perform cleaning of the pipes and pressurizing the whole system; the compressed air line is necessary to the correct function of the pneumatic valves and finally the cooling water line to chill the system.

Demineralized water is essential for the electrolysis process. Water is demineralized through an ion exchange resin and then it is stored manually in a tank of 11L. This water tank feeds the system through two internal loops, one to the anode side and the other to the cathode side. At the entrance of both sides there are the entrance valves; the cathodic entrance valve can be closed for experimental reason since it only provides thermal stability and thus it is not necessary for the electrolysis reaction. The products of the reactions go away from the cell,



*Figure 30 Test Bench.*

passing through the downhole valves, to go inside the two separation tanks-one for each side of the cell- due to the biphasic nature of the anodic and cathodic output. The separation process occurs in two steps. In the first phase, the products are cooled down by means of condensers placed immediately at the exit of the respective channels. The condensers are tube-in-tube type, with warm products flowing into the internal region while the cooling water flows in the annular one. The second phase is the separation itself, occurring in the gas/liquid separators which are two 1L tanks with one outlet situated in the upper part for the gas-rich mixture and the other one in the lower part for the liquid-rich mixture. The level control in the separators controls the filling and draining valves in order to maintain the level in the desired operating range. Different levels in the two separators may cause pressure unbalances in the two side of the cell affecting the correct functioning.

The water is introduced into the circuit through a volumetric pump able to work with a maximum flowrate of 10L/min. In the system is present another volumetric pump with higher



maximum flow rate both for redundancy and stack operations. The pumped water is heated by an external electric heater to reach the desired operating temperature. The heat is transferred to the fluid with a plate exchanger and the temperature is kept almost constant thanks to a PID controller. In order to regulate and maintain the pressure and temperature values in the system there are: 2 back pressure controllers, one on each side, anodic and cathodic; mass flow meter for demineralized water; conductivity probe; pressure transducers; valves and temperature thermocouples, type K.

A general control system for the test bench was developed in LabVIEW (National instruments, LabVIEW 2009). It is interfaced with the power supply, instruments and hood; it allows to control voltage, current and the other system variables and further it collects and stores data. The LabVIEW system comprised of a front panel and a block diagram as shown in *Figure 31*.

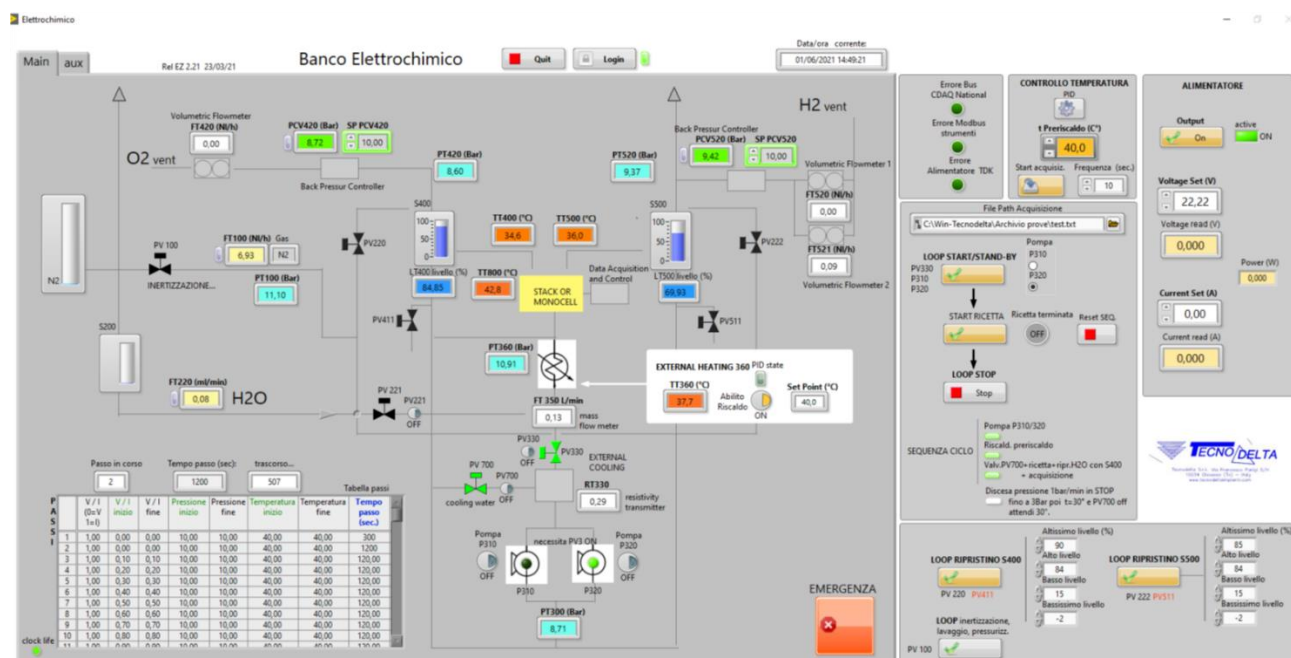
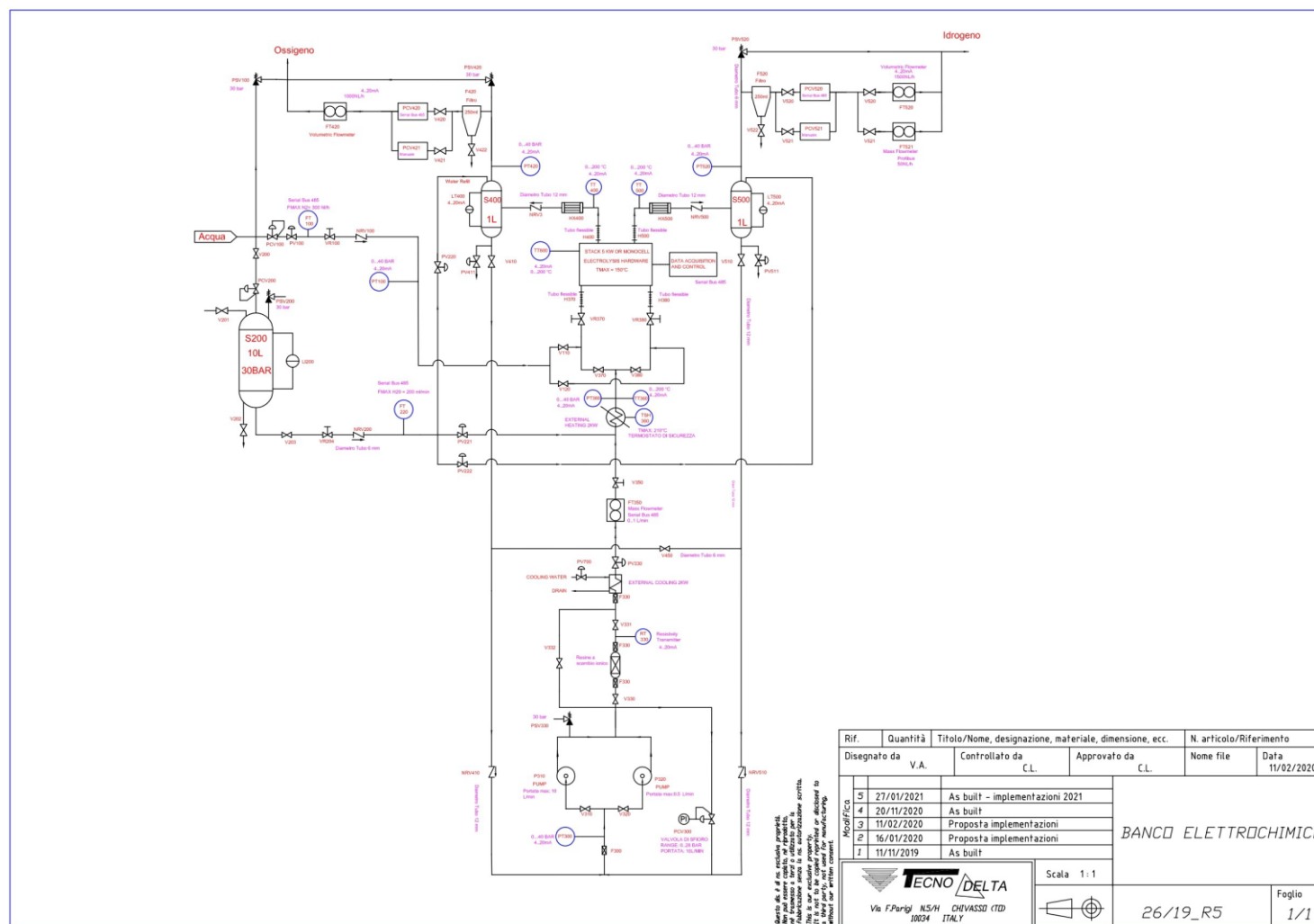


Figure 31 Software interface.

Figure 32 P&I electrochemical test bench.



---

## 4.2 Cell components

The PEM electrolytic cell under study in the *Figure 33* is a single cell with squared geometry and active area of  $25\text{ cm}^2$ . The MEA (QuinTech supplier) is made of a thin ion-conducting polymeric membrane with two porous catalytic layers attached on each side. The membrane is made of Nafion<sup>TM</sup> N117; its surface is coated with two catalytic layers, a thin layer of carbon-supported platinum with  $1\text{ mgPt/cm}^2$  at the cathode for the HER and a thicker layer of unsupported iridium with  $2\text{ mgIr/cm}^2$  at the anode for OER. The MEA is limited by the porous current collectors also called gas diffusion layer (GDL), one for each side. In the anodic compartment the GDL is a Titanium mesh of  $180\text{ }\mu\text{m}$  thickness while for the cathodic compartment there is a Freudenberg H23 C6 carbon paper GDL (treated with MPL) of  $250\text{ }\mu\text{m}$ , in which one side with E15 GDL (without hydrophobic treatment) of  $124\text{ }\mu\text{m}$  and the other with E15 GDL (with hydrophobic treatment) of  $129\text{ }\mu\text{m}$ . Each side of the PEM is limited by a bipolar plate with a pyro-sealed triple serpentine flow pattern; the anodic one is made up by Titanium block of  $8.47\text{ mm}$  thickness while the cathodic bipolar plate is a Graphite block of  $12.45\text{ mm}$ . The bipolar plates are isolated from the GDL through a silicon gasket with PET core of  $200\text{ }\mu\text{m}$ . The current collectors are made of gold-plated copper and are equipped with high current connectors. Their thickness is of  $0.6\text{ mm}$ . Moreover, they are electrical isolated from end plates through a layer of Teflon coated with fiber-glass tape. Finally, the cell is tightened between two end plates made of aluminium alloy of  $18.65\text{ mm}$  thickness using a dynamometric torque wrench applied to a system of 8 bolts for each side up to  $10\text{ Nm}$ .

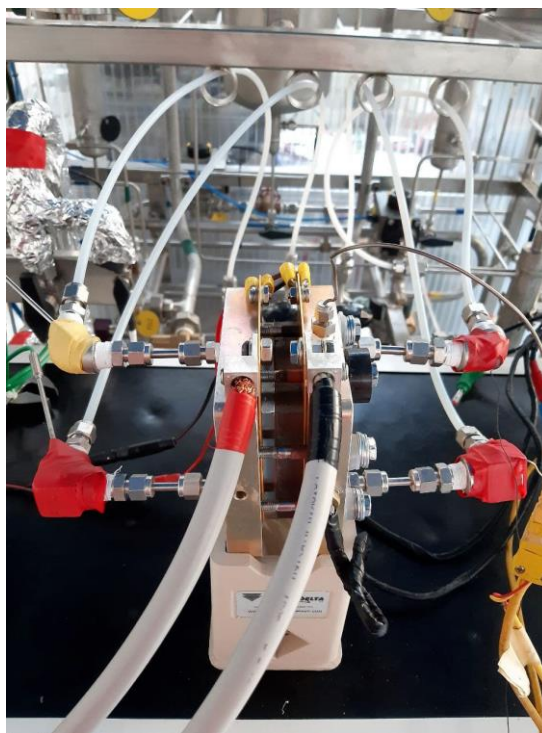


*Figure 33 PEM water electrolyser placed inside the housing on the test bench.*

---

## 4.3 EIS measurements

### 4.3.1 EIS test equipment and set-up

In order to perform EIS measurements, it is necessary to have:

- Potentiostat/Galvanostat or a load bank
- Frequency response analyser, FRA
- DC power supply

In the *Figure 34* a schematic EIS measurement configuration shows the connection between potentiostat, FRA and WE cell.

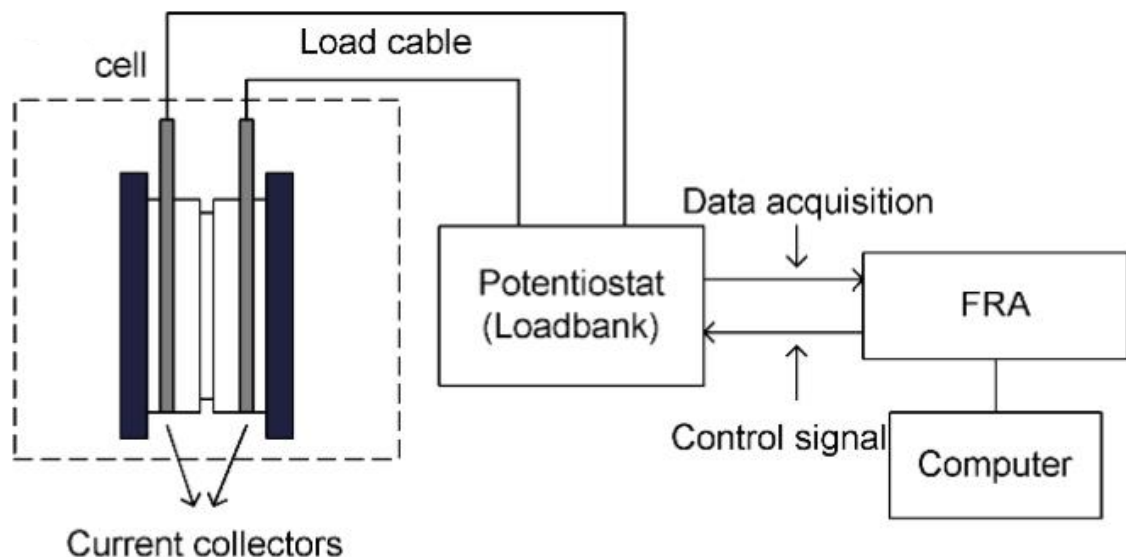


*Figure 34 Schematic EIS measurement configuration [27].*

AC impedance measurements are usually performed by a four-electrode measurement configuration with a working electrode, a counter electrode and two reference /sense electrodes [23]. The WE is the anode (positive electrode), to gain measurements of the current passing through the cell; the CE is the cathode (negative electrode), to provide a voltage or current to drive the cell and the two RE (RE1 and RE2), anode and cathode, to measure the voltage difference between two reference electrode points within the cell. Therefore, a two-wire configuration is performed.

---

To gain meaningful data from the EIS experiment, reducing as much as possible stochastic and bias errors, it is necessary to pay attention to some important specifications reported in [23]. In particular:

- the test set-up should be connected in such a way as to avoid measuring parasitic current flowing into the load
- the immediate vicinity of the test set-up should be free of electromagnetic sources to avoid interference with the EIS measurement
- low-inductance cables should be used thus they should be shielded, twisted around each other and as short as possible
- cross sections of the CE and WE should be instead as large as possible.

In the EIS experiment, the electrochemical system considered is perturbed with an input signal and the response is measured as an output signal. There are two options for controlling the perturbation to measured system: one is to control the current perturbation then record the voltage response from the system (galvanostatic mode), the other is to control the voltage perturbation then record the current response (potentiostatic mode) [27]. The working principle for a current control measurement, described below, is equivalent to that of voltage control with the only exception of constant DC value (in this case is a voltage), and input and output signals which are inverted, thus voltage and current respectively. When the leads are all connected, the electrical load is set to a DC constant current. The FRA will generate an AC current perturbation and interrupt the cell through a Potentiostat. The response to the interruption from the cell will enter into the FRA for analysis to obtain the AC impedance spectra [27]. The ratio of the frequency spectra of the response (output) and that of the perturbation (input) gives the impedance in *galvanostatic mode* and the admittance in *potentiostatic mode*. Hence, the complex impedance or admittance can be obtained at the measured frequency by dividing the response by the perturbation. This procedure is repeated again and again, with the frequency of the stimulus swept across the frequency range within the capabilities of the FRA [27]. In this way, it is possible to gain the full impedance spectrum of the electrochemical system under study.

It is necessary to pay attention to the perturbation amplitude. This needs to obey linearity as discussed before, thus it is required a small amplitude of the perturbing signal. However, too low value will result in an unacceptable signal-to-noise ratio making it difficult for the FRA to distinguish between the actual response and the noise arising from random excitations [23]. The figure below from [23] lists all the parameters to set up with their recommended value/range.

|                       | Test input   | Symbol    | Unit | Recommended value / range   |
|-----------------------|--|-----------|------|---|
|                       | Number of perturbation frequency data per decade of frequency range  | $PPD$     | -    | minimum 3   |
|                       | Number of perturbation cycles during $\tau_{ACT}$ ( $\tau_{ACT}$ precedes $\tau_{ACS}$ )                               | $n_{ACT}$ | -    | minimum 2 ( $^{\dagger}$ )  |
|                       | Number of perturbation cycles during $\tau_{ACS}$ used to record the EIS spectra ( $\tau_{ACS}$ follows $\tau_{ACT}$ ) | $n_{ACS}$ | -    | minimum 3   |
|                       | Range of perturbation frequencies  | $f$       | Hz   | $10^{-2}$ – $10^{-6}$   |
| Potentiostatic method | load (voltage) perturbation peak-to-peak amplitude   | $U_{AC}$  | V    | typically 5–10 mV <sub>rms</sub> to be less than the thermal voltage, $U_T$ (e.g. <30 mV at 80°C cell temperature) ( $^{\dagger}$ ) |
| Galvanostatic method  | load (current) perturbation peak-to-peak amplitude   | $I_{AC}$  | A    | 0.5% – 5% of $I_{DC}$ ( $^{\ddagger}$ )   |

Figure 35 Input parameters and settings for the EIS instrument [23].

The AC impedance spectrum is graphically represented by the Nyquist plot. Another type of plot is the so called Bode plot. These graphs show the tests output parameters gained from the EIS measurement.

| Output        | Parameter type | Measurement uncertainty | Sampling rate                           |                               |
|---------------|----------------|-------------------------|---|-------------------------------|
| $U_{AC,k}(f)$ | primary        | $\pm 1\%$               | $\geq 20 (\tau_{ACS}(f)/\tau_{ACT}(f))$ | Galvanostatic method          |
| $I_{AC,k}(f)$ | primary        | $\pm 1\%$               | $\geq 20 (\tau_{ACS}(f)/\tau_{ACT}(f))$ | Potentiostatic method         |
| $Z_{IM,k}(f)$ | secondary      | – ( $^{\dagger}$ )      | –                                       | Nyquist plot ( $^{\dagger}$ ) |
| $Z_{RE,k}(f)$ | secondary      | – ( $^{\dagger}$ )      | –                                       | Nyquist plot ( $^{\dagger}$ ) |
| $ Z_k (f)$    | secondary      | – ( $^{\dagger}$ )      | –                                       | Bode plot ( $^{\dagger}$ )    |
| $\theta_k(f)$ | secondary      | – ( $^{\dagger}$ )      | –                                       | Bode plot ( $^{\dagger}$ )    |

Figure 36 Output parameters for the EIS measurement [23].

---

### 4.3.2 Measurement modes

AC impedance spectroscopy foresees two methods to execute the impedance measurements; these are the *potentiostatic mode* and the *galvanostatic mode*. Each mode involves advantages and drawbacks and depending on the application one can result more adequate than the other. In general, the differences in the obtained results are almost invisible to be considered negligible [55].

With the potentiostatic mode in the operating WE cell an AC voltage perturbation signal is imposed and the response of the system is a current [55]. This method allows to use the whole spectrum provided by the FRA/potentiostat but it should be pay attention to the amplitude of the stimulus for two fundamental reasons. The amplitude must not exceed the maximum current tolerable by the potentiostat otherwise this can drift to an overloading of the cell. Moreover, the amplitude chosen must ensure the linearity of the current response [55]. This explains the recommended amplitude value of the stimulus between 5 – 15 mV [23]. However, electrolytic cells have lower impedance value ( $\approx 1\Omega$ ) thus even small impedance voltage perturbations may lead to large currents; this may affect negatively the signal-to-noise ratio. When measuring the impedance spectrum in potentiostatic mode the frequency is usually swept in a range between 100kHz and 1mHz, and the points per decades are generally 10. Potentiostatic measurements are carried out at different DC voltage levels to have a better representation of the phenomena occurring during the operation of the electrolytic cell. Rozain and Millet [37] performed EIS measurements in the potentiostatic mode at different DC voltages (1.4 – 1.8V) in the 100 kHz – 1mHz frequency range to characterize a 23cm<sup>2</sup> PEM water electrolysis cell made of Nafion as solid polymer electrolyte, iridium oxide as anodic catalyst and carbon-supported platinum as cathodic catalyst. Dedigama et al. [39] performed EIS characterization of a PEMWE of 28 cm<sup>2</sup> in a constant potentiostatic mode in a frequency range between 100kHz – 0.1Hz by frequency sweeping in the single sine mode with amplitude of 10mV and 5 frequencies per decade. Siracusano et al. [49] studied a 5 cm<sup>2</sup> PEM electrolytic cell at 1.5V and 1.8V in the frequency from 100kHz – 100mHz with an AC amplitude pk-pk of 10mV.

With the galvanostatic mode the perturbation signal applied is an AC current which spans the cell and hence the response of the system is a voltage [55]. In general, this method is characterized by a frequency range between 200 kHz and 2mHz; moreover, it has the advantage of larger perturbation current amplitude without determining a relevant change in the cell voltage; therefore, it allows a better control of the current across the cell. In fact, the amplitude value of the current perturbation determines a voltage response of mV, which is tolerated by most instrumentations. Moreover, higher current perturbation improve the signal-to-noise ratio so the EIS measurements are more accurate. Nonetheless, the amplitude of the stimulus is still critical because the response needs to be within the linear regime. In general, it is recommended a value around 0.5 – 5% of the DC value [23]. However, at high current densities, the cell voltage is unstable and this instability could impair the accuracy of

the AC impedance measurement, especially for low-frequency measurements. Elsoe et al. [40] chose a frequency range of  $100\text{kHz} - 0.01\text{Hz}$ ,  $24.5\text{ mA/cm}^2$  AC amplitude, and 12 points per decade for the galvanostatic mode measurement of a PEMEC with active electrode area of  $2.89\text{ cm}^2$  at  $0.07, 0.35, 0.69, 1\text{ A/cm}^2$ . van der Merwe et al. [26, 38] made impedance measurements on a  $25\text{ cm}^2$  PEM electrolyser in galvanostatic mode with a frequency range of  $200\text{ mHz}$  to  $200\text{ kHz}$ .

### 4.3.3 Test procedure

The EIS measurements are carried out with the Energy-Lab XM System Energy-Lab XM System provided by AMETEKSI with Solartron Analytical brand coupled with the software XM-studio ECS. The device consists of a PGSTAT potentiostat/galvanostat, an internal 2A booster and the frequency response analyser, FRA. The system is controlled through the software XM-studio ECS. The Potentiostat/galvanostat enables to perform experiment on the cell. When used on its own it is able to run many types of DC tests, while combined with the FRA it can also measure impedance. It records data with maximum rate of 1M samples/second and it is able to work in a voltage range of  $\pm 8\text{V}$  up to  $\pm 300\text{mA}$  and 1MHz bandwidth. The internal power booster is used to enhance the capability for testing higher power electrochemical systems and it is characterized by a maximum output of  $\pm 8\text{V}/\pm 2\text{A}$ . The FRA allows impedance measurements, it can generate and analyse AC waveform with good accuracy over its range of operation over its full frequency range  $10\mu\text{Hz} - 1\text{MHz}$ .



Figure 37 Energy-Lab XM System.



The test procedure foresees in order:

- the wire connection between the cell and the ModuLab XM,
- the creation of the project in the XM-studio software including the setting of the test input parameters, and finally
- the experiment running.

A proper electrode connection is required. A schematic configuration is reported in *Fig.38*. The potentiostat is connected to the internal booster and the booster is connected to the cell. The CE on the booster is connected to the positive terminal and the WE is connected to the negative terminal. The working and counter wires of the ModuLab XM are connected to the anode (positive electrode) and the cathode (negative electrode) respectively, while the reference wire is connected to both cathode and anode electrodes.

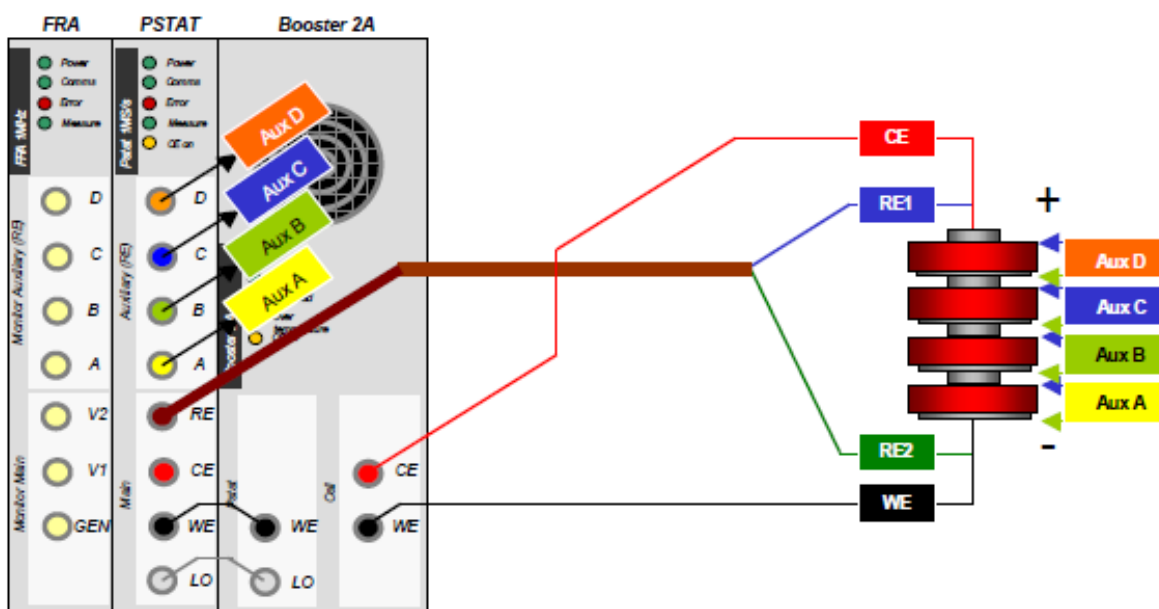


Figure 38 Schematic configuration of the connection between the cell and the device.

Prior to the running of the experiment, is the creation of the project in the XM-studio ECS software. This enables to run different experiments named *steps*: *DC voltage control*, *DC current control*, *impedance voltage control* and *impedance current control*. The focus of this work is the characterization of the electrolytic cell with the impedance spectroscopy technique thus the steps chosen are the last two: *Impedance Voltage Control* and *Impedance Current Control*.

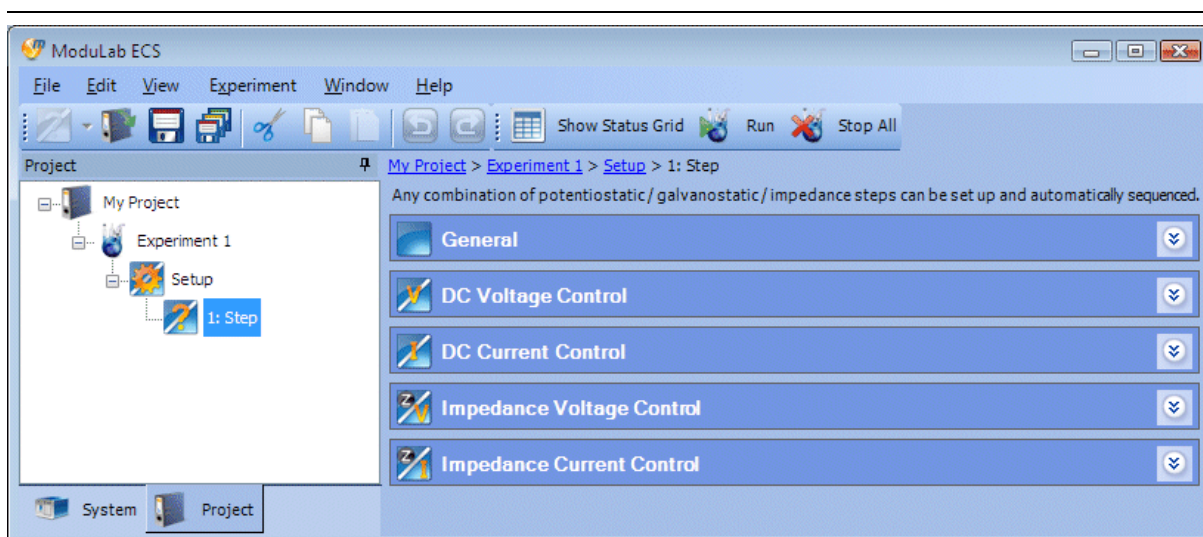


Figure 39 Types of experiments in the XM-studio ECS software.

For each step category there is a list of *step types* among which making the choice. For the impedance voltage control *Potentiostatic impedance* is selected while for the impedance current control the *Galvanostatic impedance*. These represent the two EIS measurement modes performed in this work.

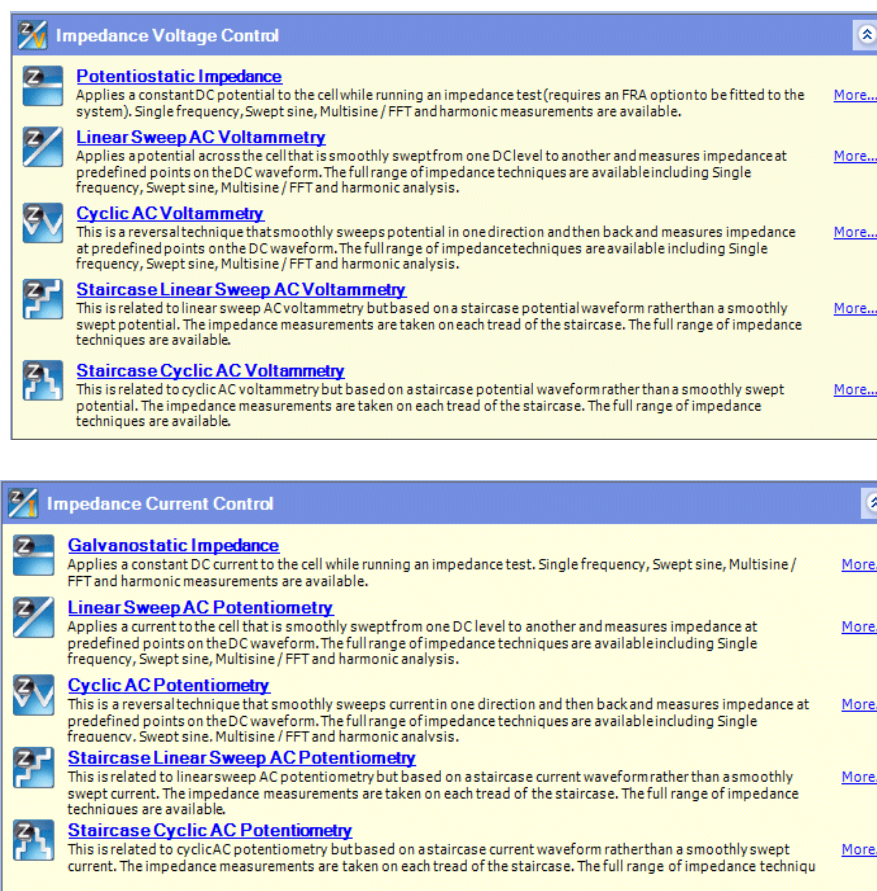


Figure 40 Possible step types for Impedance Voltage Control and Impedance Current Control.

For each EIS measurement mode the first step is the definition of the experiment *Setup* item consisting of different fields, in particular *Hardware Requirement* and *Cell Setup*.

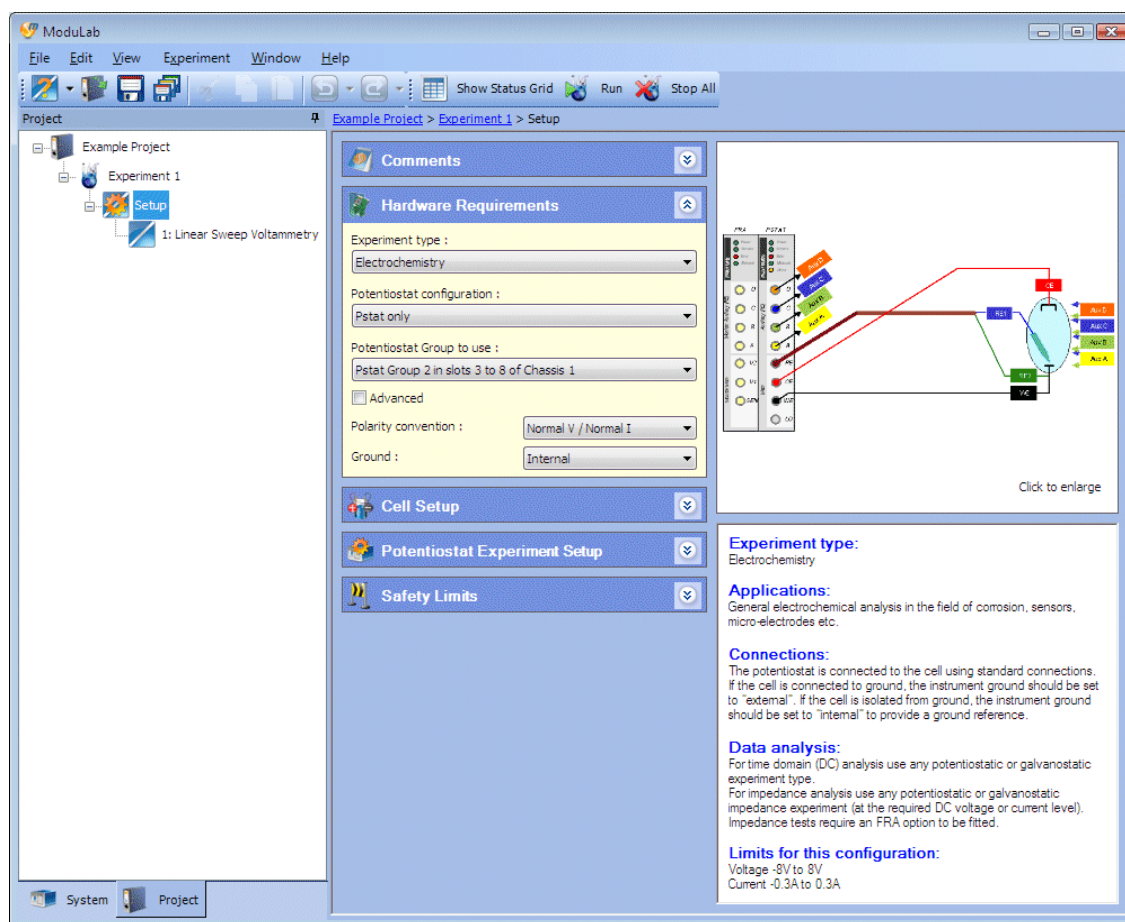


Figure 41

The *Hardware Requirement* specifies the hardware and connection configuration for the experiment while the *Cell Setup* some specification about electrochemical cell such as the electrode active area, the type of reference electrode, density and equivalent weight.

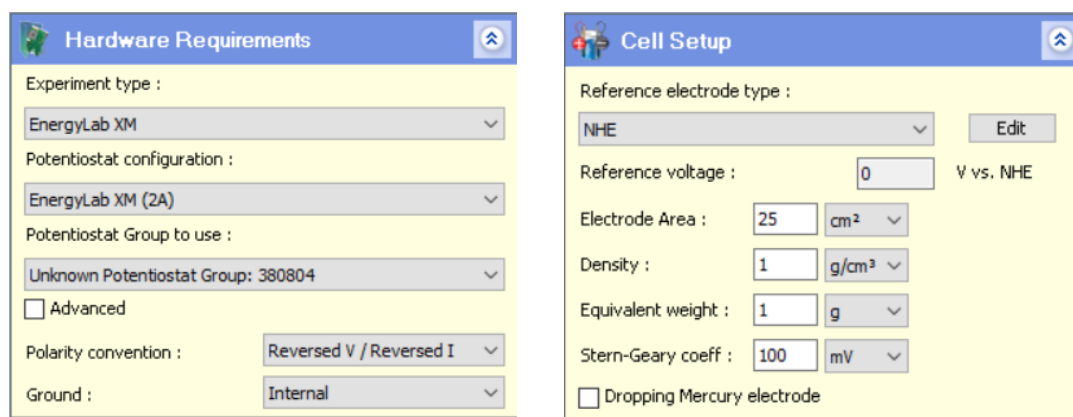


Figure 42 Hardware requirements and cell setup.

Thereafter, there is the definition of the test inputs for both the impedance experiments. These are defined into two fundamental sub-screens:

- *Scan Setup*: this sub-screen specifies values associated with the excitation signal that is applied to the cell.
- *Impedance Setup*: it specifies the frequency range to be tested since the system superimposes a frequency, or a range of frequencies, on top of the DC scan that has been specified from the Scan Setup.

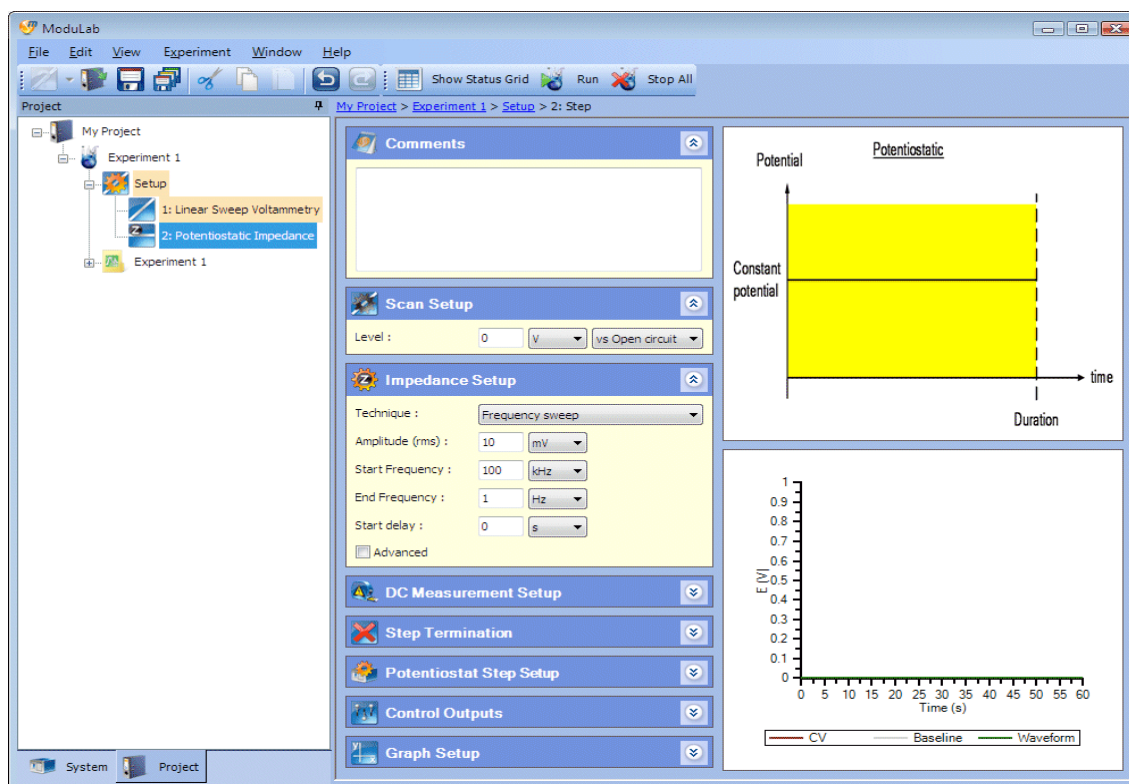
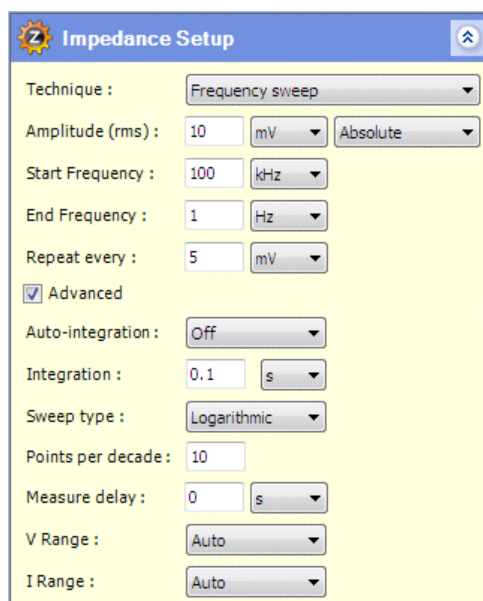


Figure 43

The *Impedance Setup* contains several fields to specify as shown in the Fig.44. In the *Technique* the frequency sweep- consisting of a single sinewave swept from the start frequency to the end frequency- is chosen as the type of the AC stimulus. Other possibilities are the single frequency where a single sinewave is applied to the cell at a fixed frequency or the multi-sine where multiple sinewaves, according to a Fast Fourier Transform, are swept from the start frequency to the end frequency.





**Impedance Setup**

Technique : Frequency sweep

Amplitude (rms) : 10 mV Absolute

Start Frequency : 100 kHz

End Frequency : 1 Hz

Repeat every : 5 mV

☒ Advanced

Auto-integration : Off

Integration : 0.1 s

Sweep type : Logarithmic

Points per decade : 10

Measure delay : 0 s

V Range : Auto

I Range : Auto

Figure 44 Impedance setup.

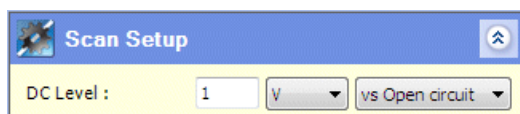
The *amplitude* defines the RMS amplitude of the AC signal, maintained at a fixed level during the step. This value is specified in absolute terms without reference to any other values, therefore in both potentiostatic and galvanostatic tests the absolute field is selected. As discussed in the previous section, the amplitude of the stimulus must be carefully chosen to ensure the linearity of the system response but also to provide a reasonable signal-to-noise ratio. Since the Frequency sweep is selected in the frequency field there are two fields representing the *Start Frequency* and *End Frequency* of the sweep. Generally, the frequency range used is between  $10^{-3} - 10^6$ .

The signal applied to the FRA can be integrated to reject noise. The effect is to narrow the measurement bandwidth and thus increase the signal-to-noise ratio. Integration increases the measurement time, so there is a trade-off between the accuracy you require and the measurement speed. *Auto-integration* can be used when there is uncertainty about the degree of interference generated by the cell, so that the integration time is adjusted automatically to obtain a specified statistical accuracy in the measurement result. When auto-integration is off, this field can be used to specify a fixed integration time. The units can be seconds or cycles, and a value in seconds is rounded up to cover the nearest number of whole cycles.

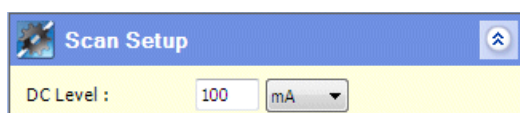
The *Sweep type* defines the method of variation of frequency during the sweep. Among linear and logarithmic the latter one is chosen. Also, the number of measurement points per decade during a logarithmic sweep should be at least 10.

The other field is the *Scan Setup* where the DC value of the stimulus is defined. Voltage, or potential as it is otherwise called, is always defined as a difference between two values. For the potentiostatic the potential has to be specified against no obvious reference value; there

are many options but the most suitable is the *vs. Reference* where the value is specified relative to the reference voltage in the Cell Setup.



The galvanostatic impedance do not require a referencing method, thus the Scan Setup appears as follows



Finally, once that the wires are connected and the project has been created and set, the experiment is run.

## 4.4 Measurement Data Quality

The error structure of the measurement data plays a fundamental role in the modelling and fitting steps. Particular attention should be paid to stochastic errors and systematic bias errors. While bias errors can be defined to be those that result inconsistent with the Kramers-Kroning relations, the stochastic errors can be consider under control by selecting suitable experimental parameters. In this regard, the magnitude of the perturbation should be small enough to avoid non-linear response, minimizing stochastic errors [56].

The *Lin-KK tool* is used to check the Kramers-Kroning compliancy of the impedance spectra. The test result is given as residuals representing the relative deviation between experimental data and an ideal fitting with KK over frequency. Low residuals over the whole frequency range indicate a good quality impedance spectrum, i.e. data are not affected by noise and time-variance. All impedance spectra have been evaluated with *Lin-KK tool* using *complex-fit* and *RC-auto* mode.

Some examples of impedance spectra with good and low quality are reported in the figures below. The first two show valid impedance spectra whereas the last one is considered invalid due to the exhibition of biased residuals, which indicates time-variance.

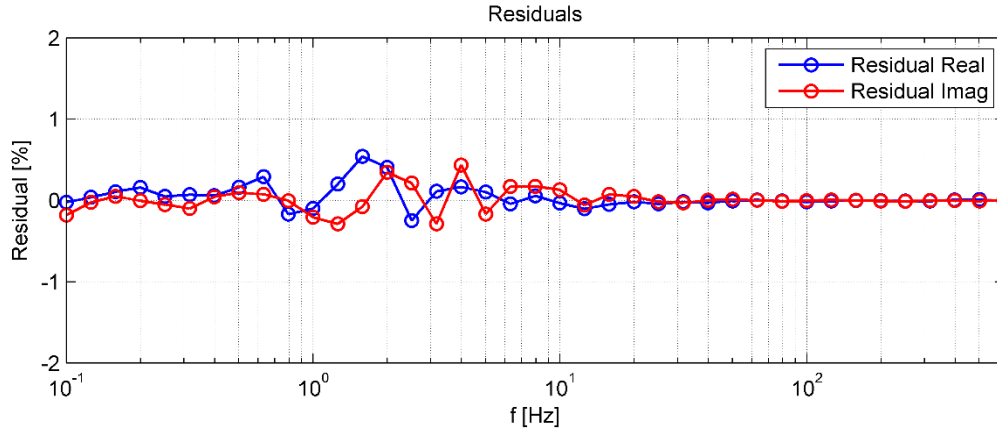


Figure 45 Impedance spectrum with low noise and describing a time-invariant system.

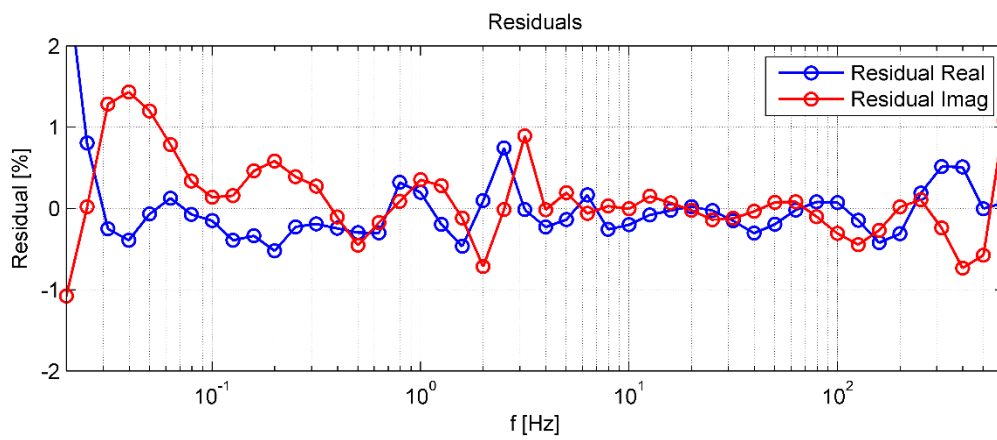


Figure 46 Impedance spectrum giving noisy residuals but still acceptable quality.

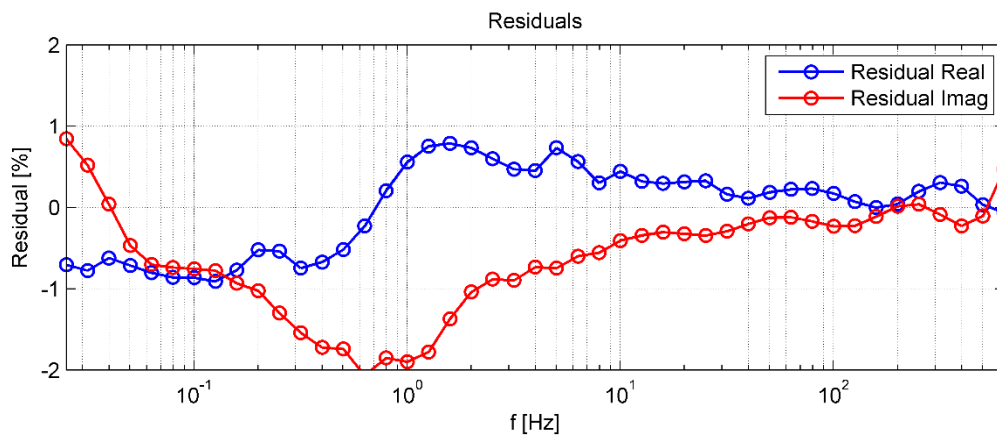


Figure 47 Impedance spectrum with time-variant behaviour.

An important stage to improve the identification of the model and its parametrization is the *data pre-processing*, allowing to evaluate the quality of the recorded data. Data pre-processing foresees different steps, in particular data monitoring and filtration [28].

---

Impedance data are monitored by checking their graphical representation, thus Nyquist and Bode plots. These diagrams can give additional information especially at high frequency where artefact impedance data appear due to wires connected to the cell and cell windings. Electrical leads have self-inductance that produces a typical shape with positive imaginary values (inductive behaviour).

In the filtration stage data points deteriorated by errors are detected and eliminated. Erroneous data are typically outliers, wild points, recorded data coinciding with the electrical grid frequency and harmonics. About the latter, it is known that measurements at frequencies near the power supply frequency, as well as to its harmonics- 50, 100, 150, 250 Hz, produce erroneous data which should be rejected when possible. Instead, wild points are points that do not obey the general behaviour of a given ensemble of points [28].

EIS spectra are not corrected for parasite inductive effects determined by wires.

## 4.5 Cell measurement

The electrochemical characterization includes polarization curves and electrochemical impedance spectroscopy under potentiostatic and galvanostatic modes.

Polarization curves are performed by recording the cell voltage vs. the imposed current density with maximum current density reached of  $2\text{ A/cm}^2$ .

Electrochemical impedance spectroscopy analysis is carried out using an electrochemical setup consisting of PGSTAT potentiostat/galvanostat (Solartron analytical), an internal 2A booster and the frequency response analyser, FRA, properly connected with the PEM electrolyser as described in the previous section. The impedance measurement are performed under potentiostatic and galvanostatic modes. In the potentiostatic mode the AC voltage perturbation signal is superimposed on the DC voltage level. The latter is selected in the range between 0 – 1.5V while the AC voltage is a single sinewave with amplitude of 10 mV (RMS) swept in the frequency range of 20kHz – 2mHz. In the galvanostatic mode the AC current signal is superimposed on the DC current level, which is selected in the range between 0 – 2000mA. The AC current is again a single sinewave with amplitude of 1000mA (RSM) swept in the frequency range of 10kHz – 1mHz. Due to the instrumentation limits, the impedance measurements are executed at low current densities corresponding to the system operation under activation control. As a consequence, the impedance analysis allows to observe phenomena principally linked to the electrocatalyst behaviour.

Either polarization curves or EIS tests have been performed at different temperature, pressure, cathode configuration and mass flow rate.



---

Temperature is varied between  $40^{\circ}\text{C}$  and  $80^{\circ}\text{C}$  whereas the relative pressure range is  $0.5\text{ bar} - 7.5\text{ bar}$ . The cathode configuration is changed by acting on the entrance valve situated at the entrance of the cathode side. In the test bench both anode and cathode have entrance valves which allows water feeding as depicted in Fig. xx. The water stream to the cathodic side provides only thermal stability. Hence, the aim of changing the configuration of the cathode is to study if there are evident differences on the performance of the cell under different cathode configuration. The mass flow rate is set by varying the chamber percentage of the recirculating pump or by changing manually the needle valve. Whether the recirculating pump or the needle valve is used, the mass flow rate introduced in the system is divided between the entrance of anode and cathode; thus, both compartments have same mass flow rate. Hence, tests that use the pump have just indicated the pump percentage whereas in case of needle valve the mass flow rate will be exactly given in  $\text{mL}/\text{m}^3$ .

Tests have been performed varying one or more operating parameter, while keeping all the other operating parameters constant. This enables the identification of the several processes occurring within the PEM water electrolyser, which clearly have dependencies on operating parameters. All tests' typologies are listed below.

- a) Test performed at constant temperature with different pressure. Cathode open and fixed mass flow rate imposed with the recirculating pump.
- b) Tests performed at constant pressure with different temperature. cathode open and fixed mass flow rate imposed with the recirculating pump.
- c) Test performed at constant temperature and pressure with different cathode configuration. The mass flow rates is varied between open and closed cathode with the recirculating pump.
- d) Test performed at constant temperature and pressure with different cathode configuration. The mass flow rates is varied between open and closed cathode with the needle valve.
- e) Test performed at constant temperature and pressure with different cathode configuration. The mass flow rates kept constant and imposed by the needle valve.

---

# Modelling

In this chapter the relevant features of the impedance spectra obtained from the electrolytic cell are presented. Typical circuit elements used to model the impedance spectrum are reported. Further on, the procedure for the development of the equivalent circuit model (ECM) is delineated. Finally, some critical aspects of ECM are discussed.

## 5.1 AC impedance spectra features

Impedance measurements on electrolytic cells can give impedance spectra with variable shape. In fact, impedance spectra are affected by the several operating parameters such as current density, voltage, temperature, pressure or relative humidity, or they can change according to catalysts loadings, membrane thickness, additional components to improve the performance and so on. In addition, some features of the impedance spectrum can show stronger correlation to a specific component within the cell or operating parameters may have a different impact depending on the level of ageing of the cell.

Generally, the impedance spectrum of an electrolytic cell consists of one or more semicircles, which usually can also be depressed or incomplete. Furthermore, sometimes it can happen that semicircles merge forming a sort of arc. These arcs or semicircles account for the different processes occurring inside the cell and each of them is characterized by a time constant.

In the impedance spectrum usually three features are observed [55]:

- high frequency ( $f > 1\text{kHz}$ ), in which double layer charging effects and proton transport dominate on the faradaic processes of the electrode response.
- mid frequency ( $1\text{Hz} < f < 1\text{kHz}$ ), related to the electrochemical processes occurring at the electrode/electrolyte interface (so called faradaic processes), so OER at the anode and HER at the cathode.
- low frequency ( $f < 1\text{Hz}$ ), which reflects mass transfer limitations due to reactants ( $H_2O$ ) and products ( $H_2, O_2$ ) removal or starving in the cell.

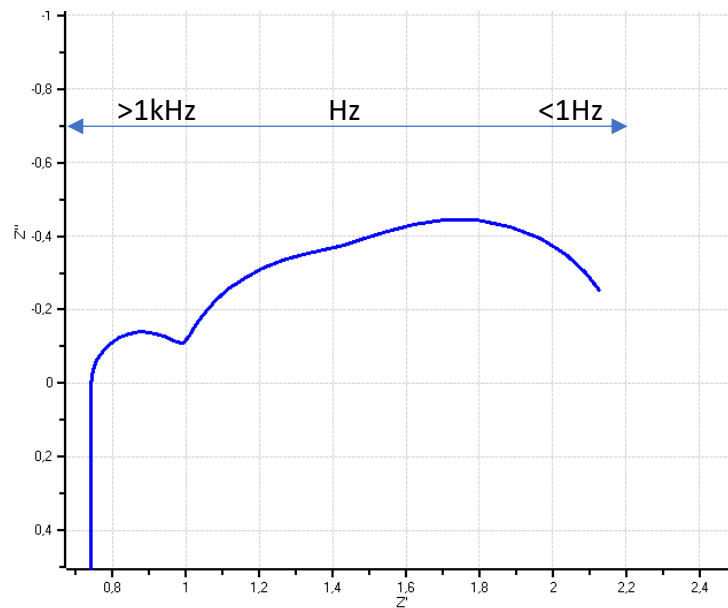


Figure 48

### High frequency feature

The high frequency region is potential independent and it may be attributed to:

- Distributed resistance effects in the electrolyte within the catalyst layer
- MEA structure characteristics

This high-frequency feature- in case of current constrictions- is characterized by combined resistive and capacitive effects and it can be detected as:

- Complete semicircle
- Incomplete semicircle
- Straight line at 45° angle, mostly associated to protonic conductivity limitations in the catalyst layer

Generally, current constriction derives from bad contact between the membrane and the catalyst layer. Bad contact has many causes, principally correlated to the MEA characteristics (catalyst loading, ionomer content, fabrication method, porosity) but all converge to the same consequence, less efficient three phase boundary (TPB). With bad contact a two-phase boundary instead of the three-phase boundary occurs at the anode surface hindering the proton conduction in the electrolyte surface [57].

The high frequency intercept of the HF feature with the real axis allows to determine an important parameter, the ohmic resistance  $R_{\Omega}$ , accounting for contact resistances between components and proton/electron transport through electrolyte and conductive components of the cell respectively. A change in the ohmic resistance value is associated to temperature and membrane hydration, as well as variation of the membrane thickness due to degradation issues. It should be noted that in this region it is possible to detect inductive effects due to connecting wires and cell windings that affect the impedance spectrum.

These features- inductive effects, ohmic losses and current constrictions- are modelled through a series connection of different circuit elements. An inductance models inductive effects whether a series resistance is used to simulate ohmic losses. Instead, current constriction appearing as a semicircle at HF- when present- is modelled with a resistance in parallel with a constant phase element (CPE). So, the high frequency feature is simulated by a series connection of inductance, ohmic resistance and parallel between a resistance and a CPE.

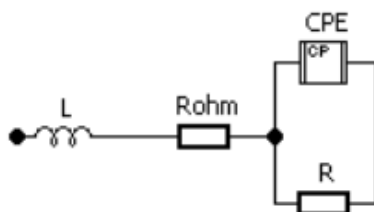


Figure 49

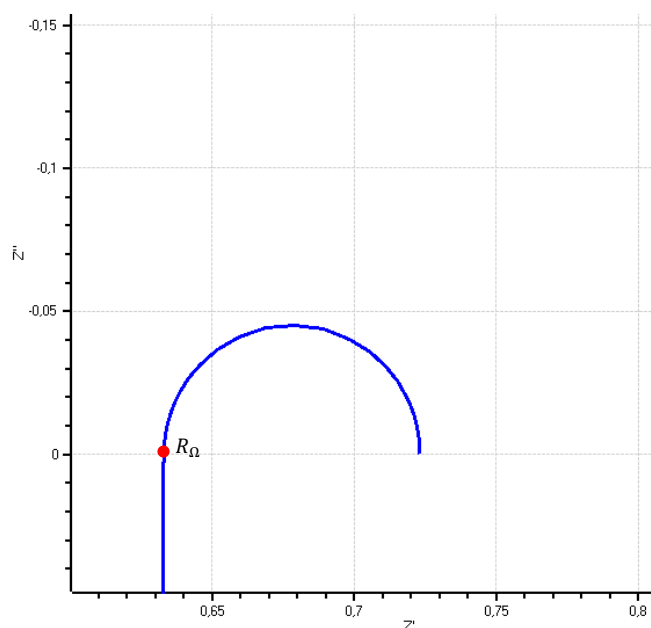


Figure 50

### Mid frequency feature

The mid frequency region shows a dependency on potential; in general, it decreases with increasing overpotential due to the rapid increase of the kinetics. It is usually associated to the kinetics of the anode (OER) but in some papers it is also attributed to the HER at the cathode. This mid frequency region appears in the Nyquist plot as one arc or even two more

or less merged semicircles. Each of these charge transfer processes is modelled by a parallel of a resistance (called charge transfer resistance) and a CPE.



Figure 51

In general, when only one arc is visible in the mid frequency region in the Nyquist plot (corresponding to a single peak in the same frequency range in the Bode plot), this is modelled with a single  $R_{ct}||CPE$ ; instead, two merged semicircles with two visible peaks in the Bode plot are simulated with two  $R_{ct}||CPE$  in series.

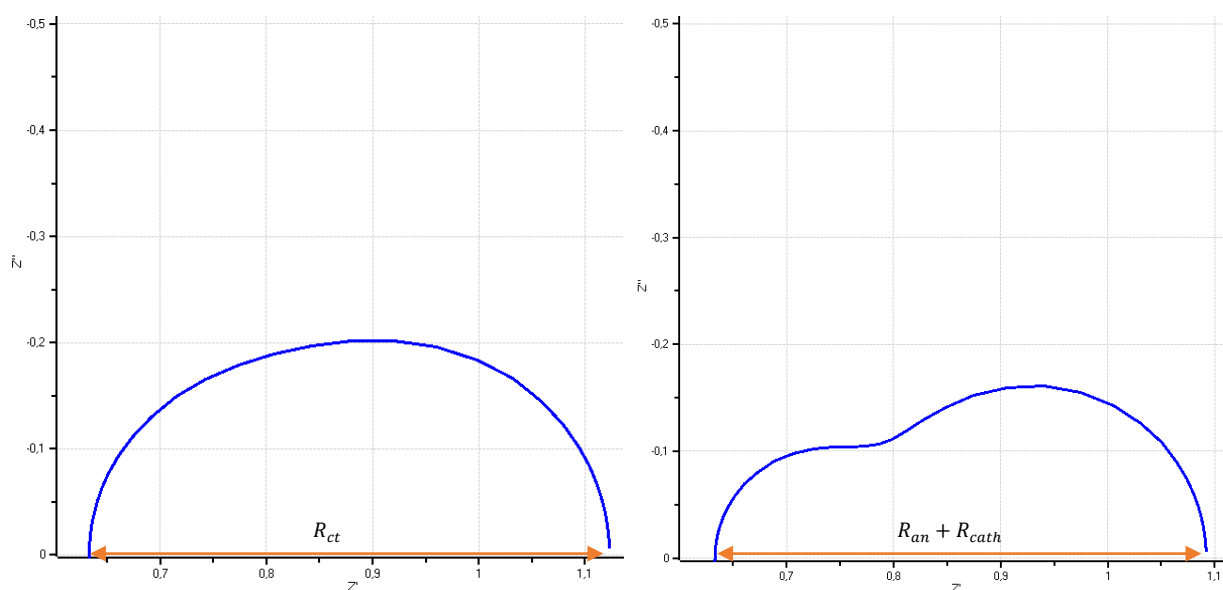


Figure 52

The charge transfer resistance  $R_{ct}$ , corresponding to the diameter of the arc, is associated with the charge transfer mechanism for the electrode reactions (mostly the OER) and it is function of temperature and potential. The constant phase element is mainly used rather than capacitor because by adjusting its parameters it allows to fit data quite well- function very useful in case of overlapping arcs- and moreover, it represents the imperfect nature of electrodes (surface roughness, irregular properties distribution, non-uniform current distribution, etc.). In any case, by using its parameters with maximum frequency or charge transfer resistance, it is possible to determine the capacitance  $C_{dl}$  as expressed in Eq.5.1.

---


$$C_{dl} = Q \cdot (\omega_{max})^{n-1} = \frac{(R_{ct}Q)^{\frac{1}{n}}}{R_{ct}} \quad (Eq. 5.1)$$

The capacitance value gives some insight of the electrode properties, such as catalyst surface area, active sites, catalyst loading and utilization [55]. Higher value of the capacitance means good properties and behaviour of the electrode and it is graphically represented by small semicircles/arcs; in contrast, lower value are related to possible degradation of the electrode with consequently decreasing performance.

#### Low frequency feature

The low frequency feature is also potential dependent, increasing with increasing overpotential and it is related to mass transport limitations. Its graphical representation at low frequency is generally another semicircle (finite diffusion) rather than a straight line or tail (semi-infinite diffusion) [55]. It is modelled with Warburg elements, which can be added in series to the overall  $R_{ct}||CPE$  modelling the mid frequency region or in series only to the charge transfer resistance as shown in Fig.47.



Figure 53

To conclude, the number of semicircles/arcs depends on the phenomena occurring in the cell. When only one arc is present probably mass transport limitation are negligible, whereas two or three arcs -more or less pronounced and merged- appear in case of both faradaic and mass transport processes.

## 5.2 Data fitting procedure

### 5.2.1 Qualitative analysis

The impedance spectra are subject to a qualitative analysis. It foresees validation by Kramers Kronig relationships, data pre-processing and structural identification. The aim of the data pre-processing is to individuate and discard data affected by error and noise, wild points, outliers and to delete data affected by inductive effects as well. This first step allows to individuate the frequency range where impedance data are reliable. In the structural identification an inspection of the available complex plane plots provides the number of time constants while the setup of the EIS test- in this case the DC value – can give information about the presence/absence of transport limitations.

### 5.2.2 Parameters initial estimation

A first modelling with the *Circle fitting option* allows to have an initial estimation of the principal parameters such as resistances, capacitances, at high and low frequencies. This first approximation is useful for the CNLS fit to the model function obtained from the ECM. The Circle fitting method foresees two option among which make a choice. The Prefit option is selected allowing to fit circles through three points selected in the impedance.

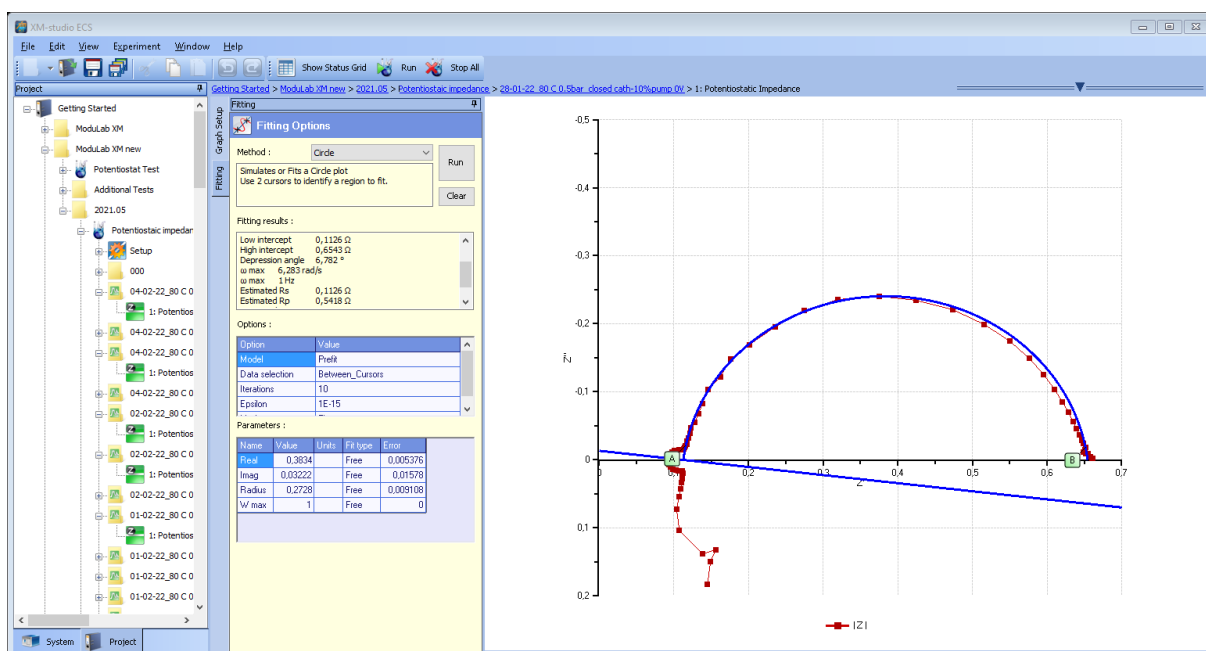


Figure 54

### 5.2.3 Model development and CNLS approximation

The model construction and the CNLS approximation to the equivalent circuit model are both performed with the software. To get a good fit of the impedance data a multi-step procedure is carried out.

#### 1. ECM construction

On the basis of the qualitative analysis of the impedance diagram the ECM is built using the tool available in the software. The ECM usually consists of a series connection of inductance, ohmic resistance and two R || CPE elements.

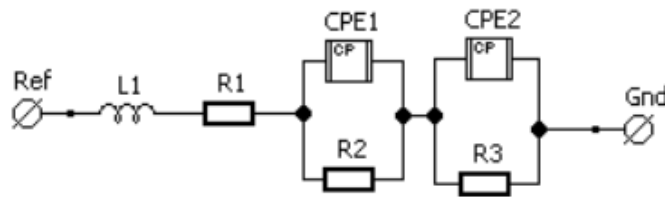


Figure 55

#### 2. First approximation

ECM in Fig.53 is used to get a first approximation. In this step different parameter such as ohmic resistance  $R_1$  and charge transfer resistances  $R_2, R_3$  are fixed using the values gained by the Circle pre-fit. The CPE has two variables as depicted in Fig.53; TDE represents the Q parameter of the formulas whereas PHIDE represents the exponent  $n$ .

The screenshot shows a dialog box titled "Set Constant Phase Element (CPE) parameters". It contains a table with parameters for the CPE. The parameters are TDE and PHIDE. TDE has a value of 1E-06, a fit type of Positive, and an error of 0. PHIDE has a value of 1, a fit type of Fixed, and an error of 0. There are OK and Cancel buttons at the bottom.

|       | Value | Fit type | Error |
|-------|-------|----------|-------|
| TDE   | 1E-06 | Positive | 0     |
| PHIDE | 1     | Fixed    | 0     |

Figure 56

It is necessary to lock  $n = 1$  and leave Q with its default value. Before running the fitting, it is necessary to set the weighting, generally modulus weight is preferred, and also it is important to choose points A and B, which individuate the range of data points to fit in the impedance spectrum.



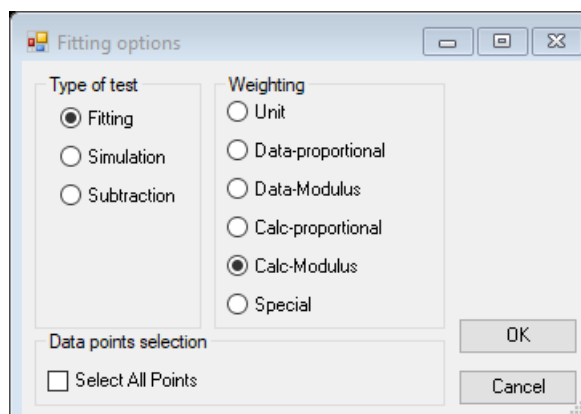


Figure 57

Thereafter, it is possible to run the software. After the first run,  $n$  in both CPE is unlocked and by running again it is possible to get the first data approximation.

### 3. Analysis of obtained fitting data

It is necessary to note that the anode reaction should occur at lower frequency with respect to the cathode reaction occurring at higher frequency. So, if both anode and cathode reactions are considered, the first Randle element should be related to cathode and the second one to the anode. If from the fitting the opposite is obtained (first Randle element to the anode and second to the cathode) it is necessary to restart again the fitting procedure. If the data obtained from the fitting are consistent with the impedance spectrum it is possible to pass to the next step.

### 4. Build a new circuit adding a Warburg element

Note that if diffusion is present, it should be accounted, hence it is necessary to add a Warburg element usually in parallel to the CPE, since mass transport processes occur in parallel to the charge transfer reaction. The Warburg element used is the so-called short Warburg ( $W_s$ ), it has three variables:  $R$  represents  $R_0$ ,  $T$  is  $Q$  and  $\text{PHI}$  is the exponent  $n$ .

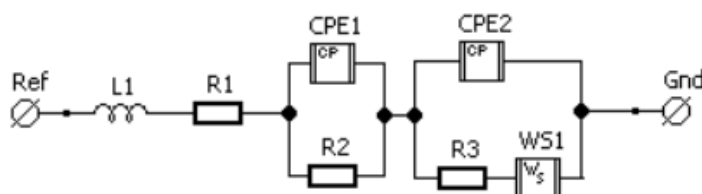
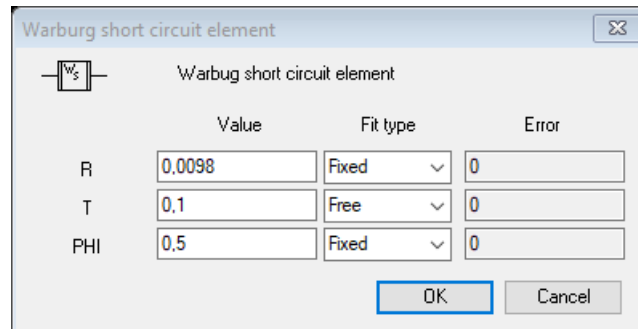


Figure 58

---

#### 5. Get final results

The final ECM is depicted in *Fig.54*. In this case, all the data obtained from the first approximation are fixed whereas in the short Warburg element  $R_0$  is fixed with a small value and  $n$  is locked to its default value 0.5.



The screenshot shows a dialog box titled "Warburg short circuit element". Inside, there is a table with three columns: "Value", "Fit type", and "Error". The rows correspond to parameters R, T, and PHI. The values are 0.0098, 0.1, and 0.5 respectively. The fit types are Fixed, Free, and Fixed. The error values are all 0. There are OK and Cancel buttons at the bottom right.

|     | Value  | Fit type | Error |
|-----|--------|----------|-------|
| R   | 0.0098 | Fixed    | 0     |
| T   | 0.1    | Free     | 0     |
| PHI | 0.5    | Fixed    | 0     |

Figure 59

After the run, all the parameters are unlocked and with another running the final results are obtained.

#### 5.2.4 Final results

The final results of the fitting are the model parameters and a quantity characterizing the goodness of the fit. The error associated with the model is used to decide whether the model gives a poor or a good fit. If a high value of the error is gained the possible reason could be (i) inappropriate equivalent circuit model, (ii) poor initial estimation of the parameter. In both cases, it is necessary to repeat the fitting procedure with some modifications on the ECM or with new initial parameters.

---

## 5.3 Ambiguities

The application of equivalent electrical circuits as models shows several ambiguities.

ECMs, generally chosen a priori, do not describe the physicochemical properties of the system, they simply reproduce the experimental data whereas physical models not only reproduce but also account for the mechanism occurring at the interface [58]. Hence, this is an incomplete method that needs to be coupled with others. In fact, an EEC containing a sufficient number of elements adequately connected can fit closely the experimental impedance data but at the end the information gained are very limited because the ECM is not clearly based on the physicochemical processes involved in the system.

To overcome the lack of correlation with the physics, only pre-knowledge of the system under study can give some hints on the choice of the circuit elements to get meaningful results. If it is known a priori that a specific process occurs, then it is possible to construct the ECM with elements that could be identified with that process.

It is also important to stress out that the same impedance spectrum may be simulated by different circuits giving rise to difficulties in the interpretation of the experimental data. Orazem et al. [59] presented some examples of ambiguous model identification. Different equivalent circuit models- each modelling to different phenomena (charge transfer, adsorption, diffusion, etc.)- were used to fit two synthetic data samples. The results of the regression of all these models to the synthetic data showed that the models provided acceptable fits to the data. This demonstrates that the phenomena governing the system cannot be identified by the model giving the best fit, but a prior knowledge suggesting a reasonable model is required.

Ambiguities become more relevant with system characterized by several processes, usually modelled with multiple time constant circuits. A circuit with  $n$  time constants has at least  $n$  solutions for the circuit elements. So, although the equation of the ECM shows a high degree of simulation for each  $n$  solutions- i.e. a good fit to the experimental data is achieved- the choice will fall among the most adequate one from a physicochemical point of view [60]. Moreover, it may happen that the contributions of the processes to the impedance spectrum overlap because their time constants are very close. Therefore, there are not visible by simple inspection of the impedance diagram, thus it is not possible to consider them in the ECM.

Another issue comes from the weakness of the weighting strategy in the CNLS approximation for the model identification. This because the real and imaginary part in the impedance spectra vary over many order of magnitude.

These figures show a clear example of ambiguity in the fitting procedure. Different equivalent circuit models have produced a quite similar fit; all parameters found from the modelling have errors with same order of magnitude hence it is troublesome to choose among the two solutions.

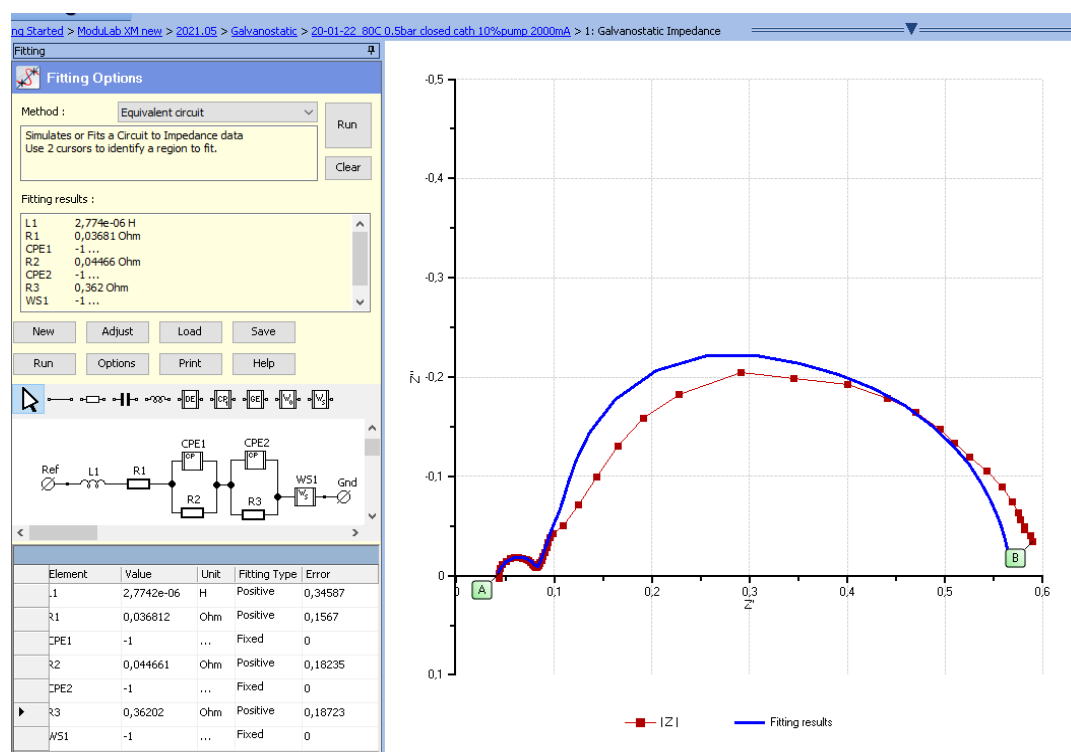


Figure 60

| ELEMENT     | SUB-PARAMETERS | VALUE    | ERROR    | FITTING  |
|-------------|----------------|----------|----------|----------|
| <b>L1</b>   |                | 2,77E-06 | 0,34587  | positive |
| <b>R1</b>   |                | 0,036812 | 0,1567   | positive |
| <b>CPE1</b> | TDE            | 0,026114 | 0,53769  | positive |
|             | PHIDE          | 0,94813  | 0,11356  | free     |
| <b>R2</b>   |                | 0,044661 | 0,18235  | positive |
| <b>CPE2</b> | TDE            | 5,3878   | 0,37091  | positive |
|             | PHIDE          | 0,93802  | 0,051539 | free     |
| <b>R3</b>   |                | 0,36202  | 0,18723  | positive |
| <b>WS1</b>  | R              | 0,12424  | 0,53275  | positive |
|             | T              | 1,7307   | 0,1158   | free     |
|             | PHI            | 0,66556  | 0,083576 | free     |

Table 5.1 Fitting results with LR(QR)(QR)WS.

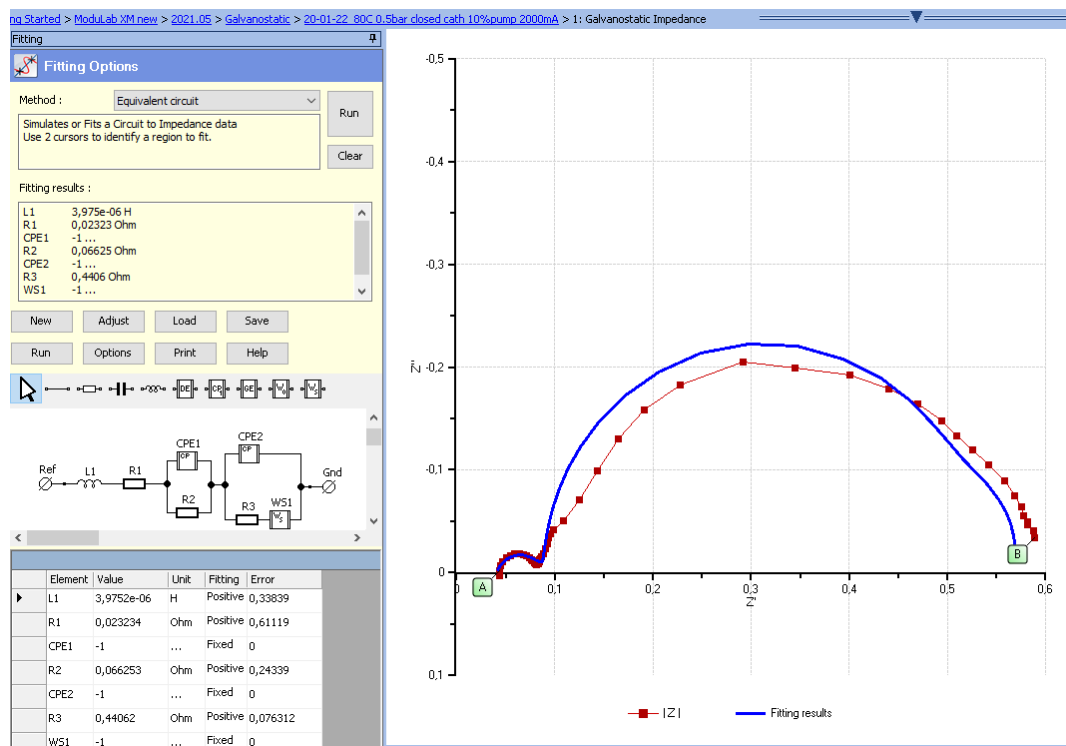


Figure 61

| ELEMENT | SUB-PARAMETERS | VALUE    | ERROR    | FITTING  |
|---------|----------------|----------|----------|----------|
| L1      |                | 3,38E-01 | 0,33839  | positive |
| R1      |                | 0,023234 | 0,61119  | positive |
| CPE1    | TDE            | 0,071583 | 0,39248  | positive |
|         | PHIDE          | 0,73087  | 0,14882  | free     |
| R2      |                | 0,066253 | 0,24339  | positive |
| CPE2    | TDE            | 2,9869   | 0,037519 | positive |
|         | PHIDE          | 0,99969  | 0,030631 | free     |
| R3      |                | 0,44062  | 0,076312 | positive |
| WS1     | R              | 0,039049 | 1,0474   | positive |
|         | T              | 19,097   | 0,70333  | free     |
|         | PHI            | 0,61451  | 0,56276  | free     |

Table 5.2 Fitting results with LR(QR)(QRWS).

---

# Results and discussion

This section presents the results obtained from the tests performed on the PEM electrolytic cell in which two MEAs- having same characteristic but different ageing conditions- were studied. The tests are divided in four categories:

- Open cathode tests
- Closed cathode tests
- Open/closed cathode tests
- Degradation tests

In each test two fundamental parts are provided: results- containing data quality assessment and modelling- and discussion. Parameters gained from the model and their error are reported in the appendix.

## 6.1 Open cathode tests

### 6.1.1 Test Performed At 60°C, Imposed Gauge Pressure 0.5 bar, with 200 mL/min by needle valve with open cathode configuration

The aim of the test to perform electrochemical characterization of the new cell by carrying out EIS measurements. The test is performed at 60°C, 0.5 bar imposed gauge pressure, mass flow rate of 200 mL/min with needle valve and open cathode configuration.

Two types of EIS measurements have been used:

- Potentiostatic test, performed at different DC value of voltage (0 V, 0.5 V, 1 V, 1.5 V) vs Reference by varying the frequency from 100 kHz to 0,001 Hz in single sine mode and using a sinusoidal excitation signal of 10 mV root mean square (rms)
- Galvanostatic test, performed at different DC current -0 mA, 1000 mA, 1500 mA, 2000 mA- by varying the frequency from 200 kHz to 0,002 Hz in single sine mode and using a sinusoidal excitation signal of 1000 mA root mean square (rms).

During the test, the cell temperature was 61.5°C whereas the fluid temperature at the heater was 59.2°C; the real gauge pressure in both side of the cell was around 0.9 bar.

## RESULTS

### Data quality assessment

The KK validation shows a general better quality of the measurements under voltage control, whereas those obtained with galvanostatic mode are affected by time variance hence higher residuals are observed. By visual inspection of both Nyquist and Bode plots two time constants are individuated in both potentiostatic and galvanostatic tests. Hence, the ECM used to model experimental data consists of three elements: LR(QR)(QR).

### Modelling

Impedance spectra under voltage control are characterized by an arc at high frequency and a second arc at mid-low frequency. The low frequency features shows a dependence on voltage: as the DC value of potential increases this tends to reduce its diameter. Same consideration for tests performed under current control, i.e. the LF arc shows a dependence on the DC current and it tends to reduce as the current density is increased.

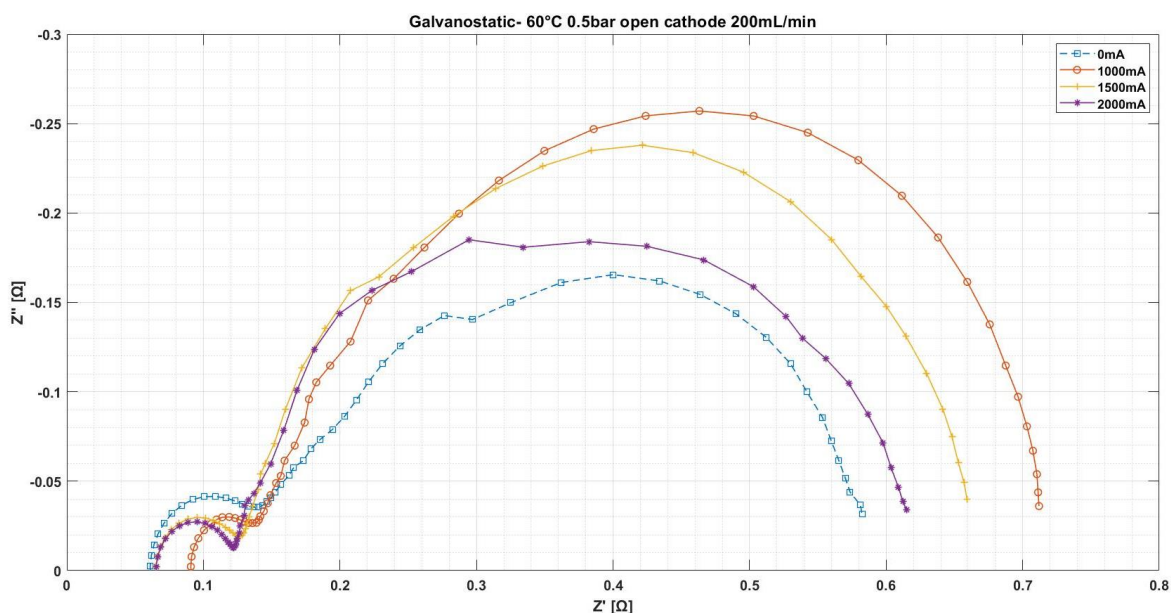


Figure 62 Nyquist plot under current control at 60°C 0.5bar open cathode 200mL/min.

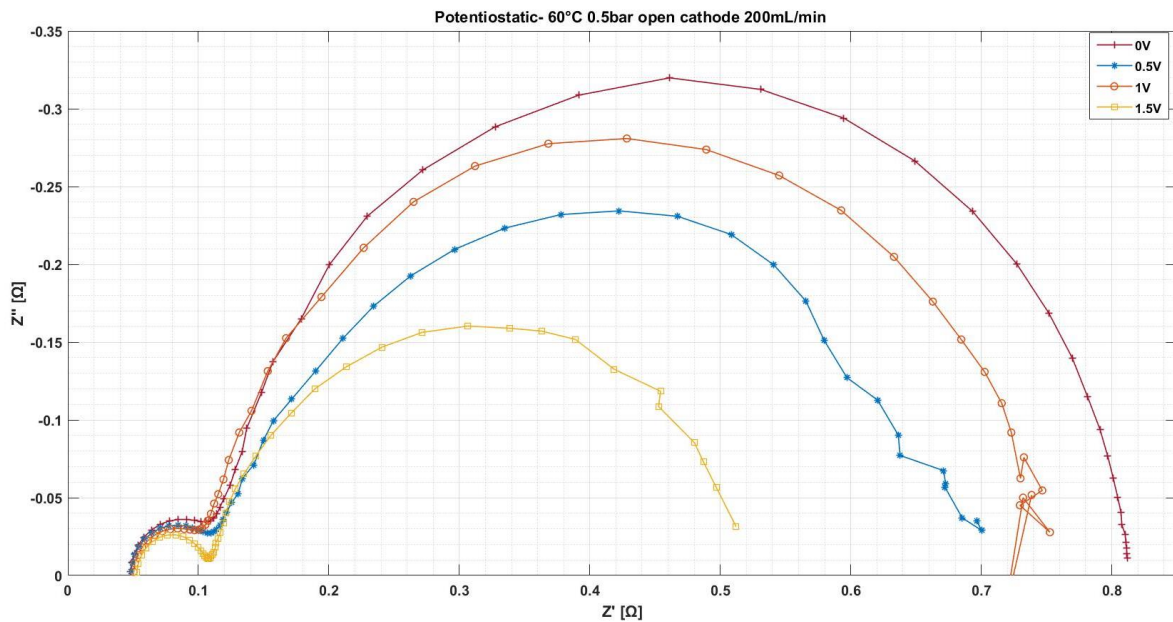


Figure 63 Nyquist plot under voltage control at 60°C 0.5bar open cathode 200mL/min.

Table 6.1 Characteristic frequency at high and low frequency and correlated time constant for both types of EIS test.

|          | POTENTIOSTATIC   |               |                  |               |          | GALVANOSTATIC    |               |                  |               |
|----------|------------------|---------------|------------------|---------------|----------|------------------|---------------|------------------|---------------|
| DC VALUE | $\omega$ HF [Hz] | $\tau$ HF [s] | $\omega$ LF [Hz] | $\tau$ LF [s] | DC VALUE | $\omega$ HF [Hz] | $\tau$ HF [s] | $\omega$ LF [Hz] | $\tau$ LF [s] |
| 0V       | 79.43            | 0.0020        | 0.631            | 0.2524        | 0mA      | 79.62            | 0.0020        | 0.1589           | 1.0021        |
| 0.5V     | 100              | 0.0016        | 0.2512           | 0.6339        | 1000mA   | 100.2            | 0.0016        | 0.1589           | 1.0021        |
| 1V       | 100              | 0.0016        | 0.3921           | 0.4061        | 1500mA   | 100.2            | 0.0016        | 0.1589           | 1.0021        |
| 1.5V     | 125.9            | 0.0013        | 0.07943          | 2.0047        | 2000mA   | 126.2            | 0.0013        | 0.1002           | 1.5892        |

## DISCUSSION

The analysis is focused on the EIS measurements providing good impedance spectra. Hence, 1500 mA and 2000 mA for the galvanostatic mode and the range 0-1.5 V for the potentiostatic mode.

As the current increases in the range 1.5-2 A we have that at LF the charge transfer resistance decreases from 14.4 to 12.3  $\Omega\text{cm}^2$  and the capacitance  $C$  increase from 1.84 to 3.18 F, so the LF semicircle becomes smaller. Instead, the HF arc in the same range is characterized by a less dependent behaviour from the current density since it shows very small variation of the charge transfer resistance HF (from 0.13 to 1.34  $\Omega\text{cm}^2$ ) and capacitance (0.025 F), whereas the ohmic resistance is almost constant around 1.69  $\Omega\text{cm}^2$ .



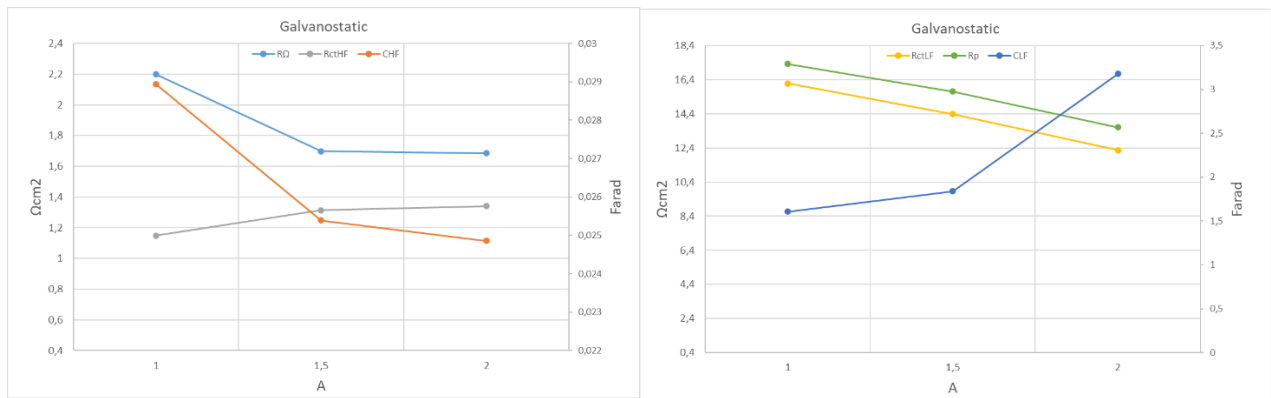


Figure 64 Trend of the parameters with galvanostatic mode.

Considering the range 0-1.5 V, it is possible to notice that the ohmic resistance is not varying significantly with voltage (from 1.05 to 1.17  $\Omega\text{cm}^2$ ), whereas as the voltage increases it observed a decrease of the LF arc. About the LF arc, the charge transfer resistance decreases (from 17.4 to 10.3  $\Omega\text{cm}^2$ ) and its capacitance  $C$  increases (from 0.37 to 5.37 F). The high frequency arc shows a very slight decrease with voltage: in particular, capacitance is constant around 0.018 F while the charge transfer resistance shows lower value with higher voltage level (from 1.85 to 1.53  $\Omega\text{cm}^2$ ).

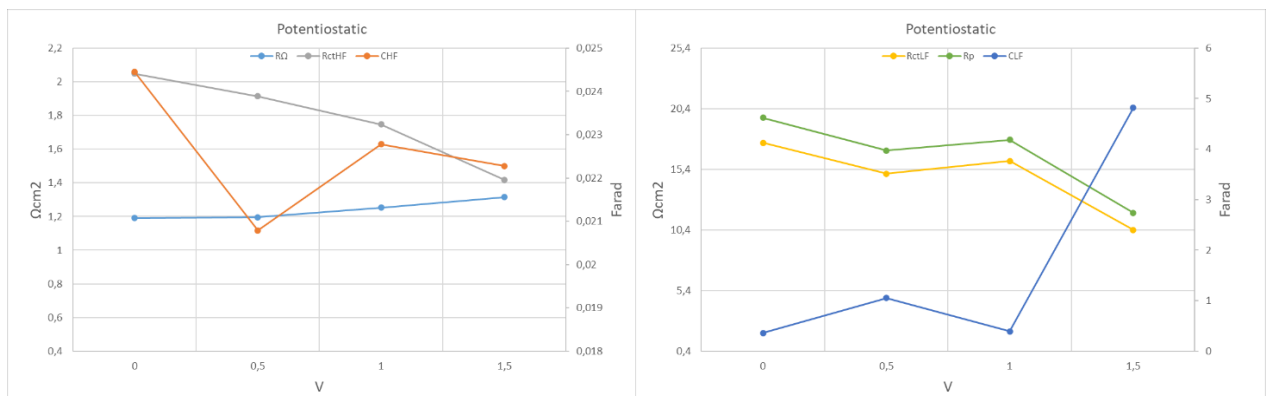


Figure 65 Trend of the parameters with potentiostatic mode.

### 6.1.2 Test Performed At 60°C and 74°C, Imposed Gauge Pressure 0.5bar, with 10% by pump with open cathode configuration

The aim of the test to perform electrochemical characterization of the new cell by carrying out EIS measurements to investigate the temperature effect on the cell impedance. The test consists of two series, first performed at 60°C and the second at 74°C, both characterized by same operating conditions of 0.5 bar imposed gauge pressure, 10% pump and open cathode configuration.

---

Two types of EIS measurements have been used:

- Potentiostatic test, performed at different DC value of voltage (0 V, 0.5 V, 1 V, 1.5 V) vs Reference by varying the frequency from 100 kHz to 0,001 Hz in single sine mode and using a sinusoidal excitation signal of 10 mV root mean square (rms)
- Galvanostatic test, performed at different DC current -0 mA, 1000 mA, 1500 mA, 2000 mA- by varying the frequency from 200 kHz to 0,002 Hz in single sine mode and using a sinusoidal excitation signal of 1000 mA root mean square (rms).

During the test at 60°C, the cell temperature was 61.3°C whereas the fluid temperature at the heater was 59.7°C; the real gauge pressure in both side of the cell was around 0.6 bar. On the other hand, at 74°C the cell temperature was 74.2°C, fluid temperature 79°C and real gauge pressure was around 0.7 bar.

## RESULTS

### *Data quality assessment*

The KK validation shows a general better quality of the measurements under voltage control, whereas those obtained with galvanostatic mode are affected by time variance hence higher residuals. By visual inspection of both Nyquist and Bode plots two time constants are observed in both potentiostatic and galvanostatic tests. The ECM used is LR(QR)(QR).

### *Modelling*

Impedance spectra under voltage control are characterized by an arc at high frequency and a second arc at mid-low frequency. The low frequency features shows a dependence on voltage: as the DC value of potential increases this tends to reduce its diameter. Same consideration for tests performed under current control, i.e. the LF arc shows a dependence on the DC current and it tends to reduce as the current density is increased.

*Table 6.2 Characteristic frequency at high and low frequency and correlated time constant for both types of EIS test at 60°C.*

| 60°C        | POTENTIOSTATIC      |               |                  |               |             | GALVANOSTATIC       |                  |                     |               |
|-------------|---------------------|---------------|------------------|---------------|-------------|---------------------|------------------|---------------------|---------------|
| DC<br>VALUE | $\omega$ HF<br>[Hz] | $\tau$ HF [s] | $\omega$ LF [Hz] | $\tau$ LF [s] | DC<br>VALUE | $\omega$ HF<br>[Hz] | $\tau$ HF<br>[s] | $\omega$ LF<br>[Hz] | $\tau$ LF [s] |
| 0V          | 79.43               | 0.0020        | 0.631            | 0.2524        | 0mA         | 79.62               | 0.0020           | 0.1262              | 1.2618        |
| 1V          | 100                 | 0.0016        | 0.2512           | 0.6339        | 1000mA      | 79.62               | 0.0020           | 0.1589              | 1.0021        |
| 1.2V        | 125.9               | 0.0013        | 0.1585           | 1.0046        | 1500mA      | 100.2               | 0.0016           | 0.1262              | 1.2618        |
| 1.5V        | 125.9               | 0.0013        | 0.0631           | 2.5235        | 2000mA      | 126.2               | 0.0013           | 0.1002              | 1.5892        |

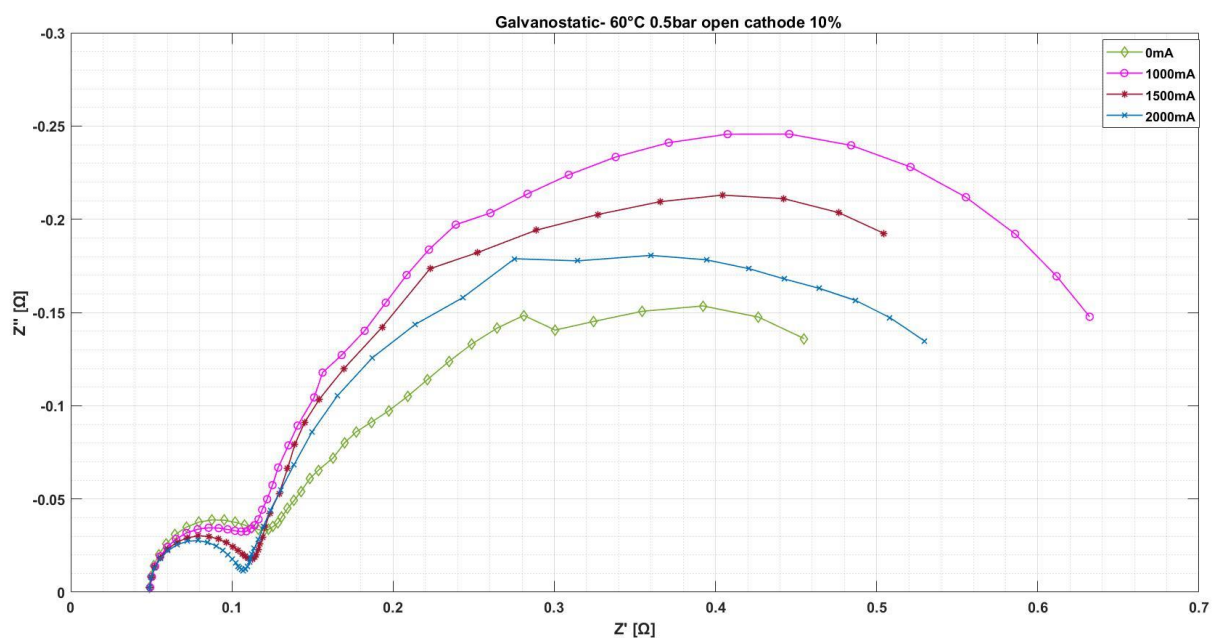


Figure 66 Nyquist plot under current control at 60°C 0.5bar open cathode 10%.

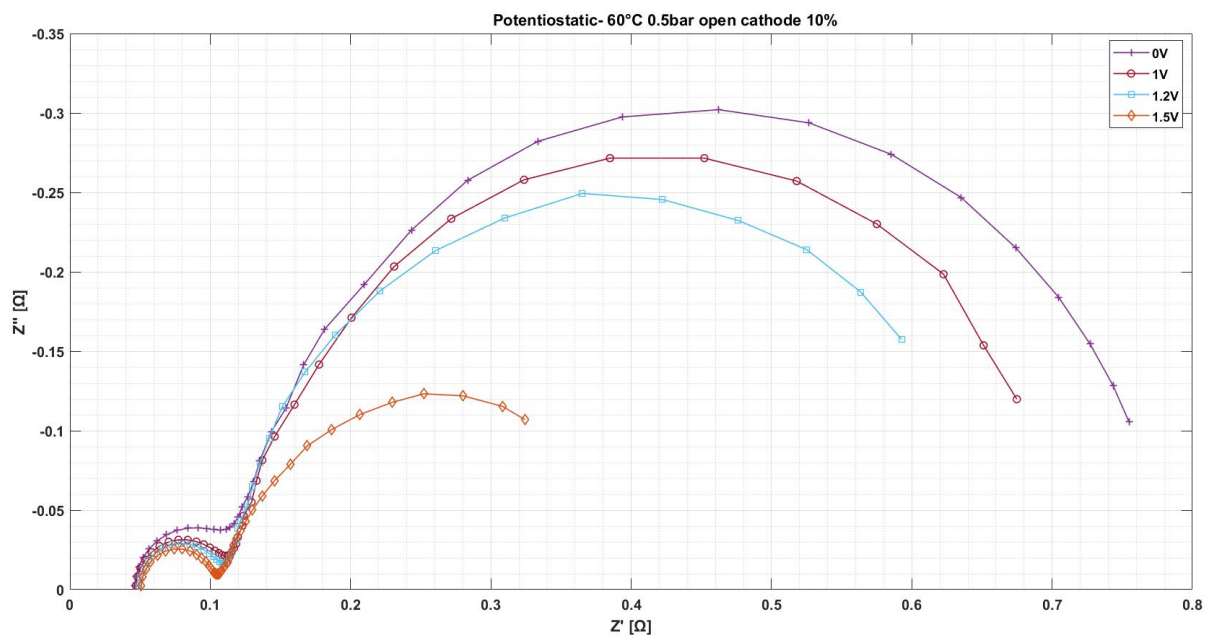


Figure 67 Nyquist plot under voltage control at 60°C 0.5bar open cathode 10%.

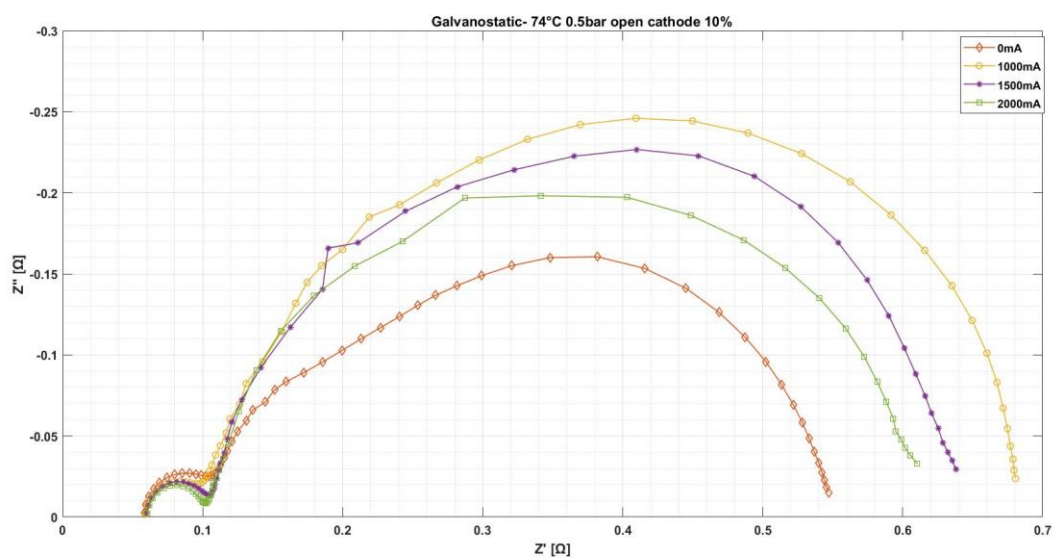


Figure 68 Nyquist plot under current control at 74°C 0.5bar open cathode 10%.

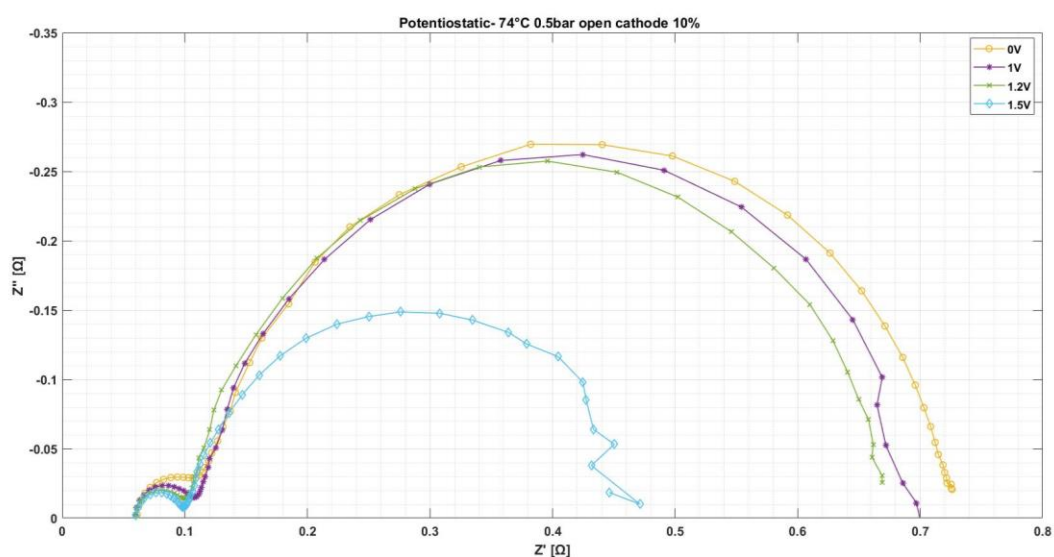


Figure 69 Nyquist plot under voltage control at 74°C 0.5bar open cathode 10%.

Table 6.3 Characteristic frequency at high and low frequency and correlated time constant for both types of EIS test at 74°C.

| 74°C     | POTENTIOSTATIC   |               |                  |               |          | GALVANOSTATIC    |               |                  |               |
|----------|------------------|---------------|------------------|---------------|----------|------------------|---------------|------------------|---------------|
| DC VALUE | $\omega$ HF [Hz] | $\tau$ HF [s] | $\omega$ LF [Hz] | $\tau$ LF [s] | DC VALUE | $\omega$ HF [Hz] | $\tau$ HF [s] | $\omega$ LF [Hz] | $\tau$ LF [s] |
| 0V       | 100              | 0.0016        | 0.631            | 0.2524        | 0mA      | 100.2            | 0.0016        | 0.1589           | 1.0021        |
| 1V       | 125.9            | 0.0013        | 0.1585           | 1.0046        | 1000mA   | 126.2            | 0.0013        | 0.1589           | 1.0021        |
| 1.2V     | 158.5            | 0.0010        | 0.1995           | 0.7982        | 1500mA   | 126.2            | 0.0013        | 0.1589           | 1.0021        |
| 1.5V     | 158.5            | 0.0010        | 0.0631           | 2.5235        | 2000mA   | 126.2            | 0.0013        | 0.1262           | 1.2618        |

## DISCUSSION

Figures below show the parameters' trend obtained from the fitting results at 60°C and 74°C.

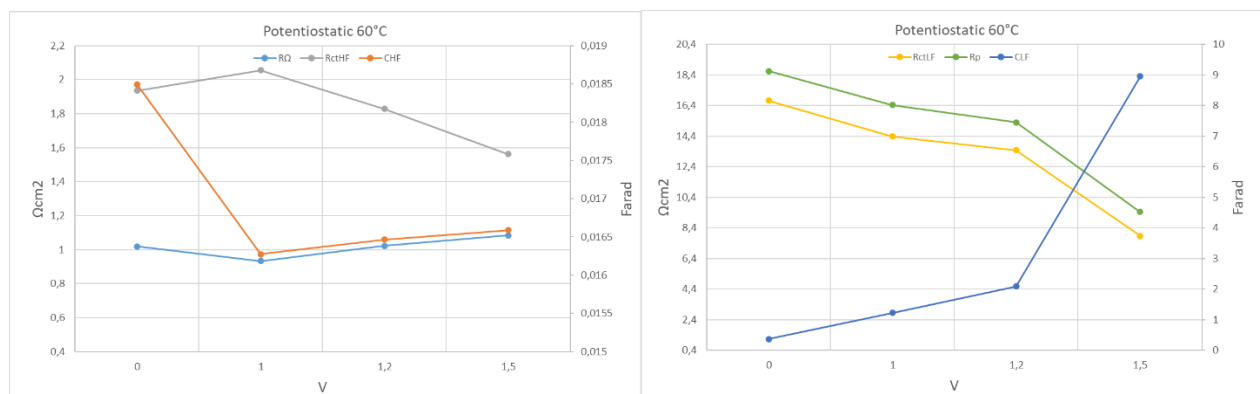


Figure 70 Parameters' trend obtained from potentiostatic test at 60°C.

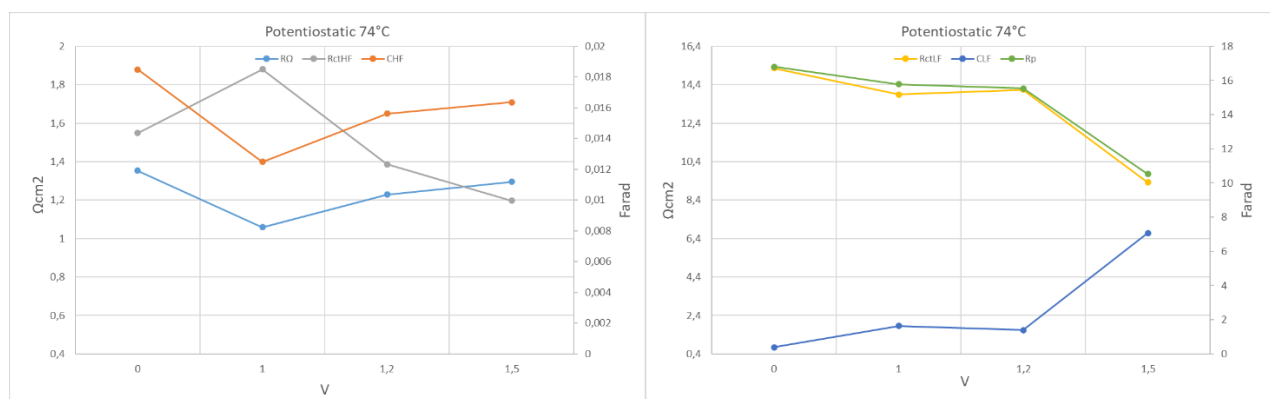


Figure 71 Parameters' trend obtained from potentiostatic test at 74°C.

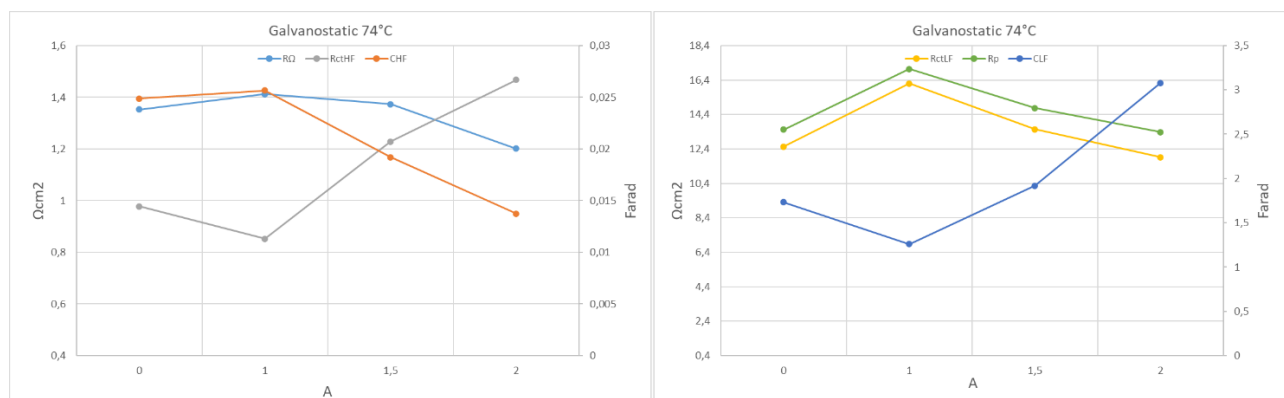


Figure 72 Parameters' trend obtained from galvanostatic test at 74°C.

The comparison between the 60°C and 74°C is carried out by considering EIS measurements in the range 0-1.5 V in the potentiostatic mode. Trends show that they have same behaviour as voltage increases, but two parameters-ohmic resistance and charge transfer resistance at HF- have different values. Ohmic resistance is generally smaller whereas charge transfer resistance at high frequency is higher at 60°C; instead, opposite behaviour is observed at 74°C. Nevertheless, both temperatures have similar values of the total polarization resistance and the other parameters do not show relevant variation with temperature.

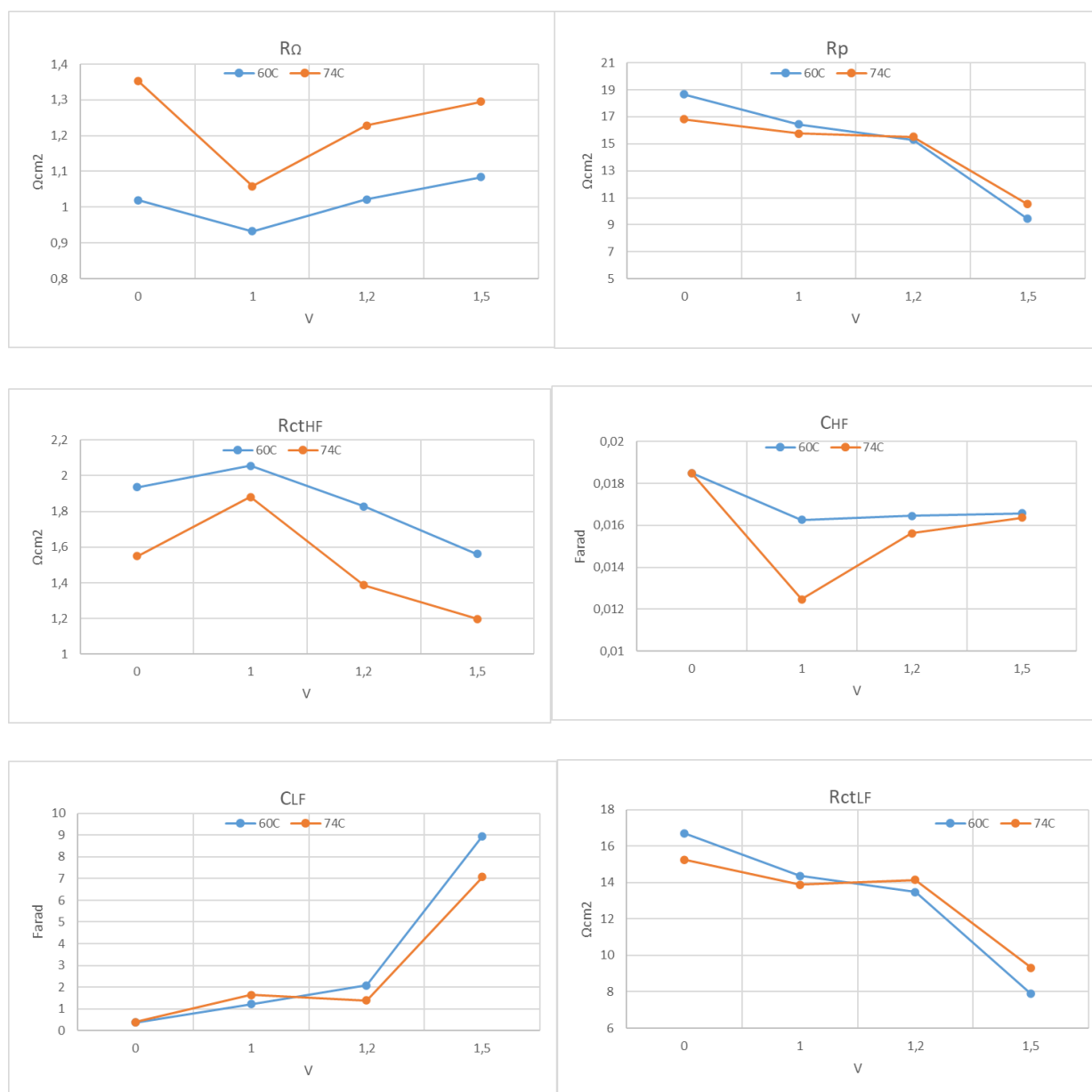


Figure 73 Comparison of the parameters gained from potentiostatic measurements between 60°C and 74°C.

Concluding, it is observed that the high frequency arc is particularly affected by temperature whereas the low frequency arc is less temperature dependent although a benefit from higher temperature is noticed.

---

### 6.1.3 Tests performed at T=79°C & T=71°C, with open cathode at different gauge pressure

The objective of the experiment is to investigate the influence of temperature and pressure on cell impedance through EIS measurements.

The experiment is executed with open cathode at fixed temperature of 79°C, increasing the imposed gauge pressure from 1.4 bar to 7.5 bar. Then, temperature is decreased up to 71°C and kept fixed while imposed gauge pressure is decreased from 7.5 bar to 1.4 bar. EIS measurements are performed after stabilization of the cell at the desired value of temperature and pressure. Two types of EIS tests have been used:

- Potentiostatic test, performed at 0 DC V vs Open circuit by varying the frequency from 100kHz to 1Hz in single sine mode and using a sinusoidal excitation signal of 10 mV root mean square (rms).
- Galvanostatic test, performed at 0 DC mA by varying the frequency from 200 kHz to 0,2 Hz in single sine mode and using a sinusoidal excitation signal of 1000 mA root mean square (rms).

Note that the real pressure in both sides of the cell is given taking the average between the imposed pressure and the pressure at the heater. Hence, real pressures are different as shown in the table below.

Table 6.4 Values of pressure during the test.

| Imposed gauge pressure | Pressure at the heater @79°C | Real gauge pressure @79°C | Pressure at the heater @71°C | Real gauge pressure @71°C |
|------------------------|------------------------------|---------------------------|------------------------------|---------------------------|
| <b>1.4</b>             | 2,19                         | 1,8                       | 2,27                         | 1,8                       |
| <b>2.4</b>             | 3,08                         | 2,7                       | 3,28                         | 2,8                       |
| <b>5</b>               | 5,46                         | 5,1                       | 5,70                         | 5,3                       |
| <b>7.5</b>             | 8,08                         | 7,7                       | 8,00                         | 7,6                       |

Real gauge pressure is the same for anode and cathode as depicted in *Figure 75*.

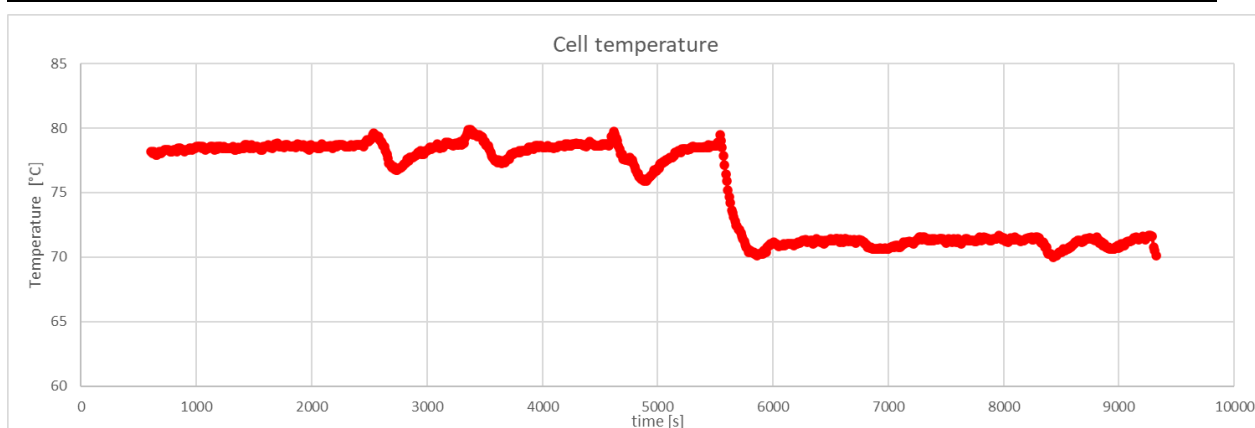


Figure 74 Cell temperature measured during the test.

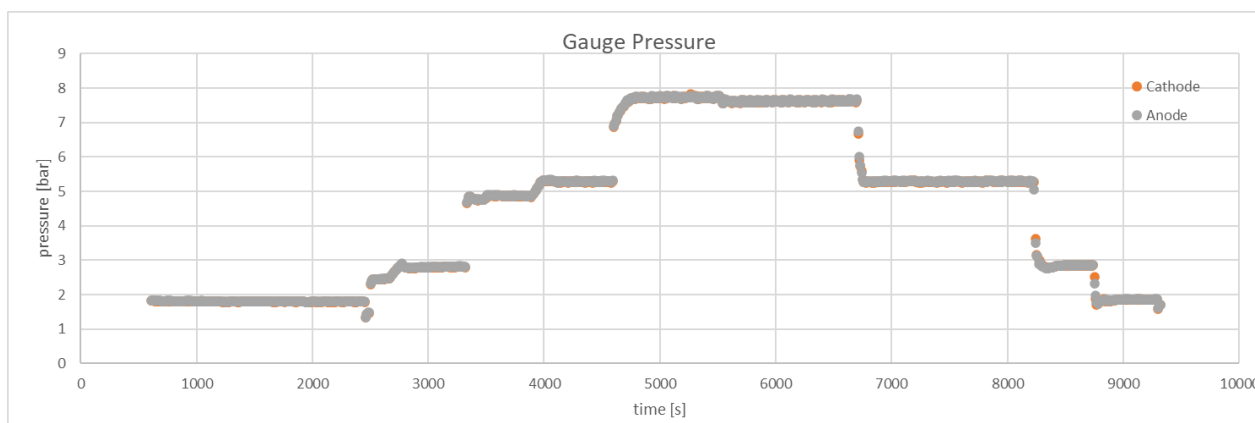


Figure 75 Gauge pressure in the anode and cathode measured during the test.

## RESULTS

### Data quality assessment

The KK validation shows that impedance spectra obtained under voltage control are characterized by residuals in the range  $\pm 1\%$ , whereas impedance data gained with galvanostatic tests are affected by time variance. In Nyquist plots it is observed that the shape is made of a semicircle in the HF and a second incomplete semicircle in the mid frequency region, corresponding to two time constants visible in the Bode plots. Hence, the ECM used to fit is LR(QR)(QR).

### Modelling

Figure 76 and 77 show impedance spectra obtained respectively at 79°C and 71°C at different gauge pressure with potentiostatic tests. The high frequency arc seems not affected by the



pressure whereas the second incomplete arc bends down to the real axis with decreasing pressures. The imaginary part of all HF arcs at 79°C reaches a maximum at  $\omega_{max}$  equal to 158.5 Hz.

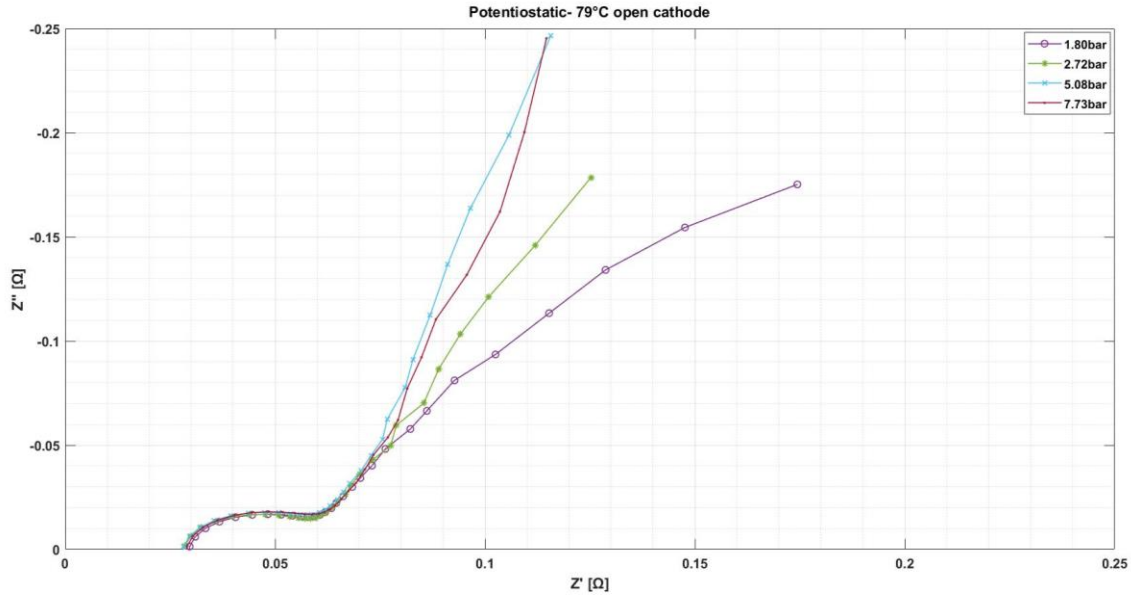


Figure 76 Nyquist plot under voltage control at 79°C open cathode at different gauge pressures.

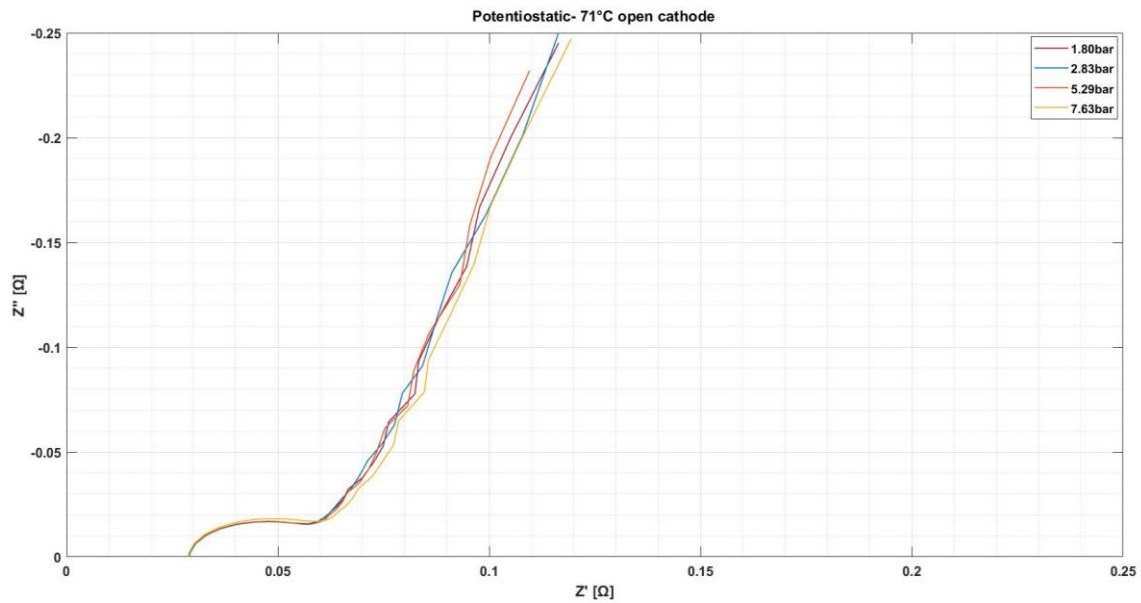


Figure 77 Nyquist plot under voltage control at 71°C open cathode at different gauge pressures.

Figure 78 and 79 show impedance spectra obtained respectively at 79°C at different gauge pressure with galvanostatic tests. The high frequency arc is not affected by the pressure as well as the second incomplete arc in the mid frequency region. A tail appears at lower

frequencies, maybe it is an insight of a third semicircle. The imaginary part of all HF arcs reaches a maximum at  $\omega_{max}$  equal to 158.9 Hz.

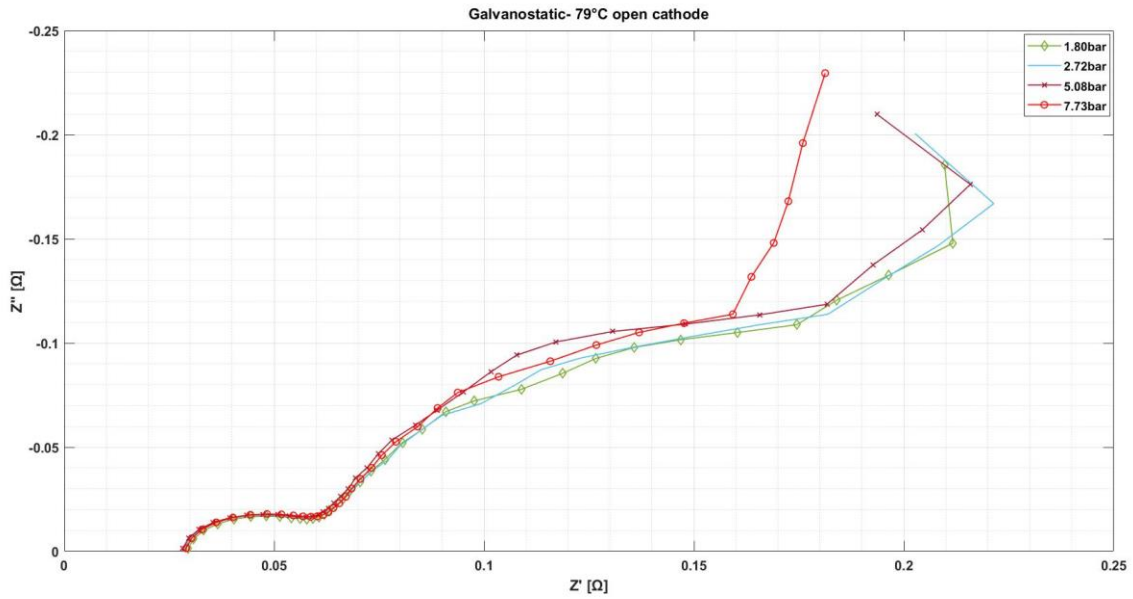


Figure 78 Nyquist plot under current control at 79°C open cathode at different gauge pressures.

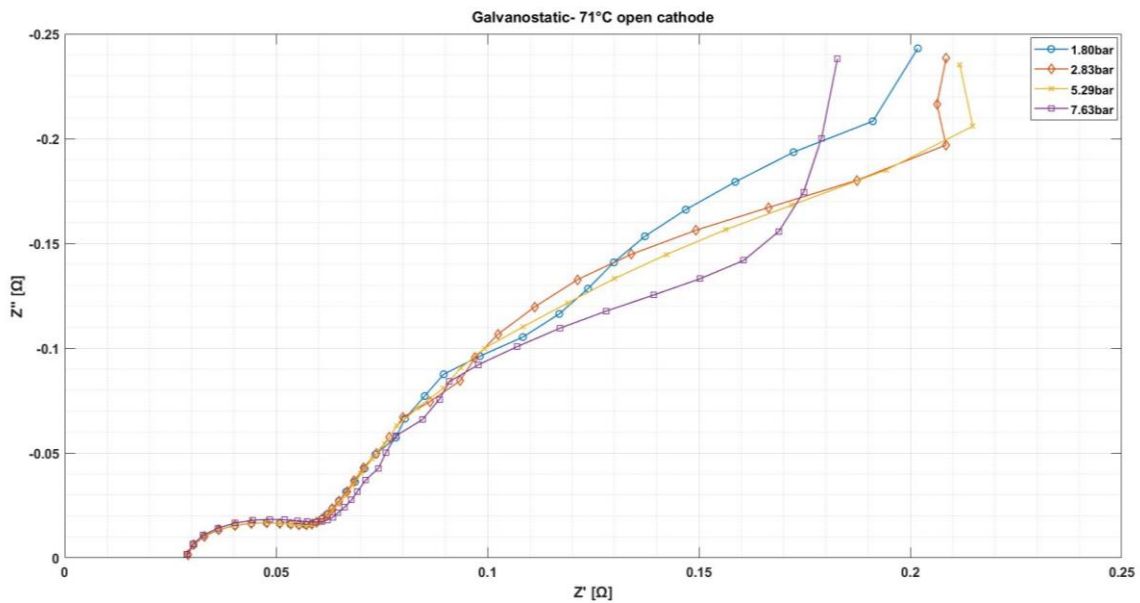


Figure 79 Nyquist plot under current control at 71°C open cathode at different gauge pressures.

## DISCUSSION

Potentiostatic tests are considered for further analysis. The impedance spectra shows two regions: one at high frequency and another at mid-low frequency. Since the EIS tests are performed using a limited range of frequency (in order to have a fast test), it is not possible to

say much about the second region aforementioned. Instead, the high frequency region- represented by the semicircle- can be analysed because we can clearly see the ohmic resistance, intercept of the high frequency arc with the real axes, and the charge transfer resistance, represented by the intercept at mid frequency.

The increase of pressure at 71°C has negligible effects on the high frequency arc; on the other hand, at 79°C it determines a relative decrease of the ohmic resistance (from 0.625 to 0.568  $\Omega\text{cm}^2$ ) as well as the capacitance (from 0.021 to 0.019 F), and an increase of the charge transfer resistance from 0.847 to 0.983  $\Omega\text{cm}^2$ .

Increasing temperature, considering constant pressure, has a positive effects on capacitance and charge transfer resistance, but it tends to become negligible as pressure increases. Instead, too high temperature (>71°C) causes an increase of the ohmic resistance probably due to dehydration effects, but this negative effects is mitigated by increase of pressure, at least up to 5 bar.

In conclusion, lower pressure and higher temperature have positive effects on the capacitance and the charge transfer resistance (higher capacitance and lower charge transfer resistance), whereas ohmic resistance at high temperature (>70°C) benefits from higher pressure.

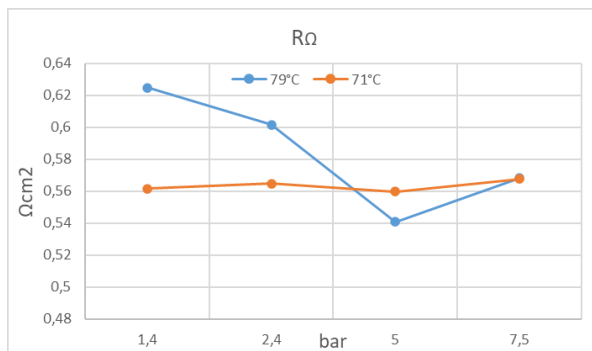


Figure 80 Trend of the ohmic resistance at 79°C and 71°C.

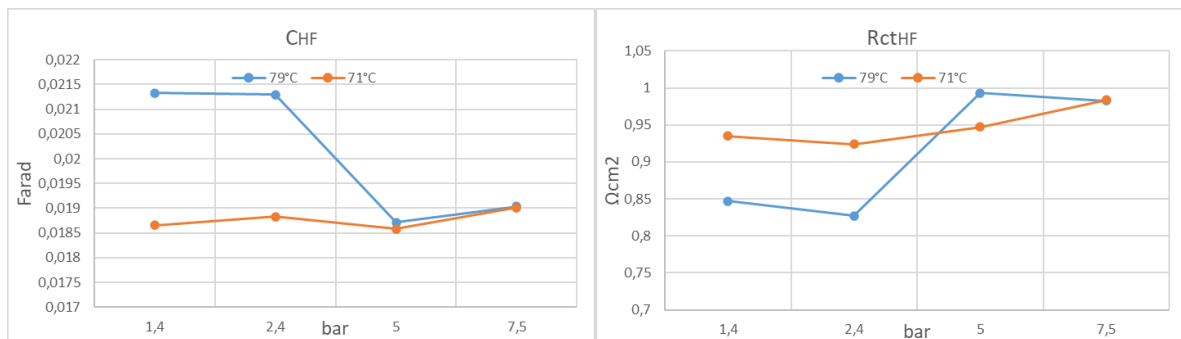


Figure 81 Trend of charge transfer resistance and capacitance in the HF region at 79°C and 71°C.

---

## Conclusion

Results gained from the open cathode tests suggest the following assumptions:

1. The HF features and the ohmic resistance are not showing a strong dependence on current and/or voltage, but rather they are mostly temperature dependent. These findings suggest that it is not related to kinetics processes but rather to the MEA structure. In particular, it is related to hinder of proton conduction which strictly depends on the characteristics of the membrane electrode assembly, like the presence of big catalyst agglomerates in the active surface of the anode or bad contact between the electrolyte and the anode catalyst layer [40,57]. However, the attribution of the HF arc is generally troublesome. Some researchers attribute its origin to the HER in the cathode, others correlate this feature to a hinder of the proton conduction in the electrolyte, principally due to the MEA characteristics.
2. Considering that in the range 0-2 A (so 0-0,08 A/cm<sup>2</sup> current density) we are in the activation domain and that the LF arc shows a dependence on current density and on voltage, it is suggested that the LF arc is controlled by the charge-transfer kinetics. It means that in the Nyquist plot the LF arc is related to both OER and HER.
3. A general improvement is observed as temperature is increased. Instead, pressure determines substantial enhancement at higher temperature rather than at lower. Moreover, it is noticed that when temperature is too high (>71°C) ohmic losses are increased and this is probably related to the loss of humidity. Increasing pressure, at least up to 5 bar, can reduce ohmic resistance at high temperature.

## 6.2 Closed cathode tests

Note that with open cathode the real pressure in both sides of the cell is given by taking the average between the imposed pressure and the pressure at the heater. During closed cathode the average is taken only for the anode.

---

### 6.2.1 Tests performed at constant current density of 1 A/cm<sup>2</sup> with 60°C, 0.5 bar, closed cathode imposing different mass flow rate by recirculating pump

The aim of the experiment is to investigate the influence of mass flow rate on cell impedance at fixed operating condition and with closed cathode.

The test is performed at constant current density of 1 A/cm<sup>2</sup> with fixed operating conditions of 60°C and 0,55 bar @ anode -0,44 bar @cathode and different mass flow rates changed by the usage of the pump from 10% to 100%. A change of the mass flow rate by pump causes a variation of the pressure at the heater during the experiment.

*Table 6.5 Values of temperatures, pressure at the heater and voltage at different percentage of mass flow rates during the test.*

|                    | Voltage [V] | Fluid pressure at heater [bar] | Cell Temperature [°C] | Fluid Temperature at Heater Outlet [°C] |
|--------------------|-------------|--------------------------------|-----------------------|---|
| <b>10%</b>         | 2,79        | 1,31                           | 61,26                 | 61,82                                   |
| <b>EIS at 10%</b>  | -           | 1,10                           | 61,14                 | 62,03                                   |
| <b>30%</b>         | 2,79        | 2,46                           | 61,30                 | 59,17                                   |
| <b>EIS at 30%</b>  | -           | 2,57                           | 61,08                 | 58,70                                   |
| <b>50%</b>         | 2,87        | 4,36                           | 61,32                 | 58,71                                   |
| <b>EIS at 50%</b>  | -           | 4,45                           | 61,23                 | 59,05                                   |
| <b>70%</b>         | 3,00        | 6,32                           | 61,32                 | 58,86                                   |
| <b>EIS at 70%</b>  | -           | 6,19                           | 61,11                 | 59,10                                   |
| <b>100%</b>        | 3,19        | 8,71                           | 61,34                 | 58,97                                   |
| <b>EIS at 100%</b> | -           | 8,86                           | 61,24                 | 59,07                                   |

During the experiment two types of EIS tests have been used:

- Potentiostatic test is performed at 0 DC V vs Open circuit by varying the frequency from 100 kHz to 1 Hz in single sine mode and using a sinusoidal excitation signal of 10 mV root mean square (rms);
- Galvanostatic test is performed at 0 DC mA by varying the frequency from 200 kHz to 0,2 Hz in single sine mode and using a sinusoidal excitation signal of 1000 mA root mean square (rms).

## **RESULTS**

### *Data quality assessment*

The KK validation shows that impedance spectra obtained under voltage control are characterized by acceptable values of the residuals, whereas impedance data gained with galvanostatic tests are more affected by biased behaviour. In general, the shape is made of a

semicircle in the HF and second incomplete semicircle/straight line in the mid frequency region. Hence, the ECM used to fit is LR(QR)(QR).

### Modelling

Figure 82 shows impedance spectra obtained with potentiostatic tests. The high frequency intercept with the real axis is not much affected by mass flow rate variation, instead height and diameter of the HF arc show a substantial increase with increasing mass flow rates.

The imaginary part of all HF arcs reaches a maximum at  $\omega_{max}$  equal to 199.5 Hz and it tends to decrease up to 158.9 Hz with increasing mass flow rates.

Same considerations can be done on the impedance spectra obtained with galvanostatic tests in Figure 83. In this case, the  $\omega_{max}$  is equal to 200 Hz and it tends to decrease up to 158.9 Hz with increasing mass flow rates.

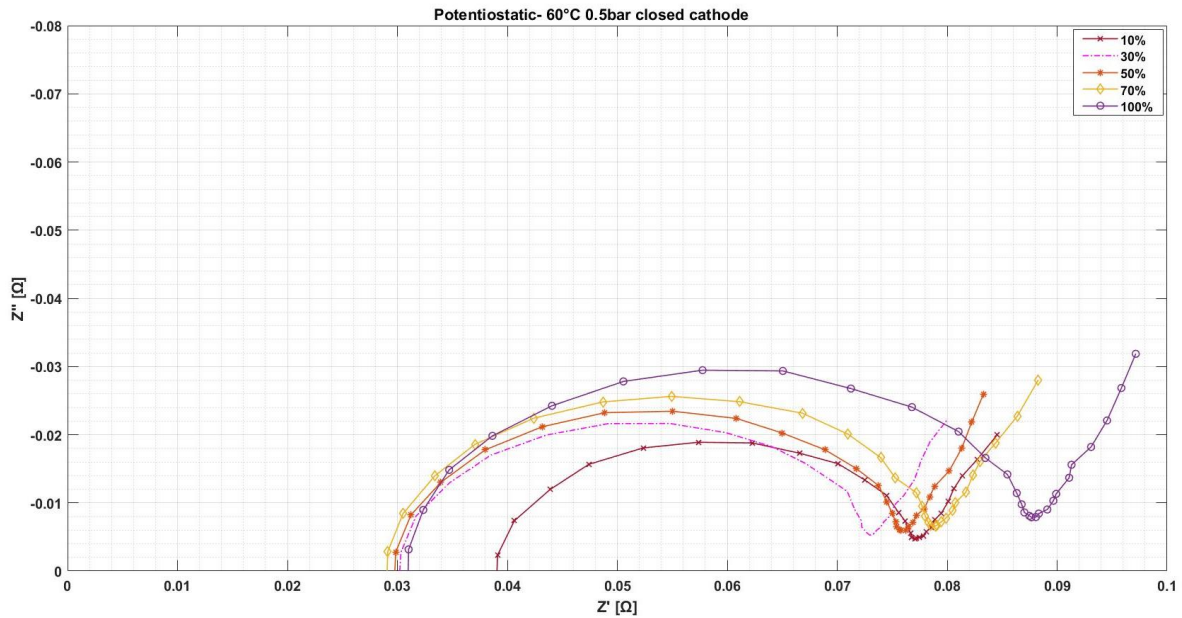


Figure 82 Nyquist plot under voltage control at 60°C 0.5bar closed cathode at different percentage of mass flow rates.

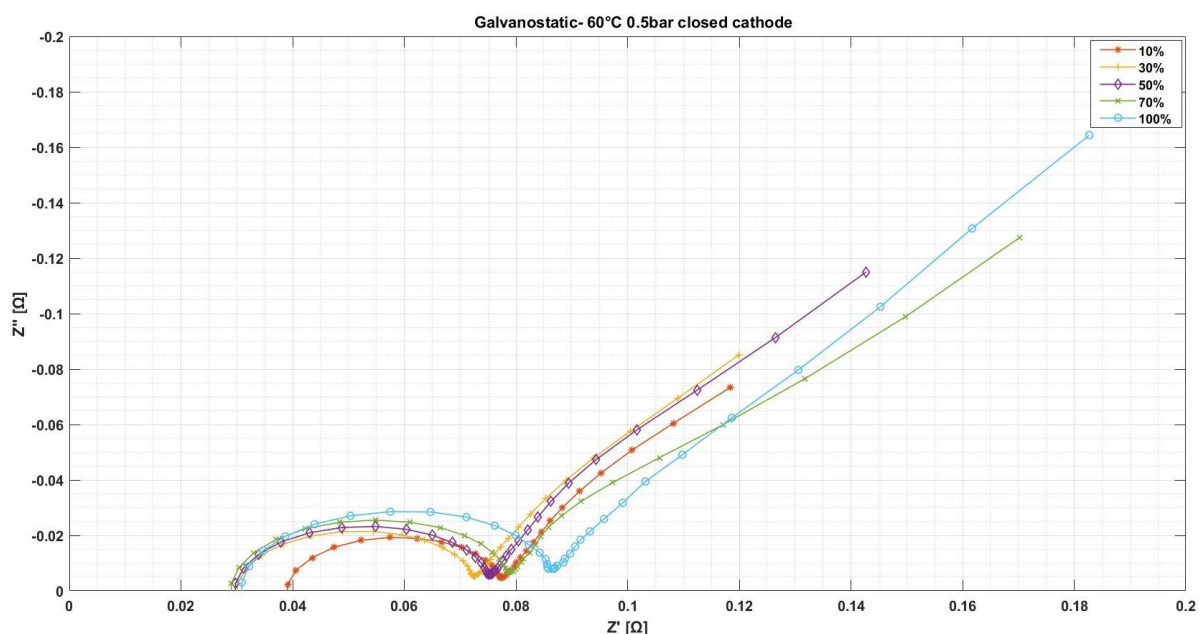


Figure 83 Nyquist plot under current control at 60°C 0.5bar closed cathode at different percentage of mass flow rates.

## DISCUSSION

The analysis is carried out by discussing the results obtained from the potentiostatic tests.

The impedance spectra shows two regions: one at high frequency and another at mid-low frequency. EIS tests are performed using a limited range of frequency, thus only the -HF arc is analysed by measuring the ohmic resistance, intercept of the high frequency arc with the real axes, and the charge transfer resistance, which is the diameter of the high frequency arc.

The increase of mass flow rate determines a relative decrease of the ohmic resistance (from 0.898 to 0.716  $\Omega\text{cm}^2$ ) as well as the capacitance (from 0.0187 to 0.0172 F), and an increase of the charge transfer resistance from 1.010 to 1.447  $\Omega\text{cm}^2$ . The increase of the charge transfer resistance is higher with respect to the decrease of the ohmic resistance. Hence, it may be assumed that the total polarization resistance is increasing as well; this agree with high values of voltage obtained with higher mass flow rate percentage (higher total polarization resistance means higher voltage).

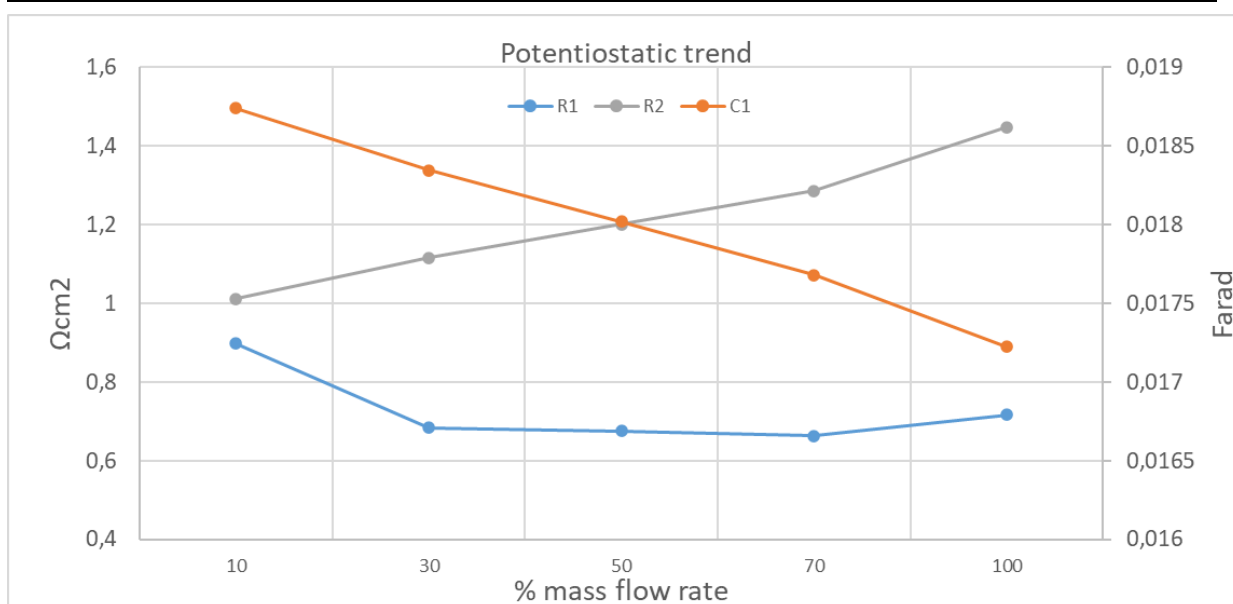


Figure 84

The analysis shows that from 10% to 100% of mass flow rate percentage, voltage and pressure at the heater increase instead average cell temperature (61,08°C-61,35°C) is almost constant. Only fluid temperature at the heater is characterized by a decreasing behaviour from 61,8°C up to 59°C, maybe because with higher percentage of the pump the flow is faster and so thermal stabilization is improved. Hence, increasing the percentage of mass flow rate determines an increment of fluid pressure at the heater and a decrease of the temperature at the heater. As a consequence, voltage increases so the cell performance is negatively affected by increment of mass flow rates.

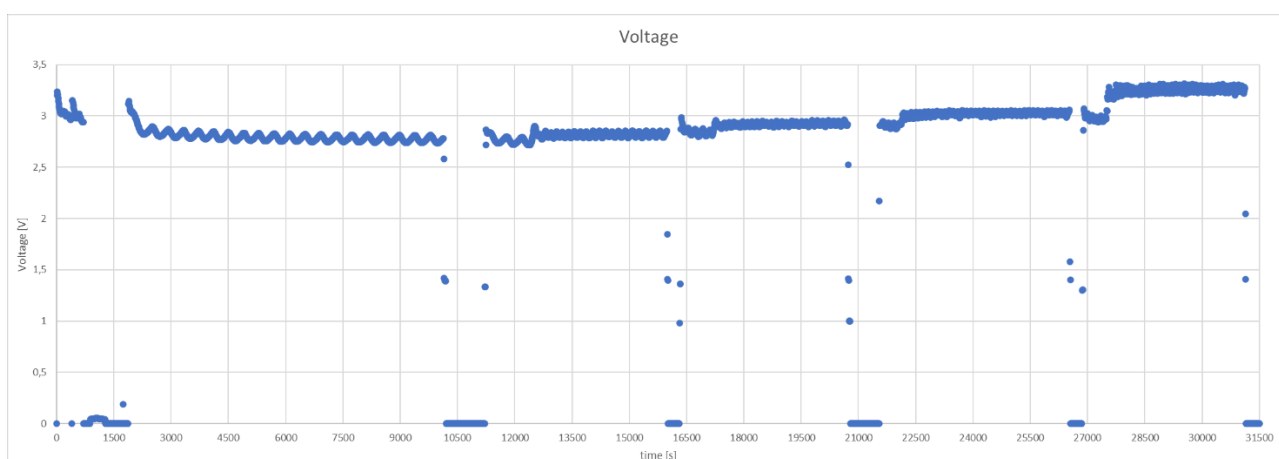


Figure 85 Trend of the voltage during the test.



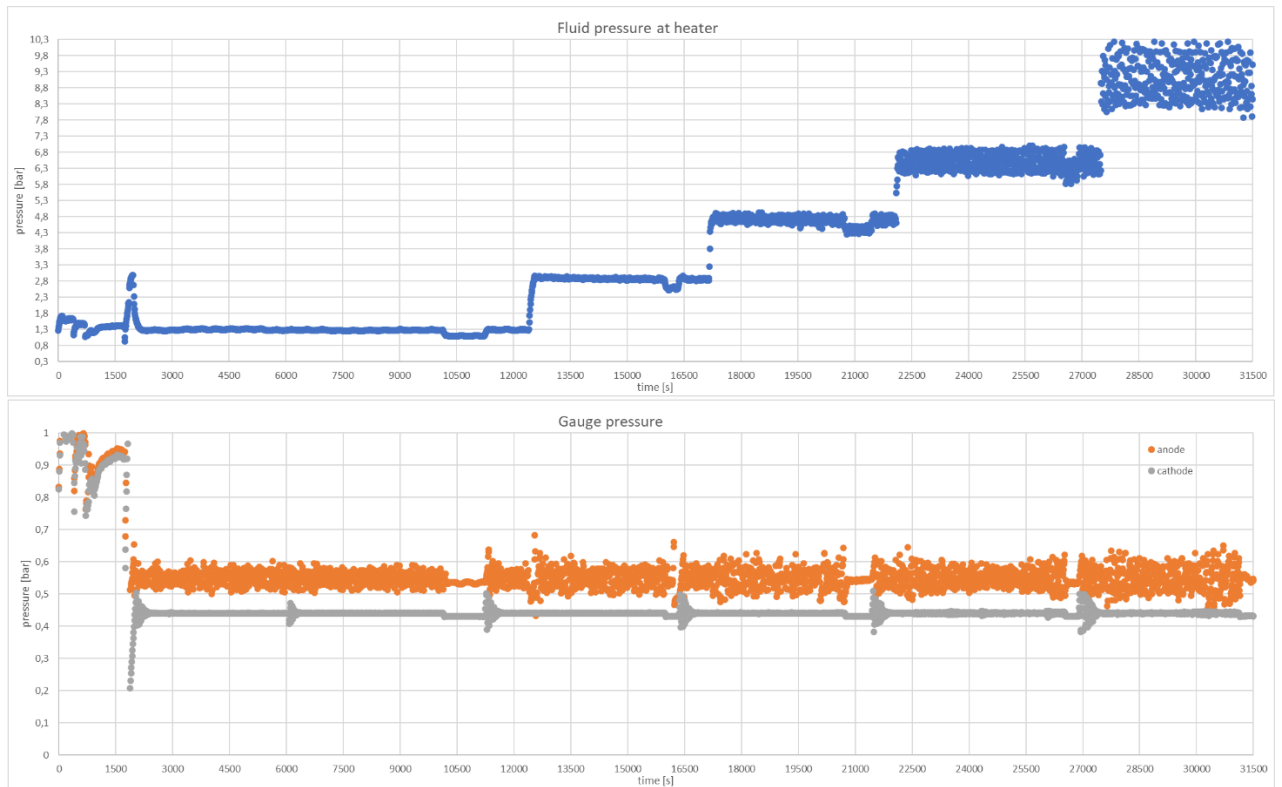


Figure 86 Trend of the pressures- anode, cathode, heater- during the test.

In conclusion, with closed cathode at 60°C and with constant current density of 1 A/cm<sup>2</sup>, an increase of the mass flow rate determines an increment of pressure which negatively affects the performance of the cell, i.e. higher voltages are measured.

---

### 6.2.2 Test Performed At 60°C And 80°C With Closed Cathode, Imposed Gauge Pressure 0.5bar, 105% Mass Low Rate by Pump

The aim of the test to perform electrochemical characterization of the new cell by carrying out polarization curves and EIS measurements.

The test consists of two series, first performed at 60°C and the second at 80°C, both characterized by same operating conditions of 0.5 bar imposed gauge pressure, 105% pump and closed cathode configuration. Polarization curves were measured by current control up to 1.6 A/cm<sup>2</sup> whereas two types of EIS measurements have been used:

- Potentiostatic test, performed at 0 DC V vs Reference by varying the frequency from 100 kHz to 0,001 Hz in single sine mode and using a sinusoidal excitation signal of 10 mV root mean square (rms)
- Galvanostatic test, performed at 0 DC mA by varying the frequency from 200 kHz to 0,002 Hz in single sine mode and using a sinusoidal excitation signal of 1000 mA root mean square (rms).

During the test performed at 60°C the real gauge pressure at the anode side of the cell is almost 4.6 bar at the anode and 0.44 bar at the cathode, whether the real temperature of the cell is around 61.5°C and fluid temperature at the heater is 59°C. As a matter of fact, during EIS test operating conditions are unvaried. During the test performed at 80°C the real gauge pressure as before is 4.6 bar in the anode and 0.44 bar in the cathode, whether the real temperature of the cell is around 79.6°C and fluid temperature at the heater is 78.1°C. No changes of pressure during EIS tests at 80°C are seen.

## **RESULTS**

### *Data quality assessment*

The KK validation shows a poor quality of the impedance spectra obtained under galvanostatic measurements whereas those obtained with potentiostatic still show high residuals but at least the HF is not much affected by noise or time variance. By visual inspection of both Nyquist and Bode plots two time constants are observed in the measurements under voltage control and at least three under current control. The ECM used to fit experimental data is LR(QR)(QR) due to the presence of noise at low frequency which makes difficult to get good results.

## Modelling

The comparison between 60°C and 80°C for both EIS measurements is shown in the figures below.

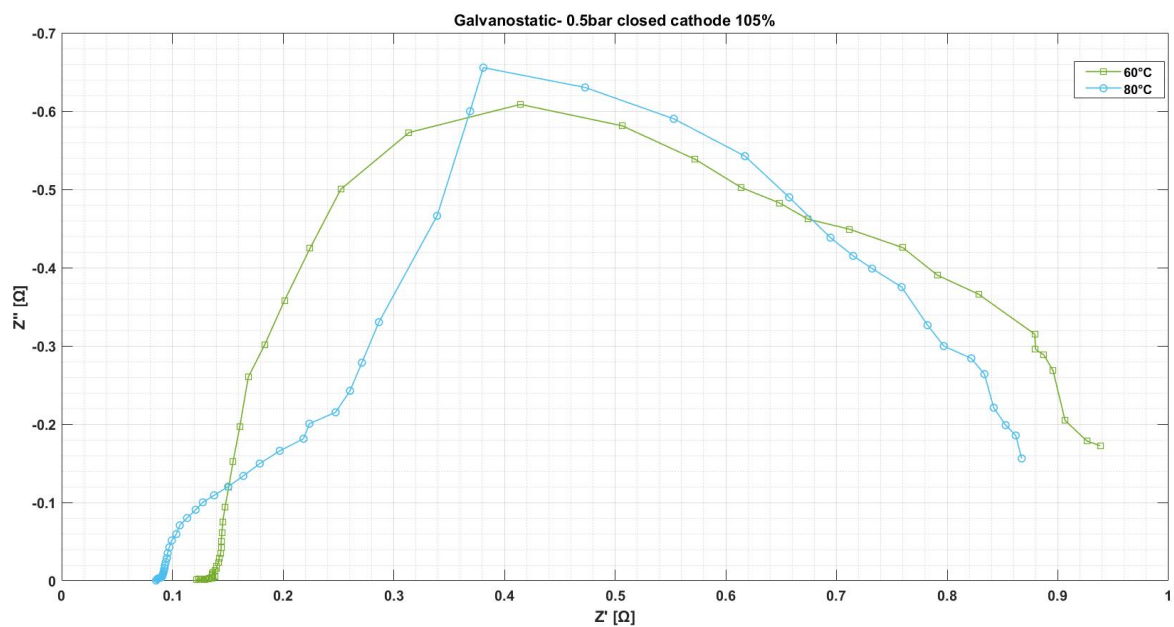


Figure 87 Nyquist plot under current control at 0.5bar closed cathode with 105% at different temperatures.

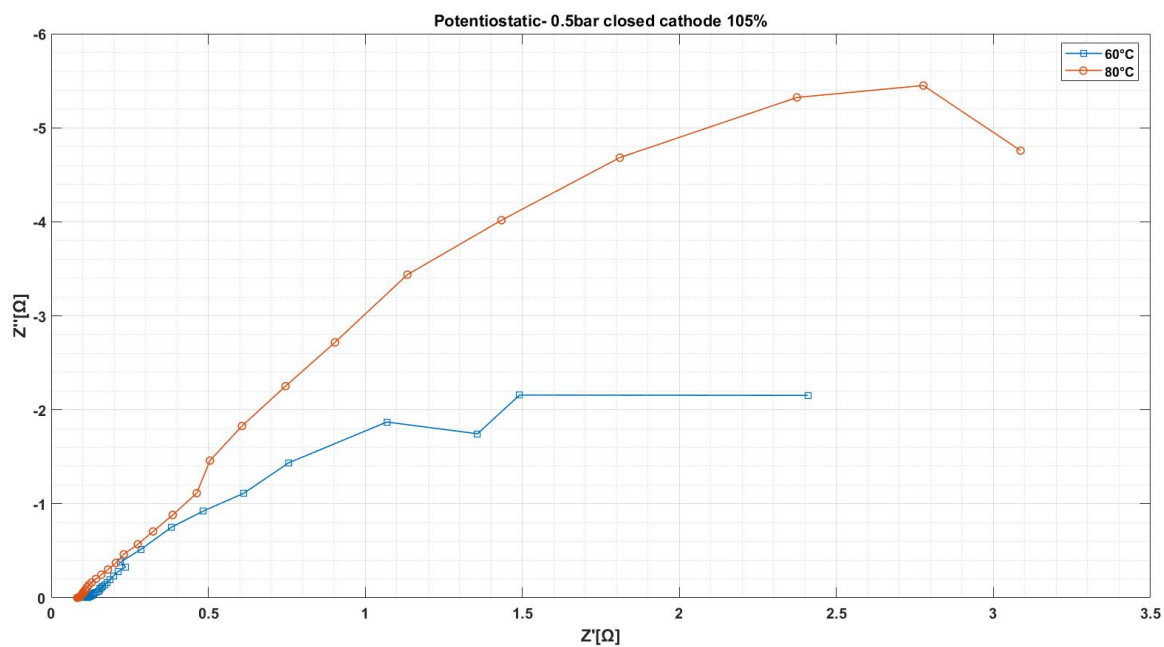


Figure 88 Nyquist plot under voltage control at 0.5bar closed cathode with 105% at different temperatures.

Potentiostatic measurements have one semicircle in the HF region and a second incomplete arc in the mid-low frequency range; same behaviour at high frequency for the galvanostatic which instead shows in the mid low frequency range two other arcs, mostly affected by noise. In both EIS modes the HF intercept with the real axis has lower values at 80°C. Impedance spectra of galvanostatic tests are considered only qualitatively due to the KK non-compliant behaviour, hence they have not been fitted. On the other hand, impedance spectra of the potentiostatic mode have been fitted only considering the HF region, which shows a relative acceptable quality. Tables with all parameters and their errors are presented in the appendix.

## DISCUSSION

Results obtained with potentiostatic tests are subject to a verification through a comparison with the iV-curves measured at 60°C and 80°C.

Both tests are performed at 0V and they have an arc in the high frequency region and a curved line at low frequencies which can be assumed as an uncompleted arc. As the temperature increases, it is observed a general decrease of the ohmic resistance from  $2.572 \Omega/cm^2$  to  $2.012 \Omega/cm^2$ . Instead, capacitance and charge transfer resistance of the HF arc do not show significant variations. The decrease of the ohmic resistance may be related to higher T which has a positive effects on the proton conductivity. The figures below show a comparison between ECM fit and Circle fit. In both cases the trend are the same although there is a small difference between parameters.

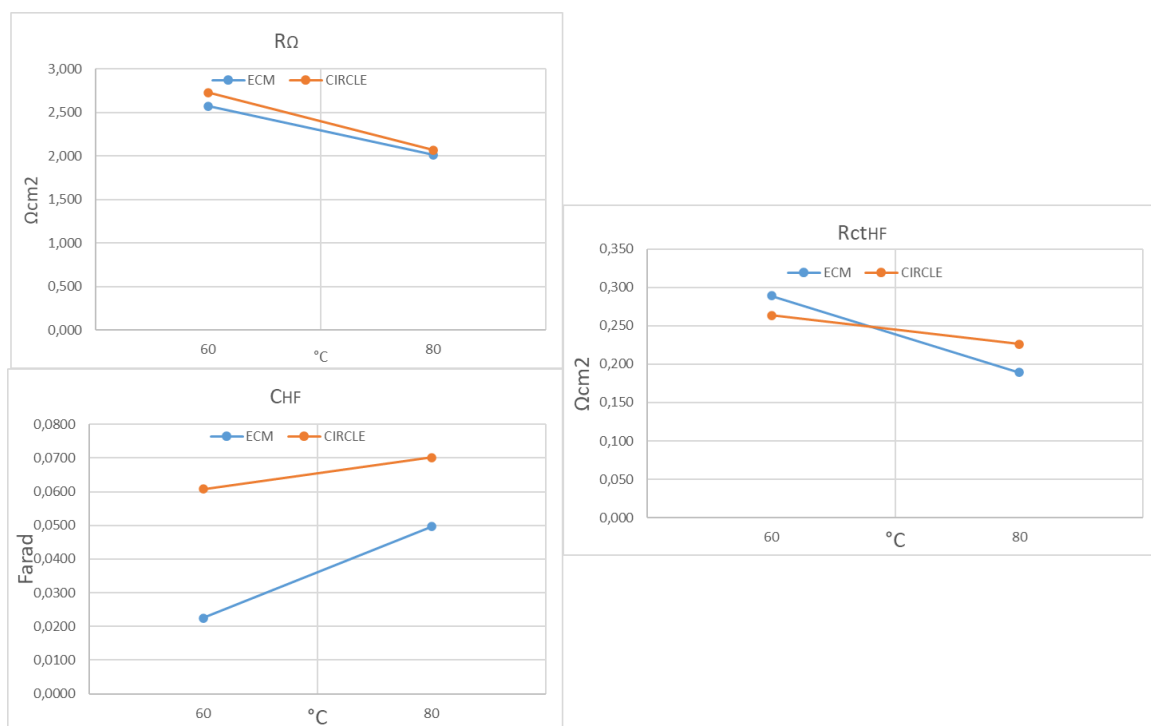


Figure 89

Although galvanostatic tests have shown low quality from KK validation, a qualitative analysis can be done. From the Nyquist plot at OCV it is observed that the total polarization resistance and the ohmic resistance are lower at 80°C, hence it suggests that the test at 80°C has lower voltage near the OCV.

The results obtained from EIS measurement under voltage control and the qualitative analysis of galvanostatic tests are in accordance with the polarization curves. The figure below shows a comparison between the two iV-curves, each taken before performing EIS tests. It is observed that at low current density- where activation losses are dominant- high temperature has a positive effect on the cell performance, i.e. lower voltage at 80°C. This trend is opposite at higher current densities where maybe dehydration effects and/or mass transport limitations become more relevant. The latter is a hypothesis because EIS measurements at high current densities or voltages are not possible due to the device limitations.

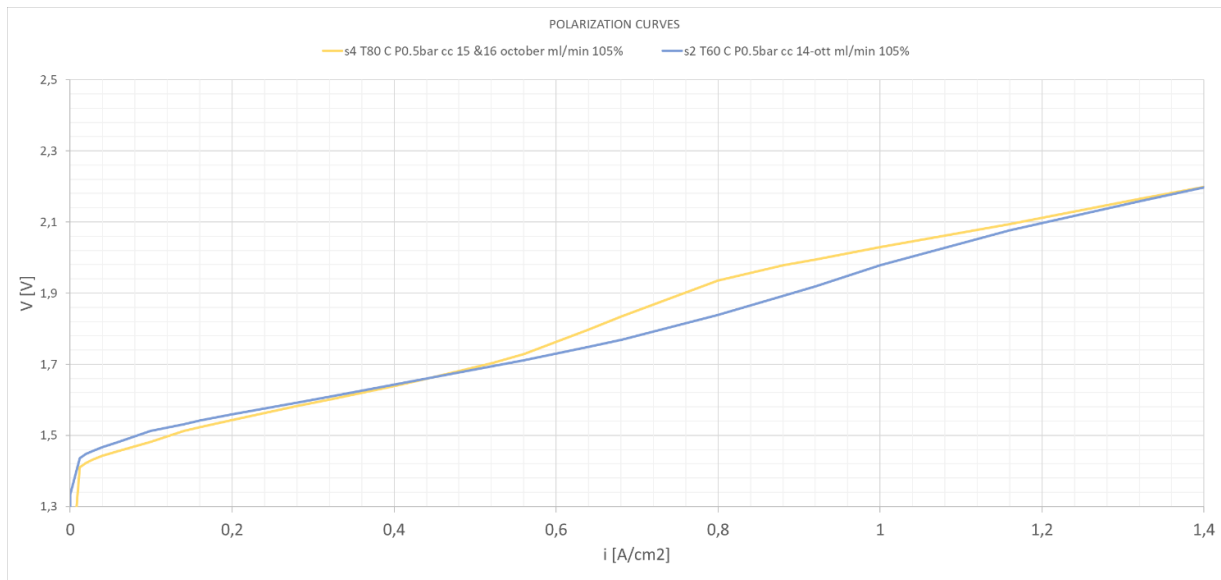


Figure 90 Polarization curves at 60°C and 80°C.

---

### 6.2.3 Test Performed At 80°C With Closed Cathode, Imposed Gauge Pressure 0.5 bar, with different Mass Flow Rates by Pump

The objective of the test is to investigate the effect of mass flow rates on the cell impedance obtained by changing the DC values of the EIS setup. The test is performed at 80°C and 0.5 bar imposed gauge pressure, with closed cathode configuration by imposing the percentage of the chamber displacement of the pump first at 5% then at 20%. Two types of EIS measurements have been used:

- Potentiostatic test, performed at different DC value of voltage (0 V and 1 V) vs Reference by varying the frequency from 100 kHz to 0,001 Hz in single sine mode and using a sinusoidal excitation signal of 10 mV root mean square (rms)
- Galvanostatic test, performed at different DC current -0 mA, 1000 mA, 1500 mA, 2000 mA- by varying the frequency from 200 kHz to 0,002 Hz in single sine mode and using a sinusoidal excitation signal of 1000 mA root mean square (rms).

During the test with 5% pump, the cell temperature was 79.3°C whereas the fluid temperature at the heater was quite high 85°C; the real gauge pressure was 0.4 bar in the anode and 0.2 bar in the cathode. On the other hand, at 20% the cell temperature was 79.5°C, fluid temperature 80°C and real gauge pressure was around 1 bar and 0.4 bar in the anode and cathode respectively.

## **RESULTS**

### *Data quality assessment*

The KK validation shows that both potentiostatic and galvanostatic modes have some tests with low quality impedance spectra which are invalid so not used in the analysis. By visual inspection of both Nyquist and Bode plots two time constants are observed in the impedance spectra under voltage control and at least two for those obtained with the galvanostatic mode. The ECM used to fit experimental data is LR(QR)(QR) due to the presence of noise at low frequency which makes difficult to get good results.

### *Modelling*

The figure below shows a comparison between impedance spectra obtained with potentiostatic mode at 0 V and 1 V with different percentage of the displacement pump. The shape of the impedance consists of an arc at high frequency and a second incomplete semicircle at mid-low frequency.

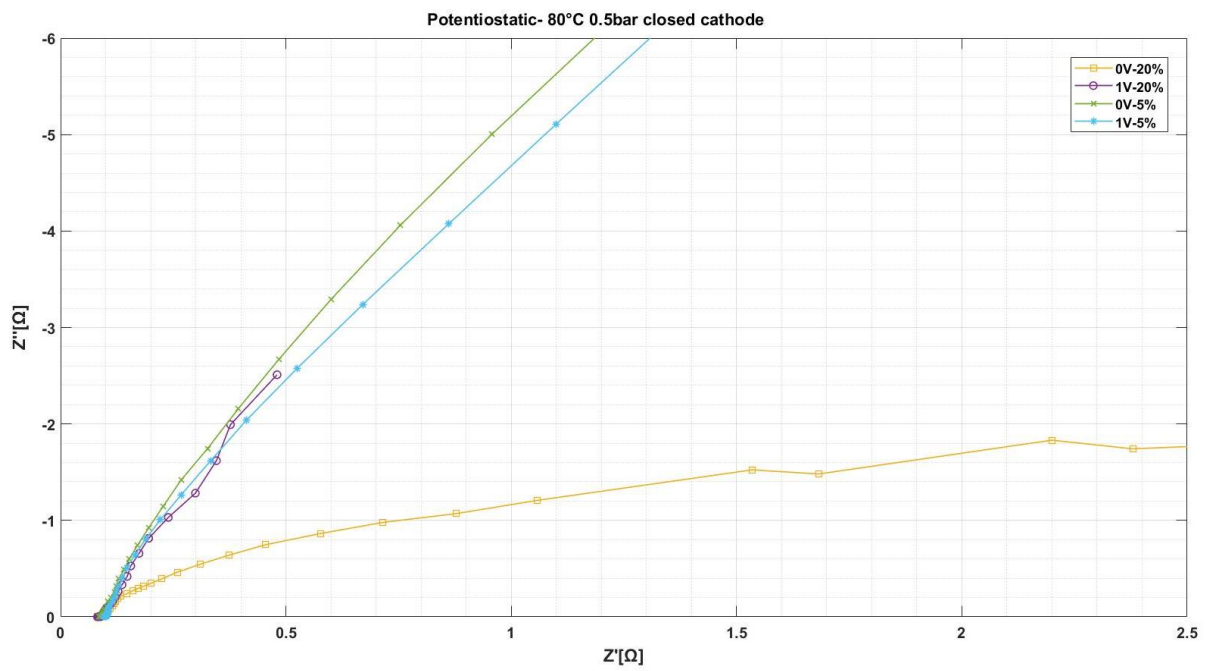


Figure 91 Nyquist plot under voltage control at 80°C 0.5bar closed cathode with different mass flow rates.

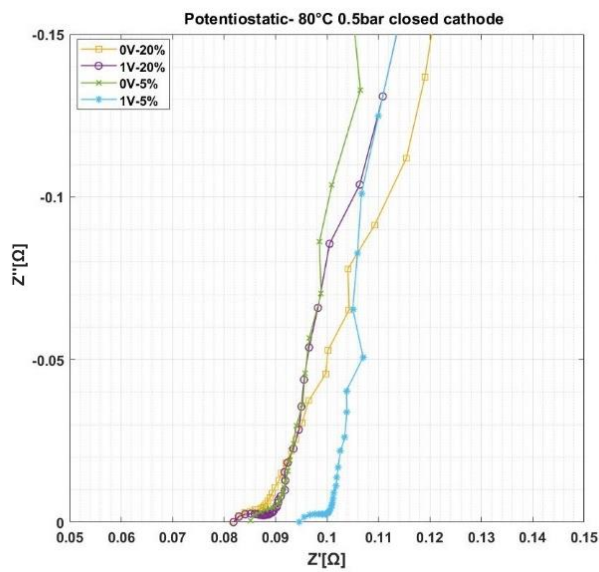


Figure 92

The figure below shows all impedance spectra measured with galvanostatic tests. The shape changes as the DC value is increased. At 0 mA and 1000 mA there are three arcs, one at HF

and the others at mid-low frequency. As the DC current is increased up to 2000 mA the arcs become two and the LF arc tends to reduce as well.

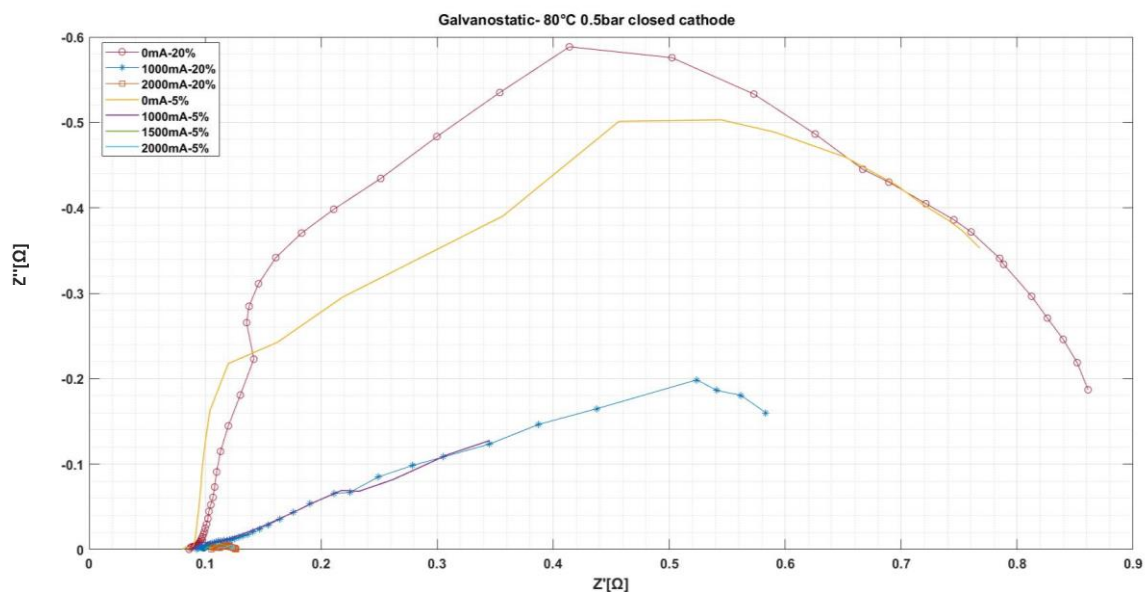


Figure 93 Nyquist plot under current control at 80°C 0.5bar closed cathode with different mass flow rates.

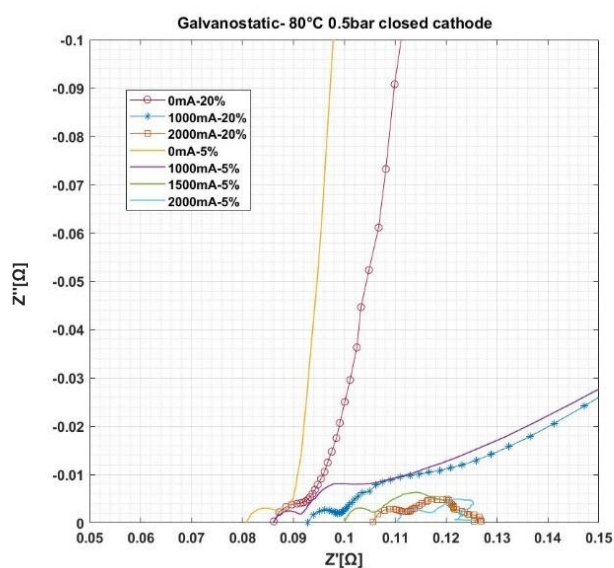


Figure 94

Impedance spectra have been fitted only considering the HF region, which shows a relative acceptable quality. Tables with all parameters and their errors are presented in the appendix.



## DISCUSSION

The analysis is made considering only the results obtained by fitting the HF arc of valid impedance spectra measurements under current control, which are characterized by a better quality with respect to those of the potentiostatic mode. It is observed that at low current densities the ohmic resistance decreases sensibly when the mass flow rates is decreased from 20% to 5%. This may be related to lower pressures with low mass flow rate as shown in *Figure 96*.

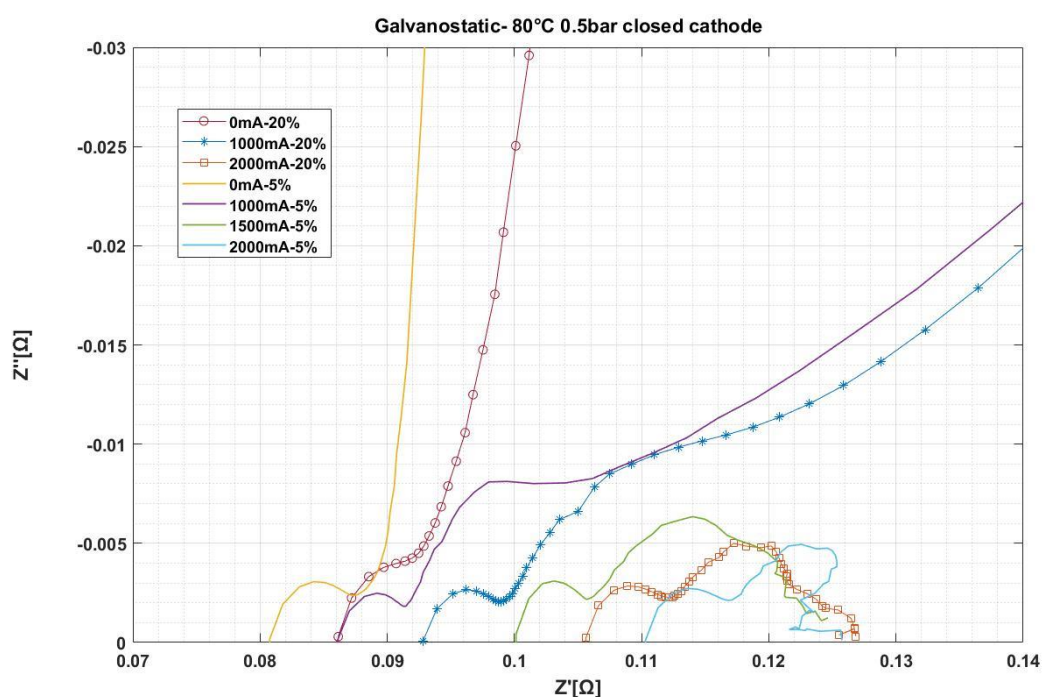


Figure 95

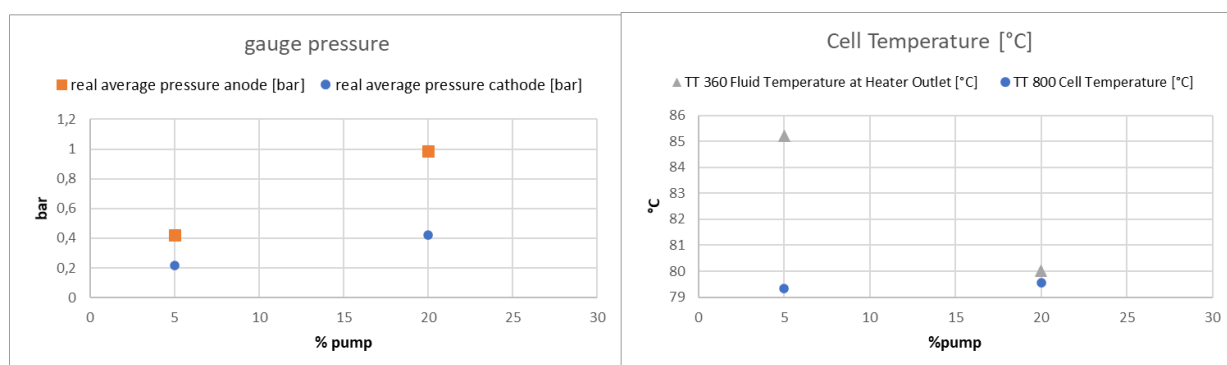


Figure 96

Considering capacitance and charge transfer resistance of the HF arc, these show an unperceivable improvement, i.e. the capacitance slightly increases and the  $R_{ct}$  decreases. Instead, qualitatively it is possible to notice equivalent value of the total polarization resistance between the two pump percentage.

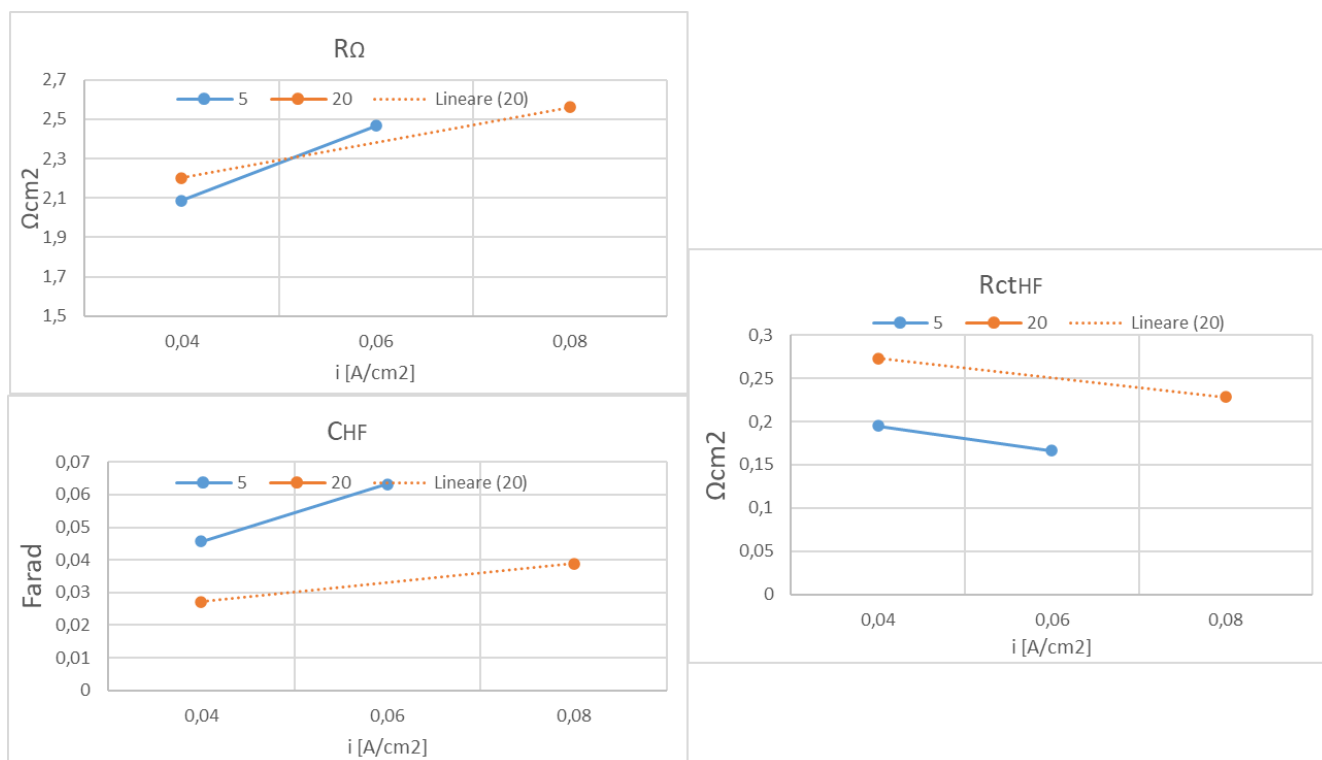


Figure 97

In conclusion, at low current densities and higher temperature, lower mass flow rates thus lower pressures can enhance the performance of the cell.

---

#### 6.2.4 Test performed at 80°C and 60°C, With Closed Cathode, Imposed Gauge Pressure 0.5bar, with 20% Mass Low Rates by Pump

The aim of the test to perform electrochemical characterization of the new cell by carrying out polarization curves and EIS measurements. The test consists of two series, first performed at 80°C and the second at 60°C, both characterized by same operating conditions of 0.5 bar imposed gauge pressure, 20% pump and closed cathode configuration.

Polarization curves were measured by current control up to 2 A/cm<sup>2</sup> whereas two types of EIS measurements have been used:

- Potentiostatic test, performed at different DC value of voltage (from 0 V to 1.5 V) vs Reference by varying the frequency from 100 kHz to 0,001 Hz in single sine mode and using a sinusoidal excitation signal of 10 mV root mean square (rms)
- Galvanostatic test, performed at different DC current -0 mA, 1000 mA, 1500 mA, 2000 mA- by varying the frequency from 200 kHz to 0,002 Hz in single sine mode and using a sinusoidal excitation signal of 1000 mA root mean square (rms).

During the test at 80°C, the cell temperature was 79.5° whereas the fluid temperature at the heater was 80.5°C; the real gauge pressure was around 1 bar in the anode and 0.4 bar in the cathode. On the other hand, during the test at 60°C the cell temperature was 61.5°C, fluid temperature 60.8°C and real gauge pressure was 1 bar and 0.4 bar at the anode and cathode respectively.

## **RESULTS**

### *Data quality assessment*

The KK validation shows a general poor quality of the impedance spectra, especially those obtained with galvanostatic tests. Potentiostatic mode has produced impedance measurements with acceptable quality only in the HF range. The main reason of non-validity of the impedance spectra obtained with galvanostatic tests is the time variance of the cell during its execution, as shown in *Figure 98*. In these figures the larger oscillations of pressure individuate when galvanostatic test have been performed.

The number of time constants observed in the graphical representation are two for potentiostatic and at least three for galvanostatic. The ECM used to fit experimental data is LR(QR)(QR) due to the presence of noise at low frequency which makes difficult to get good results.

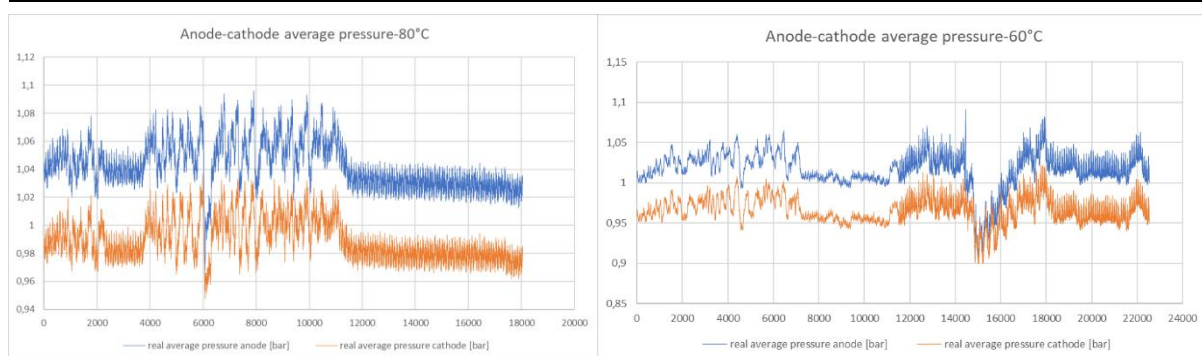


Figure 98 Trend of pressure during potentiostatic and galvanostatic measurements.

### Modelling at 80°C

Nyquist plot below shows the impedance measurement at 80°C, both potentiostatic and galvanostatic. Impedance spectra under voltage control are characterized by an arc at high frequency and a straight line/second incomplete arc at mid-low frequency (some tests were interrupted before reaching the lowest frequency due to noise, this explains the difference in shape at lower frequencies). On the other hand, under current control the shape changes as the DC value is increased. At 0 mA and 1000 mA there are three arcs, one at HF and the others at mid-low frequency. As the DC current is increased up to 2000 mA the arcs become two and the LF arc tends to reduce.

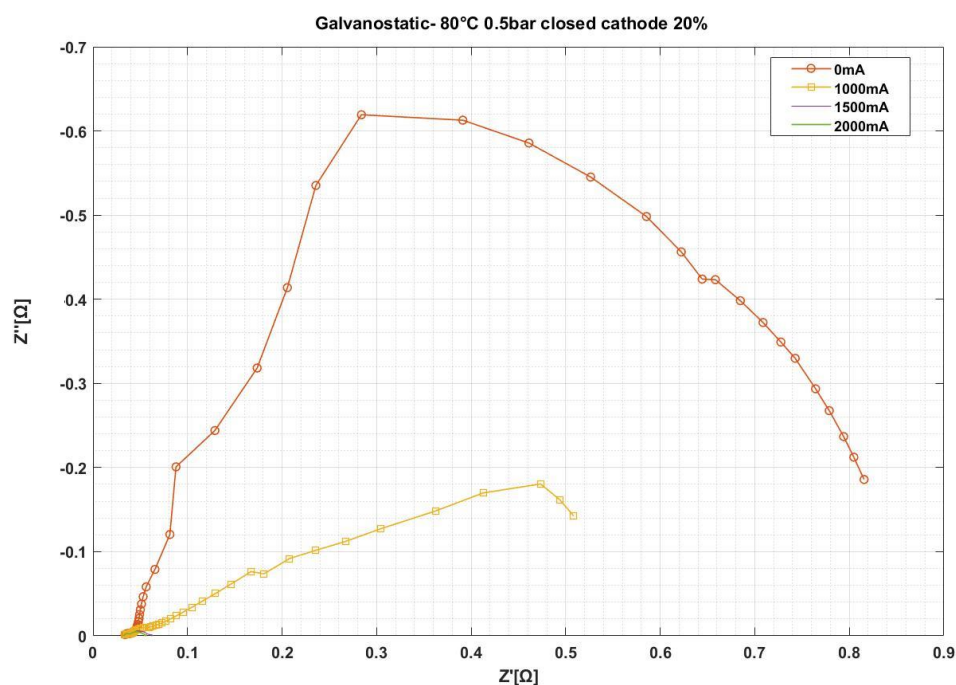


Figure 99 Nyquist plot under current control at 80°C 0.5bar closed cathode with 20% pump.

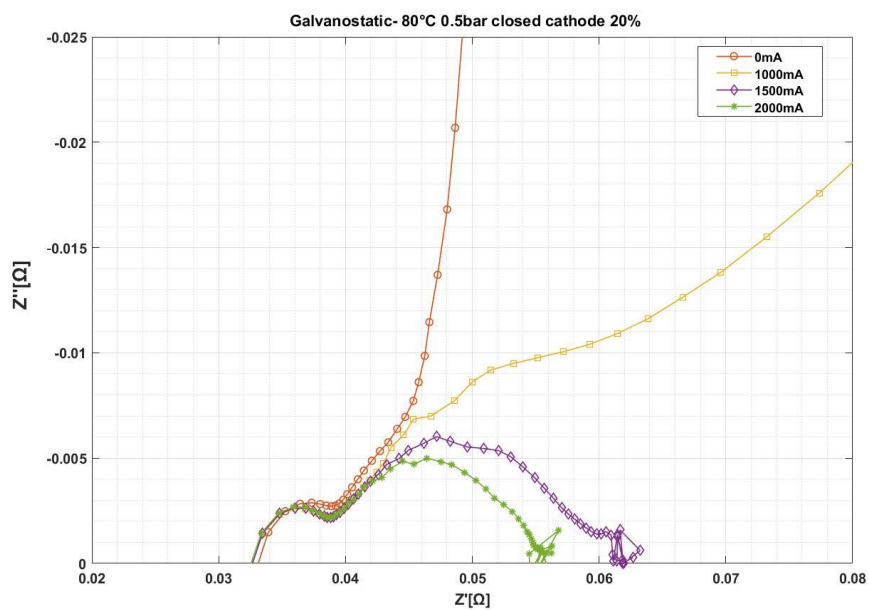


Figure 100 Zoom of Nyquist plot under current control at 80°C 0.5bar closed cathode with 20% pump.

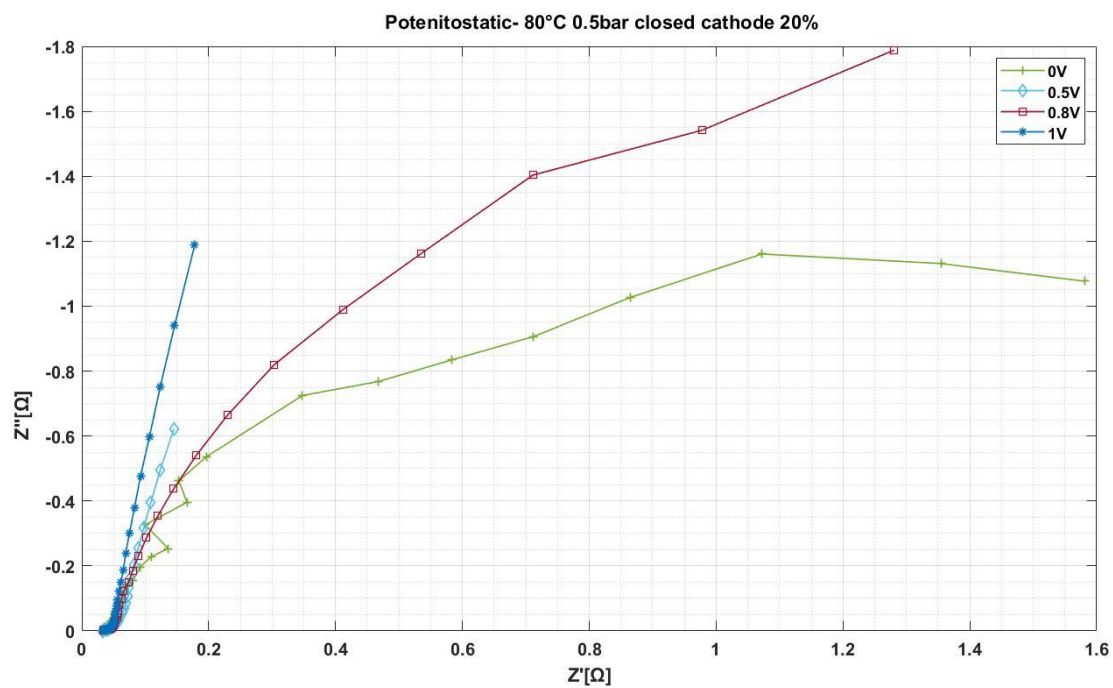


Figure 101 Nyquist plot under voltage control at 80°C 0.5bar closed cathode with 20% pump.

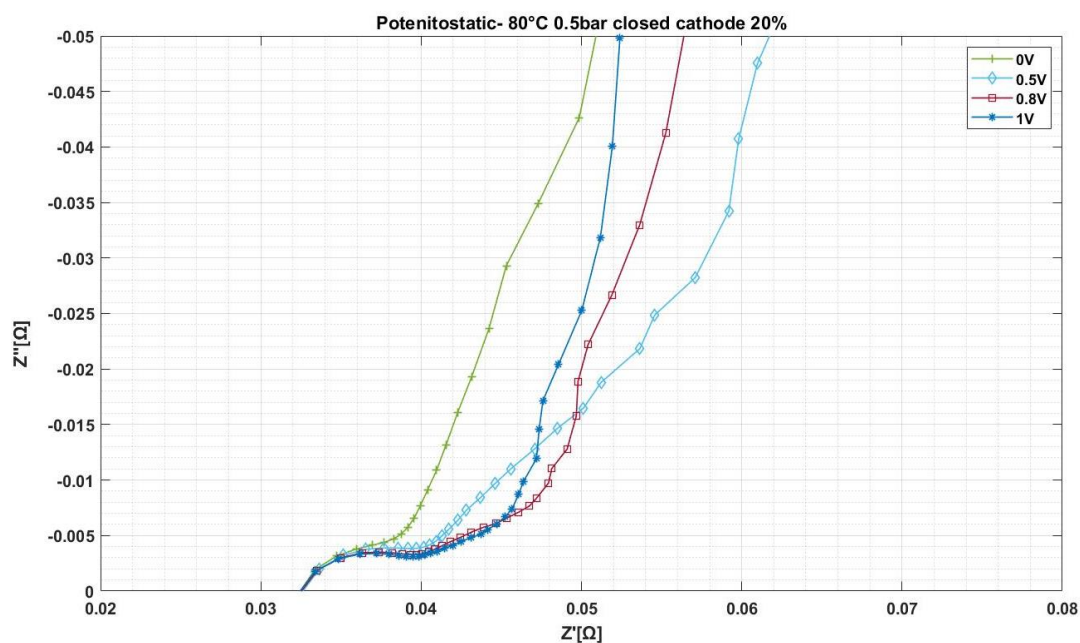


Figure 102 Zoom of Nyquist plot under voltage control at 80°C 0.5bar closed cathode with 20% pump.

### Modelling at 60°C

Figures below show the EIS measurements at the end of the test at 60°C.

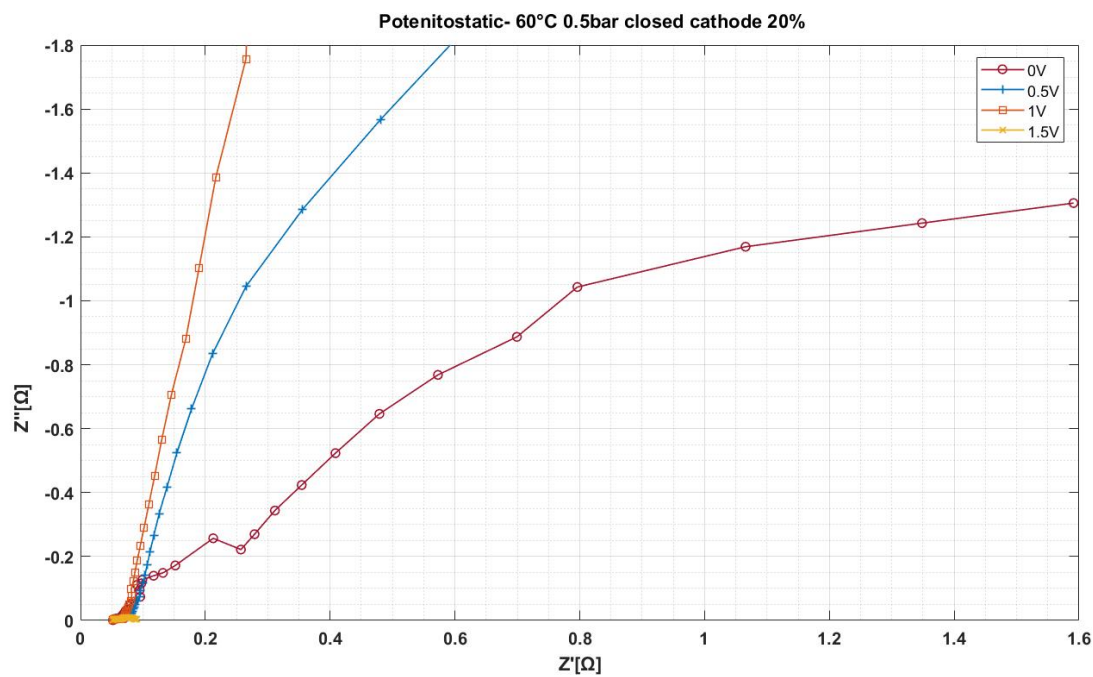


Figure 103 Nyquist plot under voltage control at 60°C 0.5bar closed cathode with 20% pump.



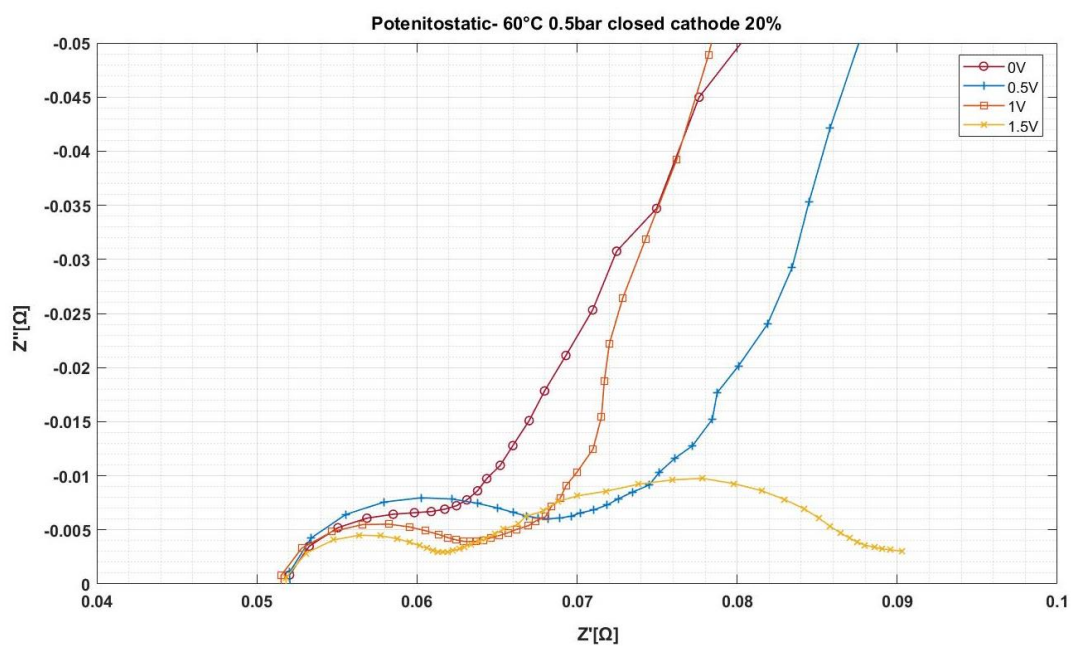


Figure 104 Zoom of Nyquist plot under voltage control at 60°C 0.5bar closed cathode with 20% pump.

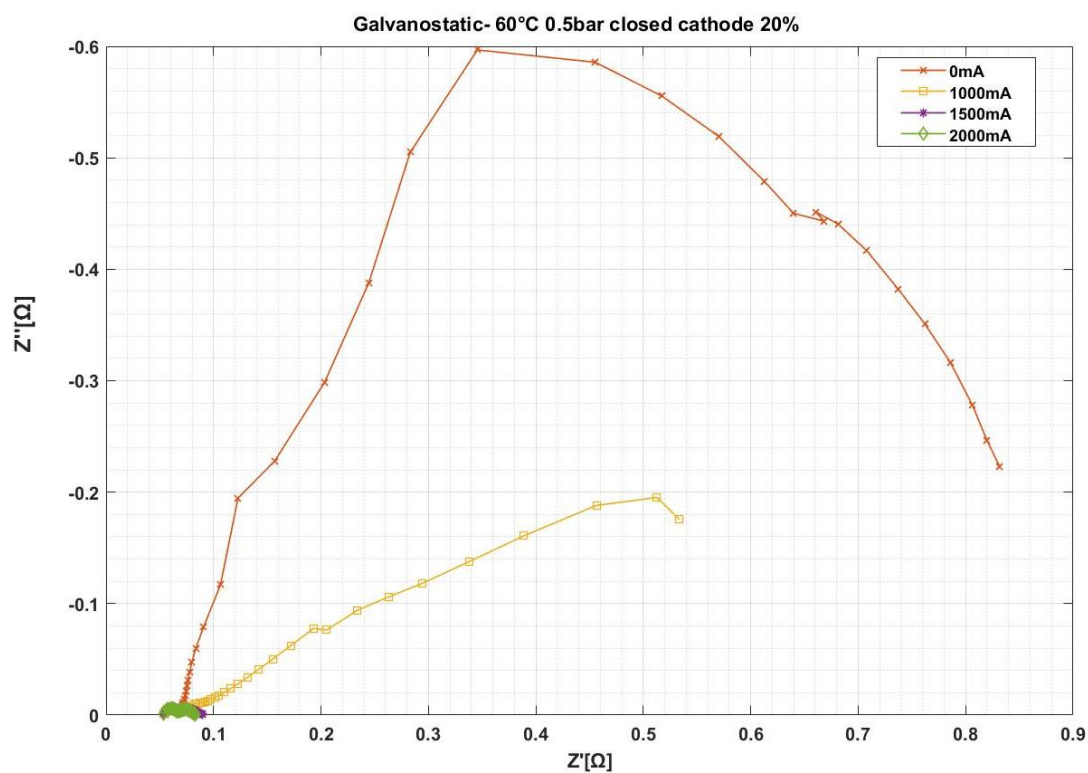


Figure 105 Nyquist plot under current control at 60°C 0.5bar closed cathode with 20% pump.

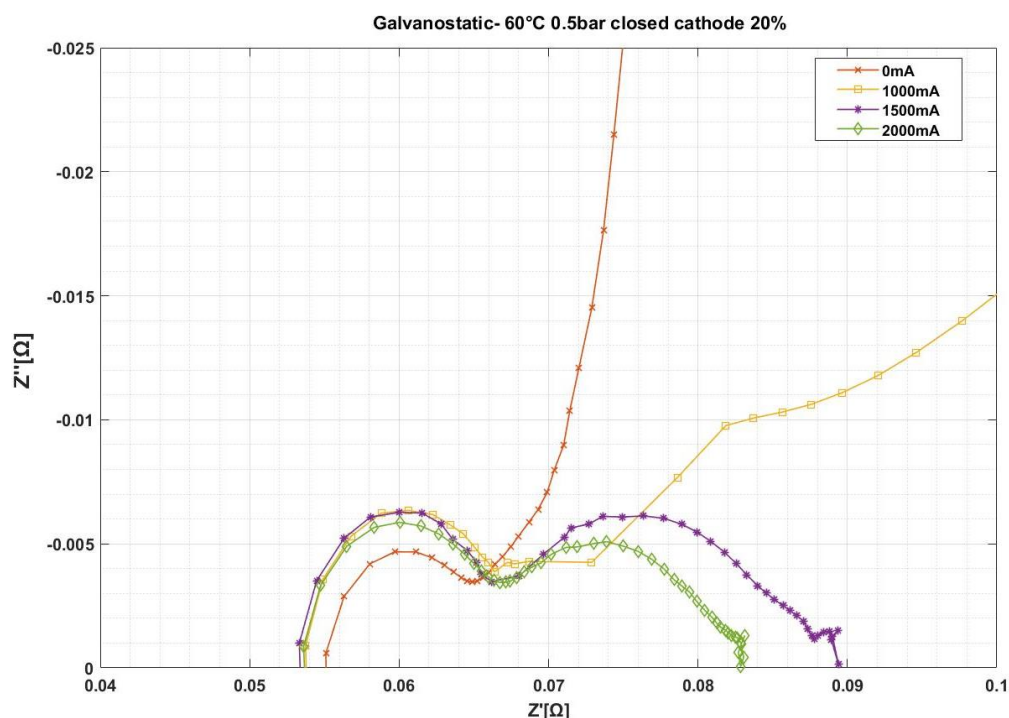


Figure 106 Zoom of Nyquist plot under current control at 60°C 0.5bar closed cathode with 20% pump.

Impedance spectra under voltage control are characterized by an arc at high frequency and a straight line/second incomplete arc at mid-low frequency. The low frequency features shows a dependence on voltage: as the DC value of potential increases, this tends to bend down towards the real axis. In fact, at 1.5 V a second arc is clearly visible. Same consideration for tests performed under current control, i.e. the shape changes as the DC value is increased.

## DISCUSSION

### Considerations on tests performed at 80°C

Results obtained by fitting the impedance spectra measured under current control are analysed from a qualitative point of view. First, it is observed a dependence on current density principally related to the LF arc. As the current density increases it is noticed that the LF arc is characterized by a decrease of charge transfer resistance while its capacitance  $C$  increases; so the LF semicircle becomes smaller. Considering that in the range 0-2 A (so 0-0,08 A/cm<sup>2</sup> current density) we are in the activation domain and that the LF arc shows a dependence on current density, it is suggested that the LF arc is controlled by the charge-transfer kinetics. It means that in the Nyquist plot the LF arc is related to OER and HER. The presence of noise makes impossible to say if mass transport processes are present.



Instead, the HF arc and the ohmic resistance show an almost constant trend. Hence, it is possible to assess that the HF arc is current independent. This means that is not related to kinetics processes but rather to the MEA structure.

About potentiostatic tests, the analysis of the fitting results concerns only valid spectra which are those obtained in the range 0.5-1 V and it is focused on the HF region of the spectra where quality is higher. It is possible to notice that the ohmic resistance is not varying significantly with voltage (from 0.770 to 0.730  $\Omega\text{cm}^2$ ), the same thing for the HF arc which remains almost constant in this range. In fact, the maximum frequency is constant at 251.2 Hz. Figures below show a comparison between ECM fit and Circle fit. The trend is similar for both types of fit. In the ECM fit mode the result at 0.8 V is considered an outlier due to higher error of the fit.

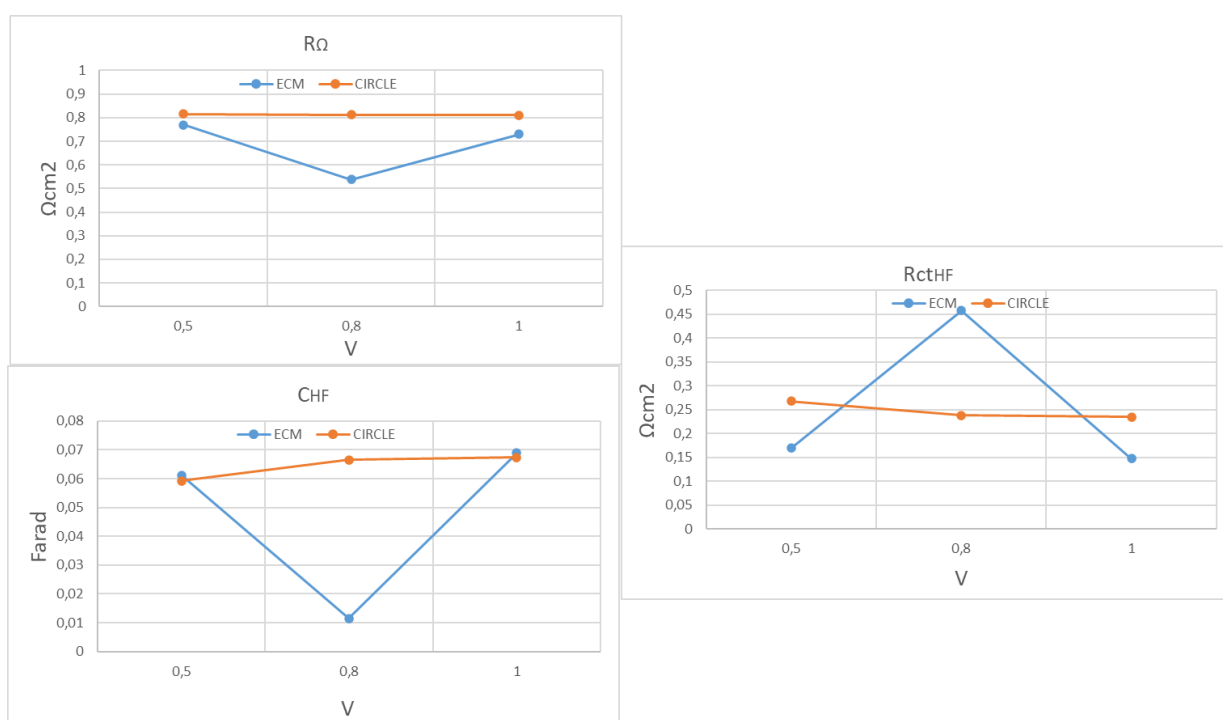


Figure 107 Trend of the HF parameters at 60°C with 20% pump.

### Considerations on tests performed at 60°C

The analysis is focused on the EIS measurements performed at the end of the test. Only good impedance spectra are considered, thus 1500 mA and 2000 mA for the galvanostatic mode and the range 0.5-1.5 V for the potentiostatic mode.

As the current increases in the range 1.5-2 A we have that at LF the charge transfer resistance decreases from 0.583 to 0.428  $\Omega\text{cm}^2$  and the capacitance C is almost constant at 4-4.1 F, so the LF semicircle becomes smaller. Instead, the HF arc in the same range is characterized by an almost constant value of the charge transfer resistance HF (from 0.37 to 0.39  $\Omega\text{cm}^2$ ) and capacitance (from 0.034 to 0.03 F), whereas the ohmic resistance is almost constant around 1.25-1.24  $\Omega\text{cm}^2$ .

Considering the range 0.5-1.5 V, it is possible to notice that the ohmic resistance is not varying significantly with voltage (from 1.178 to 1.200  $\Omega\text{cm}^2$ ), whereas as the voltage increases, we have that the LF arc bends down to the real axis. Moreover, at LF the charge transfer resistance decreases and the capacitance C increases, so the LF semicircle becomes smaller. The high frequency arc, characterized by  $R_{ct}$  and C, shows a very slight decrease with voltage: in particular, capacitance is increased while the charge transfer resistance shows lower value with higher voltage level.

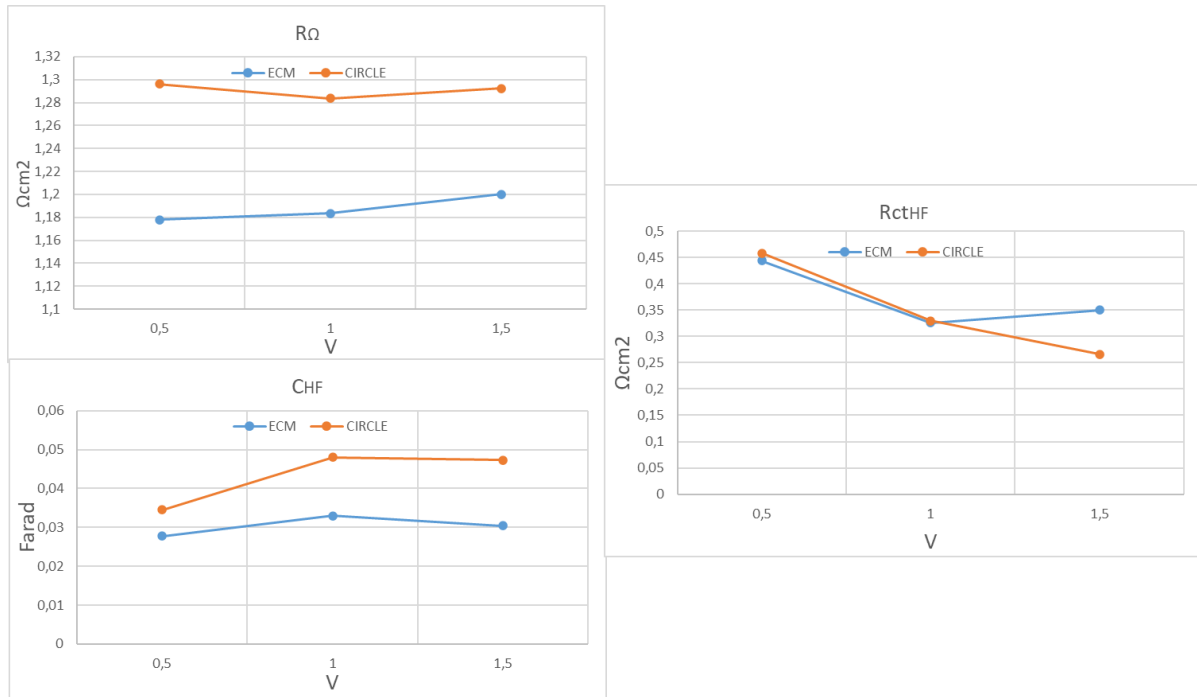


Figure 108 Trend of the HF parameters at 80°C with 20%pump.

### Comparison Between 80°C And 60°C At 20% Pump

Polarization curves show that the performance of the cell improves at higher temperatures. This result is in accordance with the findings of the EIS tests. First of all, the trends in *Figure 110* show that the HF feature is improved at higher temperature. Further on, a qualitative comparison between impedance spectra obtained with galvanostatic tests allows to say that total polarization resistance is smaller at 80°C, hence not only the electrolyte benefits from higher temperature but also the anode.

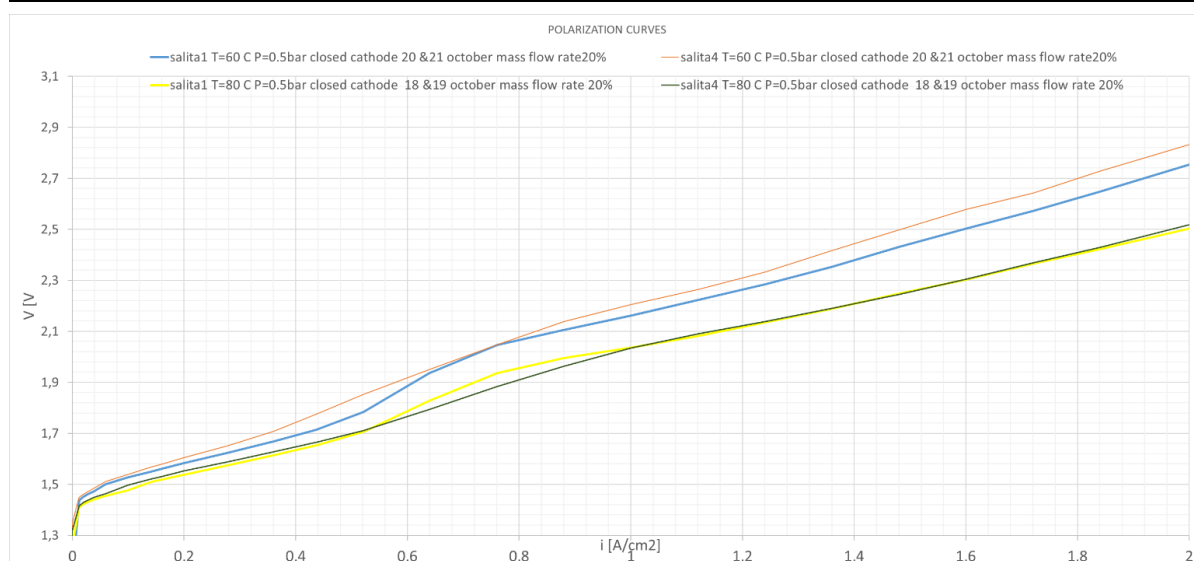


Figure 109

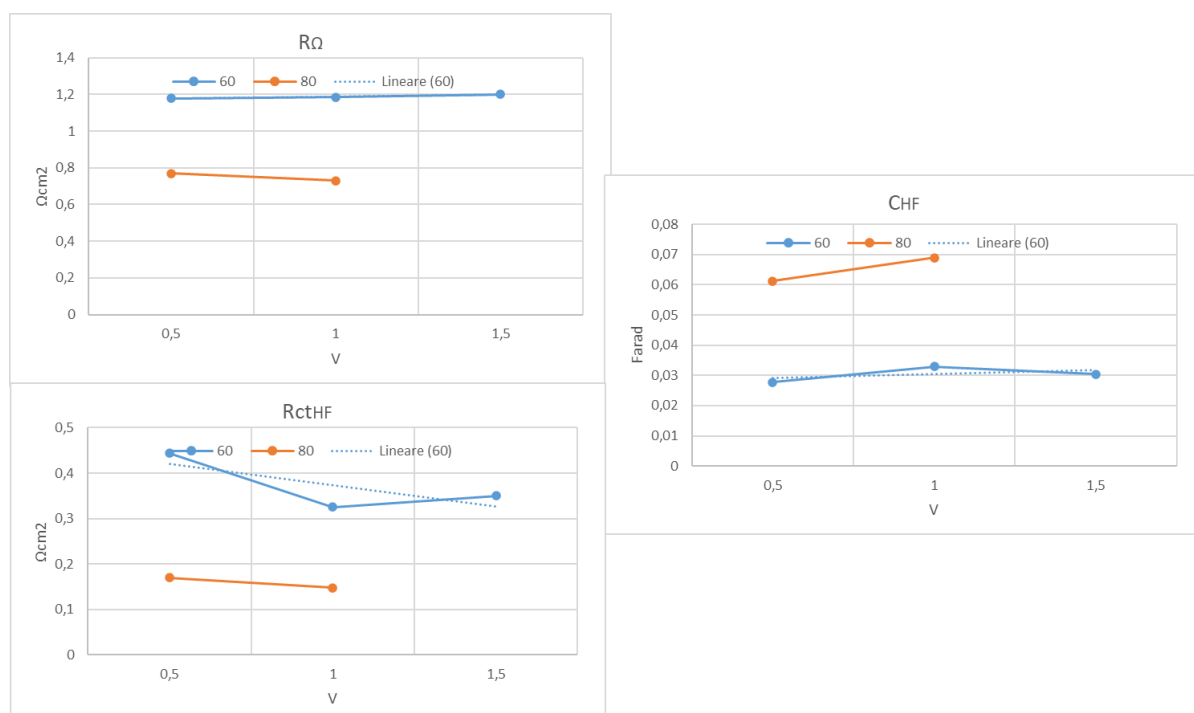


Figure 110 Comparison between 80°C and 60°C of the HF parameters with 20% pump.

---

#### 6.2.5 Test Performed At 60°C, Imposed Gauge Pressure 0.5bar, with 10% Mass Low Rates by Pump With closed Cathode configuration

The aim of the test to perform electrochemical characterization of the new cell by carrying out polarization curves and EIS measurements. The test is performed at 60°C and 0.5 bar imposed gauge pressure, with closed cathode configuration and 10% pump. Polarization curves are carried out by imposing the current and measuring the voltage whereas two types of EIS measurements have been used:

- Potentiostatic test, performed at different DC value of voltage (0 V, 0.5 V, 1 V, 1.5 V) vs Reference by varying the frequency from 100 kHz to 0,001 Hz in single sine mode and using a sinusoidal excitation signal of 10 mV root mean square (rms)
- Galvanostatic test, performed at different DC current -0 mA, 1000 mA, 1500 mA, 2000 mA- by varying the frequency from 200 kHz to 0,002 Hz in single sine mode and using a sinusoidal excitation signal of 1000 mA root mean square (rms).

During the test the cell temperature was 61.5°C whereas the fluid temperature at the heater was 60°C; the real gauge pressure is 0.75 bar in the anode and 0.4 bar in the cathode.

### **RESULTS**

#### *Data quality assessment*

The KK validation shows a general poor quality of the impedance spectra, especially those obtained with galvanostatic tests. Potentiostatic mode has produced impedance measurements with acceptable quality only in the HF range. The ECM used to fit experimental data is LR(QR)(QR) due to the presence of noise at low frequency which makes difficult to get good results.

#### *Modelling*

Impedance spectra under voltage control are characterized by an arc at high frequency and a straight line/second incomplete arc at mid-low frequency. The low frequency features shows a dependence on voltage: as the DC value of potential increases this tends to bend down towards the real axis. In fact, at 1.5 V a second arc is clearly visible. Same consideration for tests performed under current control, i.e. the shape changes as the DC value is increased. At 0mA and 1000 mA there are three arcs, one at HF and the others at mid-low frequency. As the DC current is increased up to 2000 mA the arcs become two and the LF arc tends to reduce.

Figures below show the EIS measurements at the end of the tests at 60°C.

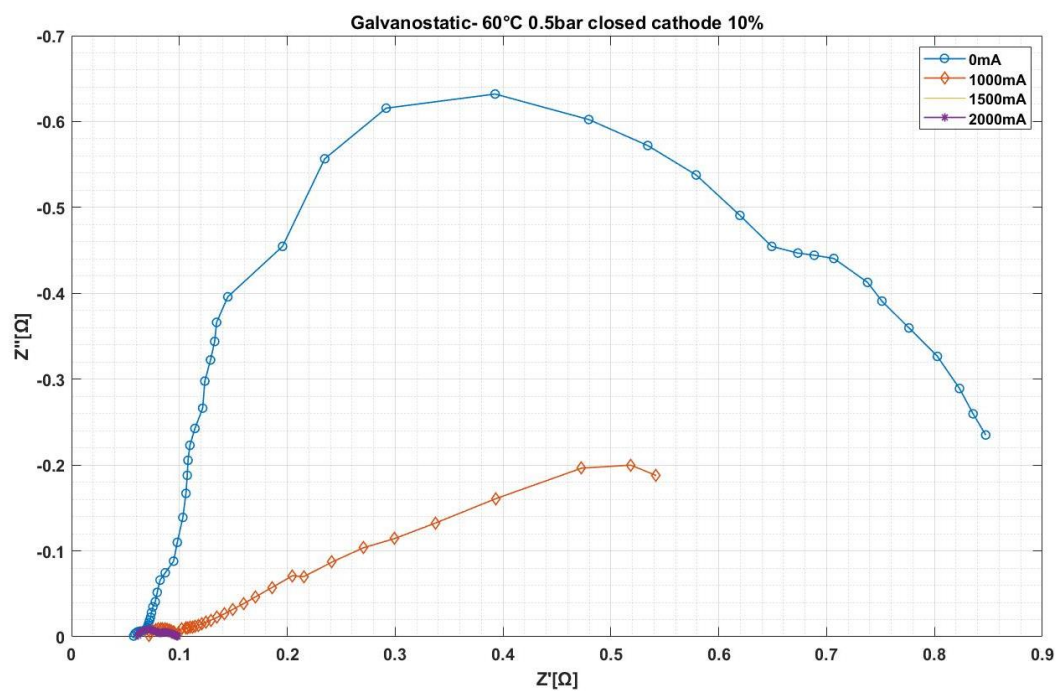


Figure 111 Nyquist plot under current control at 60°C 0.5bar closed cathode with 10% pump.

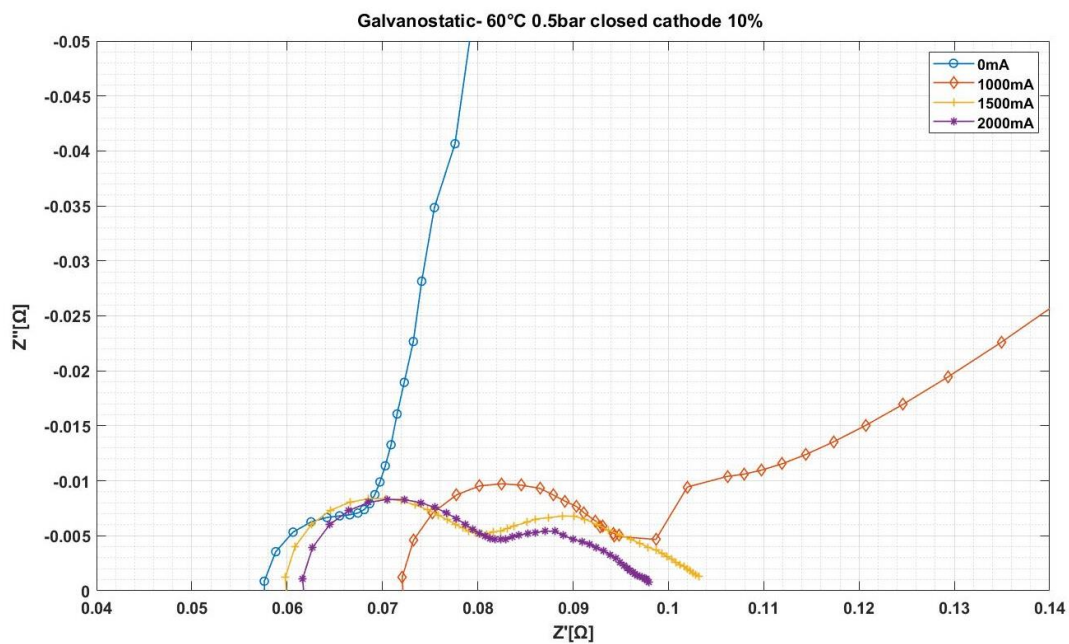


Figure 112 Zoom of Nyquist plot under current control at 60°C 0.5bar closed cathode with 10% pump.

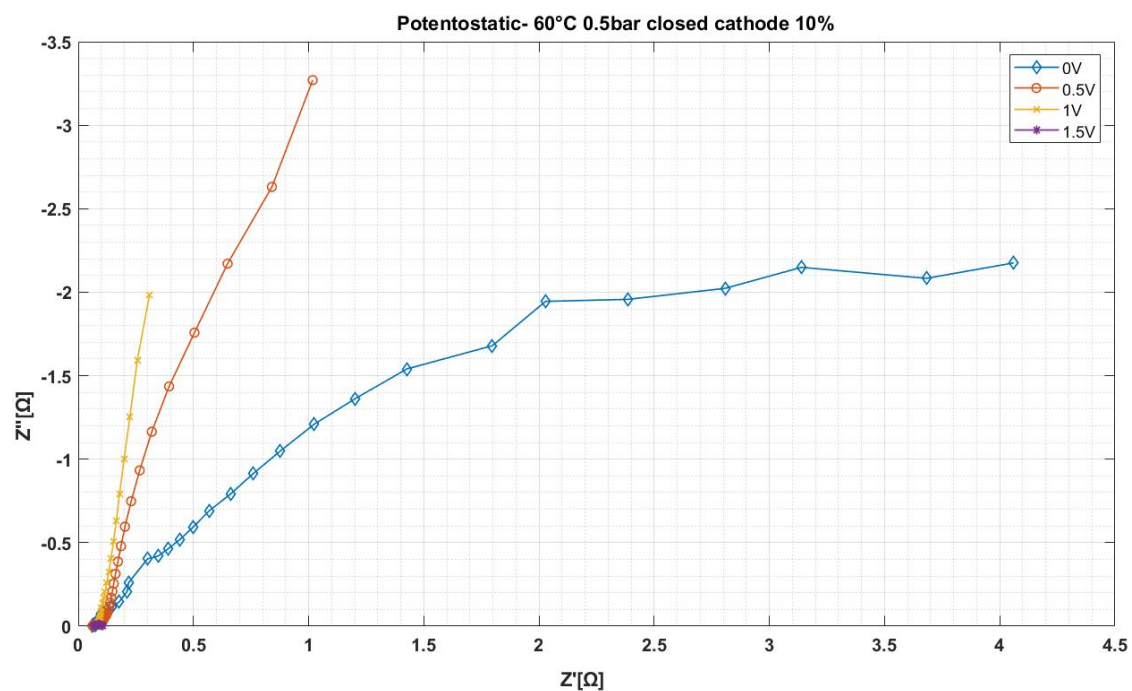


Figure 113 Nyquist plot under voltage control at 60°C 0.5bar closed cathode with 10% pump.

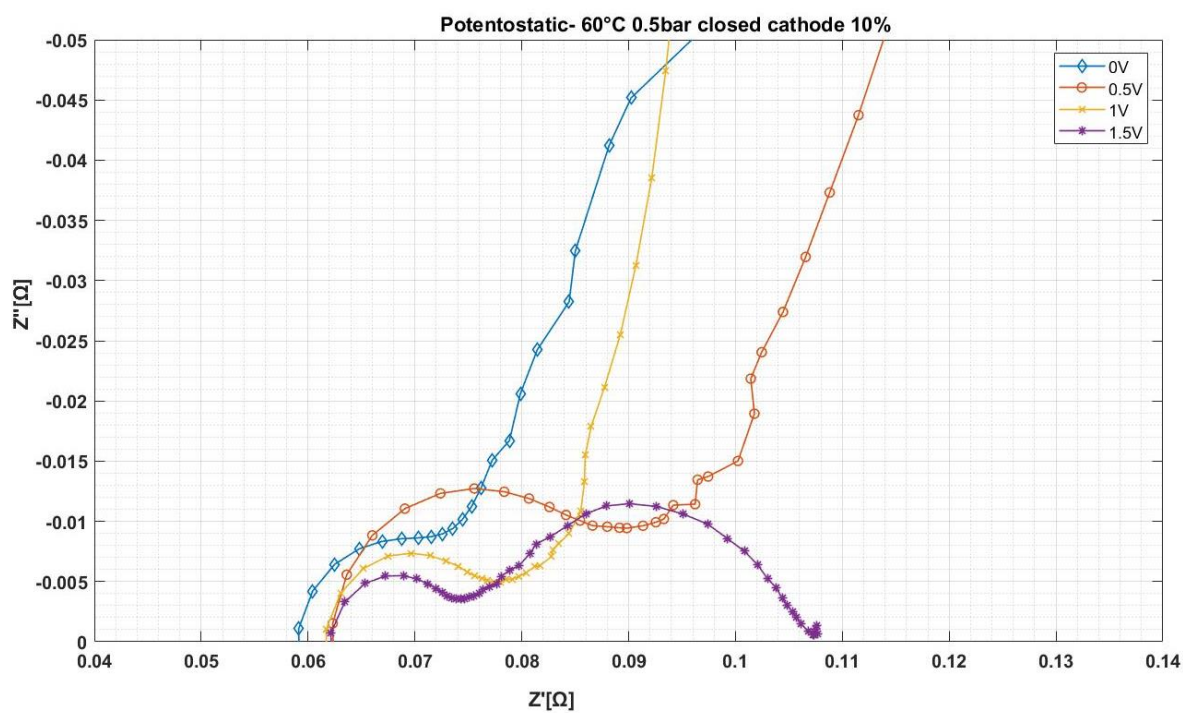


Figure 114 Nyquist plot under voltage control at 60°C 0.5bar closed cathode with 10% pump.

## DISCUSSION

The analysis is performed using the results of the potentiostatic tests in the range 0.5-1.5 V done at the end of the test. Considering the range 0.5-1.5V, it is possible to notice that the ohmic resistance is not varying significantly with voltage (from 1.34 to 1.37  $\Omega\text{cm}^2$ ), whereas as the voltage increases, we have that the LF arc bends down to the real axis. Moreover, at LF the charge transfer resistance decreases and the capacitance C increases, so the LF semicircle becomes smaller. The high frequency arc, characterized by  $R_{ct}$  and C, shows a very slight decrease with voltage: in particular, capacitance is increased while the charge transfer resistance shows lower value with higher voltage level. The figures below make a comparison between two types of fitting, ECM and Circle fit. The high difference shown by these trends is probably related to the not perfect modelling of ECM fit to the experimental data.

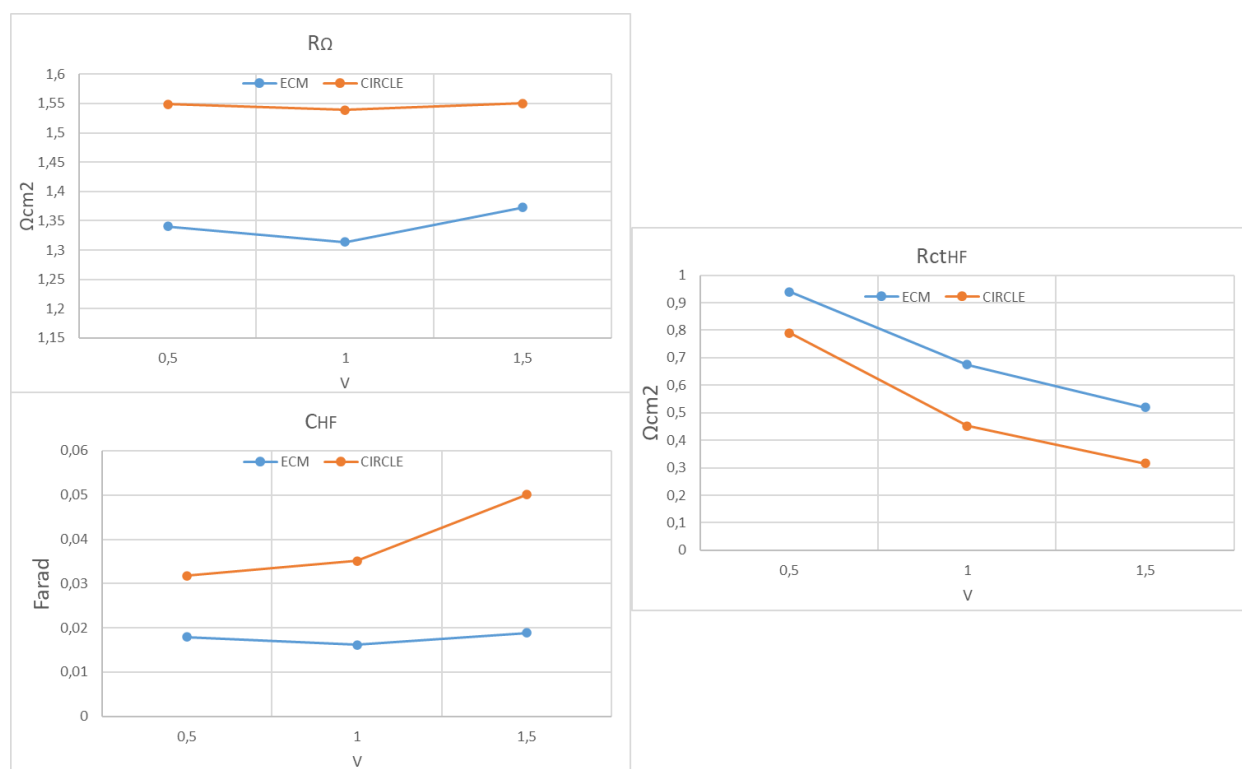


Figure 115 Trend of the HF parameters at 60°C and 10%pump.

---

## Conclusion

EIS tests performed in both modes- potentiostatic and galvanostatic- at different DC value have produced results in accordance with the findings of the open cathode tests: high frequency is current/voltage independent thus related to the MEA structure whereas the mid-low frequency arc is correlated to kinetics process due to its dependence on the current density and voltage.



## 6.3 Open vs Closed cathode tests

### 6.3.1 Tests performed at gauge pressure 1.4 bar, with open/closed cathode at different temperatures

The objective of the experiment is to investigate the influence of temperature and different cathode configurations on the cell impedance by carrying out EIS tests.

It consists of two series: the *first series* is done with *open cathode* with real imposed gauge pressure of 1,84bar in the anode and 1,83bar in the cathode and T going from 70°C to 40°C. The *second series* is done with *closed cathode* with real imposed gauge pressure of 2,38bar in the anode and 1,35bar in the cathode and T going from 50°C up to 80°C. After stabilization of the system at each value of temperature, EIS tests are executed. These are:

- Potentiostatic test, performed at 0 DC V vs Open circuit by varying the frequency from 100kHz to 1Hz in single sine mode and using a sinusoidal excitation signal of 10mV root mean square (rms).
- Galvanostatic test, performed at 0 DC mA by varying the frequency from 200kHz to 0,2Hz in single sine mode and using a sinusoidal excitation signal of 1000 mA root mean square (rms).

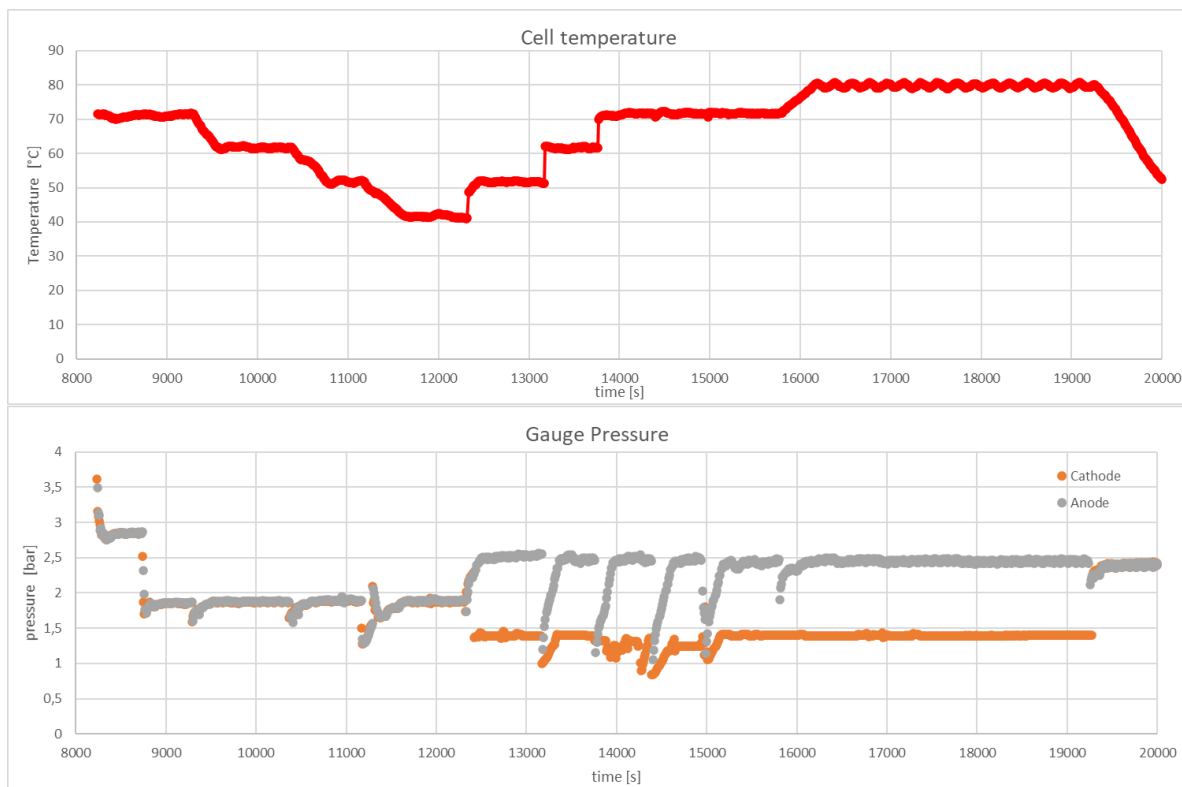


Figure 116 Trend of cell temperature and gauge pressure in the anode and cathode.

---

## RESULTS OF OPEN AND CLOSED CATHODE

### Data quality assessment

The KK validation shows that impedance spectra obtained under voltage control are characterized by lower residuals, whereas impedance data gained with galvanostatic tests are affected by time variance of the cell behaviour. In Nyquist spectra the shape is made of a semicircle in the HF and a second incomplete semicircle/straight line in the mid frequency region, corresponding to two time constants in the Bode plots. Hence, the ECM used to fit is LR(QR)(QR).

### Modelling

Figure 117 and 118 show impedance spectra obtained with potentiostatic tests, with open and closed cathode respectively. The high frequency arc is not much affected by the temperature in both cathode configurations, whereas the second incomplete arc shows a different behaviour: with open cathode no relevant changes are seen but with closed it bends down to the real axis as temperature decreases. The EIS data obtained with closed cathode at 51°C is in contrast with the trend shown by the other impedance spectra of the same series. The imaginary part of all HF arcs reaches a maximum at  $\omega_{max}$  equal to 158.5 Hz for open cathode; for closed cathode is 125.9 Hz, except for 80°C characterized by  $\omega_{max}$  equal to 158.9 Hz.

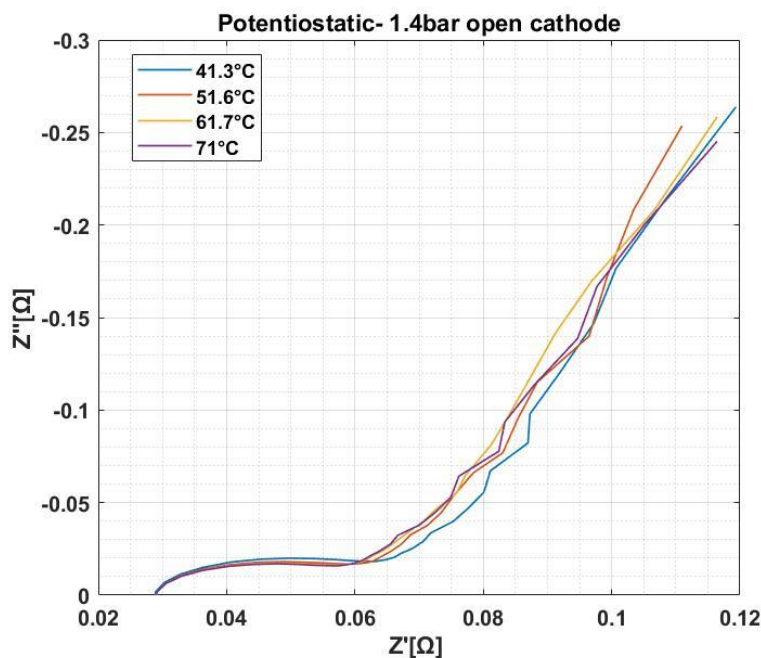


Figure 117 Nyquist plot under voltage control at 1.4bar open cathode with different temperatures.

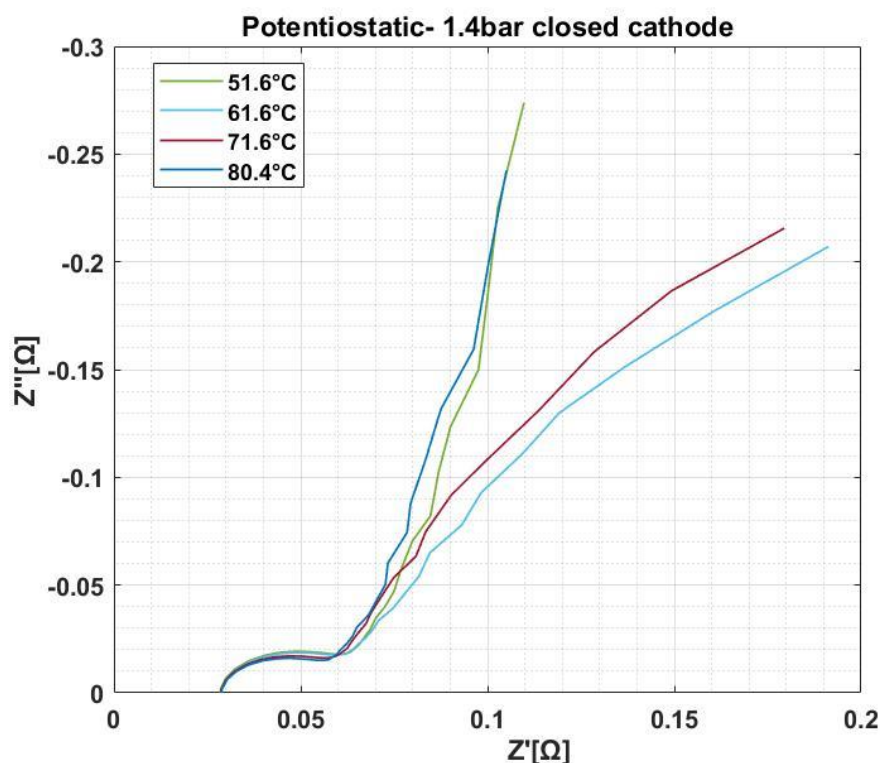


Figure 118 Nyquist plot under voltage control at 1.4bar closed cathode with different temperatures.

Figure 119 and 120 show impedance spectra obtained with open and closed cathode during galvanostatic tests. As before, the high frequency arc is not much affected by temperature in both cathode configurations, whereas the second incomplete arc shows a different behaviour: with open cathode no relevant changes are seen but with closed it bends down to the real axis as temperature decreases. The EIS data at low frequency obtained with closed cathode at 51°C are in contrast with the trend shown by the other impedance spectra of the same series. The imaginary part of all HF arcs reaches a maximum at  $\omega_{max}$  equal to 158.5 Hz for open cathode except for 41°C characterized by  $\omega_{max}$  equal to 126.2 Hz.; for closed cathode is 126.2 Hz at 71°C and 601°C, whereas 80°C and 51°C have  $\omega_{max}$  equal to 158.9 Hz.

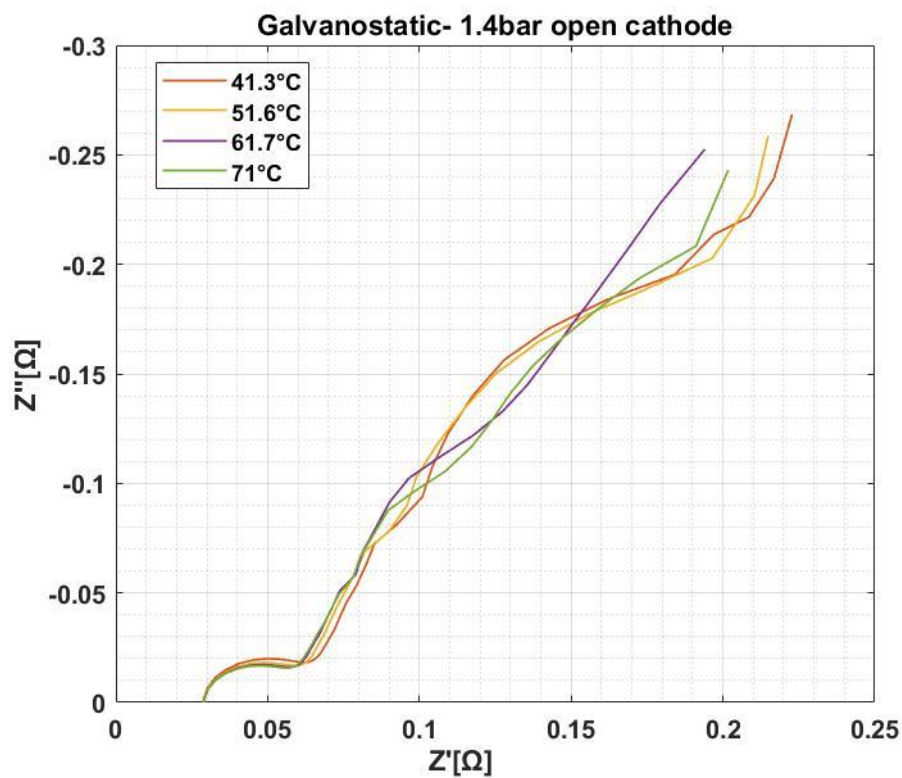


Figure 119 Nyquist plot under current control at 1.4bar open cathode with different temperatures.

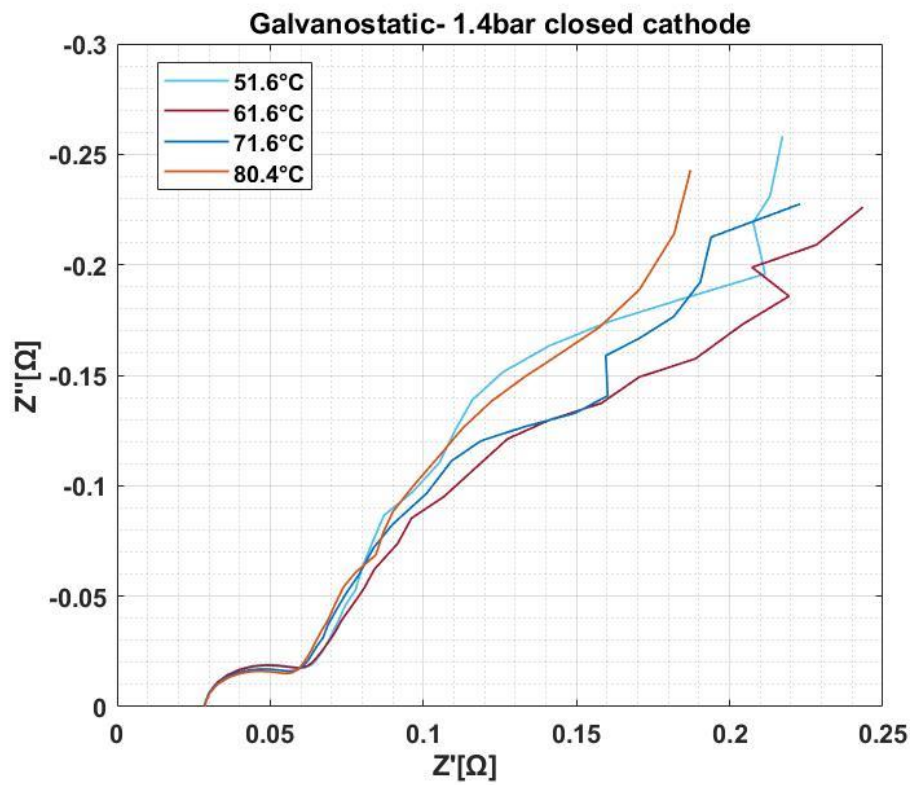


Figure 120 Nyquist plot under current control at 1.4bar closed cathode with different temperatures.

## DISCUSSION

Results gained from potentiostatic tests are discussed. It is possible to analyse the high frequency region- represented by the semicircle- by measuring the ohmic resistance, intercept of the high frequency arc with the real axes, and the charge transfer resistance, represented by the intercept at mid frequency.

Considering the effect of temperature, it is observed a clear dependence on T of all parameters. It is noticed a higher dependence during closed cathode whereas during open cathode the variation in the parameters values is negligible. In particular, open cathode shows an enhancement of charge transfer resistance (increment from 0.736 to 0.925  $\Omega\text{cm}^2$ ) and capacitance (from 0.035 to 0.018 F), whereas the ohmic resistance is almost constant. On the other hand, closed cathode in the 51-71°C range shows a worsening of charge transfer resistance (increment from 0.700 to 0.887  $\Omega\text{cm}^2$ ) and capacitance (from 0.0360 to 0.0208 F), whereas the ohmic resistance improves from 0.800 to 0.588  $\Omega\text{cm}^2$ . Data at 80°C of closed cathode shows an opposite trend, so worsening of the ohmic resistance – maybe due to dehydration effects- and improvement of capacitance and charge transfer resistance.

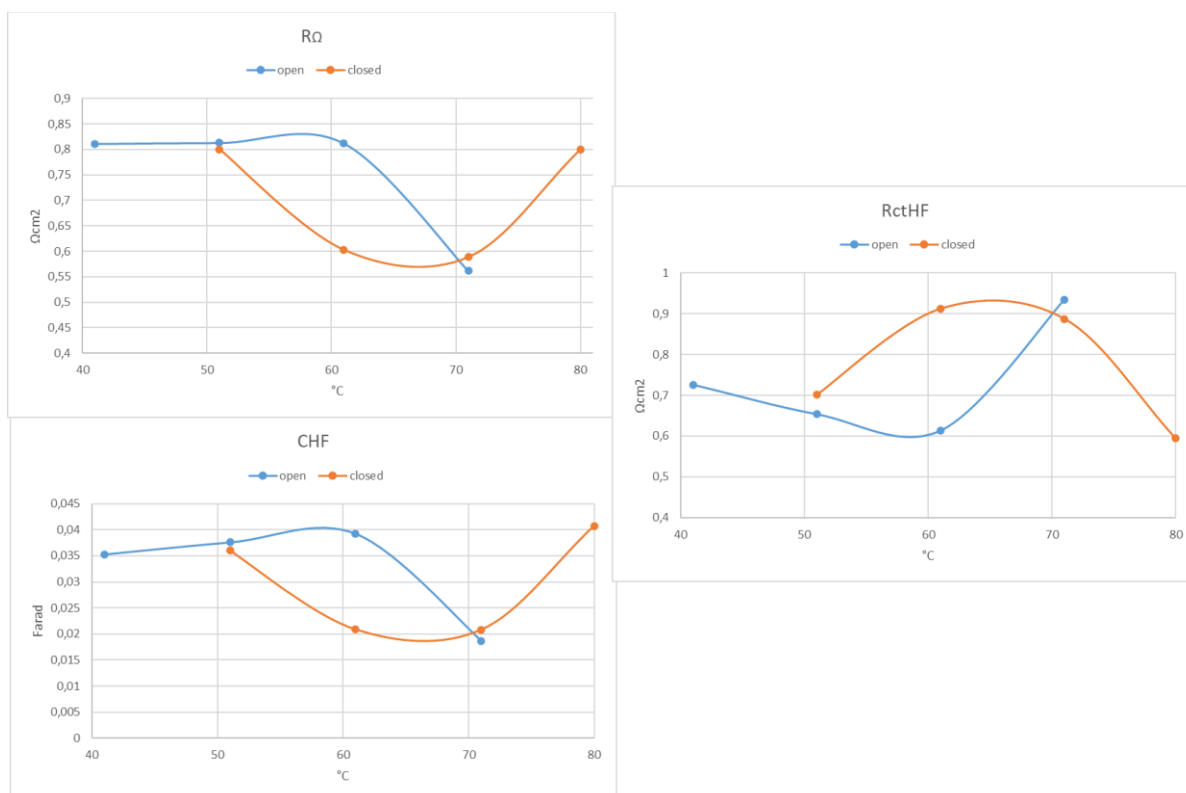


Figure 121 Comparison between open and closed cathode of the HF parameters.

---

In conclusion, open cathode is less affected by the increase of temperature- in the range from 40 to 60°C -with respect to the closed cathode configuration which benefits from an increase of temperature. Making a comparison between open and closed cathode configuration at constant temperature in the range 40-60°C, EIS parameters obtained during the open cathode test have better trend although it is characterized by higher pressure if compared at constant temperature. A possible reason is a better thermal stabilization of the system (temperature at the heater has less oscillations). On the other hand, closed cathode seems to perform better at higher temperature (>70°C)- lower value of the charge transfer resistance and capacitance- but still the ohmic resistance is not improving because too higher T cause dehydration effects.

### 6.3.2 Tests performed with open/closed cathode with different mass flow rates

The objective is to investigate the influence of the cathode configuration on the cell performance. The only variable changed between open and closed cathode configuration is the mass flow rate; this is done to keep the mass flow rate per channel at the anode side constant between the two configurations.

Moreover, two modalities are used to vary the mass flow rate: variation of the pump displacement chamber and usage of the needle valve. On the bases of these two possibilities, two series of experiments are identified:

- **First series** with recirculating pump
  - 1) test executed at 60°C
    - Open, 60% pump- 2,47 bar @anode & 2,42 bar @cathode
    - Closed, 10% pump- 1,73 bar @anode & 1,35 bar @cathode
  - 2) test executed at 80°C
    - Open, 60% pump- 2,36 bar @anode & 2,32 bar @cathode
    - Closed, 10% pump- 1,70 bar @anode & 1,30 bar @cathode
- **Second series** with needle valve
  - 1) test executed at 60°C
    - Open, 200ml/min, 1,65 bar @anode & 1,64 bar @cathode
    - Closed, 100ml/min, 1,56 bar @anode & 1,30 bar @cathode
  - 2) test executed at 70° C
    - Open, 200ml/min, 1,65 bar @anode & 1,64 bar @cathode
    - Closed, 100ml/min, 1,67 bar @anode & 1,36 bar @cathode
  - 3) test executed at 80°C
    - Open, 200ml/min, 1,66 bar @anode & 1,67 bar @cathode
    - Closed, 100ml/min, 1,59 bar @anode & 1,26 bar @cathode

---

The electrochemical characterization is performed with polarization curves and EIS measurements. Polarization curves are carried out by imposing the current and measuring the voltage. Two types of EIS tests have been used:

- Potentiostatic test, performed at 0 DC V vs Reference by varying the frequency from 100 kHz to 0,001 Hz in single sine mode and using a sinusoidal excitation signal of 10 mV root mean square (rms)
- Galvanostatic test, performed at 0 DC mA by varying the frequency from 200 kHz to 0,002 Hz in single sine mode and using a sinusoidal excitation signal of 1000 mA root mean square (rms).

## **RESULTS FIRST SERIES**

### *Data quality assessment for tests performed at 60°C and 80°C*

The KK validation shows impedance spectra of both EIS experiments affected by time variance behaviour, so high residuals values at almost all frequencies. By visual inspection a difference between potentiostatic and galvanostatic modes is observed in both Nyquist and Bode plots. Galvanostatic has produced impedance spectra with three time constants, whether the potentiostatic has two. In any case, the ECM used to fit is LR(QR)(QR) because the LF range is affected by noise.

### *Modelling*

#### 1. 60°C open/closed cathode

*Figure 122* shows Nyquist plots of EIS data measured at 0V. It is possible to notice the presence of an arc at high frequency, and an incomplete second arc in the mid frequency region. In the closed cathode configuration, it is observed a general increase of HF arc, and a decrease of the second arc; the trend is opposite in case of open cathode.

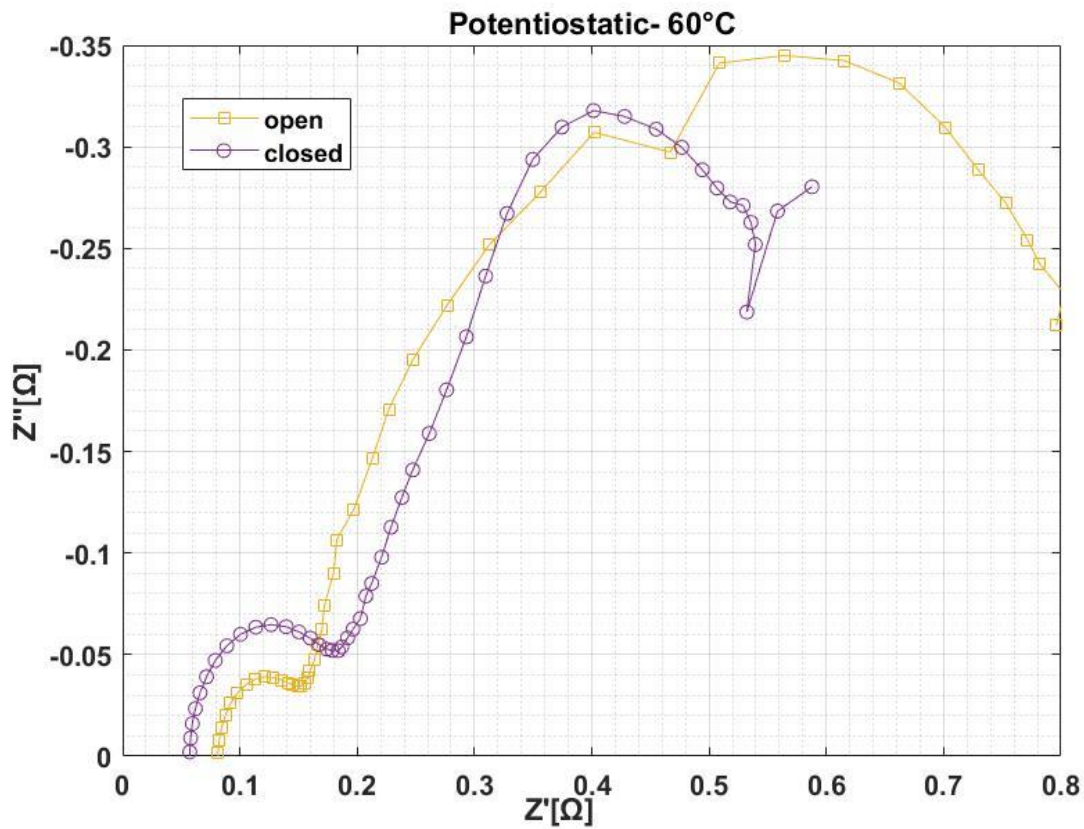


Figure 122 Nyquist plot under voltage control at 60°C- open vs closed cathode.

| POT    | $\omega$ HF [Hz] | $\tau$ HF [s] | $\omega$ mid-LF [Hz] | $\tau$ mid-low F [s] |
|--------|------------------|---------------|----------------------|----------------------|
| open   | 100              | 0,001592357   | 0,3162               | 0,503591615          |
| closed | 63,1             | 0,002523545   | -                    | -                    |

Table 6.6 Characteristic frequency at high and low frequency and correlated time constant for potentiostatic test at 60°C.

Figure 123 shows Nyquist plots of EIS data measured at 0 mA, corresponding to the open circuit voltage of the cell. It is observed the presence of an arc at high frequency, and a second arc in the mid-low frequency region affected by noise. The latter seems made of two merged semicircles. The comparison between open and closed cathode shows that the mid frequency arc is larger in case of open cathode, same consideration for the low frequency region. Instead, the HF arc intercept with the real axis is higher in case of closed cathode.



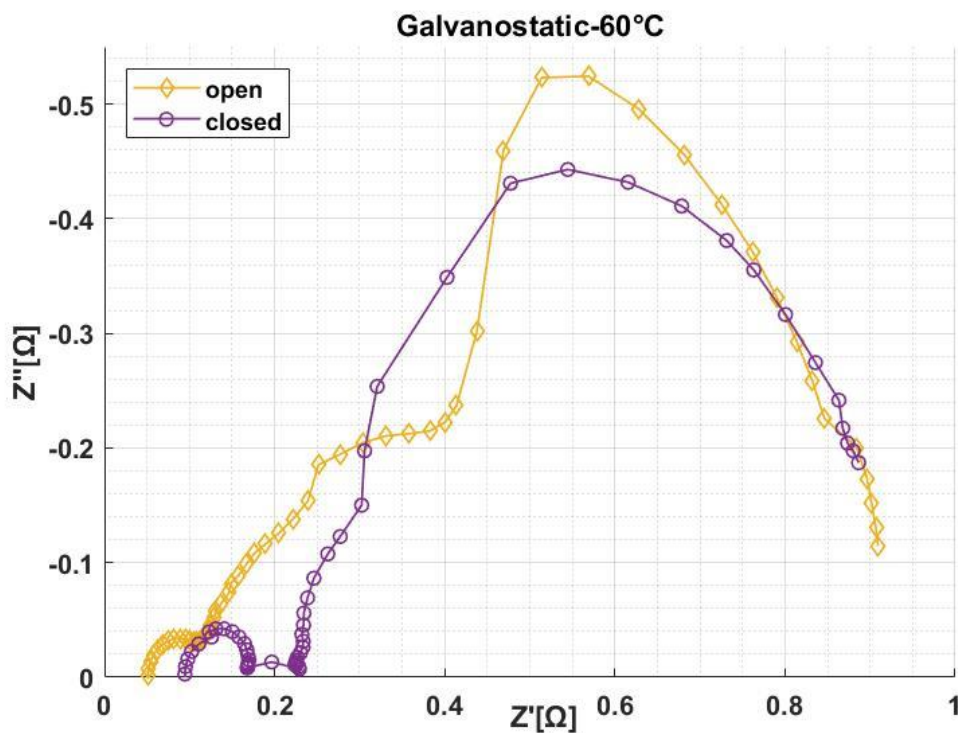


Figure 123 Nyquist plot under current control at 60°C- open vs closed cathode.

| GALV   | $\omega$ HF [Hz] | $\tau$ HF [s] | $\omega$ mid-LF [Hz] | $\tau$ mid-low F [s] | $\omega$ LF [Hz] | $\tau$ LF [s] |
|--------|------------------|---------------|----------------------|----------------------|------------------|---------------|
| open   | 100,2            | 0,001589178   | 0,1262               | 1,261772336          | 0,05024          | 3,169499777   |
| closed | 126,2            | 0,001261772   | -                    | -                    | 0,0317           | 5,023207217   |

Table 6.7 Characteristic frequency at high and low frequency and correlated time constant for galvanostatic test at 60°C.

## 2. 80°C open/closed cathode

Figure 124 shows Nyquist plots of EIS data measured at 0V. It is possible to notice the presence of an arc at high frequency, and an incomplete second arc in the mid frequency region affected by noise. In the closed cathode configuration, it is observed a general increase of HF arc, and a decrease of the second arc; the trend is opposite in case of open cathode.

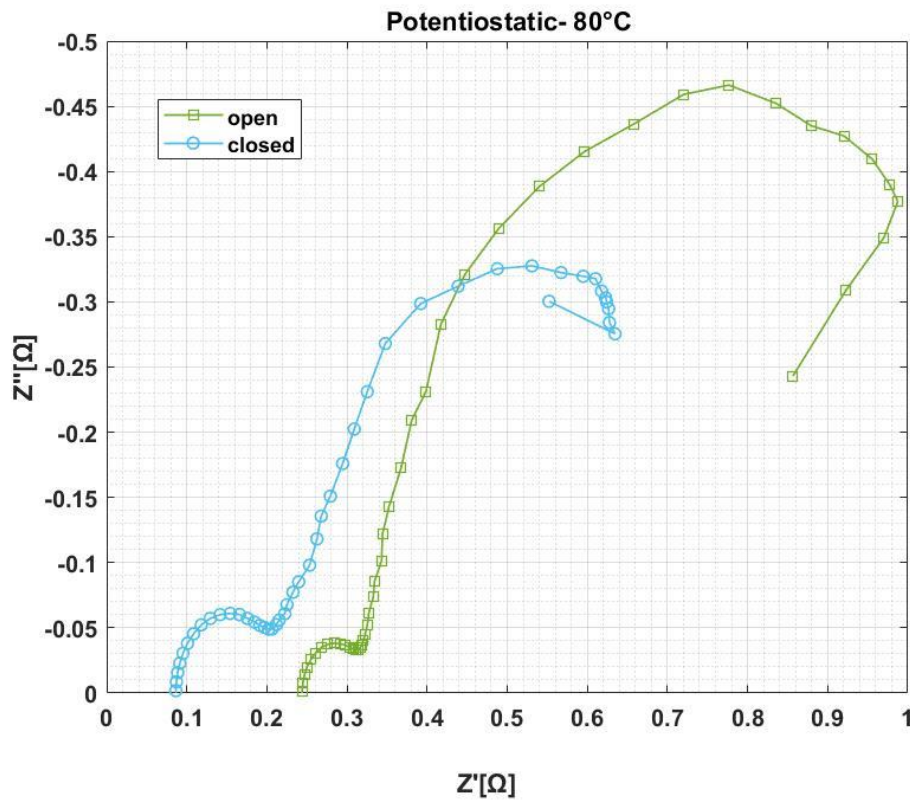


Figure 124 Nyquist plot under voltage control at 80°C- open vs closed cathode.

| POT    | $\omega$ HF [Hz] | $\tau$ HF [s] | $\omega$ mid-LF [Hz] | $\tau$ mid-LF [s] |
|--------|------------------|---------------|----------------------|-------------------|
| open   | 79,4             | 0,002005487   | 0,1585               | 1,004641443       |
| closed | 63,1             | 0,002523545   | 0,2512               | 0,633899955       |

Table 6.8 Characteristic frequency at high and low frequency and correlated time constant for potentiostatic test at 80°C.

Figure 125 shows Nyquist plots of EIS data measured at 0 mA, corresponding to the open circuit voltage of the cell. It is observed the presence of an arc at high frequency, and a second arc in the mid-low frequency region made of two merged semicircles.

The comparison between open and closed cathode shows that the mid frequency arc is smaller in case of open cathode, same consideration for the low frequency region. Instead, the HF arc intercept with the real axis is lower in case of closed cathode.

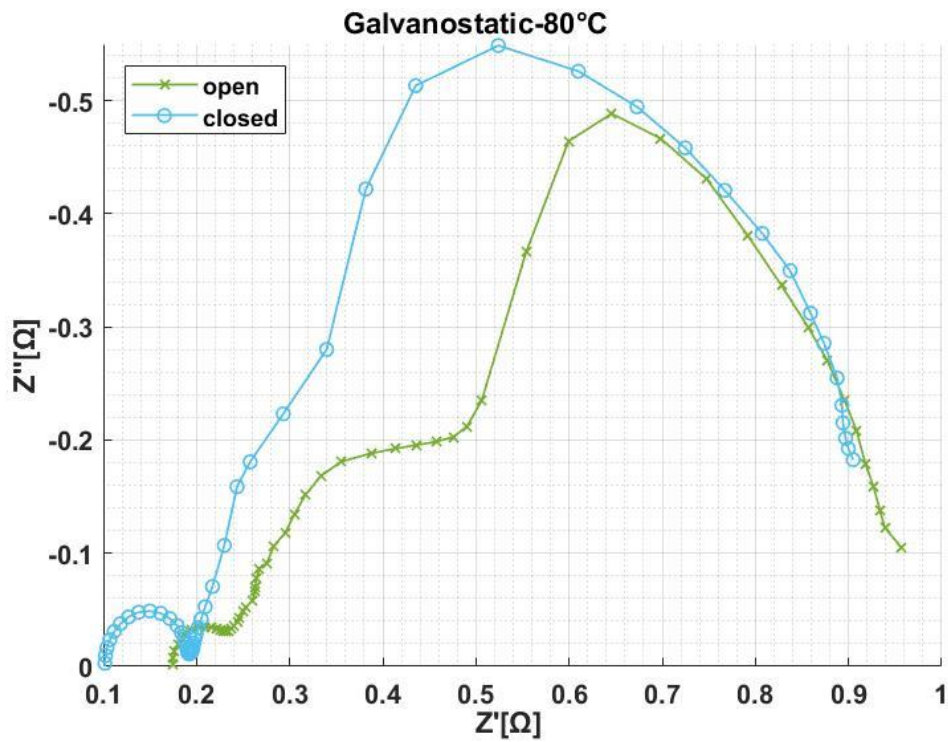


Figure 125 Nyquist plot under current control at 80°C- open vs closed cathode.

| GALV   | $\omega$ HF [Hz] | $\tau$ HF [s] | $\omega$ mid-LF [Hz] | $\tau$ mid-LF [s] | $\omega$ LF [Hz] | $\tau$ LF [s] |
|--------|------------------|---------------|----------------------|-------------------|------------------|---------------|
| open   | 100,2            | 0,001589178   | 0,1262               | 1,261772336       | 0,05024          | 3,169499777   |
| closed | 100,2            | 0,001589178   | -                    | -                 | 0,06325          | 2,517559981   |

Table 6.9 Characteristic frequency at high and low frequency and correlated time constant for galvanostatic test at 80°C.

Table 6.10 Pressure and temperature comparison between open and closed cathode

| Average value                                 | 60°C  | 80°C  |
|---|-------|-------|
| T cell open cathode [°C]                      | 61,63 | 79,47 |
| T cell closed cathode [°C]                    | 61,64 | 79,64 |
| T fluid open cathode [°C]                     | 58,15 | 77,37 |
| T fluid closed cathode [°C]                   | 63,14 | 82,05 |
| Fluid pressure at heater open cathode [bar]   | 3,51  | 3,30  |
| Fluid pressure at heater closed cathode [bar] | 2,01  | 1,98  |

### DISCUSSION FIRST SERIES-model validation with iV curves

Considering the test performed at 60°C the presence of noise in both EIS tests do not allow to quantify accurately the parameters gained from the fitting of the experimental data. Nevertheless, from galvanostatic test it seems that near the OCV closed cathode is performing better since it has a lower total polarization resistance- given by the difference between high intercept and low intercept with the real axis - even if the ohmic resistance is higher. The higher value of the ohmic resistance can have role at higher current densities, where ohmic losses are dominant, determining a lower performance of the closed cathode.

The first observation does not find correspondence in the polarization curves where near the OCV iV curves overlap. Meanwhile higher voltage values at higher current densities are observed for closed cathode in the comparison between iV curves, hence this is in agreement with higher ohmic resistance of the closed cathode.

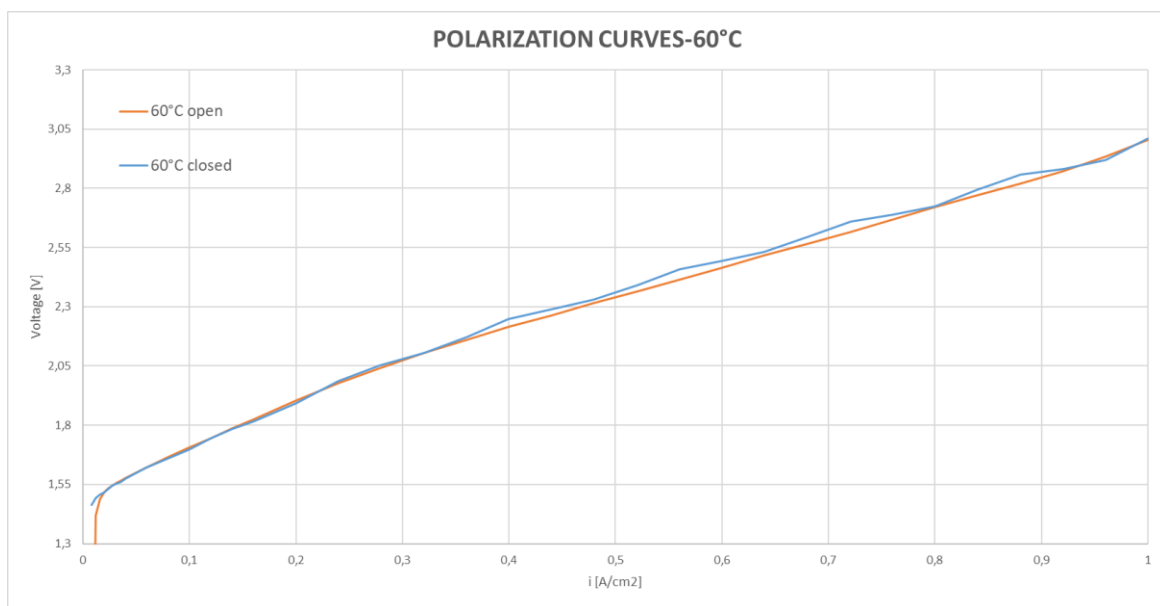


Figure 126 Polarization curves at 60°C- open vs closed cathode.

The comparison between the polarization curves at 60°C shows a **better performance of the open cathode configuration** since its curve is lower with respect to the closed cathode one. The analysis shows that the cell temperature is the same during open and closed cathode (61.6°C), while fluid temperature and fluid pressure at the heater between open and closed cathode configuration are different. In particular, during open cathode experiment the fluid temperature is lower and pressure is higher compared to closed cathode.

EIS tests at 80°C have produced still low quality impedance spectra but a trend can be seen from galvanostatic results to check the consistency with the polarization curves near the OCV. The most meaningful parameter obtained qualitatively by visual inspection is the polarization resistance, which gives an insight of the activation losses within the cell. It is possible to say that the overall polarization resistance is unvaried between open and closed cathode; only ohmic resistance of the open is higher compared to that of the closed cathode. The higher ohmic resistance with open cathode should determine lower performance at higher current densities, but this hypothesis is not in agreement with the findings of the polarization curves where it is generally observed a better performance of the open cathode configuration.

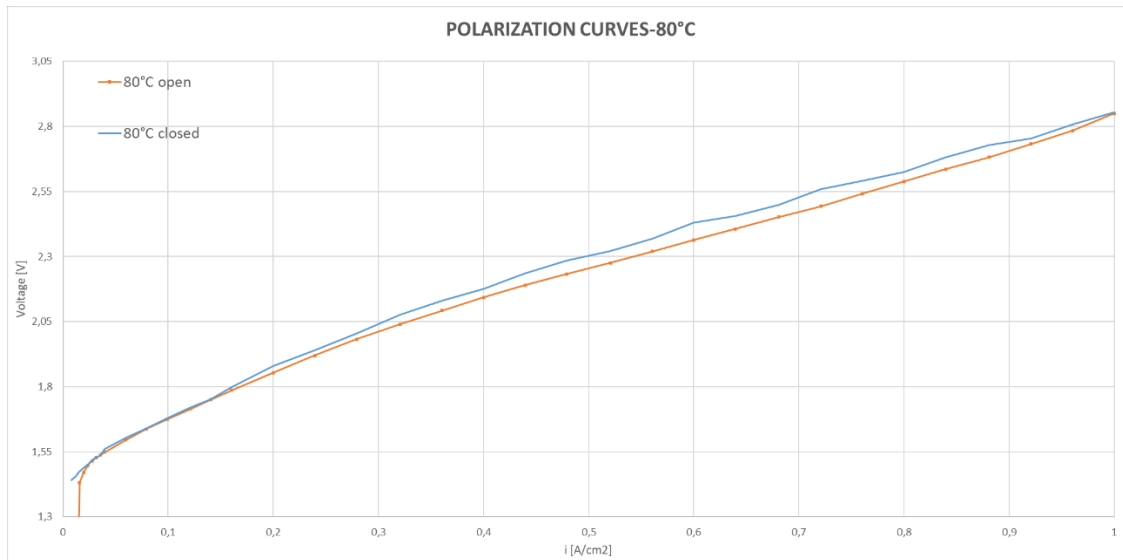


Figure 127 Polarization curves at 80°C- open vs closed cathode.

The analysis shows that the cell temperature is around 79,5-79,6°C, instead fluid temperature and fluid pressure at the heater between open and closed cathode configuration are different. In particular, during open cathode experiment the fluid temperature is lower and pressure is higher compared to closed cathode. Again, although the closed cathode has higher T and lower p it shows a lower performance.

## RESULTS SECOND SERIES

### Data quality assessment

The KK validation shows impedance spectra of both EIS experiments affected by time variance behaviour, so high residuals values, mainly larger at lower frequencies. By visual inspection a difference between potentiostatic and galvanostatic modes is observed in both Nyquist and Bode plots. As before, galvanostatic has produced impedance spectra with three time constants, whether the potentiostatic is characterized by two time constants. In any case, the

impedance spectra have poor quality especially at low frequency for both potentiostatic and galvanostatic modes, hence the ECM used to fit is LR(QR)(QR).

### Modelling

#### 1. 60°C open/closed cathode

Figure 128 shows Nyquist plots of EIS data measured at 0V. The shape of the impedance spectra changes between open and closed cathode. In the open cathode it is possible to notice the presence of an arc at high frequency, and a second arc in the mid-low frequency region. In the closed cathode configuration, there is a semicircle in the HF region followed by a straight line mostly affected by noise.

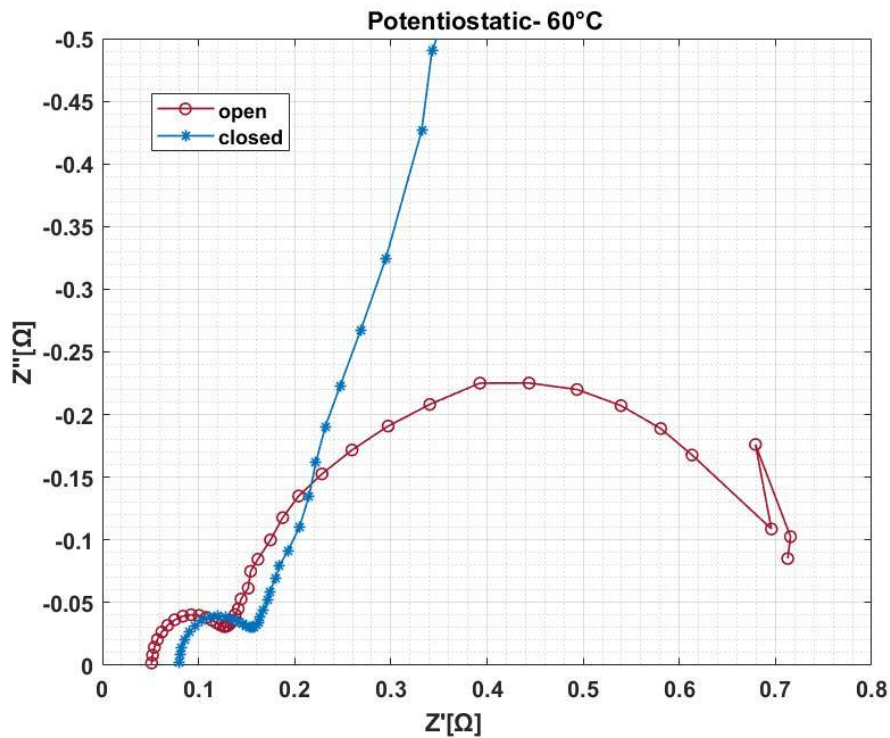


Figure 128 Nyquist plot under voltage control at 60°C- open vs closed cathode.

Table 6.11 Characteristic frequency at high and low frequency and correlated time constant for potentiostatic test at 60°C.

| POT    | $\omega$ HF [Hz] | $\tau$ HF [s] | $\omega$ mid-LF [Hz] | $\tau$ mid-LF [s] |
|--------|------------------|---------------|----------------------|-------------------|
| open   | 79,43            | 0,002005      | 0,3162               | 0,503591615       |
| closed | 79,43            | 0,002005      | -                    | -                 |

Figure 129 shows Nyquist plots of EIS data measured at 0 mA, corresponding to the open circuit voltage of the cell. It is observed the presence of an arc at high frequency, and a second arc- made of two merged semicircles- in the mid-low frequency region affected by noise.

The comparison between open and closed cathode shows that the high frequency arc is smaller in case of open cathode whereas the closed cathode has smaller mid-low frequency arc.

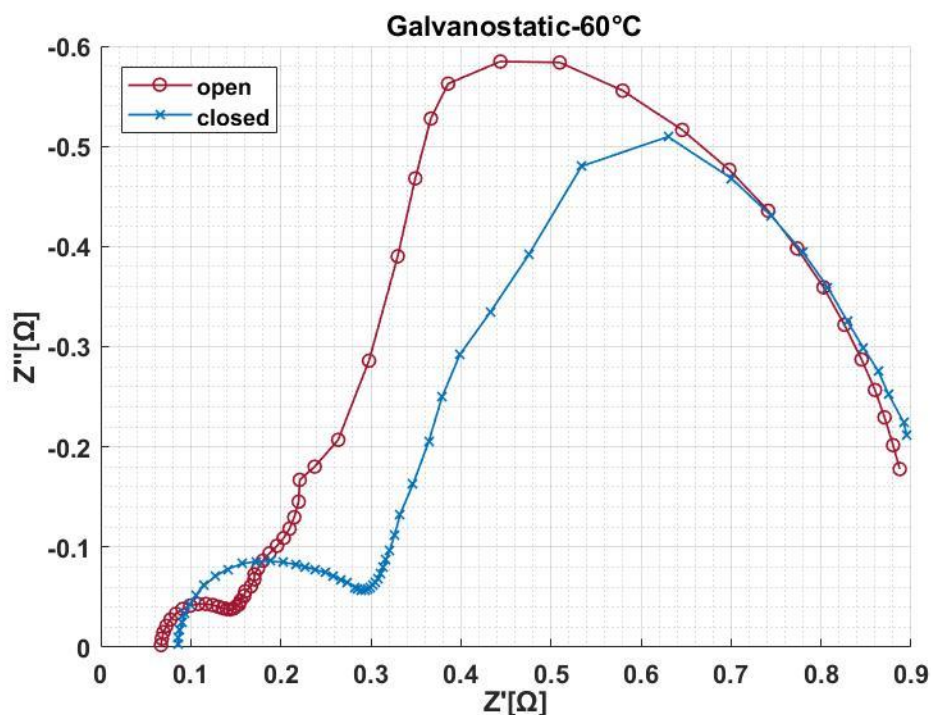


Figure 129 Nyquist plot under current control at 60°C- open vs closed cathode.

Table 6.12 Characteristic frequency at high and low frequency and correlated time constant for galvanostatic test at 60°C.

| GALV   | $\omega$ HF [Hz] | $\tau$ HF [s] | $\omega$ mid-LF [Hz] | $\tau$ mid-LF [s] | $\omega$ LF [Hz] | $\tau$ LF [s] |
|--------|------------------|---------------|----------------------|-------------------|------------------|---------------|
| open   | 79,62            | 0,001999946   | -                    | -                 | 0,06325          | 2,51756       |
| closed | 31,7             | 0,005023207   | -                    | -                 | 0,0317           | 5,023207      |

## 2. 70°C open/closed cathode

Figure 130 shows Nyquist plots of EIS data measured at 0V. The shape of the impedance spectra is similar for both open and closed cathode. It is possible to notice the presence of a small arc at high frequency, and a second incomplete arc in the mid-low frequency region. A lower intercept with the real axis at high frequency is observed for the closed cathode tests.



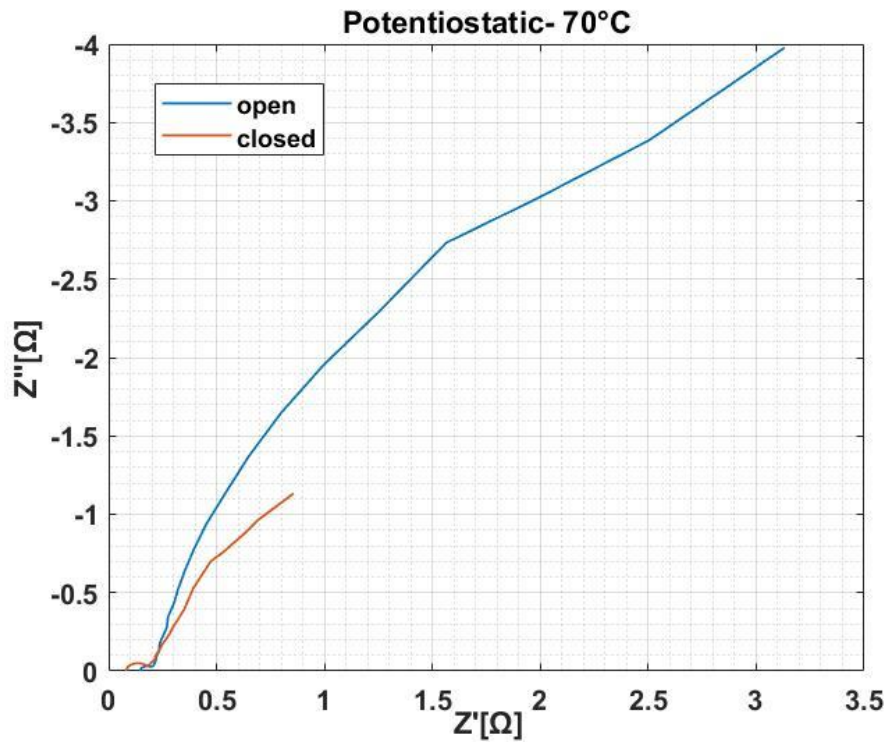


Figure 130 Nyquist plot under voltage control at 70°C- open vs closed cathode.

Table 6.13 Characteristic frequency at high and low frequency and correlated time constant for potentiostatic test at 70°C.

| POT    | $\omega$ HF [Hz] | $\tau$ HF [s] | $\omega$ mid-LF [Hz] | $\tau$ mid-LF [s] |
|--------|------------------|---------------|----------------------|-------------------|
| open   | 100              | 0,0015924     | 0,01995              | 7,981737784       |
| closed | 63,1             | 0,0025235     | -                    | -                 |

Figure 131 shows Nyquist plots of EIS data measured at 0 mA, corresponding to the open circuit voltage of the cell. It is observed the presence of an arc at high frequency, and a second arc in the mid-low frequency region affected by noise.

The comparison between open and closed cathode shows some differences. The impedance spectrum of open shows an incomplete semicircle in the md frequency region, which almost disappears in the closed cathode impedance spectrum. Moreover, the high frequency arc is smaller in case of open cathode whereas the closed cathode has smaller mid frequency arc.



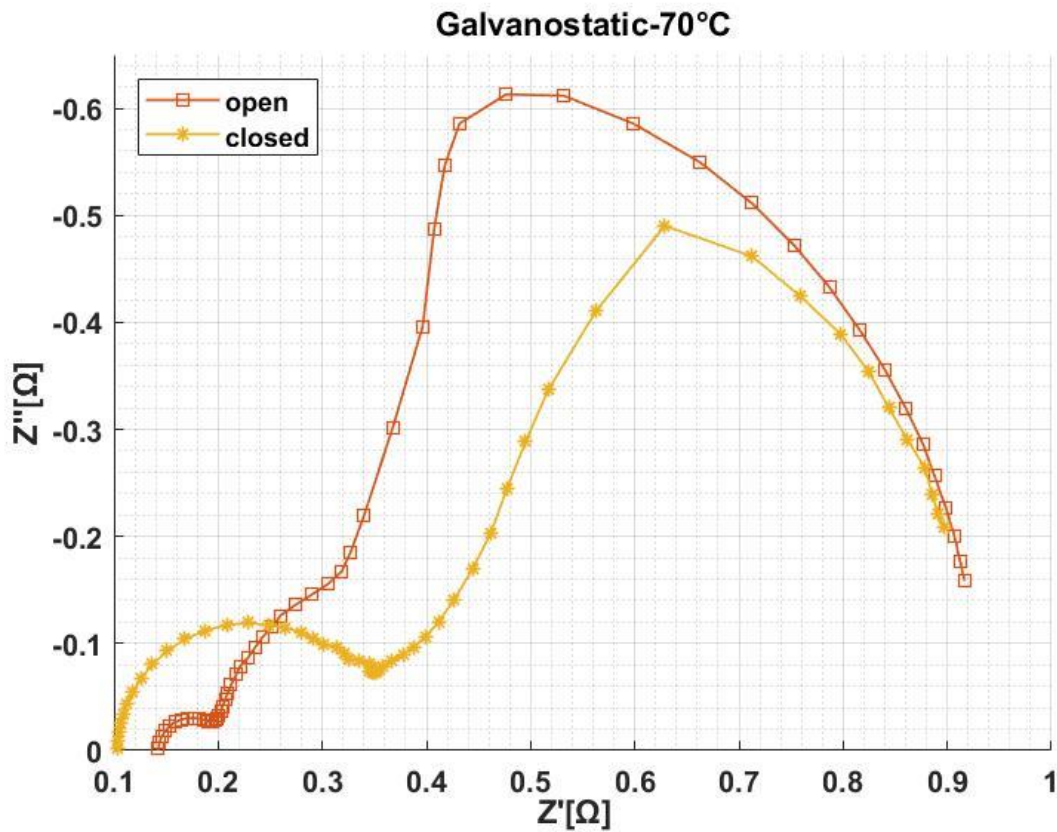


Figure 131 Nyquist plot under current control at 70°C- open vs closed cathode.

Table 6.14 Characteristic frequency at high and low frequency and correlated time constant for galvanostatic test at 70°C.

| GALV   | $\omega$ HF [Hz] | $\tau$ HF [s] | $\omega$ mid-LF [Hz] | $\tau$ mid-LF [s] | $\omega$ LF [Hz] | $\tau$ LF [s] |
|--------|------------------|---------------|----------------------|-------------------|------------------|---------------|
| open   | 100,2            | 0,001589178   | 0,3991               | 0,398986892       | 0,06325          | 2,51756       |
| closed | 25,18            | 0,006323895   | -                    | -                 | 0,0317           | 5,023207217   |

### 3. 80°C open/closed cathode

Figure 132 shows Nyquist plots of EIS data measured at 0V. The shape of the impedance spectra is similar for both open and closed cathode. It is possible to notice the presence of an arc at high frequency, and a second arc in the mid-low frequency region. The main difference occurs in the mid-low frequency region where the open shows a smaller arc with respect to that appearing in the closed cathode impedance.

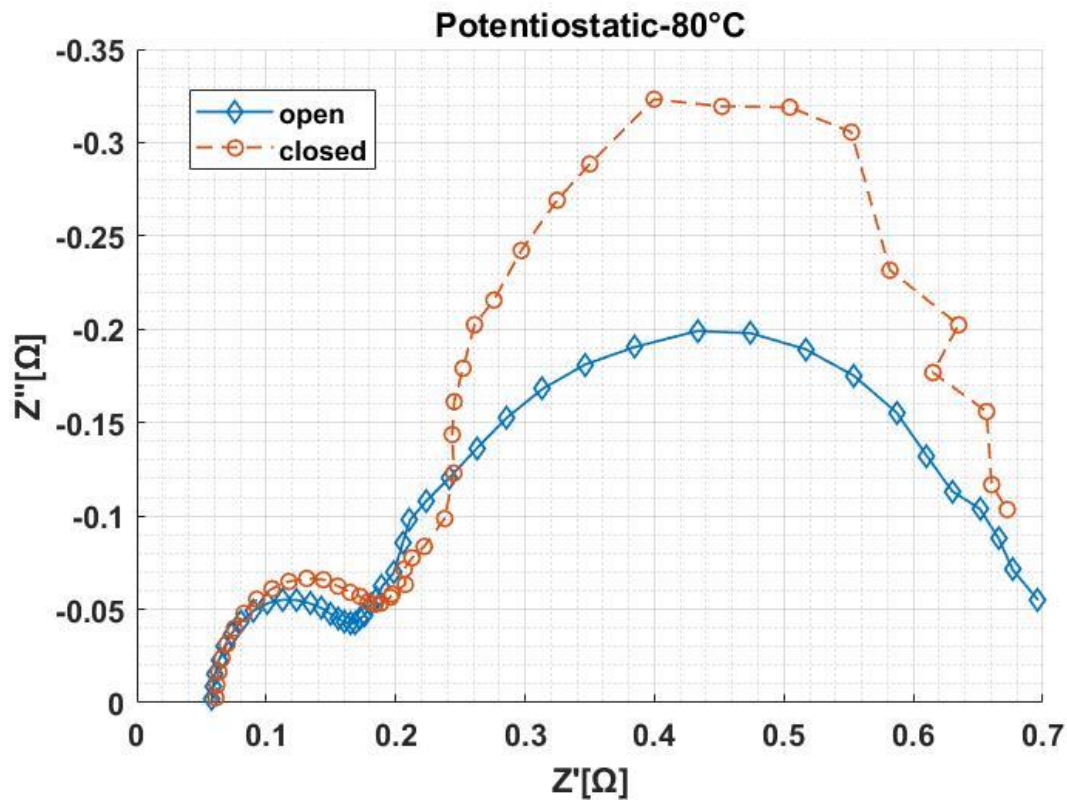


Figure 132 Nyquist plot under voltage control at 80°C- open vs closed cathode.

Table 6.15 Characteristic frequency at high and low frequency and correlated time constant for potentiostatic test at 80°C.

| POT    | $\omega$ HF [Hz] | $\tau$ HF [s] | $\omega$ mid-LF [Hz] | $\tau$ mid-LF [s] |
|--------|------------------|---------------|----------------------|-------------------|
| open   | 63,1             | 0,002524      | 0,3162               | 0,503592          |
| closed | 63,1             | 0,002524      | 0,2512               | 0,6339            |

Figure 133 shows Nyquist plots of EIS data measured at 0 mA, corresponding to the open circuit voltage of the cell. It is observed the presence of an arc at high frequency, and a second arc in the mid-low frequency region affected by noise.

The comparison between open and closed cathode shows some differences. The impedance spectrum of open shows an incomplete and very small semicircle in the mid frequency region, which disappears in the closed cathode impedance spectrum. The high and low frequency arc do not show significant variations between the two cathode configurations.

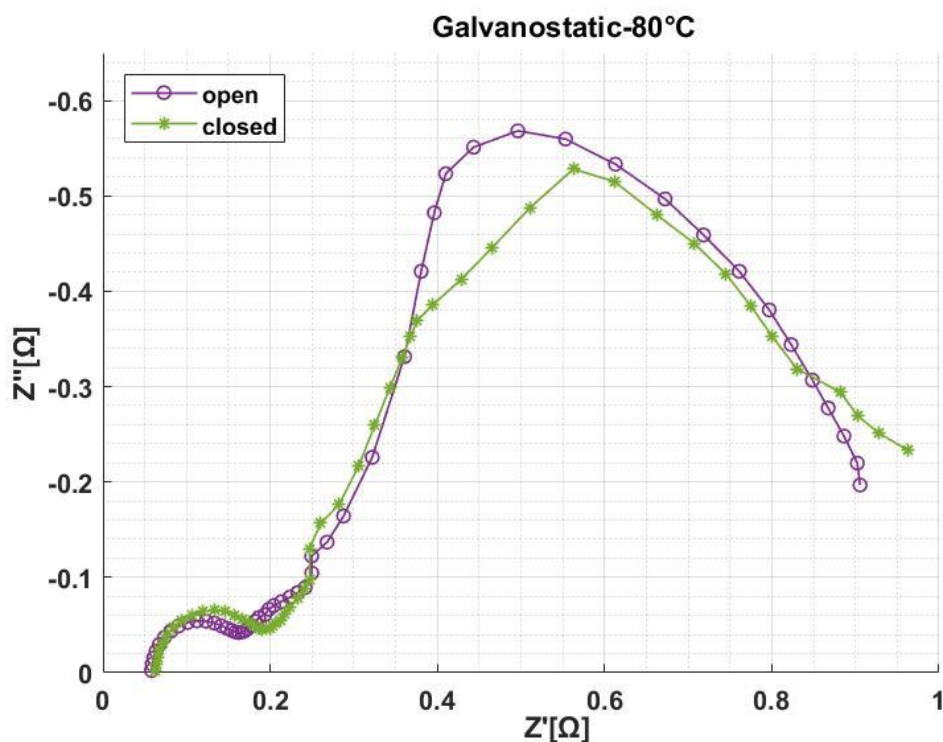


Figure 133 Nyquist plot under current control at 80°C- open vs closed cathode.

Table 6.16 Characteristic frequency at high and low frequency and correlated time constant for galvanostatic test at 80°C.

| GALV   | $\omega$ HF [Hz] | $\tau$ HF [s] | $\omega$ mid-LF [Hz] | $\tau$ mid-LF [s] | $\omega$ LF [Hz] | $\tau$ LF [s] |
|--------|------------------|---------------|----------------------|-------------------|------------------|---------------|
| open   | 63,25            | 0,00251756    | -                    | -                 | 0,7962           | 0,199995      |
| closed | 63,25            | 0,00251756    | -                    | -                 | 0,05024          | 3,1695        |

### DISCUSSION SECOND SERIES-model validation with *iV* curves

Tests performed at 60°C and 70°C under current control show a similar behaviour, i.e the high frequency arc is smaller in case of open cathode whereas the closed cathode has smaller mid-low frequency arc. All EIS tests have shown poor quality in the overall frequency range, but it is possible a qualitative analysis of the impedance spectra gained under galvanostatic mode.

Galvanostatic tests at 60°C shows that closed cathode configuration has lower total polarization resistance; hence it may be assumed a better performance of closed cathode near the OCV. On the other hand, open cathode has lower ohmic resistance which may determine lower voltage value at higher current densities but this assumption is not in accordance with the polarization results. The comparison between the polarization curves at 60°C shows a better performance of the closed cathode configuration since its curve is slightly lower with respect to the open cathode one. The analysis shows that the cell temperature and fluid

pressure at the heater are unvaried –respectively 61,5-61,6°C and 1,99-1,89 bar- while fluid temperature between open and closed cathode configuration is different. In particular, during open cathode experiment the fluid temperature is lower compared to closed cathode.

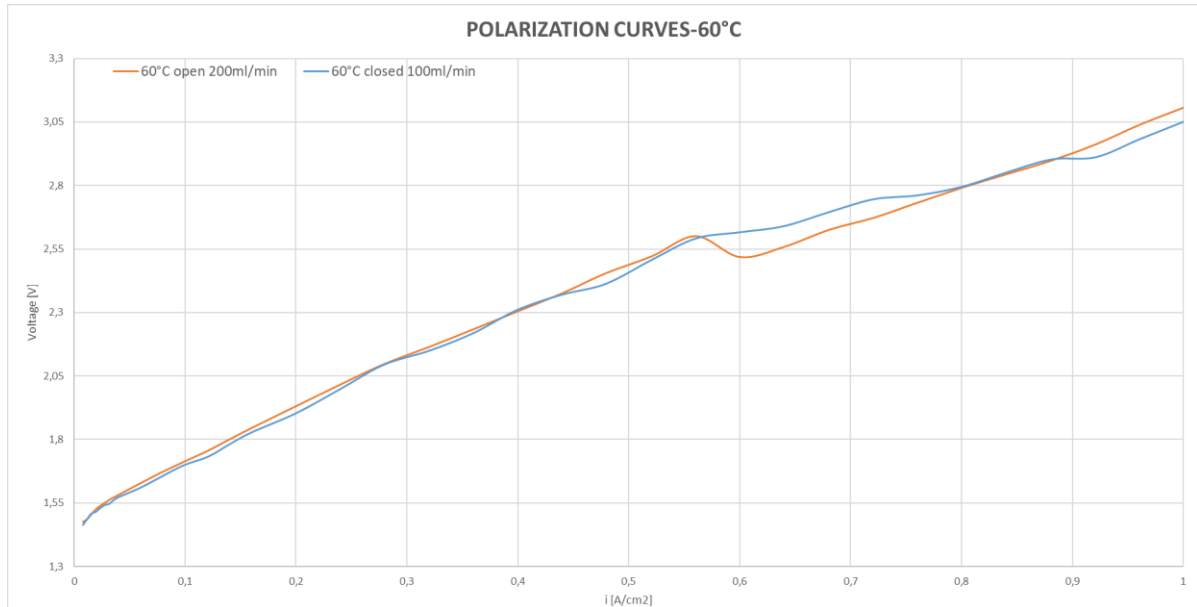


Figure 134 Polarization curves at 60°C- open vs closed cathode.

Galvanostatic tests at 70°C shows that both configurations have similar total polarization resistance. However, closed cathode has lower ohmic resistance so this suggests that it has better performance at high current density. The comparison between the polarization curves at 70°C seems to show an overlapping of the two curves. At high current density closed cathode has lower voltage values and hence this finding is in agreement with the previous hypothesis of lower ohmic resistance during closed cathode. The analysis shows that fluid pressure at the heater is around 2 bar, instead fluid temperature and cell temperature between open and closed cathode configuration are different. In particular, during the open cathode experiment both temperatures are lower compared to closed cathode. The higher temperature of the cell during closed cathode with almost unvaried pressure in both sides of the cell for open/closed cathode configuration may be considered the reason of the better performance with respect to the open cathode at higher current densities.

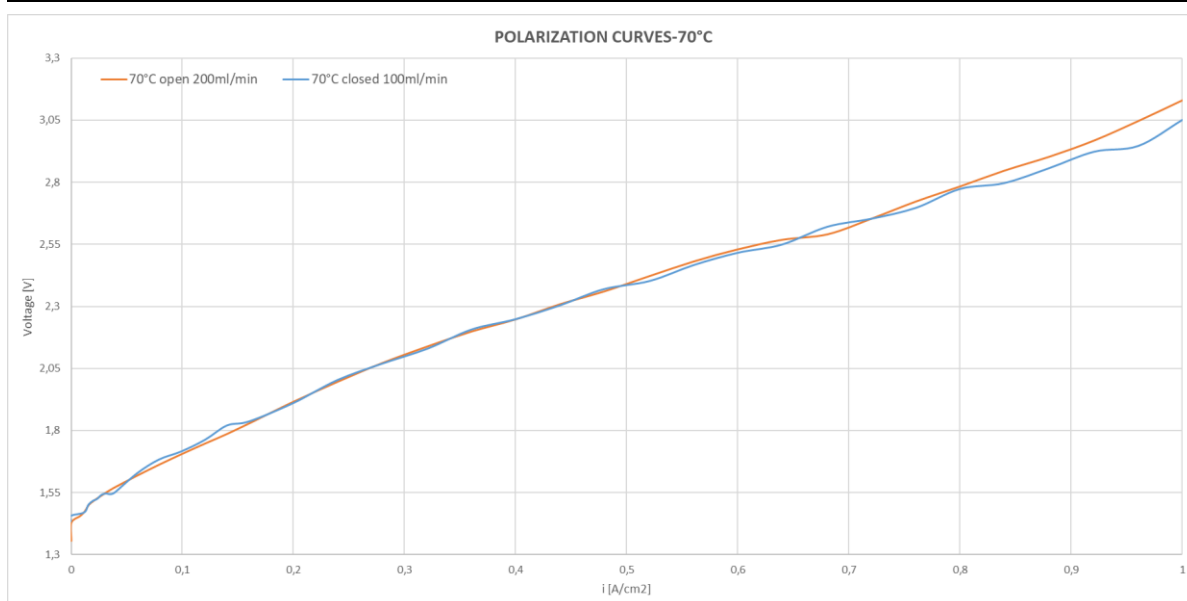


Figure 135 Polarization curves at 70°C- open vs closed cathode.

Tests performed at 80°C under current control show that open and closed cathode have similar impedance spectra but the comparison between the polarization curves at 80°C shows generally a better performance of the open cathode configuration since its curve is lower with respect to the closed cathode one. Moreover, it is found that open cathode has a slightly lower value of the ohmic resistance. The analysis shows that the fluid pressure at the heater is around 2 bar, instead fluid temperature and cell temperature between open and closed cathode configuration are different. During the open cathode experiment both temperatures are lower compared to closed cathode.

Table 6.17 Pressure and temperature comparison between open and closed cathode

| Average value                                 | 60°C  | 70°C  | 80°C  |
|---|-------|-------|-------|
| T cell open cathode [°C]                      | 61,54 | 69,36 | 78,06 |
| T cell closed cathode [°C]                    | 61,62 | 71,37 | 79,49 |
| T fluid open cathode [°C]                     | 58,50 | 67,79 | 77,75 |
| T fluid closed cathode [°C]                   | 61,48 | 71,56 | 79,44 |
| Fluid pressure at heater open cathode [bar]   | 1,99  | 2,02  | 2,04  |
| Fluid pressure at heater closed cathode [bar] | 1,89  | 2,01  | 1,99  |

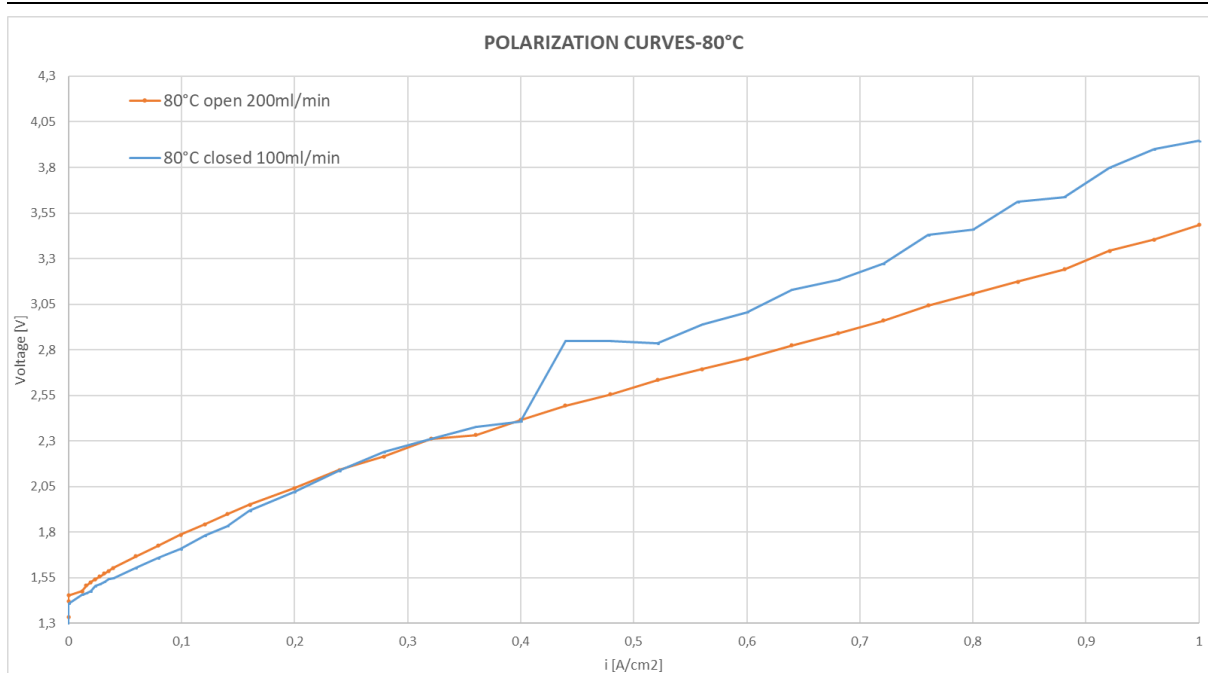


Figure 136 Polarization curves at 80°C- open vs closed cathode.

## Conclusion

1. Making a comparison between open and closed cathode configuration at constant temperature in the range 40-60°C, EIS parameters obtained during the open cathode test have better trend. A possible reason is a better thermal stabilization of the system (temperature at the heater has less oscillations). On the other hand, closed cathode seems to perform better at higher temperature (>70°C)- lower value of the charge transfer resistance and capacitance- but still the ohmic resistance is not improving because too higher T cause dehydration effects.
2. The improvement seen in the open cathode in both cases could be related to the more homogeneous temperature distribution in the housing during the test.
3. EIS tests show that closed cathode has generally a larger high frequency arc which could be related to a worsening of current constrictions.

## 6.4 Degradation tests

### 6.4.1 Degradation test performed at 60°C and 80°C, 0.5bar, closed cathode, 10% mass flow rate, constant current density of 0.5 A/cm<sup>2</sup>

The degradation test is carried out at a constant current density of 0.5 A/cm<sup>2</sup> and the cell voltage increase over time is monitored. It consists of two series: the first series is performed at 60°C while the second at 80°C; both have an imposed gauge pressure of 0.5bar in the anode and cathode, and closed cathode configuration. During the first series EIS tests have been performed each twelve hours which means two tests each day (early morning and evening) whereas each 24 hours (one test each evening) while performing the second series of the degradation test. Two types of EIS tests have been used:

- Potentiostatic test, performed at 0 DC V by varying the frequency from 100 kHz to 0,001 Hz in single sine mode and using a sinusoidal excitation signal of 10mV root mean square (rms)
- Galvanostatic test, performed at 0 DC mA by varying the frequency from 200 kHz to 0,002 Hz in single sine mode and using a sinusoidal excitation signal of 1000 mA root mean square (rms).

It is expected to have an increase of the cell potential therefore a decrease of the cell performance.

### **RESULTS FIRST SERIES**

After around 168 h of operation at 0.5 A/cm<sup>2</sup> the cell has shown a degradation rate of 1080  $\mu$ V/h.

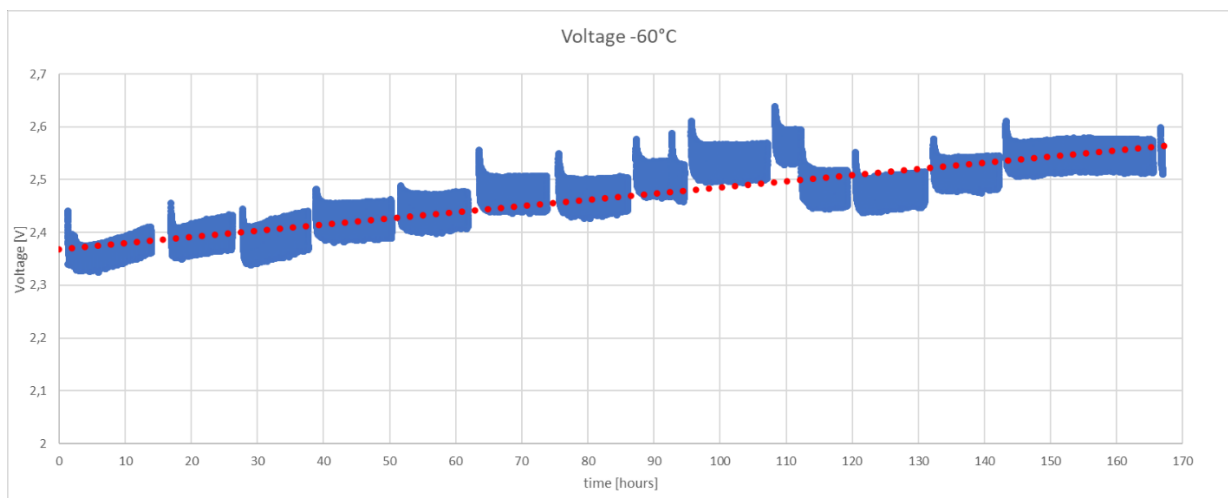


Figure 137 Voltage trend during the degradation test at 60°C.

The effective temperature during the experiment oscillates around 61°C whereas the real gauge pressure at the anode and cathode was 0,89 bar and 0,44 bar respectively.

The study shows an increase of pressure at the heater (from 1 to 1.3 bar), instead cell temperature remains in a range of values between 61-61,39°C and fluid temperature at the heater between 61,35-63,32°C.

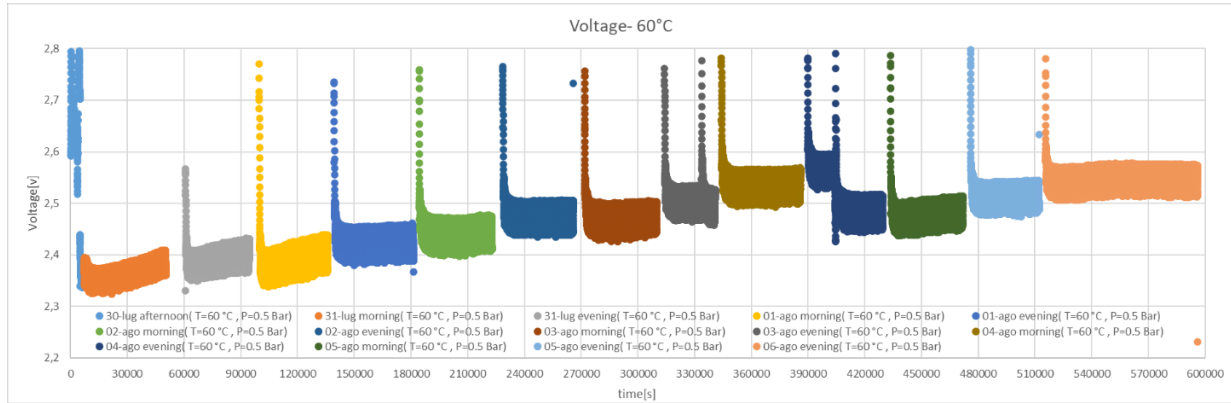


Figure 138

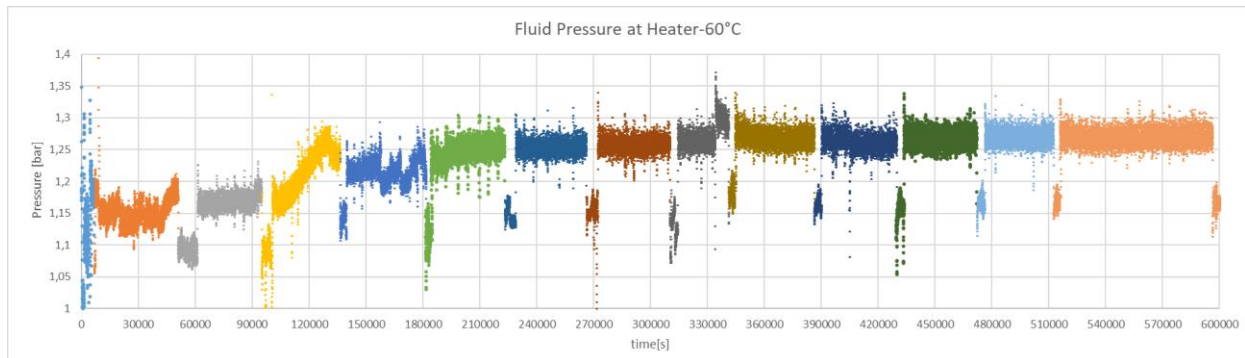


Figure 139

During the experiment there was a fault of the system on 3<sup>rd</sup> August afternoon that explains the anomaly on the cell voltage. Another remark should be done for the measurement done on 4<sup>th</sup> August. In the cell voltage graph a steep increase of the voltage is noticed, probably related to a decrease of the pressure at the heater, which also caused a decrease of cell temperature and fluid temperature.

Figures 140 and 141 show the overall EIS measurements performed under voltage and current control during the degradation test at 60°C.



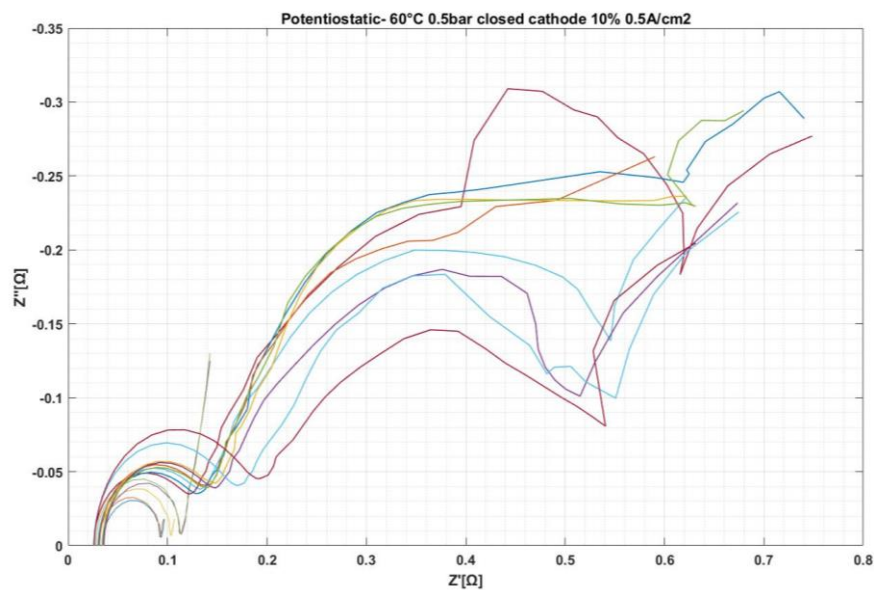


Figure 140 All EIS measurements with potentiostatic mode.

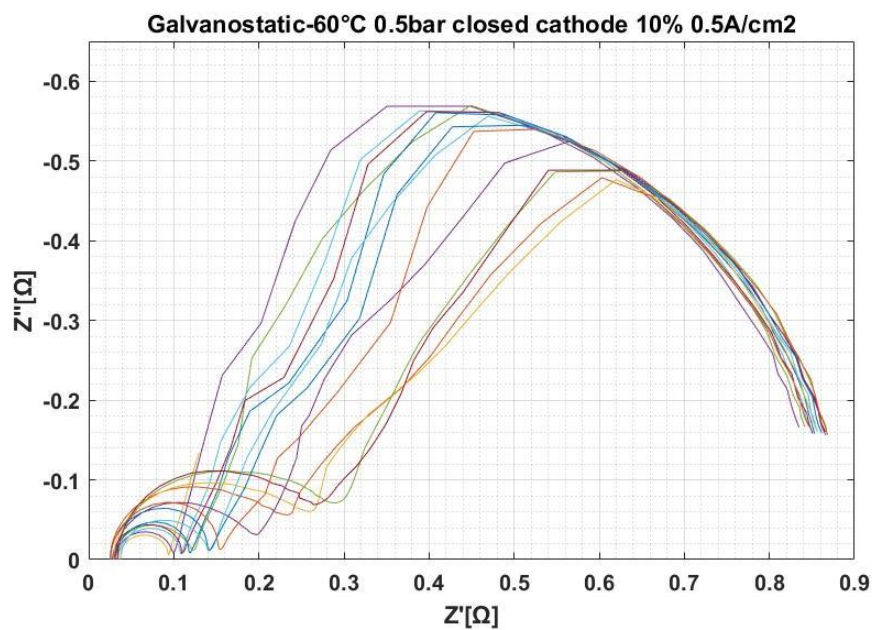


Figure 141 All EIS measurements with galvanostatic mode.

### Data quality assessment

Validation through KK relations shows that impedance spectra obtained with both modes have similar residuals behaviour, i.e. low residuals of high frequency data and larger residuals as data are collected at lower frequencies. This is probably related to the drift of the system during the measurements at low frequency, which are more time consuming.

Impedance spectra showing very high residuals in all frequency range are discarded. These are 2<sup>nd</sup>, 4<sup>th</sup> and 5<sup>th</sup> morning for the potentiostatic and 2<sup>nd</sup> evening, 3<sup>rd</sup> 4<sup>th</sup> and 5<sup>th</sup> morning for the galvanostatic. Another EIS test not considered due to tripping of the system is the one performed on the 3<sup>rd</sup> evening.

By visual inspection of the Nyquist and Bode plots it is possible to say that EIS measurements with galvanostatic and potentiostatic mode have produced impedance spectra characterized by at least two time constants. The low frequency impedance spectra in both modes- particularly in the potentiostatic mode- is affected by noise and/or time variance of the cell behaviour. Consequently, the impedance spectra obtained at lower frequencies is considered only from a qualitative point of view because its approximation to an ECM will probably produce a poor fit. Hence, the impedance spectra are fitted up to where data show a good trend, typically the first semicircle at HF and the initial part of the second semicircle appearing in the mid frequency range. Accordingly, the ECM used is LR(QR)(QR).

## Modelling

Figure 142 shows Nyquist plots of EIS data measured at 0V, with invalid spectra removed. It is possible to notice the presence of an arc at high frequency, and an incomplete second arc in the mid frequency region. The low frequency data are affected by noise but it is possible to notice a third semicircle.

It is observed a general increase of HF arc, and a decrease of the second arc in favour of an increment of the LF arc even if it is affected by noise.

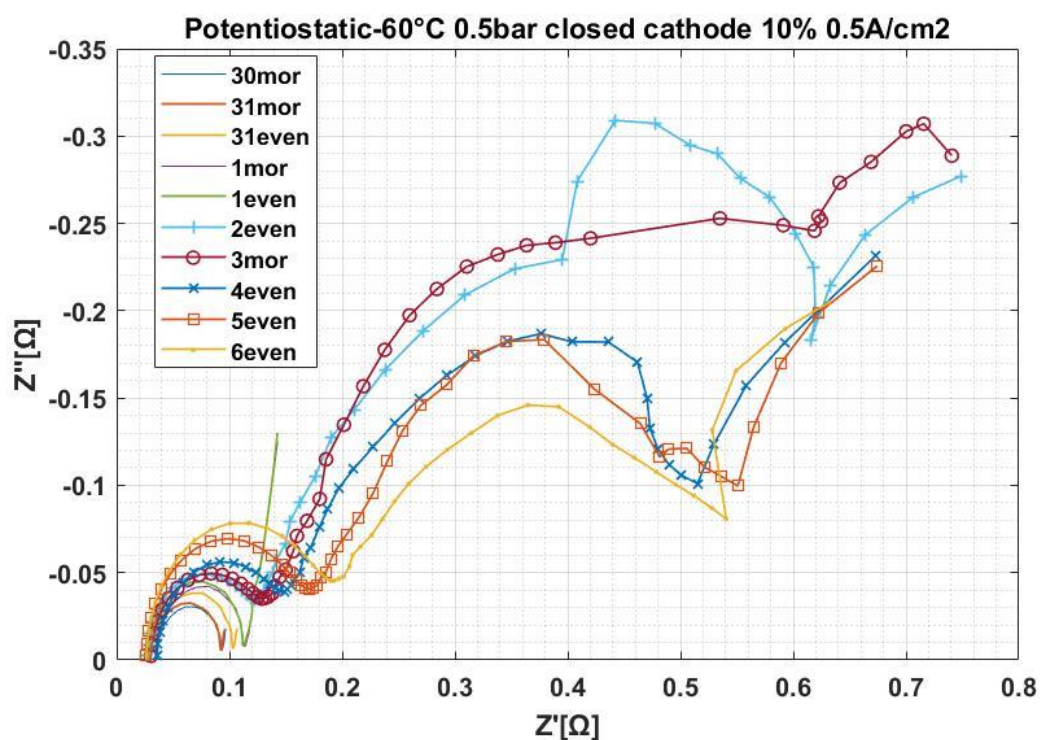


Figure 142 EIS measurements with potentiostatic mode- removed invalid impedance spectra.

Figure 143 shows Nyquist plots of EIS data measured at 0 mA, corresponding to the open circuit voltage of the cell, with invalid spectra removed. It is observed the presence of an arc at high frequency, and a second arc in the mid-low frequency region affected by noise. The latter seems to be made of two merged semicircles.

It seems that the HF arc increases but the second arc shows a decreasing behaviour.

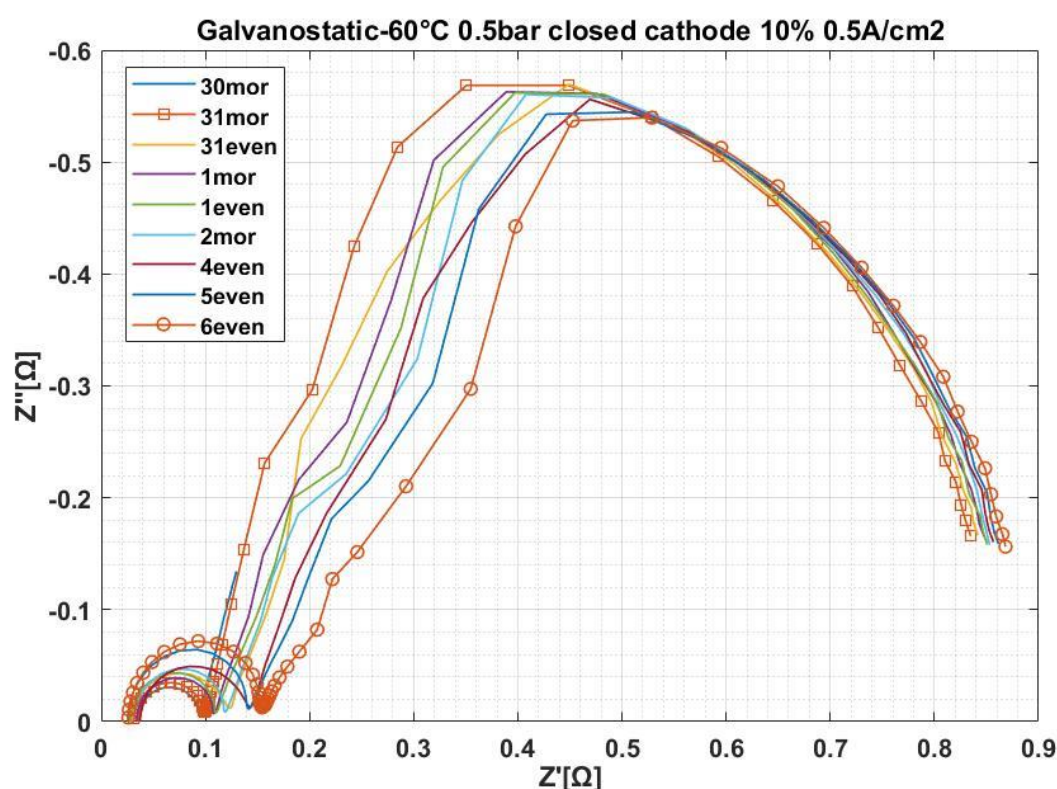


Figure 143 EIS measurements with galvanostatic mode- removed invalid impedance spectra.

## DISCUSSION

The analysis considers both EIS results gained from potentiostatic and galvanostatic modes. The trend of ohmic resistance, high frequency charge transfer resistance and capacitance is shown in Figures 144 and 145.

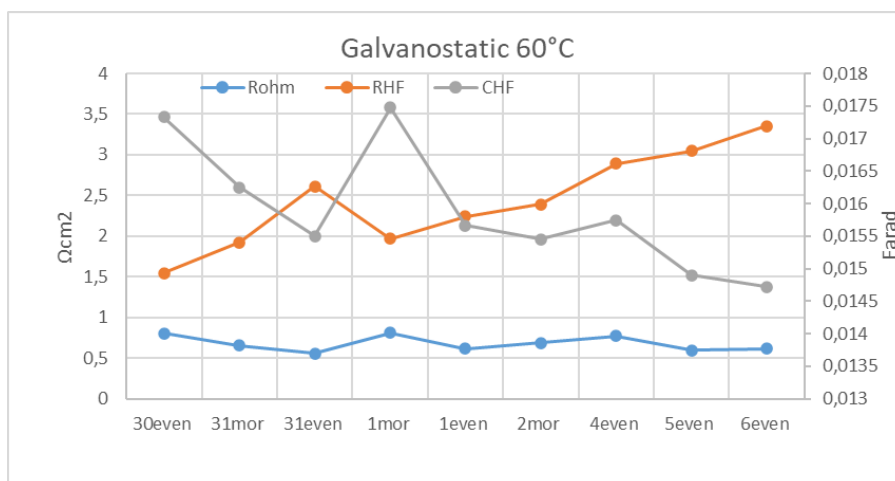


Figure 144

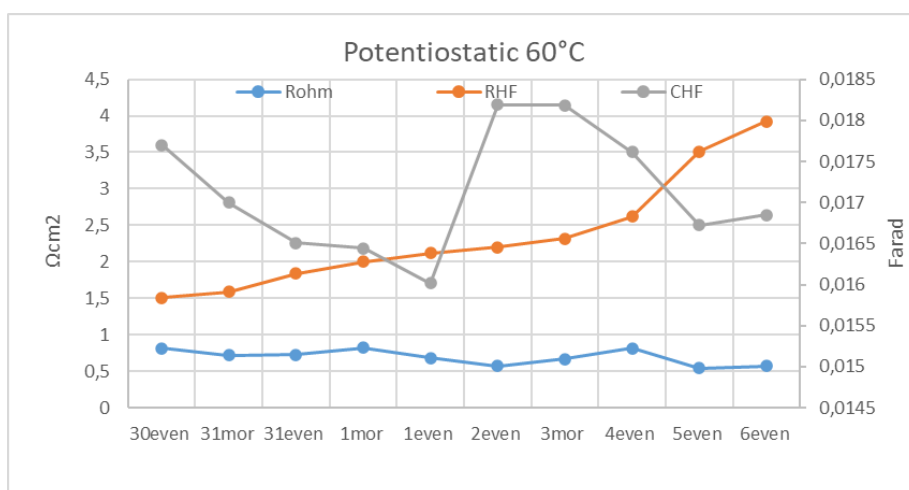


Figure 145

For both EIS tests the ohmic resistance seems to have a very slight decrease- although an oscillating behaviour between 0.818-0.542  $\Omega\text{cm}^2$  and 0.0806- 0.593  $\Omega\text{cm}^2$  is noticed for potentiostatic and galvanostatic respectively- whereas the charge transfer resistance increment is much more evident from 1.51 to 3.92  $\Omega\text{cm}^2$  for potentiostatic and 1.55 to 3.35  $\Omega\text{cm}^2$  for galvanostatic. The capacitance of the high frequency arc is characterized by a decreasing trend, at least during the first part of the test. Anyway, possible oscillations of the value may be related to time-variance of the system during the whole test but if the start and the end are considered, a decrease can be observed. It is not possible to say much about the low frequency arc due to the presence of noise, particularly in the impedance spectra obtained with voltage control. Hence, it is not possible to gain a quantitative and reliable measurement of the overall polarization resistance. On the other hand, some qualitative considerations can be done for the LF results gained with galvanostatic tests. The low frequency intercept with the real axis seems to show increasing values, hence it is suggested an increase of the total

polarization resistance. As it is shown in the figure below, the trend of the total polarization resistance is mainly due to that of the charge transfer resistance of the HF arc.

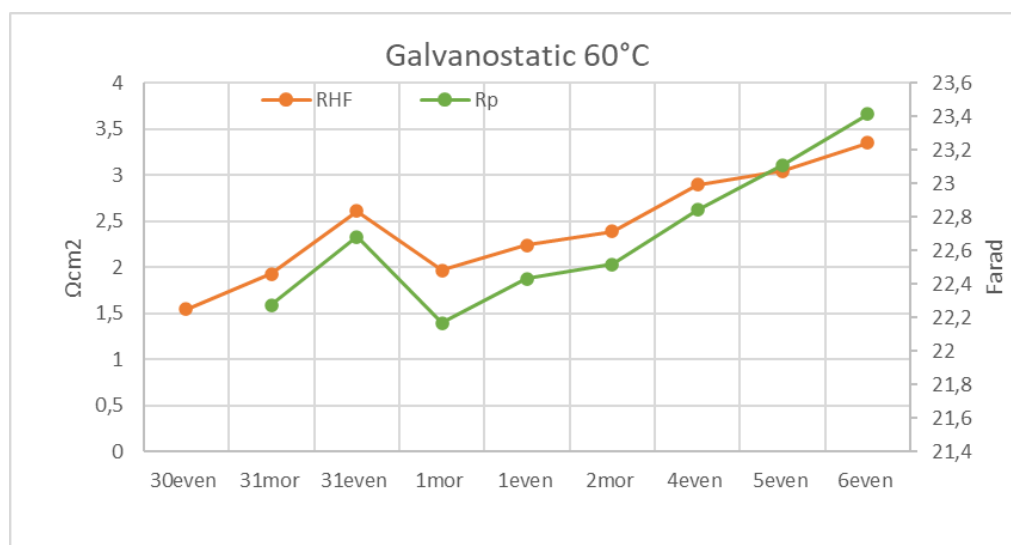


Figure 146

Considering the trends of *Figures 144* and *145*, it is assumed that the HF feature is related to current constrictions, whereas the second incomplete semicircle and third one are respectively associated to charge transfer kinetics in the anode and mass transport limitations.

Concluding, the EIS results are in accordance with the increase of voltage during the degradation test. A probable reason of the ohmic resistance decrease (from 0.8 to 0.6  $\Omega\text{cm}^2$ ) is the thinning of the membrane. It is suggested a loss of material from the aged membrane, which can also explain the decrease of the capacitance at high frequency. A loss of materials or agglomeration of catalyst particles can cause an increase of the distributed contact resistances at the electrolyte/anode interface. This determines current constrictions and thus a lower performance of the cell. About the low frequency region, qualitatively it is possible to say that the larger arc in the galvanostatic tests or the increment of the third arc in the potentiostatic tests may be insights of the anode degradation. Large arcs are characterized by lower value of the capacitance, which in turn is linked to the number of active sites in the electrode surface. A low value of the capacitance demonstrates the occurrence of degradation processes in the catalyst layer. Instead, the presence of a third arc at low frequencies suggests important mass transport limitations, another sign of degradation.

## RESULTS SECOND SERIES

After around 135 h of operation at 0.5  $\text{A}/\text{cm}^2$  the cell has shown a degradation rate of about 720  $\mu\text{V}/\text{h}$ .

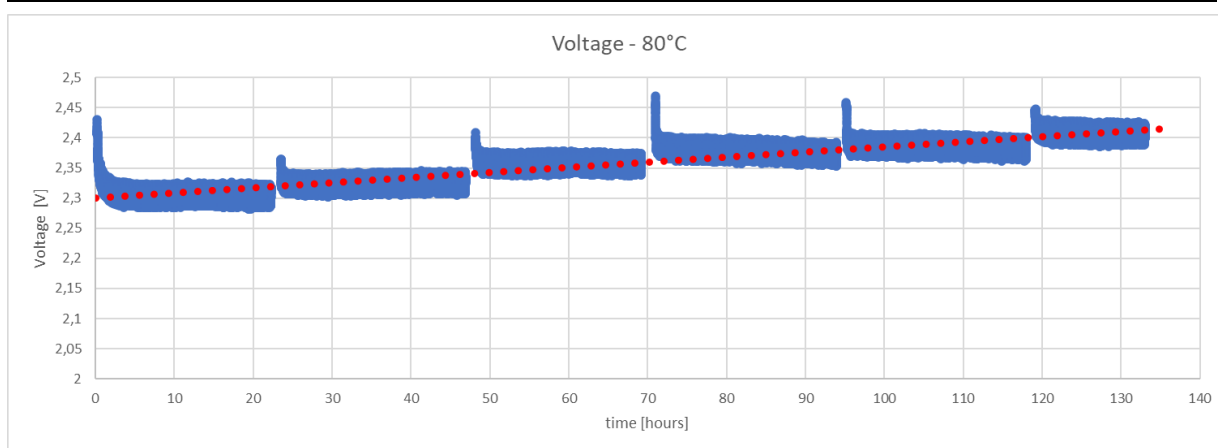


Figure 147 Voltage trend during the degradation test at 80°C.

The effective temperature during the experiment oscillates around 79°C whereas real gauge pressure at the anode and cathode was 0,91 bar and 0,44 bar respectively.

The study shows an increase of the cell potential, instead pressure at the heater remains in a range between 1,14 bar-1,29bar, temperature at the heater between 79,3°C -79,8°C and cell temperature remain 79,5°C -79,7°C.

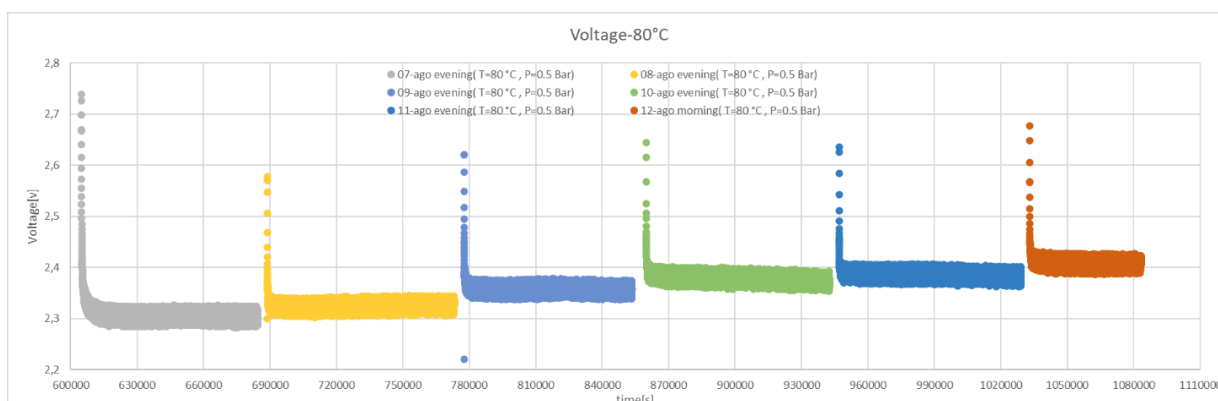


Figure 148

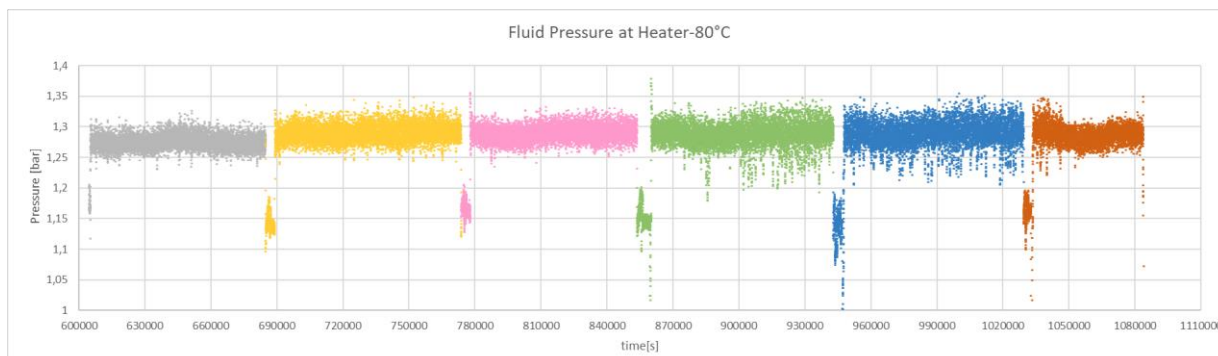


Figure 149



Figures 150 and 151 show the overall EIS measurements performed under voltage and current control during the degradation test.

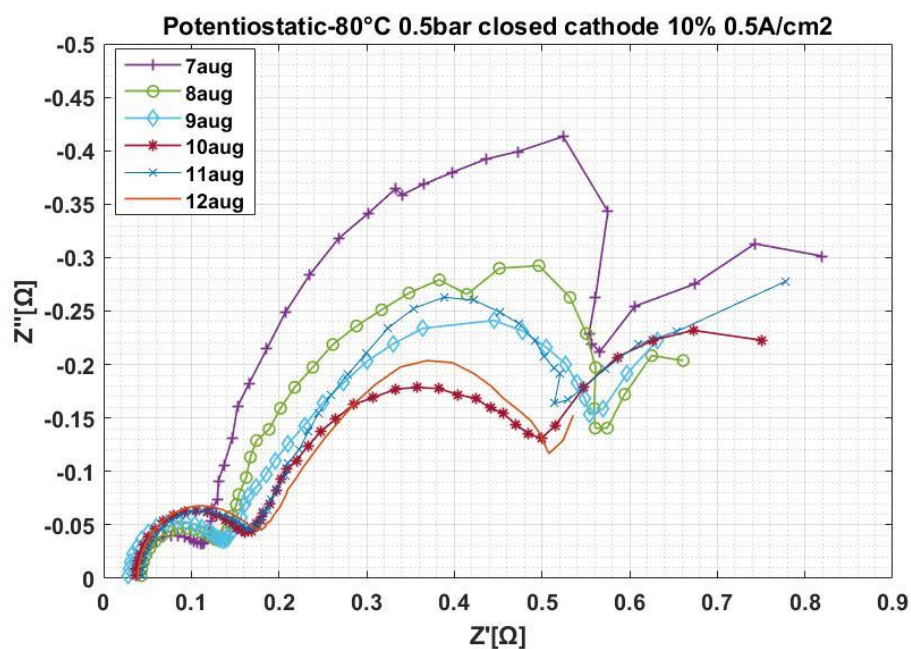


Figure 150 EIS measurements with potentiostatic mode.

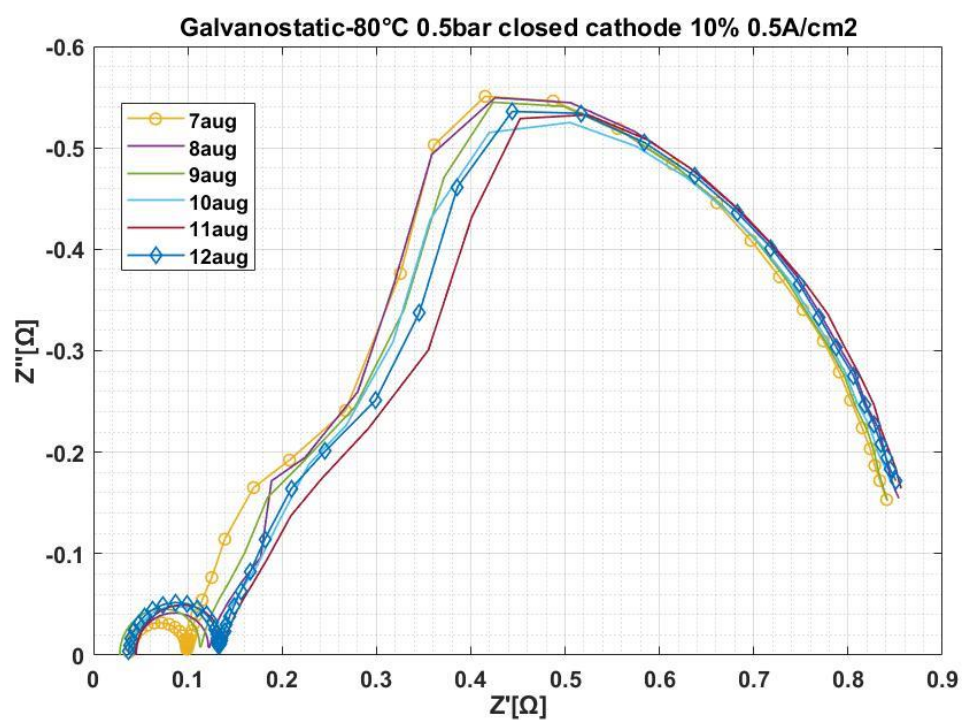


Figure 151 All EIS measurements with galvanostatic mode.

### Data quality assessment

Validation through KK relations shows that impedance spectra obtained with both modes have similar residuals behaviour, i.e. low residuals of high frequency data and larger residuals as data are collected at lower frequencies. Data quality is mostly affected by time variance rather than noise.

By visual inspection of both Nyquist and Bode plots, at least two time constants are individuated, so two distinguishable features are observed: high frequency arc and a mid-frequency arc, mainly affected by noise. As previously said, due to high level of noise the LF data are considered only in a qualitative way. Therefore, the ECM used to fit the experimental data is LR(QR)(QR).

### DISCUSSION

The analysis is carried out with both EIS results gained from potentiostatic and galvanostatic modes. The trend of ohmic resistance, high frequency charge transfer resistance and capacitance is shown in the figures below.

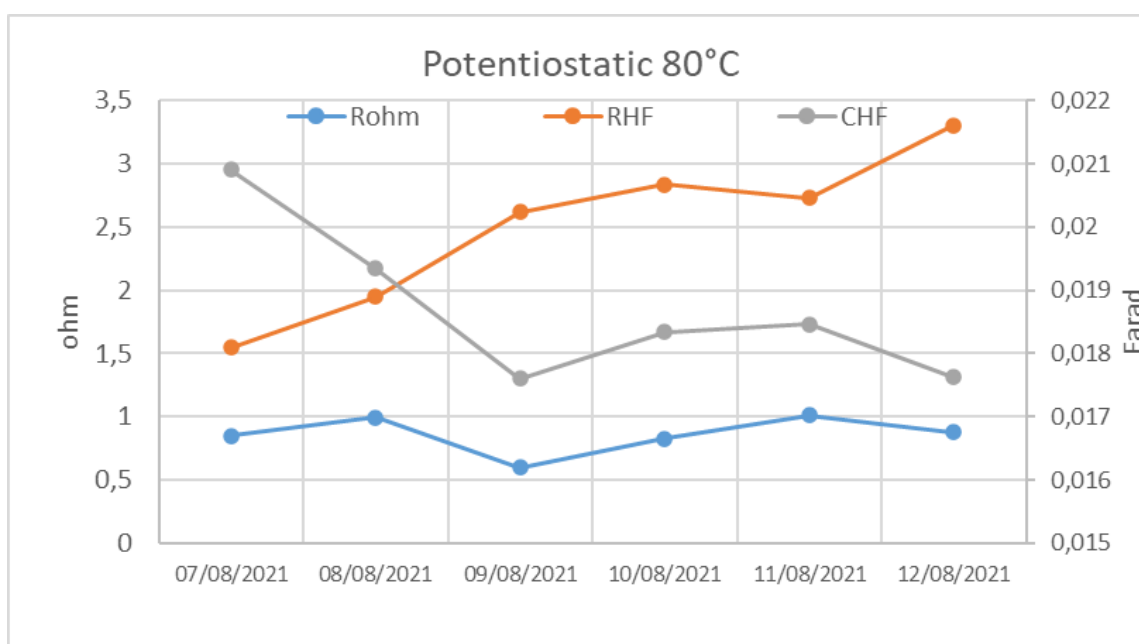


Figure 152



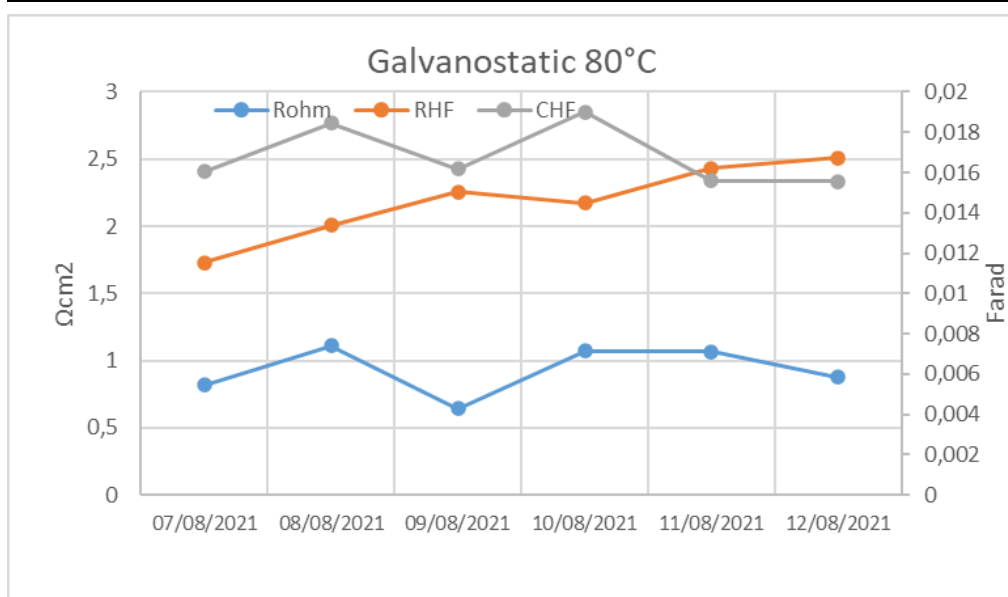


Figure 153

For both EIS tests the high frequency arc shows a moderate increase: the ohmic resistance seems to oscillate in the between  $0.8\text{--}1.1\ \Omega\text{cm}^2$  whereas there is an evident increment of the charge transfer resistance. Instead, the HF capacitance shows a small decrease, higher in the potentiostatic test (from 0.0209 to 0.0176 F) rather than in the galvanostatic (from 0.0160 to 0.0155). As before, it is possible to get a qualitative trend of the LF feature from the galvanostatic measurements. It is observed an increase of the diameter of the mid-low frequency arc; hence, it can be assumed an increase of the total polarization resistance.

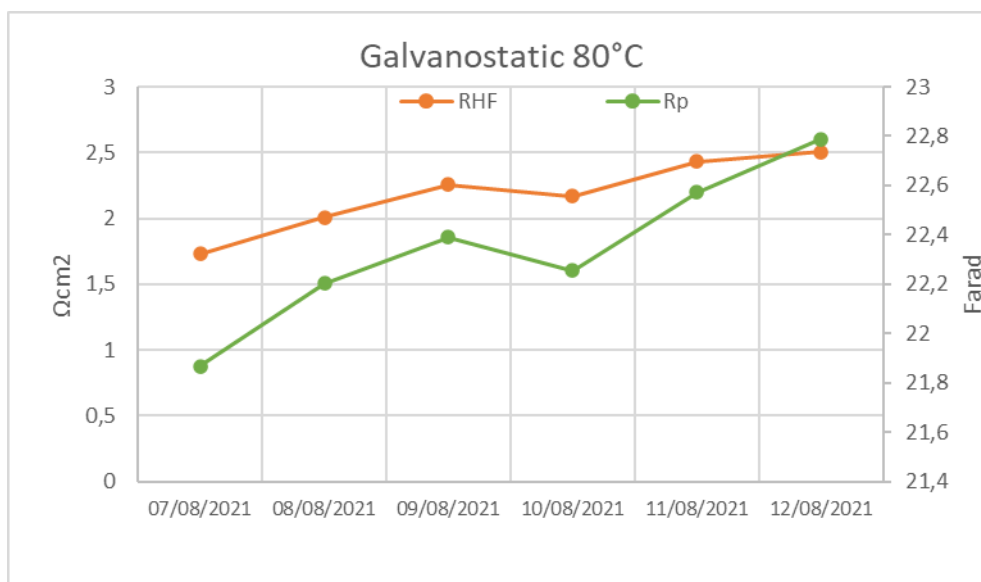


Figure 154

These results are consistent with the voltage increase during the experiment at 80°C. Therefore, the cell is experiencing degradation mainly of the anode even if some loss of performance are individuated also in the membrane.

#### 6.4.2 Degradation test performed at 80°C, 0.5bar, closed cathode, 10% mass flow rate, constant current density of 1 A/cm<sup>2</sup>

The degradation test is carried out at a constant current density of 1 A/cm<sup>2</sup> and the cell voltage increase over time is monitored. It is performed at 80°C, imposed gauge pressure of 0.5bar at the anode and cathode, and closed cathode configuration.

Two types of EIS tests have been used:

- Potentiostatic test is performed at 0 DC V by varying the frequency from 100 kHz to 0,001 Hz in single sine mode and using a sinusoidal excitation signal of 10mV root mean square (rms);
- Galvanostatic test is performed at 0 DC mA by varying the frequency from 200 kHz to 0,002 Hz in single sine mode and using a sinusoidal excitation signal of 1000 mA root mean square (rms).

## **RESULTS**

After around 350 h of operation at 1 A/cm<sup>2</sup> the cell has shown a degradation rate of about 180  $\mu$ V/h.

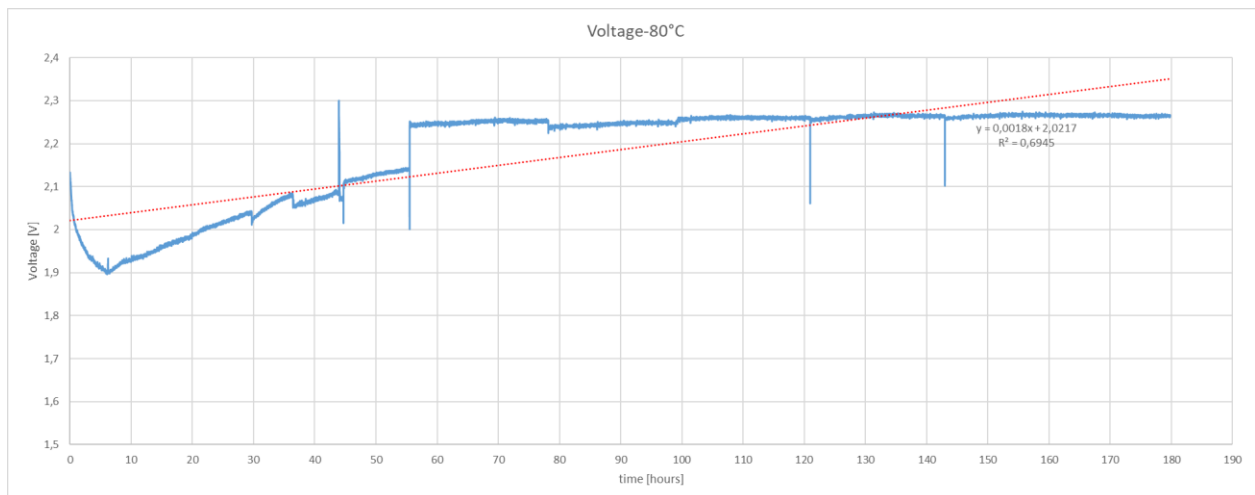


Figure 155

The effective temperature during the experiment oscillates around 80°C whereas real gauge pressure at the anode and cathode was 0,95 bar and 0,42 bar respectively. The study shows

---

an increase of the cell potential and of the pressure at the heater; instead, temperature at the heater and cell temperature remain almost unvaried.

#### *Data quality assessment*

All impedance spectra are subject to a quality validation through KK relations. It is noticed that impedance measurements gained with galvanostatic mode have quite high residuals due mostly to the instability of the cell during their execution. Conversely, potentiostatic test have provided measurement with lower residuals thus higher quality. A visual inspection of Nyquist and Bode plots clearly show two time constants for the potentiostatic tests and three for the galvanostatic tests.

#### *Modelling*

Nyquist plot below shows the impedance spectra measured during potentiostatic tests.

Impedance spectra obtained under voltage control are characterized by two semicircles, appearing at high and mid-low frequency respectively. On the other hand, the shape of the impedance spectra produced by galvanostatic tests changes depending on the DC value of the current. Three semicircle are detected at 0mA, one at high frequency and two merged in the mid-low frequency range. As the current increases the mid frequency arc tends to disappear so at the end there are two arcs.

### **DISCUSSION**

The degradation test has a duration of around 350 hours in which the cell behaviour is under dynamic conditions, i.e. several perturbations occur during its execution. After perturbation the system tends to reach a new equilibrium hence there is always a period of stabilization after each perturbation.

The first part of the test (60 hours) is of stabilization of the cell voltage, then there is the start of the degradation test. At around 120 h there is a perturbation of the cell hence the time lapse up to 200h is of stabilization. After that, the degradation test continues till the end at around 350h.

As a consequence, parts of the test where perturbations and stabilization occur are not considered in the analysis. This means that EIS measurements gained during these part of the test are not considered as well.

The validation with KK relations put in evidence the inconsistency of the impedance spectra measured with galvanostatic mode whereas almost all impedance data under potentiostatic mode showed good quality, i.e. residuals below 0.5%. As a result, only potentiostatic tests are used for the analysis. The EIS tests considered are those shown in the figure below.

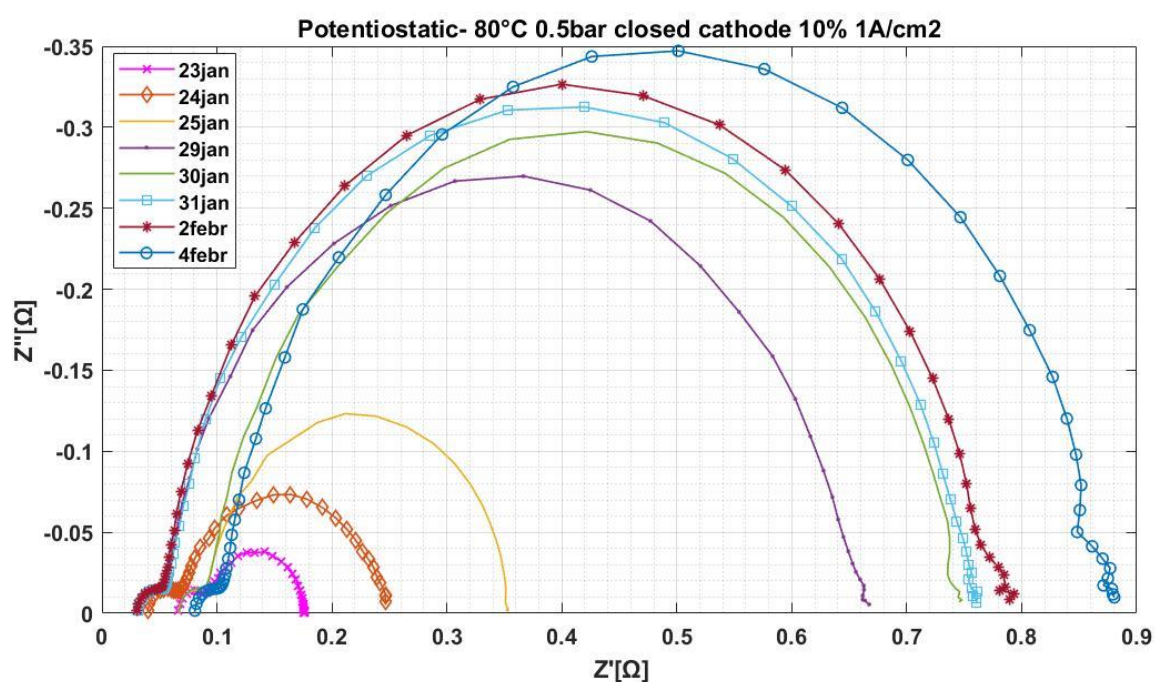


Figure 156

It is observed an increase of the low frequency arc whereas the dimension of the high frequency arc seems not to vary. Further on, a third semicircle affected by noise appears at very low frequency as the degradation test goes on.

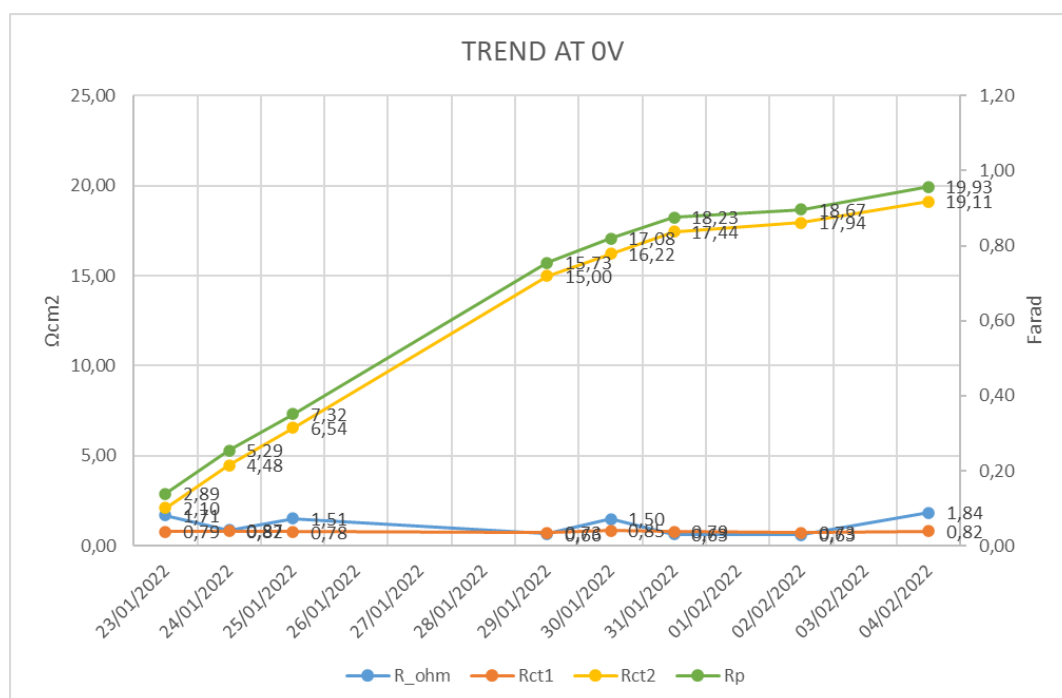


Figure 157

---

The ohmic resistance shows an oscillating behaviour, so it is not possible to say whether or not a degradation process is occurring in the MEA. Its value goes from a maximum of  $1.84 \Omega\text{cm}^2$  and a minimum of  $0.63 \Omega\text{cm}^2$ . The high frequency arc seems not change during the operation of the cell, the charge transfer resistance is around  $0.73\text{-}0.82 \Omega\text{cm}^2$  and the capacitance is constant at  $0.02 \text{ F}$ . What shows a substantial increase is the low frequency arc, i.e. the charge transfer resistance increases from  $2.10$  to  $19.11 \Omega\text{cm}^2$  whereas the capacitance decreases from  $0.5$  to  $0.3 \text{ F}$ . As a consequence, the polarization resistance-corresponding to the sum of the diameters of the two arcs- increases from  $2.9$  to  $19.9 \Omega\text{cm}^2$ .

The results of the EIS tests shows that a component affected by degradation process is the anode. This is in accordance with the increase of voltage during the degradation test of about  $350 \text{ mV}$ , corresponding to a degradation rate of  $180 \mu\text{V/h}$ .

---

---

# Conclusion

The present work has the purpose of investigating the performance and durability of the PEM water electrolyser through the execution of impedance spectroscopy measurements.

PEM electrolytic cells are complex electrochemical system in which several processes occur. Among the different techniques available to study such system, AC impedance spectroscopy is one of the most promising. The main advantages are the possibility of individuating and distinguishing the phenomena, quantifying their impact on the cell performance and identifying the critical component. Moreover, it is a non-destructive method so it is applied during the operation of the cell. Impedance spectra measured during the performance of EIS tests are then analysed by complex non-linear least square (CNLS) approximation to a model function obtained by an equivalent circuit model used to fit the experimental data. the principal drawback of this technique is the time required to get a full impedance spectrum. Measurements at low frequency are time consuming and during this lapse of time the drift of the system can occur affecting in turn the measurements.

The experimental part has been conducted by operating the PEMWE under different test condition to obtain the electrochemical characterization of the two MEAs under study. Polarization curves and electrochemical impedance spectroscopy tests have been performed at different temperatures, pressures, cathode configurations and mass flow rates. Four principal categories of experiment are individuated: open cathode tests, closed cathode tests, comparison between open and closed cathode and finally degradation tests. The main outcomes are briefly reported below.

The results obtained from open cathode measurements have suggested to attribute the high frequency feature to the properties of the MEA, due to its non-dependence on current density and voltage. The capacitive behaviour at high frequency may be related to catalysts agglomerates or to bad contact between the anode catalyst layer and the electrolyte. This hypothesis is confirmed also from the fact that it is also present in both the MEAs studied and it is showing the same behaviour. On the other hand, the mid-low frequency semicircle comes from kinetics processes, related to the OER and HER. In this regard, it is assumed that the low frequency feature is mostly linked to the anode, characterized by a sluggish kinetics with respect to the faster cathode.

The open/closed cathode series of experiments puts in evidence that open cathode has better performance probably because of the higher thermal stability. It was also observed that EIS measurements during closed cathode show a more pronounced high frequency arc, thus the presence of more relevant current constrictions are possible.

---

Finally, the most important and time-taking tests performed are the degradation tests. The first series of degradation is performed on an already aged MEA at two different temperatures but at the same constant current densities of  $0.5 \text{ A/cm}^2$ . It is found a degradation rate of  $1080 \text{ } \mu\text{V/h}$  during the 168 hours of test at  $60^\circ\text{C}$  and  $720 \text{ } \mu\text{V/h}$  for the test performed at  $80^\circ\text{C}$  with a duration of around 135 hours. Although the first test shows a higher degradation rate, it is possible to say that degradation is faster during the test performed at  $80^\circ\text{C}$ . Hence, temperature is a stressor for the cell because it accelerates its loss of performance. The impedance spectra results suggest that both anode and electrolyte are subject to degradation since both charge transfer resistances of the HF arc- related to MEA structure as said before- and of the low frequency arc- attributed to the anode- have shown an increasing behaviour. Regarding the second series performed on the new MEA at  $80^\circ\text{C}$  and with constant current density of  $1 \text{ A/cm}^2$ , it has a longer duration with respect to the others, 350 hours, and a degradation rate of  $180 \text{ } \mu\text{V/h}$ . In this case, only the anode shows the presence of degradation effects.

In future works, a fundamental aspect is to account for the ambiguity related to the equivalent circuit model used to simulate the experimental impedance spectrum. ECMs, generally chosen a priori, do not describe the physicochemical properties of the system, they simply reproduce the experimental data. Only a pre-knowledge of the system under study can guide on the choice of the ECM to get meaningful results. Therefore, other methods such as distribution of relaxation times (DRT), can assist to the identification of a proper number of circuit element avoiding problem of under- or over fitting as well as lack of correlation with the physics.



---

# Appendix-TABLES

Tests performed at T=79°C & T=71°C, with open cathode at different gauge pressure

Table 1 Fitting results of potentiostatic at 79°C -1.4 bar

|                  |                   |                                       |                   |
|------------------|-------------------|---------------------------------------|-------------------|
| <b>Pressure</b>  | 1.4 bar           | <b>T</b>                              | <b>79°C</b>       |
| <b>circuit</b>   | <b>LR(QR)(QR)</b> |                                       | <b>POT</b>        |
| <b>weighting</b> | modulus           |                                       |                   |
|                  |                   | <b>open</b>                           |                   |
| <b>element</b>   | sub-parameters    | value                                 | error             |
| <b>L1</b>        |                   | 2,48E-06                              | 0,041055          |
| <b>R1</b>        |                   | 0,024984                              | 0,024412          |
| <b>CPE1</b>      | TDE               | 0,022912                              | 0,078978          |
|                  | PHIDE             | 0,99012                               | 0,015618          |
| <b>R2</b>        |                   | 0,033887                              | 0,028028          |
| <b>CPE2</b>      | TDE               | 0,93772                               | 0,018362          |
|                  | PHIDE             | 0,8201                                | 0,0079397         |
| <b>R3</b>        |                   | 6,98E-01                              | 0,042531          |
|                  |                   | <b>C with <math>\omega</math> max</b> | <b>C with Rct</b> |
|                  | C1 [F]            | 0,021792944                           | 0,02133195        |

Table 2 Fitting results of potentiostatic at 79°C -2.4 bar

|                  |                   |                                       |                   |
|------------------|-------------------|---------------------------------------|-------------------|
| <b>Pressure</b>  | 2.4 bar           | <b>T</b>                              | <b>79°C</b>       |
| <b>circuit</b>   | <b>LR(QR)(QR)</b> |                                       | <b>POT</b>        |
| <b>weighting</b> | modulus           |                                       |                   |
|                  |                   | <b>open</b>                           |                   |
| <b>element</b>   | sub-parameters    | value                                 | error             |
| <b>L1</b>        |                   | 2,41E-06                              | 0,039563          |
| <b>R1</b>        |                   | 0,024061                              | 0,022457          |
| <b>CPE1</b>      | TDE               | 0,019981                              | 0,066981          |
|                  | PHIDE             | 1,0088                                | 0,013046          |
| <b>R2</b>        |                   | 0,033078                              | 0,022938          |
| <b>CPE2</b>      | TDE               | 1,3002                                | 0,0080092         |
|                  | PHIDE             | 0,77188                               | 0,0040824         |
| <b>R3</b>        |                   | 2,67E+07                              | 0,20668           |
|                  |                   | <b>C with <math>\omega</math> max</b> | <b>C with Rct</b> |
|                  | C1 [F]            | 0,020891878                           | 0,02129883        |

Table 3 Fitting results of potentiostatic at 79°C -5 bar

|                  |                   |                                       |                   |
|------------------|-------------------|---------------------------------------|-------------------|
| <b>Pressure</b>  | 5 bar             | <b>T</b>                              | <b>79°C</b>       |
| <b>circuit</b>   | <b>LR(QR)(QR)</b> |                                       | POT               |
| <b>weighting</b> | modulus           |                                       |                   |
|                  |                   | <b>open</b>                           |                   |
| <b>element</b>   | sub-parameters    | value                                 | error             |
| <b>L1</b>        |                   | 2,74E-06                              | 5,75E-02          |
| <b>R1</b>        |                   | 0,021623                              | 0,04819           |
| <b>CPE1</b>      | TDE               | 0,031538                              | 0,10177           |
|                  | PHIDE             | 0,92756                               | 0,022399          |
| <b>R2</b>        |                   | 0,03972                               | 0,036541          |
| <b>CPE2</b>      | TDE               | 0,83334                               | 0,011824          |
|                  | PHIDE             | 0,84966                               | 0,0053407         |
| <b>R3</b>        |                   | 1,35E+07                              | 0,6782            |
|                  |                   | <b>C with <math>\omega</math> max</b> | <b>C with Rct</b> |
|                  | C1 [F]            | 0,021850633                           | 0,01871472        |

Table 4 Fitting results of potentiostatic at 79°C -7.5 bar

|                  |                   |                                       |                   |
|------------------|-------------------|---------------------------------------|-------------------|
| <b>Pressure</b>  | 7.5 bar           | <b>T</b>                              | <b>79°C</b>       |
| <b>circuit</b>   | <b>LR(QR)(QR)</b> |                                       | POT               |
| <b>weighting</b> | modulus           |                                       |                   |
|                  |                   | <b>open</b>                           |                   |
| <b>element</b>   | sub-parameters    | value                                 | error             |
| <b>L1</b>        |                   | 2,71E-06                              | 0,057697          |
| <b>R1</b>        |                   | 0,02272                               | 0,044385          |
| <b>CPE1</b>      | TDE               | 0,029877                              | 0,10155           |
|                  | PHIDE             | 0,93736                               | 0,021956          |
| <b>R2</b>        |                   | 0,03931                               | 0,035952          |
| <b>CPE2</b>      | TDE               | 0,85459                               | 0,011708          |
|                  | PHIDE             | 0,84096                               | 0,0053581         |
| <b>R3</b>        |                   | 5,78E+10                              | 0,0001585         |
|                  |                   | <b>C with <math>\omega</math> max</b> | <b>C with Rct</b> |
|                  | C1 [F]            | 0,0217534                             | 0,01903383        |

Table 5 Fitting results of galvanostatic at 79°C -1.4 bar

|                  |                   |                                       |                   |
|------------------|-------------------|---------------------------------------|-------------------|
| <b>Pressure</b>  | 1.4 bar           | <b>T</b>                              | <b>79°C</b>       |
| <b>circuit</b>   | <b>LR(QR)(QR)</b> |                                       | <b>GALV</b>       |
| <b>weighting</b> | modulus           |                                       |                   |
|                  |                   | <b>open</b>                           |                   |
| <b>element</b>   | sub-parameters    | value                                 | error             |
| <b>L1</b>        |                   | 1,81E-06                              | 0,23958           |
| <b>R1</b>        |                   | 0,027397                              | 0,063703          |
| <b>CPE1</b>      | TDE               | 0,0090788                             | 0,44692           |
|                  | PHIDE             | 1,1755                                | 0,070207          |
| <b>R2</b>        |                   | 0,021112                              | 0,1574            |
| <b>CPE2</b>      | TDE               | 2,1001                                | 0,097065          |
|                  | PHIDE             | 0,60497                               | 0,05732           |
| <b>R3</b>        |                   | 7,45E-01                              | 0,29594           |
|                  |                   | <b>C with <math>\omega</math> max</b> | <b>C with Rct</b> |
|                  | C1 [F]            | 0,022096612                           | 0,032586354       |

Table 6 Fitting results of galvanostatic at 79°C -2.4 bar

|                  |                   |                                       |                   |
|------------------|-------------------|---------------------------------------|-------------------|
| <b>Pressure</b>  | 2.4 bar           | <b>T</b>                              | <b>79°C</b>       |
| <b>circuit</b>   | <b>LR(QR)(QR)</b> |                                       | <b>GALV</b>       |
| <b>weighting</b> | modulus           |                                       |                   |
|                  |                   | <b>open</b>                           |                   |
| <b>element</b>   | sub-parameters    | value                                 | error             |
| <b>L1</b>        |                   | 1,90E-06                              | 0,20717           |
| <b>R1</b>        |                   | 0,026306                              | 0,062309          |
| <b>CPE1</b>      | TDE               | 0,010164                              | 0,39037           |
|                  | PHIDE             | 1,1517                                | 0,06274           |
| <b>R2</b>        |                   | 0,023066                              | 0,13634           |
| <b>CPE2</b>      | TDE               | 2,0435                                | 0,087349          |
|                  | PHIDE             | 0,61679                               | 0,051455          |
| <b>R3</b>        |                   | 7,30E-01                              | 0,25897           |
|                  |                   | <b>C with <math>\omega</math> max</b> | <b>C with Rct</b> |
|                  | C1 [F]            | 0,021926795                           | 0,030563095       |

Table 7 Fitting results of galvanostatic at 79°C -5 bar

|                  |                   |                                       |                   |
|------------------|-------------------|---------------------------------------|-------------------|
| <b>Pressure</b>  | 5 bar             | <b>T</b>                              | <b>79°C</b>       |
| <b>circuit</b>   | <b>LR(QR)(QR)</b> |                                       | <b>GALV</b>       |
| <b>weighting</b> | modulus           |                                       |                   |
|                  |                   | <b>open</b>                           |                   |
| <b>element</b>   | sub-parameters    | value                                 | error             |
| <b>L1</b>        |                   | 1,79E-06                              | 2,86E-01          |
| <b>R1</b>        |                   | 0,026115                              | 0,079868          |
| <b>CPE1</b>      | TDE               | 0,0098384                             | 0,50569           |
|                  | PHIDE             | 1,1586                                | 0,080398          |
| <b>R2</b>        |                   | 0,022813                              | 0,17387           |
| <b>CPE2</b>      | TDE               | 2,0202                                | 0,1112            |
|                  | PHIDE             | 0,61993                               | 0,06456           |
| <b>R3</b>        |                   | 9,66E-01                              | 0,42387           |
|                  |                   | <b>C with <math>\omega</math> max</b> | <b>C with Rct</b> |
|                  | C1 [F]            | 0,021979749                           | 0,031075568       |

Table 8 Fitting results of galvanostatic at 79°C -7.5 bar

|                  |                   |                                       |                   |
|------------------|-------------------|---------------------------------------|-------------------|
| <b>Pressure</b>  | 7.5 bar           | <b>T</b>                              | <b>79°C</b>       |
| <b>circuit</b>   | <b>LR(QR)(QR)</b> |                                       | <b>GALV</b>       |
| <b>weighting</b> | modulus           |                                       |                   |
|                  |                   | <b>open</b>                           |                   |
| <b>element</b>   | sub-parameters    | value                                 | error             |
| <b>L1</b>        |                   | 1,80E-06                              | 0,24481           |
| <b>R1</b>        |                   | 0,026565                              | 0,06386           |
| <b>CPE1</b>      | TDE               | 0,0082114                             | 0,4315            |
|                  | PHIDE             | 1,1941                                | 0,06532           |
| <b>R2</b>        |                   | 0,020771                              | 0,13662           |
| <b>CPE2</b>      | TDE               | 2,4462                                | 0,035784          |
|                  | PHIDE             | 0,56101                               | 0,028862          |
| <b>R3</b>        |                   | 7,03E+08                              | 0,048406          |
|                  |                   | <b>C with <math>\omega</math> max</b> | <b>C with Rct</b> |
|                  | C1 [F]            | 0,021961164                           | 0,033645189       |

Table 9 Fitting results of potentiostatic at 71°C -7.5 bar

|                  |                   |                                       |                   |
|------------------|-------------------|---------------------------------------|-------------------|
| <b>Pressure</b>  | 7.5 bar           | <b>Temperature</b>                    | <b>71°C</b>       |
| <b>circuit</b>   | <b>LR(QR)(QR)</b> |                                       | POT               |
| <b>weighting</b> | modulus           |                                       |                   |
|                  |                   | <b>open</b>                           |                   |
| <b>element</b>   | sub-parameters    | value                                 | error             |
| <b>L1</b>        |                   | 2,71E-06                              | 0,055397          |
| <b>R1</b>        |                   | 0,022703                              | 0,04201           |
| <b>CPE1</b>      | TDE               | 0,02838                               | 0,097435          |
|                  | PHIDE             | 0,94434                               | 0,020785          |
| <b>R2</b>        |                   | 0,039351                              | 0,034109          |
| <b>CPE2</b>      | TDE               | 0,83664                               | 0,011267          |
|                  | PHIDE             | 0,84023                               | 0,0051276         |
| <b>R3</b>        |                   | 5,69E+10                              | 0,00015729        |
|                  |                   | <b>C with <math>\omega</math> max</b> | <b>C with Rct</b> |
|                  | C1 [F]            | 0,021407146                           | 0,01901156        |

Table 10 Fitting results of potentiostatic at 71°C -5 bar

|                  |                   |                                       |                   |
|------------------|-------------------|---------------------------------------|-------------------|
| <b>Pressure</b>  | 5 bar             | <b>Temperature</b>                    | <b>71°C</b>       |
| <b>circuit</b>   | <b>LR(QR)(QR)</b> |                                       | POT               |
| <b>weighting</b> | modulus           |                                       |                   |
|                  |                   | <b>open</b>                           |                   |
| <b>element</b>   | sub-parameters    | value                                 | error             |
| <b>L1</b>        |                   | 2,67E-06                              | 0,06042           |
| <b>R1</b>        |                   | 0,022382                              | 0,047909          |
| <b>CPE1</b>      | TDE               | 0,029347                              | 0,10285           |
|                  | PHIDE             | 0,93701                               | 0,022658          |
| <b>R2</b>        |                   | 0,037878                              | 0,038212          |
| <b>CPE2</b>      | TDE               | 0,87991                               | 0,011667          |
|                  | PHIDE             | 0,84681                               | 0,0052696         |
| <b>R3</b>        |                   | 8,65E+10                              | 0,00010276        |
|                  |                   | <b>C with <math>\omega</math> max</b> | <b>C with Rct</b> |
|                  | C1 [F]            | 0,021329657                           | 0,01857716        |

Table 11 Fitting results of potentiostatic at 71°C -2.5 bar

|                  |                   |                                       |                   |
|------------------|-------------------|---------------------------------------|-------------------|
| <b>Pressure</b>  | 2.5 bar           | <b>Temperature</b>                    | <b>71°C</b>       |
| <b>circuit</b>   | <b>LR(QR)(QR)</b> |                                       | POT               |
| <b>weighting</b> | modulus           |                                       |                   |
|                  |                   | <b>open</b>                           |                   |
| <b>element</b>   | sub-parameters    | value                                 | error             |
| <b>L1</b>        |                   | 2,65E-06                              | 6,36E-02          |
| <b>R1</b>        |                   | 0,022589                              | 0,049951          |
| <b>CPE1</b>      | TDE               | 0,029659                              | 0,10989           |
|                  | PHIDE             | 0,93748                               | 0,024249          |
| <b>R2</b>        |                   | 0,036968                              | 0,041303          |
| <b>CPE2</b>      | TDE               | 0,84606                               | 0,01185           |
|                  | PHIDE             | 0,8395                                | 0,0053856         |
| <b>R3</b>        |                   | 8,65E+10                              | 0,00010762        |
|                  |                   | <b>C with <math>\omega</math> max</b> | <b>C with Rct</b> |
|                  | C1 [F]            | 0,021607806                           | 0,018825852       |

Table 12 Fitting results of potentiostatic at 71°C -1.4 bar

|                  |                   |                                       |                   |
|------------------|-------------------|---------------------------------------|-------------------|
| <b>Pressure</b>  | 1.4 bar           | <b>Temperature</b>                    | <b>71°C</b>       |
| <b>circuit</b>   | <b>LR(QR)(QR)</b> |                                       | POT               |
| <b>weighting</b> | modulus           |                                       |                   |
|                  |                   | <b>open</b>                           |                   |
| <b>element</b>   | sub-parameters    | value                                 | error             |
| <b>L1</b>        |                   | 2,68E-06                              | 0,061001          |
| <b>R1</b>        |                   | 0,022461                              | 0,048914          |
| <b>CPE1</b>      | TDE               | 0,029913                              | 0,10579           |
|                  | PHIDE             | 0,93502                               | 0,023425          |
| <b>R2</b>        |                   | 0,037401                              | 0,03978           |
| <b>CPE2</b>      | TDE               | 0,84197                               | 0,011494          |
|                  | PHIDE             | 0,84042                               | 0,0052185         |
| <b>R3</b>        |                   | 8,65E+10                              | 0,00010439        |
|                  |                   | <b>C with <math>\omega</math> max</b> | <b>C with Rct</b> |
|                  | C1 [F]            | 0,021522964                           | 0,018653481       |

Table 13 Fitting results of galvanostatic at 71°C -7.5 bar

|                  |                   |                                       |                   |
|------------------|-------------------|---------------------------------------|-------------------|
| <b>Pressure</b>  | 7.5 bar           | <b>Temperature</b>                    | <b>71°C</b>       |
| <b>circuit</b>   | <b>LR(QR)(QR)</b> |                                       | <b>GALV</b>       |
| <b>weighting</b> | modulus           |                                       |                   |
|                  |                   | <b>open</b>                           |                   |
| <b>element</b>   | sub-parameters    | value                                 | error             |
| <b>L1</b>        |                   | 3,96E-10                              | 0,074902          |
| <b>R1</b>        |                   | 0,030652                              | 0,040595          |
| <b>CPE1</b>      | TDE               | 0,0057532                             | 0,54576           |
|                  | PHIDE             | 1,3048                                | 0,066475          |
| <b>R2</b>        |                   | 0,016723                              | 0,13539           |
| <b>CPE2</b>      | TDE               | 2,229                                 | 0,046241          |
|                  | PHIDE             | 0,58546                               | 0,034504          |
| <b>R3</b>        |                   | 2,97E+08                              | 0,17862           |
|                  |                   | <b>C with <math>\omega</math> max</b> | <b>C with Rct</b> |
|                  | C1 [F]            | 0,026965721                           | 0,049914242       |

Table 14 Fitting results of galvanostatic at 71°C -5 bar

|                  |                   |                                       |                   |
|------------------|-------------------|---------------------------------------|-------------------|
| <b>Pressure</b>  | 5 bar             | <b>Temperature</b>                    | <b>71°C</b>       |
| <b>circuit</b>   | <b>LR(QR)(QR)</b> |                                       | <b>GALV</b>       |
| <b>weighting</b> | modulus           |                                       |                   |
|                  |                   | <b>open</b>                           |                   |
| <b>element</b>   | sub-parameters    | value                                 | error             |
| <b>L1</b>        |                   | 1,65E-06                              | 0,38144           |
| <b>R1</b>        |                   | 0,02692                               | 0,092425          |
| <b>CPE1</b>      | TDE               | 0,0084026                             | 0,6122            |
|                  | PHIDE             | 1,1874                                | 0,094207          |
| <b>R2</b>        |                   | 0,020593                              | 0,20151           |
| <b>CPE2</b>      | TDE               | 2,3107                                | 0,085427          |
|                  | PHIDE             | 0,59872                               | 0,055357          |
| <b>R3</b>        |                   | 3,15E+06                              | 753640            |
|                  |                   | <b>C with <math>\omega</math> max</b> | <b>C with Rct</b> |
|                  | C1 [F]            | 0,021722225                           | 0,032970524       |



Table 15 Fitting results of galvanostatic at 71°C -2.5 bar

|                  |                   |                                       |                   |
|------------------|-------------------|---------------------------------------|-------------------|
| <b>Pressure</b>  | 2.5 bar           | Temperature                           | <b>71°C</b>       |
| <b>circuit</b>   | <b>LR(QR)(QR)</b> |                                       | GALV              |
| <b>weighting</b> | modulus           |                                       |                   |
|                  |                   | <b>open</b>                           |                   |
| <b>element</b>   | sub-parameters    | value                                 | error             |
| <b>L1</b>        |                   | 1,64E-06                              | 3,70E-01          |
| <b>R1</b>        |                   | 0,027143                              | 0,087685          |
| <b>CPE1</b>      | TDE               | 0,00795                               | 0,58127           |
|                  | PHIDE             | 1,1996                                | 0,087619          |
| <b>R2</b>        |                   | 0,019641                              | 0,18007           |
| <b>CPE2</b>      | TDE               | 2,1484                                | 0,033645          |
|                  | PHIDE             | 0,59973                               | 0,026115          |
| <b>R3</b>        |                   | 2,50E+09                              | 0,020655          |
|                  |                   | <b>C with <math>\omega</math> max</b> | <b>C with Rct</b> |
|                  | C1 [F]            | 0,021863086                           | 0,034175979       |

Table 16 Fitting results of galvanostatic at 71°C -1.4 bar

|                  |                   |                                       |                   |
|------------------|-------------------|---------------------------------------|-------------------|
| <b>Pressure</b>  | 1.4 bar           | Temperature                           | <b>71°C</b>       |
| <b>circuit</b>   | <b>LR(QR)(QR)</b> |                                       | GALV              |
| <b>weighting</b> | modulus           |                                       |                   |
|                  |                   | <b>open</b>                           |                   |
| <b>element</b>   | sub-parameters    | value                                 | error             |
| <b>L1</b>        |                   | 1,63E-06                              | 0,45984           |
| <b>R1</b>        |                   | 0,026835                              | 0,11082           |
| <b>CPE1</b>      | TDE               | 0,008363                              | 0,7207            |
|                  | PHIDE             | 1,1929                                | 0,10949           |
| <b>R2</b>        |                   | 0,01967                               | 0,22287           |
| <b>CPE2</b>      | TDE               | 2,2738                                | 0,038053          |
|                  | PHIDE             | 0,59111                               | 0,030919          |
| <b>R3</b>        |                   | 2,57E+09                              | 0,025672          |
|                  |                   | <b>C with <math>\omega</math> max</b> | <b>C with Rct</b> |
|                  | C1 [F]            | 0,022230995                           | 0,034216342       |

Tests performed at gauge pressure 1.4bar, with open/closed cathode at different temperatures

## POTENTIOSTATIC

Table 17 Fitting results of potentiostatic at 71°C -1.4 bar-open cathode

|                  |                   |                                       |                    |
|------------------|-------------------|---------------------------------------|--------------------|
| <b>Pressure</b>  | 1.4 bar           | <b>T</b>                              | <b>71°C (OPEN)</b> |
| <b>circuit</b>   | <b>LR(QR)(QR)</b> |                                       | POT                |
| <b>weighting</b> | modulus           |                                       |                    |
| <b>open</b>      |                   |                                       |                    |
| <b>element</b>   | sub-parameters    | value                                 | error              |
| <b>L1</b>        |                   | 2,68E-06                              | 0,061001           |
| <b>R1</b>        |                   | 0,022461                              | 0,048914           |
| <b>CPE1</b>      | TDE               | 0,029913                              | 0,10579            |
|                  | PHIDE             | 0,93502                               | 0,023425           |
| <b>R2</b>        |                   | 0,037401                              | 0,03978            |
| <b>CPE2</b>      | TDE               | 0,84197                               | 0,011494           |
|                  | PHIDE             | 0,84042                               | 0,0052185          |
| <b>R3</b>        |                   | 8,65E+10                              | 0,00010439         |
|                  |                   |                                       |                    |
|                  |                   | <b>C with <math>\omega</math> max</b> | <b>C with Rct</b>  |
| C1 [F]           |                   | 0,021522964                           | 0,018653481        |

Table 18 Fitting results of potentiostatic at 61.7°C -1.4 bar-open cathode

|                  |                   |                                       |                      |
|------------------|-------------------|---------------------------------------|----------------------|
| <b>Pressure</b>  | 1.4 bar           | <b>T</b>                              | <b>61.7°C (OPEN)</b> |
| <b>circuit</b>   | <b>LR(QR)(QR)</b> |                                       | POT                  |
| <b>weighting</b> | modulus           |                                       |                      |
| <b>open</b>      |                   |                                       |                      |
| <b>element</b>   | sub-parameters    | value                                 | error                |
| <b>L1</b>        |                   | 2,33E-10                              | 0,084951             |
| <b>R1</b>        |                   | 0,032473                              | 0,025725             |
| <b>CPE1</b>      | TDE               | 0,01409                               | 0,28347              |
|                  | PHIDE             | 1,1475                                | 0,039542             |
| <b>R2</b>        |                   | 0,024548                              | 0,061101             |
| <b>CPE2</b>      | TDE               | 0,8356                                | 0,033244             |
|                  | PHIDE             | 0,82962                               | 0,014527             |
| <b>R3</b>        |                   | 9,90E+08                              | 0,028464             |
|                  |                   |                                       |                      |
|                  |                   | <b>C with <math>\omega</math> max</b> | <b>C with Rct</b>    |
| C1 [F]           |                   | 0,029745092                           | 0,039246267          |

Table 19 Fitting results of potentiostatic at 51.6°C -1.4 bar-open cathode

|                  |                   |                                       |                      |
|------------------|-------------------|---------------------------------------|----------------------|
| <b>Pressure</b>  | 1.4 bar           | <b>T</b>                              | <b>51.6°C (OPEN)</b> |
| <b>circuit</b>   | <b>LR(QR)(QR)</b> |                                       | POT                  |
| <b>weighting</b> | modulus           |                                       |                      |
|                  |                   | <b>open</b>                           |                      |
| <b>element</b>   | sub-parameters    | value                                 | error                |
| <b>L1</b>        |                   | 2,06E-10                              | 3,34E-02             |
| <b>R1</b>        |                   | 0,03251                               | 0,025712             |
| <b>CPE1</b>      | TDE               | 0,013625                              | 0,27029              |
|                  | PHIDE             | 1,1466                                | 0,037666             |
| <b>R2</b>        |                   | 0,026147                              | 0,057695             |
| <b>CPE2</b>      | TDE               | 0,83435                               | 0,033004             |
|                  | PHIDE             | 0,83464                               | 0,014219             |
| <b>R3</b>        |                   | 9,90E+08                              | 0,02882              |
|                  |                   | <b>C with <math>\omega</math> max</b> | <b>C with Rct</b>    |
|                  | C1 [F]            | 0,028632601                           | 0,037602423          |

Table 20 Fitting results of potentiostatic at 41.3°C -1.4 bar-open cathode

|                  |                   |                                       |                      |
|------------------|-------------------|---------------------------------------|----------------------|
| <b>Pressure</b>  | 1.4 bar           | <b>T</b>                              | <b>41.3°C (OPEN)</b> |
| <b>circuit</b>   | <b>LR(QR)(QR)</b> |                                       | POT                  |
| <b>weighting</b> | modulus           |                                       |                      |
|                  |                   | <b>open</b>                           |                      |
| <b>element</b>   | sub-parameters    | value                                 | error                |
| <b>L1</b>        |                   | 2,34E-10                              | 0,063867             |
| <b>R1</b>        |                   | 0,032434                              | 0,026982             |
| <b>CPE1</b>      | TDE               | 0,013017                              | 0,26453              |
|                  | PHIDE             | 1,1449                                | 0,036862             |
| <b>R2</b>        |                   | 0,029044                              | 0,056787             |
| <b>CPE2</b>      | TDE               | 0,8026                                | 0,035103             |
|                  | PHIDE             | 0,83578                               | 0,015206             |
| <b>R3</b>        |                   | 9,90E+08                              | 0,03147              |
|                  |                   | <b>C with <math>\omega</math> max</b> | <b>C with Rct</b>    |
|                  | C1 [F]            | 0,027120341                           | 0,035290543          |

Table 21 Fitting results of potentiostatic at 51.6°C -1.4 bar-closed cathode

|                  |                   |                                       |                   |
|------------------|-------------------|---------------------------------------|-------------------|
| <b>Pressure</b>  | 1.4 bar           | <b>T</b>                              | <b>51.6°C</b>     |
| <b>circuit</b>   | <b>LR(QR)(QR)</b> |                                       | POT               |
| <b>weighting</b> | modulus           |                                       |                   |
|                  |                   | <b>closed</b>                         |                   |
| <b>element</b>   | sub-parameters    | value                                 | error             |
| <b>L1</b>        |                   | 2,35E-10                              | 0,018659          |
| <b>R1</b>        |                   | 0,031988                              | 0,02718           |
| <b>CPE1</b>      | TDE               | 0,013574                              | 0,26909           |
|                  | PHIDE             | 1,1414                                | 0,037618          |
| <b>R2</b>        |                   | 0,028038                              | 0,057374          |
| <b>CPE2</b>      | TDE               | 0,75811                               | 0,034186          |
|                  | PHIDE             | 0,84566                               | 0,014277          |
| <b>R3</b>        |                   | 9,90E+08                              | 0,030963          |
|                  |                   | <b>C with <math>\omega</math> max</b> | <b>C with Rct</b> |
|                  | C1 [F]            | 0,026893757                           | 0,036002378       |

Table 22 Fitting results of potentiostatic at 61.6°C -1.4 bar-closed cathode

|                  |                   |                                       |                   |
|------------------|-------------------|---------------------------------------|-------------------|
| <b>Pressure</b>  | 1.4 bar           | <b>T</b>                              | <b>61.6°C</b>     |
| <b>circuit</b>   | <b>LR(QR)(QR)</b> |                                       | POT               |
| <b>weighting</b> | modulus           |                                       |                   |
|                  |                   | <b>closed</b>                         |                   |
| <b>element</b>   | sub-parameters    | value                                 | error             |
| <b>L1</b>        |                   | 2,61E-06                              | 0,041499          |
| <b>R1</b>        |                   | 0,024125                              | 0,02626           |
| <b>CPE1</b>      | TDE               | 0,022478                              | 0,083152          |
|                  | PHIDE             | 0,98981                               | 0,016194          |
| <b>R2</b>        |                   | 0,036482                              | 0,028604          |
| <b>CPE2</b>      | TDE               | 0,82764                               | 0,019245          |
|                  | PHIDE             | 0,81908                               | 0,0083357         |
| <b>R3</b>        |                   | 8,70E-01                              | 0,049192          |
|                  |                   | <b>C with <math>\omega</math> max</b> | <b>C with Rct</b> |
|                  | C1 [F]            | 0,021397272                           | 0,020892283       |

Table 23 Fitting results of potentiostatic at 71.6°C -1.4 bar-closed cathode

|                  |                   |                                       |                   |
|------------------|-------------------|---------------------------------------|-------------------|
| <b>Pressure</b>  | 1.4 bar           | <b>T</b>                              | <b>71.6°C</b>     |
| <b>circuit</b>   | <b>LR(QR)(QR)</b> |                                       | POT               |
| <b>weighting</b> | modulus           |                                       |                   |
|                  |                   | <b>closed</b>                         |                   |
| <b>element</b>   | sub-parameters    | value                                 | error             |
| <b>L1</b>        |                   | 2,52E-06                              | 4,53E-02          |
| <b>R1</b>        |                   | 0,023554                              | 0,030099          |
| <b>CPE1</b>      | TDE               | 0,026122                              | 0,087042          |
|                  | PHIDE             | 0,96861                               | 0,017684          |
| <b>R2</b>        |                   | 0,035501                              | 0,030628          |
| <b>CPE2</b>      | TDE               | 0,77462                               | 0,018174          |
|                  | PHIDE             | 0,85386                               | 0,0076459         |
| <b>R3</b>        |                   | 8,83E-01                              | 0,047748          |
|                  |                   | <b>C with <math>\omega</math> max</b> | <b>C with Rct</b> |
|                  | C1 [F]            | 0,022443295                           | 0,020831627       |

Table 24 Fitting results of potentiostatic at 80°C -1.4 bar-closed cathode

|                  |                   |                                       |                   |
|------------------|-------------------|---------------------------------------|-------------------|
| <b>Pressure</b>  | 1.4 bar           | <b>T</b>                              | <b>80°C</b>       |
| <b>circuit</b>   | <b>LR(QR)(QR)</b> |                                       | POT               |
| <b>weighting</b> | modulus           |                                       |                   |
|                  |                   | <b>closed</b>                         |                   |
| <b>element</b>   | sub-parameters    | value                                 | error             |
| <b>L1</b>        |                   | 2,31E-10                              | 0,069174          |
| <b>R1</b>        |                   | 0,031963                              | 0,026005          |
| <b>CPE1</b>      | TDE               | 0,01666                               | 0,28937           |
|                  | PHIDE             | 1,1288                                | 0,041207          |
| <b>R2</b>        |                   | 0,02376                               | 0,062038          |
| <b>CPE2</b>      | TDE               | 0,88435                               | 0,032456          |
|                  | PHIDE             | 0,83562                               | 0,014075          |
| <b>R3</b>        |                   | 9,90E+08                              | 0,026837          |
|                  |                   | <b>C with <math>\omega</math> max</b> | <b>C with Rct</b> |
|                  | C1 [F]            | 0,031991807                           | 0,040729551       |

## GALVANOSTATIC

Table 24 Fitting results of galvanostatic at 71°C -1.4 bar-open cathode

|                  |                   |                                       |                   |
|------------------|-------------------|---------------------------------------|-------------------|
| <b>Pressure</b>  | 1.4 bar           | <b>T</b>                              | <b>71°C</b>       |
| <b>circuit</b>   | <b>LR(QR)(QR)</b> |                                       | <b>GALV</b>       |
| <b>weighting</b> | modulus           |                                       |                   |
|                  |                   | <b>open</b>                           |                   |
| <b>element</b>   | sub-parameters    | value                                 | error             |
| <b>L1</b>        |                   | 1,63E-06                              | 0,45984           |
| <b>R1</b>        |                   | 0,026835                              | 0,11082           |
| <b>CPE1</b>      | TDE               | 0,008363                              | 0,7207            |
|                  | PHIDE             | 1,1929                                | 0,10949           |
| <b>R2</b>        |                   | 0,01967                               | 0,22287           |
| <b>CPE2</b>      | TDE               | 2,2738                                | 0,038053          |
|                  | PHIDE             | 0,59111                               | 0,030919          |
| <b>R3</b>        |                   | 2,57E+09                              | 0,025672          |
|                  |                   | <b>C with <math>\omega</math> max</b> | <b>C with Rct</b> |
|                  | C1 [F]            | 0,022230995                           | 0,034216342       |

Table 25 Fitting results of galvanostatic at 61.7°C -1.4 bar-open cathode

|                  |                   |                                       |                   |
|------------------|-------------------|---------------------------------------|-------------------|
| <b>Pressure</b>  | 1.4 bar           | <b>T</b>                              | <b>61.7°C</b>     |
| <b>circuit</b>   | <b>LR(QR)(QR)</b> |                                       | <b>GALV</b>       |
| <b>weighting</b> | modulus           |                                       |                   |
|                  |                   | <b>open</b>                           |                   |
| <b>element</b>   | sub-parameters    | value                                 | error             |
| <b>L1</b>        |                   | 2,23E-06                              | 0,11196           |
| <b>R1</b>        |                   | 0,025399                              | 0,052975          |
| <b>CPE1</b>      | TDE               | 0,0179                                | 0,198             |
|                  | PHIDE             | 1,0364                                | 0,036889          |
| <b>R2</b>        |                   | 0,030304                              | 0,068373          |
| <b>CPE2</b>      | TDE               | 1,2329                                | 0,033538          |
|                  | PHIDE             | 0,74916                               | 0,015605          |
| <b>R3</b>        |                   | 1,22E+10                              | 0,0010946         |
|                  |                   | <b>C with <math>\omega</math> max</b> | <b>C with Rct</b> |
|                  | C1 [F]            | 0,021526526                           | 0,023310291       |

Table 26 Fitting results of galvanostatic at 51.6°C -1.4 bar-open cathode

|                  |                   |             |               |
|------------------|-------------------|-------------|---------------|
| <b>Pressure</b>  | 1.4 bar           | <b>T</b>    | <b>51.6°C</b> |
| <b>circuit</b>   | <b>LR(QR)(QR)</b> |             | <b>GALV</b>   |
| <b>weighting</b> | modulus           |             |               |
|                  |                   | <b>open</b> |               |
| <b>element</b>   | sub-parameters    | value       | error         |

|             |        |                                       |                   |
|-------------|--------|---------------------------------------|-------------------|
| <b>L1</b>   |        | 2,32E-06                              | 7,14E-02          |
| <b>R1</b>   |        | 0,02548                               | 0,03463           |
| <b>CPE1</b> | TDE    | 0,017367                              | 0,1317            |
|             | PHIDE  | 1,0364                                | 0,024298          |
| <b>R2</b>   |        | 0,032337                              | 0,045503          |
| <b>CPE2</b> | TDE    | 1,1385                                | 0,03265           |
|             | PHIDE  | 0,76323                               | 0,0138            |
| <b>R3</b>   |        | 3,22E+07                              | 0,26314           |
|             |        | <b>C with <math>\omega</math> max</b> | <b>C with Rct</b> |
|             | C1 [F] | 0,02088554                            | 0,022588643       |

Table 27 Fitting results of galvanostatic at 41.3°C -1.4 bar-open cathode

|                  |                   |                                       |                   |
|------------------|-------------------|---------------------------------------|-------------------|
| <b>Pressure</b>  | 1.4 bar           | <b>T</b>                              | <b>41.3°C</b>     |
| <b>circuit</b>   | <b>LR(QR)(QR)</b> |                                       | <b>GALV</b>       |
| <b>weighting</b> | modulus           |                                       |                   |
|                  |                   | <b>open</b>                           |                   |
| <b>element</b>   | sub-parameters    | value                                 | error             |
| <b>L1</b>        |                   | 2,36E-06                              | 0,078538          |
| <b>R1</b>        |                   | 0,025465                              | 0,036986          |
| <b>CPE1</b>      | TDE               | 0,01651                               | 0,14235           |
|                  | PHIDE             | 1,0426                                | 0,025717          |
| <b>R2</b>        |                   | 0,034435                              | 0,046958          |
| <b>CPE2</b>      | TDE               | 1,1513                                | 0,03184           |
|                  | PHIDE             | 0,75177                               | 0,014273          |
| <b>R3</b>        |                   | 7,00E+06                              | 1,5141            |
|                  |                   | <b>C with <math>\omega</math> max</b> | <b>C with Rct</b> |
|                  | C1 [F]            | 0,020288606                           | 0,022405061       |

Table 28 Fitting results of galvanostatic at 51.6°C -1.4 bar-closed cathode

|                  |                   |               |               |
|------------------|-------------------|---------------|---------------|
| <b>Pressure</b>  | 1.4 bar           | <b>T</b>      | <b>51.6°C</b> |
| <b>circuit</b>   | <b>LR(QR)(QR)</b> |               | <b>GALV</b>   |
| <b>weighting</b> | modulus           |               |               |
|                  |                   | <b>closed</b> |               |
| <b>element</b>   | sub-parameters    | value         | error         |
| <b>L1</b>        |                   | 2,33E-06      | 0,095707      |
| <b>R1</b>        |                   | 0,025206      | 0,046019      |
| <b>CPE1</b>      | TDE               | 0,017146      | 0,16975       |
|                  | PHIDE             | 1,0377        | 0,031085      |
| <b>R2</b>        |                   | 0,033207      | 0,056151      |
| <b>CPE2</b>      | TDE               | 1,1265        | 0,030796      |
|                  | PHIDE             | 0,75828       | 0,014076      |
| <b>R3</b>        |                   | 7,62E+07      | 0,16796       |

|        |                                       |                   |
|--------|---------------------------------------|-------------------|
|        |                                       |                   |
|        | <b>C with <math>\omega</math> max</b> | <b>C with Rct</b> |
| C1 [F] | 0,020756073                           | 0,022492645       |

Table 29 Fitting results of galvanostatic at 61.6°C -1.4 bar-closed cathode

|                  |                   |                                       |                   |
|------------------|-------------------|---------------------------------------|-------------------|
| <b>Pressure</b>  | 1.4 bar           | <b>T</b>                              | <b>61.6°C</b>     |
| <b>circuit</b>   | <b>LR(QR)(QR)</b> |                                       | <b>GALV</b>       |
| <b>weighting</b> | modulus           |                                       |                   |
|                  |                   | <b>closed</b>                         |                   |
| <b>element</b>   | sub-parameters    | value                                 | error             |
| <b>L1</b>        |                   | 2,04E-06                              | 0,18081           |
| <b>R1</b>        |                   | 0,02664                               | 0,058458          |
| <b>CPE1</b>      | TDE               | 0,010333                              | 0,34482           |
|                  | PHIDE             | 1,1413                                | 0,055555          |
| <b>R2</b>        |                   | 0,0252                                | 0,11652           |
| <b>CPE2</b>      | TDE               | 1,458                                 | 0,075764          |
|                  | PHIDE             | 0,6651                                | 0,039438          |
| <b>R3</b>        |                   | 1,29E+00                              | 0,3145            |
|                  |                   |                                       |                   |
|                  |                   | <b>C with <math>\omega</math> max</b> | <b>C with Rct</b> |
| C1 [F]           |                   | 0,020469447                           | 0,028707408       |

Table 30 Fitting results of galvanostatic at 71.6°C -1.4 bar-closed cathode

|                  |                   |                                       |                   |
|------------------|-------------------|---------------------------------------|-------------------|
| <b>Pressure</b>  | 1.4 bar           | <b>T</b>                              | <b>71.6°C</b>     |
| <b>circuit</b>   | <b>LR(QR)(QR)</b> |                                       | <b>GALV</b>       |
| <b>weighting</b> | modulus           |                                       |                   |
|                  |                   | <b>closed</b>                         |                   |
| <b>element</b>   | sub-parameters    | value                                 | error             |
| <b>L1</b>        |                   | 1,31E-10                              | 8,10E-02          |
| <b>R1</b>        |                   | 0,031863                              | 0,022557          |
| <b>CPE1</b>      | TDE               | 0,0084788                             | 0,31586           |
|                  | PHIDE             | 1,2415                                | 0,041384          |
| <b>R2</b>        |                   | 0,019234                              | 0,087898          |
| <b>CPE2</b>      | TDE               | 1,2711                                | 0,080937          |
|                  | PHIDE             | 0,71727                               | 0,035429          |
| <b>R3</b>        |                   | 1,82E+08                              | 0,12189           |
|                  |                   |                                       |                   |
|                  |                   | <b>C with <math>\omega</math> max</b> | <b>C with Rct</b> |
| C1 [F]           |                   | 0,027273459                           | 0,046249602       |



Table 31 Fitting results of galvanostatic at 80°C -1.4 bar-closed cathode

|                  |                   |                                       |                   |
|------------------|-------------------|---------------------------------------|-------------------|
| <b>Pressure</b>  | 1.4 bar           | <b>T</b>                              | <b>80°C</b>       |
| <b>circuit</b>   | <b>LR(QR)(QR)</b> |                                       | <b>GALV</b>       |
| <b>weighting</b> | modulus           |                                       |                   |
|                  |                   | <b>closed</b>                         |                   |
| <b>element</b>   | sub-parameters    | value                                 | error             |
| <b>L1</b>        |                   | 2,05E-06                              | 0,19232           |
| <b>R1</b>        |                   | 0,025235                              | 0,083088          |
| <b>CPE1</b>      | TDE               | 0,018007                              | 0,32335           |
|                  | PHIDE             | 1,0451                                | 0,060084          |
| <b>R2</b>        |                   | 0,027491                              | 0,1125            |
| <b>CPE2</b>      | TDE               | 1,6232                                | 0,040667          |
|                  | PHIDE             | 0,70772                               | 0,022197          |
| <b>R3</b>        |                   | 6,90E+07                              | 0,3186            |
|                  |                   | <b>C with <math>\omega</math> max</b> | <b>C with Rct</b> |
|                  | C1 [F]            | 0,022631433                           | 0,025008085       |

Tests performed at constant current density of 1 A/cm<sup>2</sup> with 60°C, 0.5bar, closed cathode imposing different mass flow rate by recirculating pump

## POTENTIOSTATIC

Table 32 Fitting results of potentiostatic at 60°C -0.5 bar-closed cathode-10%

|                  |                   |                                       |                   |
|------------------|-------------------|---------------------------------------|-------------------|
| <b>Pressure</b>  | 0.5 bar           | <b>T</b>                              | <b>60°C -10%</b>  |
| <b>circuit</b>   | <b>LR(QR)(QR)</b> |                                       | POT               |
| <b>weighting</b> | modulus           |                                       |                   |
|                  |                   | <b>closed</b>                         |                   |
| <b>element</b>   | sub-parameters    | value                                 | error             |
| <b>L1</b>        |                   | 2,40E-06                              | 0,021104          |
| <b>R1</b>        |                   | 0,035927                              | 0,0070529         |
| <b>CPE1</b>      | TDE               | 0,013264                              | 0,028519          |
|                  | PHIDE             | 1,0481                                | 0,0051871         |
| <b>R2</b>        |                   | 0,040435                              | 0,0090305         |
| <b>CPE2</b>      | TDE               | 10,755                                | 0,048997          |
|                  | PHIDE             | 0,79221                               | 0,024414          |
| <b>R3</b>        |                   | 3,54E-01                              | 0,53871           |
|                  |                   | <b>C with <math>\omega</math> max</b> | <b>C with Rct</b> |
|                  | C1 [F]            | 0,017112039                           | 0,018739987       |

Table 33 Fitting results of potentiostatic at 60°C -0.5 bar-closed cathode-30%

|                  |                   |                                       |                   |
|------------------|-------------------|---------------------------------------|-------------------|
| <b>Pressure</b>  | 0.5 bar           | <b>T</b>                              | <b>60°C -30%</b>  |
| <b>circuit</b>   | <b>LR(QR)(QR)</b> |                                       | POT               |
| <b>weighting</b> | modulus           |                                       |                   |
|                  |                   | <b>closed</b>                         |                   |
| <b>element</b>   | sub-parameters    | value                                 | error             |
| <b>L1</b>        |                   | 2,38E-06                              | 0,020584          |
| <b>R1</b>        |                   | 0,027375                              | 0,0084634         |
| <b>CPE1</b>      | TDE               | 0,012721                              | 0,02646           |
|                  | PHIDE             | 1,0515                                | 0,004662          |
| <b>R2</b>        |                   | 0,044657                              | 0,0073547         |
| <b>CPE2</b>      | TDE               | 10,034                                | 0,018072          |
|                  | PHIDE             | 0,78188                               | 0,010479          |
| <b>R3</b>        |                   | 3,67E+07                              | 0,077636          |
|                  |                   | <b>C with <math>\omega</math> max</b> | <b>C with Rct</b> |
|                  | C1 [F]            | 0,016709687                           | 0,018343516       |

Table 34 Fitting results of potentiostatic at 60°C -0.5 bar-closed cathode-50%

|                 |         |          |                  |
|-----------------|---------|----------|------------------|
| <b>Pressure</b> | 0.5 bar | <b>T</b> | <b>60°C -50%</b> |
|-----------------|---------|----------|------------------|

|                  |                   |                                       |                   |
|------------------|-------------------|---------------------------------------|-------------------|
| <b>circuit</b>   | <b>LR(QR)(QR)</b> | <b>POT</b>                            |                   |
| <b>weighting</b> | modulus           |                                       |                   |
|                  |                   | <b>closed</b>                         |                   |
| <b>element</b>   | sub-parameters    | value                                 | error             |
| <b>L1</b>        |                   | 2,46E-06                              | 1,89E-02          |
| <b>R1</b>        |                   | 0,027032                              | 0,0081119         |
| <b>CPE1</b>      | TDE               | 0,012718                              | 0,026287          |
|                  | PHIDE             | 1,0494                                | 0,0045778         |
| <b>R2</b>        |                   | 0,048044                              | 0,0073638         |
| <b>CPE2</b>      | TDE               | 8,2054                                | 0,045958          |
|                  | PHIDE             | 0,81382                               | 0,022384          |
| <b>R3</b>        |                   | 8,54E-01                              | 0,96986           |
|                  |                   | <b>C with <math>\omega</math> max</b> | <b>C with Rct</b> |
|                  | C1 [F]            | 0,01633429                            | 0,018018291       |

Table 35 Fitting results of potentiostatic at 60°C -0.5 bar-closed cathode-70%

|                  |                   |                                       |                   |
|------------------|-------------------|---------------------------------------|-------------------|
| <b>Pressure</b>  | 0.5 bar           | <b>T</b>                              | <b>60°C -70%</b>  |
| <b>circuit</b>   | <b>LR(QR)(QR)</b> | <b>POT</b>                            |                   |
| <b>weighting</b> | modulus           |                                       |                   |
|                  |                   | <b>closed</b>                         |                   |
| <b>element</b>   | sub-parameters    | value                                 | error             |
| <b>L1</b>        |                   | 2,49E-06                              | 0,020714          |
| <b>R1</b>        |                   | 0,026526                              | 0,0089102         |
| <b>CPE1</b>      | TDE               | 0,012284                              | 0,028498          |
|                  | PHIDE             | 1,052                                 | 0,0048921         |
| <b>R2</b>        |                   | 0,051411                              | 0,0077359         |
| <b>CPE2</b>      | TDE               | 7,3157                                | 0,049778          |
|                  | PHIDE             | 0,82543                               | 0,024237          |
| <b>R3</b>        |                   | 3,26E-01                              | 0,37312           |
|                  |                   | <b>C with <math>\omega</math> max</b> | <b>C with Rct</b> |
|                  | C1 [F]            | 0,015986056                           | 0,017680525       |

Table 36 Fitting results of potentiostatic at 60°C -0.5 bar-closed cathode-100%

|                  |                   |            |                   |
|------------------|-------------------|------------|-------------------|
| <b>Pressure</b>  | 0.5 bar           | <b>T</b>   | <b>60°C -100%</b> |
| <b>circuit</b>   | <b>LR(QR)(QR)</b> | <b>POT</b> |                   |
| <b>weighting</b> | modulus           |            |                   |

|                |                       | <b>closed</b>                         |                   |
|----------------|-----------------------|---------------------------------------|-------------------|
| <b>element</b> | <b>sub-parameters</b> | <b>value</b>                          | <b>error</b>      |
| <b>L1</b>      |                       | 2,52E-06                              | 0,019472          |
| <b>R1</b>      |                       | 0,028656                              | 0,0074946         |
| <b>CPE1</b>    | TDE                   | 0,012015                              | 0,025684          |
|                | PHIDE                 | 1,0521                                | 0,0043661         |
| <b>R2</b>      |                       | 0,057905                              | 0,0068737         |
| <b>CPE2</b>    | TDE                   | 6,7135                                | 0,048069          |
|                | PHIDE                 | 0,80876                               | 0,023592          |
| <b>R3</b>      |                       | 8,31E-01                              | 0,79747           |
|                |                       | <b>C with <math>\omega</math> max</b> | <b>C with Rct</b> |
|                | C1 [F]                | 0,01564391                            | 0,017222103       |

## GALVANOSTATIC

Table 37 Fitting results of galvanostatic at 60°C -0.5 bar-closed cathode-10%

| <b>Pressure</b>  | 0.5 bar               | <b>T</b>                              | <b>60°C -10%</b>  |
|------------------|-----------------------|---------------------------------------|-------------------|
| <b>circuit</b>   | <b>LR(QR)(QR)</b>     |                                       | <b>GALV</b>       |
| <b>weighting</b> | modulus               |                                       |                   |
|                  |                       | <b>closed</b>                         |                   |
| <b>element</b>   | <b>sub-parameters</b> | <b>value</b>                          | <b>error</b>      |
| <b>L1</b>        |                       | 2,47E-06                              | 0,030248          |
| <b>R1</b>        |                       | 0,035498                              | 0,010435          |
| <b>CPE1</b>      | TDE                   | 0,013981                              | 0,036435          |
|                  | PHIDE                 | 1,0373                                | 0,0067673         |
| <b>R2</b>        |                       | 0,041618                              | 0,010909          |
| <b>CPE2</b>      | TDE                   | 9,1964                                | 0,0085556         |
|                  | PHIDE                 | 0,84708                               | 0,0079384         |
| <b>R3</b>        |                       | 2,90E-01                              | 0,048047          |
|                  |                       | <b>C with <math>\omega</math> max</b> | <b>C with Rct</b> |
|                  | C1 [F]                | 0,017035962                           | 0,018275583       |

Table 38 Fitting results of galvanostatic at 60°C -0.5 bar-closed cathode-30%

| <b>Pressure</b>  | 0.5 bar               | <b>T</b>      | <b>60°C -30%</b> |
|------------------|-----------------------|---------------|------------------|
| <b>circuit</b>   | <b>LR(QR)(QR)</b>     |               | <b>GALV</b>      |
| <b>weighting</b> | modulus               |               |                  |
|                  |                       | <b>closed</b> |                  |
| <b>element</b>   | <b>sub-parameters</b> | <b>value</b>  | <b>error</b>     |
| <b>L1</b>        |                       | 2,48E-06      | 0,040215         |
| <b>R1</b>        |                       | 0,026668      | 0,018135         |
| <b>CPE1</b>      | TDE                   | 0,013795      | 0,050405         |
|                  | PHIDE                 | 1,036         | 0,0090938        |

|             |        |                                       |                   |
|-------------|--------|---------------------------------------|-------------------|
| <b>R2</b>   |        | 0,045761                              | 0,013576          |
| <b>CPE2</b> | TDE    | 7,9526                                | 0,012575          |
|             | PHIDE  | 0,86327                               | 0,011275          |
| <b>R3</b>   |        | 2,91E-01                              | 0,062624          |
|             |        | <b>C with <math>\omega</math> max</b> | <b>C with Rct</b> |
|             | C1 [F] | 0,016693938                           | 0,017820138       |

Table 39 Fitting results of galvanostatic at 60°C -0.5 bar-closed cathode-50%

|                  |                   |                                       |                   |
|------------------|-------------------|---------------------------------------|-------------------|
| <b>Pressure</b>  | 0.5 bar           | <b>T</b>                              | <b>60°C -50%</b>  |
| <b>circuit</b>   | <b>LR(QR)(QR)</b> |                                       | <b>GALV</b>       |
| <b>weighting</b> | modulus           |                                       |                   |
| <b>closed</b>    |                   |                                       |                   |
| <b>element</b>   | sub-parameters    | value                                 | error             |
| <b>L1</b>        |                   | 2,66E-06                              | 8,23E-02          |
| <b>R1</b>        |                   | 0,025702                              | 0,041708          |
| <b>CPE1</b>      | TDE               | 0,015343                              | 0,10478           |
|                  | PHIDE             | 1,0152                                | 0,019314          |
| <b>R2</b>        |                   | 0,050485                              | 0,027255          |
| <b>CPE2</b>      | TDE               | 5,9281                                | 0,022115          |
|                  | PHIDE             | 0,93377                               | 0,019028          |
| <b>R3</b>        |                   | 2,67E-01                              | 0,083574          |
|                  |                   | <b>C with <math>\omega</math> max</b> | <b>C with Rct</b> |
|                  | C1 [F]            | 0,016571712                           | 0,017080021       |

Table 40 Fitting results of galvanostatic at 60°C -0.5 bar-closed cathode-70%

|                  |                   |                                       |                   |
|------------------|-------------------|---------------------------------------|-------------------|
| <b>Pressure</b>  | 0.5 bar           | <b>T</b>                              | <b>60°C -70%</b>  |
| <b>circuit</b>   | <b>LR(QR)(QR)</b> |                                       | <b>GALV</b>       |
| <b>weighting</b> | modulus           |                                       |                   |
| <b>closed</b>    |                   |                                       |                   |
| <b>element</b>   | sub-parameters    | value                                 | error             |
| <b>L1</b>        |                   | 2,82E-06                              | 0,13113           |
| <b>R1</b>        |                   | 0,024649                              | 0,072942          |
| <b>CPE1</b>      | TDE               | 0,016036                              | 0,17209           |
|                  | PHIDE             | 1,0043                                | 0,031777          |
| <b>R2</b>        |                   | 0,055741                              | 0,042705          |
| <b>CPE2</b>      | TDE               | 5,0165                                | 0,037804          |
|                  | PHIDE             | 0,95799                               | 0,031224          |
| <b>R3</b>        |                   | 2,23E-01                              | 0,10617           |
|                  |                   | <b>C with <math>\omega</math> max</b> | <b>C with Rct</b> |
|                  | C1 [F]            | 0,016389318                           | 0,016525304       |

Table 40 Fitting results of galvanostatic at 60°C -0.5 bar-closed cathode-100%

|                  |                   |                                       |                   |
|------------------|-------------------|---------------------------------------|-------------------|
| <b>Pressure</b>  | 0.5 bar           | T                                     | <b>60°C -100%</b> |
| <b>circuit</b>   | <b>LR(QR)(QR)</b> |                                       | GALV              |
| <b>weighting</b> | modulus           |                                       |                   |
|                  |                   | <b>closed</b>                         |                   |
| <b>element</b>   | sub-parameters    | value                                 | error             |
| <b>L1</b>        |                   | 2,89E-06                              | 0,13382           |
| <b>R1</b>        |                   | 0,026626                              | 0,068136          |
| <b>CPE1</b>      | TDE               | 0,015924                              | 0,17058           |
|                  | PHIDE             | 1,0022                                | 0,031217          |
| <b>R2</b>        |                   | 0,061924                              | 0,040327          |
| <b>CPE2</b>      | TDE               | 4,218                                 | 0,035404          |
|                  | PHIDE             | 0,95464                               | 0,02955           |
| <b>R3</b>        |                   | 3,23E-01                              | 0,1199            |
|                  |                   | <b>C with <math>\omega</math> max</b> | <b>C with Rct</b> |
|                  | C1 [F]            | 0,016102549                           | 0,016167804       |

Degradation test performed at 60°C and 80°C, 0.5bar, closed cathode, 10% mass flow rate, constant current density of 0.5 A/cm<sup>2</sup>

## POTENTIOSTATIC

Table 41 Fitting results of potentiostatic-30/07/2021

|                  |                   |                                       |                   |
|------------------|-------------------|---------------------------------------|-------------------|
| <b>Pressure</b>  | 0.5 bar           | T                                     | <b>60°C</b>       |
| <b>circuit</b>   | <b>LR(QR)(QR)</b> |                                       | 30-POT            |
| <b>weighting</b> | modulus           |                                       |                   |
|                  |                   | <b>closed</b>                         |                   |
| <b>element</b>   | sub-parameters    | value                                 | error             |
| <b>L1</b>        |                   | 2,51E-06                              | 0,022696          |
| <b>R1</b>        |                   | 0,032712                              | 0,00738           |
| <b>CPE1</b>      | TDE               | 0,011807                              | 0,027196          |
|                  | PHIDE             | 1,0543                                | 0,0045973         |
| <b>R2</b>        |                   | 0,060315                              | 0,0067501         |
| <b>CPE2</b>      | TDE               | 10,432                                | 0,08264           |
|                  | PHIDE             | 0,8926                                | 0,038774          |
| <b>R3</b>        |                   | 0,40263                               | 1,2554            |
|                  |                   | <b>C with <math>\omega</math> max</b> | <b>C with Rct</b> |
|                  | C1 [F]            | 0,015545373                           | 0,017698174       |

Table 42 Fitting results of potentiostatic-31/07/2021 morning

|                  |                   |   |             |
|------------------|-------------------|---|-------------|
| <b>Pressure</b>  | 0.5 bar           | T | <b>60°C</b> |
| <b>circuit</b>   | <b>LR(QR)(QR)</b> |   | 31morn-POT  |
| <b>weighting</b> | modulus           |   |             |

|                |                       | <b>closed</b>                         |                   |
|----------------|-----------------------|---------------------------------------|-------------------|
| <b>element</b> | <b>sub-parameters</b> | <b>value</b>                          | <b>error</b>      |
| <b>L1</b>      |                       | 2,52E-06                              | 0,022388          |
| <b>R1</b>      |                       | 0,028627                              | 0,0082375         |
| <b>CPE1</b>    | TDE                   | 0,011602                              | 0,027458          |
|                | PHIDE                 | 1,0559                                | 0,0045744         |
| <b>R2</b>      |                       | 0,063521                              | 0,0066022         |
| <b>CPE2</b>    | TDE                   | 10,264                                | 0,090113          |
|                | PHIDE                 | 0,90156                               | 0,042096          |
| <b>R3</b>      |                       | 0,36759                               | 1,2575            |
|                |                       | <b>C with <math>\omega</math> max</b> | <b>C with Rct</b> |
|                | C1 [F]                | 0,015202825                           | 0,016996989       |

Table 42 Fitting results of potentiostatic-31/07/2021 evening

| <b>Pressure</b>  | 0.5 bar               | <b>T</b>                              | <b>60°C</b>       |
|------------------|-----------------------|---------------------------------------|-------------------|
| <b>circuit</b>   | <b>LR(QR)(QR)</b>     |                                       | 31even-POT        |
| <b>weighting</b> | modulus               |                                       |                   |
|                  |                       | <b>closed</b>                         |                   |
| <b>element</b>   | <b>sub-parameters</b> | <b>value</b>                          | <b>error</b>      |
| <b>L1</b>        |                       | 2,59E-06                              | 0,020481          |
| <b>R1</b>        |                       | 0,029087                              | 0,0072377         |
| <b>CPE1</b>      | TDE                   | 0,011201                              | 0,024502          |
|                  | PHIDE                 | 1,0578                                | 0,0040214         |
| <b>R2</b>        |                       | 0,073642                              | 0,0058207         |
| <b>CPE2</b>      | TDE                   | 10,297                                | 0,099377          |
|                  | PHIDE                 | 0,89073                               | 0,046987          |
| <b>R3</b>        |                       | 0,29436                               | 1,0835            |
|                  |                       | <b>C with <math>\omega</math> max</b> | <b>C with Rct</b> |
|                  | C1 [F]                | 0,014812838                           | 0,016510147       |

Table 42 Fitting results of potentiostatic-01/08/2021 morning

| <b>Pressure</b>  | 0.5 bar               | <b>T</b>      | <b>60°C</b>  |
|------------------|-----------------------|---------------|--------------|
| <b>circuit</b>   | <b>LR(QR)(QR)</b>     |               | 1morn-POT    |
| <b>weighting</b> | modulus               |               |              |
|                  |                       | <b>closed</b> |              |
| <b>element</b>   | <b>sub-parameters</b> | <b>value</b>  | <b>error</b> |
| <b>L1</b>        |                       | 2,60E-06      | 0,024433     |
| <b>R1</b>        |                       | 0,032834      | 0,0074898    |
| <b>CPE1</b>      | TDE                   | 0,011478      | 0,028178     |
|                  | PHIDE                 | 1,0542        | 0,0046542    |
| <b>R2</b>        |                       | 0,080046      | 0,0070761    |
| <b>CPE2</b>      | TDE                   | 9,6765        | 0,16271      |
|                  | PHIDE                 | 0,89363       | 0,072049     |

|           |                                       |                   |
|-----------|---------------------------------------|-------------------|
| <b>R3</b> | 0,12622                               | 0,80492           |
|           | <b>C with <math>\omega</math> max</b> | <b>C with Rct</b> |
| C1 [F]    | 0,01491721                            | 0,016443646       |

Table 42 Fitting results of potentiostatic-01/08/2021 evening

|                  |                   |                                       |                   |
|------------------|-------------------|---------------------------------------|-------------------|
| <b>Pressure</b>  | 0.5 bar           | <b>T</b>                              | <b>60°C</b>       |
| <b>circuit</b>   | <b>LR(QR)(QR)</b> |                                       | 1even-POT         |
| <b>weighting</b> | modulus           |                                       |                   |
|                  |                   | <b>closed</b>                         |                   |
| <b>element</b>   | sub-parameters    | value                                 | error             |
| <b>L1</b>        |                   | 2,63E-06                              | 0,024176          |
| <b>R1</b>        |                   | 0,027157                              | 0,0089392         |
| <b>CPE1</b>      | TDE               | 0,010738                              | 0,028996          |
|                  | PHIDE             | 1,0606                                | 0,004679          |
| <b>R2</b>        |                   | 0,084892                              | 0,0070371         |
| <b>CPE2</b>      | TDE               | 8,6539                                | 0,16947           |
|                  | PHIDE             | 0,91728                               | 0,074181          |
| <b>R3</b>        |                   | 0,10143                               | 0,65126           |
|                  |                   | <b>C with <math>\omega</math> max</b> | <b>C with Rct</b> |
| C1 [F]           |                   | 0,014394115                           | 0,016018922       |

Table 42 Fitting results of potentiostatic-02/08/2021 evening

|                  |                   |                                       |                   |
|------------------|-------------------|---------------------------------------|-------------------|
| <b>Pressure</b>  | 0.5 bar           | <b>T</b>                              | <b>60°C</b>       |
| <b>circuit</b>   | <b>LR(QR)(QR)</b> |                                       | 2even-POT         |
| <b>weighting</b> | modulus           |                                       |                   |
|                  |                   | <b>closed</b>                         |                   |
| <b>element</b>   | sub-parameters    | value                                 | error             |
| <b>L1</b>        |                   | 3,12E-06                              | 0,13928           |
| <b>R1</b>        |                   | 0,022746                              | 0,074764          |
| <b>CPE1</b>      | TDE               | 0,016841                              | 0,21792           |
|                  | PHIDE             | 1,012                                 | 0,037301          |
| <b>R2</b>        |                   | 0,08805                               | 0,05565           |
| <b>CPE2</b>      | TDE               | 1,3739                                | 0,033224          |
|                  | PHIDE             | 0,73179                               | 0,029453          |
| <b>R3</b>        |                   | 0,76329                               | 0,043163          |
|                  |                   | <b>C with <math>\omega</math> max</b> | <b>C with Rct</b> |
| C1 [F]           |                   | 0,017748747                           | 0,018193329       |
| C2 [F]           |                   | 2,11698333                            | 1,398046632       |



Table 42 Fitting results of potentiostatic-03/08/2021 morning

|                  |                   |                                       |                   |
|------------------|-------------------|---------------------------------------|-------------------|
| <b>Pressure</b>  | 0.5 bar           | T                                     | <b>60°C</b>       |
| <b>circuit</b>   | <b>LR(QR)(QR)</b> |                                       | 3morn-POT         |
| <b>weighting</b> | modulus           |                                       |                   |
|                  |                   | <b>closed</b>                         |                   |
| <b>element</b>   | sub-parameters    | value                                 | error             |
| <b>L1</b>        |                   | 3,11E-06                              | 0,16204           |
| <b>R1</b>        |                   | 0,026645                              | 0,066348          |
| <b>CPE1</b>      | TDE               | 0,019581                              | 0,16508           |
|                  | PHIDE             | 0,98841                               | 0,030984          |
| <b>R2</b>        |                   | 0,092587                              | 0,046749          |
| <b>CPE2</b>      | TDE               | 1,7317                                | 0,027207          |
|                  | PHIDE             | 0,70553                               | 0,027752          |
| <b>R3</b>        |                   | 0,81822                               | 0,057689          |
|                  |                   | <b>C with <math>\omega</math> max</b> | <b>C with Rct</b> |
|                  | C1 [F]            | 0,0186129                             | 0,018183897       |
|                  | C2 [F]            | 3,187778082                           | 2,002807509       |

Table 42 Fitting results of potentiostatic-04/08/2021 evening

|                  |                   |                                       |                   |
|------------------|-------------------|---------------------------------------|-------------------|
| <b>Pressure</b>  | 0.5 bar           | T                                     | <b>60°C</b>       |
| <b>circuit</b>   | <b>LR(QR)(QR)</b> |                                       | 4even-POT         |
| <b>weighting</b> | modulus           |                                       |                   |
|                  |                   | <b>closed</b>                         |                   |
| <b>element</b>   | sub-parameters    | value                                 | error             |
| <b>L1</b>        |                   | 3,23E-06                              | 0,038065          |
| <b>R1</b>        |                   | 0,032558                              | 0,014452          |
| <b>CPE1</b>      | TDE               | 0,018551                              | 0,052297          |
|                  | PHIDE             | 0,99179                               | 0,0093938         |
| <b>R2</b>        |                   | 0,10468                               | 0,015299          |
| <b>CPE2</b>      | TDE               | 1,5344                                | 0,014111          |
|                  | PHIDE             | 0,72809                               | 0,012798          |
| <b>R3</b>        |                   | 0,57463                               | 0,024069          |
|                  |                   | <b>C with <math>\omega</math> max</b> | <b>C with Rct</b> |
|                  | C1 [F]            | 0,017930363                           | 0,017616491       |
|                  | C2 [F]            | 2,233979846                           | 1,463930825       |

Table 42 Fitting results of potentiostatic-05/08/2021 evening

|                  |                   |               |             |
|------------------|-------------------|---------------|-------------|
| <b>Pressure</b>  | 0.5 bar           | T             | <b>60°C</b> |
| <b>circuit</b>   | <b>LR(QR)(QR)</b> |               | 5even-POT   |
| <b>weighting</b> | modulus           |               |             |
|                  |                   | <b>closed</b> |             |
| <b>element</b>   | sub-parameters    | value         | error       |

|             |        |                                       |                   |
|-------------|--------|---------------------------------------|-------------------|
| <b>L1</b>   |        | 3,53E-06                              | 0,027989          |
| <b>R1</b>   |        | 0,021688                              | 0,015215          |
| <b>CPE1</b> | TDE    | 0,020777                              | 0,029276          |
|             | PHIDE  | 0,96416                               | 0,0055632         |
| <b>R2</b>   |        | 0,14039                               | 0,0092021         |
| <b>CPE2</b> | TDE    | 2,0764                                | 0,013543          |
|             | PHIDE  | 0,73954                               | 0,013051          |
| <b>R3</b>   |        | 0,62998                               | 0,036521          |
|             |        | <b>C with <math>\omega</math> max</b> | <b>C with Rct</b> |
|             | C1 [F] | 0,017908936                           | 0,016724308       |
|             | C2 [F] | 3,159714859                           | 2,282390246       |

Table 42 Fitting results of potentiostatic-06/08/2021 evening

|                  |                   |                                       |                   |
|------------------|-------------------|---------------------------------------|-------------------|
| <b>Pressure</b>  | 0.5 bar           | <b>T</b>                              | <b>60°C</b>       |
| <b>circuit</b>   | <b>LR(QR)(QR)</b> |                                       | 6even-POT         |
| <b>weighting</b> | modulus           |                                       |                   |
|                  |                   | <b>closed</b>                         |                   |
| <b>element</b>   | sub-parameters    | value                                 | error             |
| <b>L1</b>        |                   | 3,57E-06                              | 0,011311          |
| <b>R1</b>        |                   | 0,023011                              | 0,0063983         |
| <b>CPE1</b>      | TDE               | 0,020164                              | 0,016521          |
|                  | PHIDE             | 0,9697                                | 0,003045          |
| <b>R2</b>        |                   | 0,157                                 | 0,0058684         |
| <b>CPE2</b>      | TDE               | 2,0878                                | 0,010229          |
|                  | PHIDE             | 0,72794                               | 0,010269          |
| <b>R3</b>        |                   | 0,45919                               | 0,021744          |
|                  |                   | <b>C with <math>\omega</math> max</b> | <b>C with Rct</b> |
|                  | C1 [F]            | 0,017908795                           | 0,01684514        |
|                  | C2 [F]            | 3,23702779                            | 2,055145031       |

Table 42 Fitting results of potentiostatic-07/08/2021 evening

|                  |                   |               |             |
|------------------|-------------------|---------------|-------------|
| <b>Pressure</b>  | 0.5 bar           | <b>T</b>      | <b>80°C</b> |
| <b>circuit</b>   | <b>LR(QR)(QR)</b> |               | 7even-POT   |
| <b>weighting</b> | modulus           |               |             |
|                  |                   | <b>closed</b> |             |
| <b>element</b>   | sub-parameters    | value         | error       |
| <b>L1</b>        |                   | 2,32E-06      | 0,59159     |
| <b>R1</b>        |                   | 0,033886      | 0,15058     |
| <b>CPE1</b>      | TDE               | 0,013425      | 0,70324     |
|                  | PHIDE             | 1,0666        | 0,11502     |
| <b>R2</b>        |                   | 0,061846      | 0,16616     |
| <b>CPE2</b>      | TDE               | 1,1803        | 0,075032    |

|           |        |                                       |                   |
|-----------|--------|---------------------------------------|-------------------|
|           | PHIDE  | 0,76299                               | 0,055456          |
| <b>R3</b> |        | 0,83012                               | 0,076895          |
|           |        |                                       |                   |
|           |        | <b>C with <math>\omega</math> max</b> | <b>C with Rct</b> |
|           | C1 [F] | 0,017966077                           | 0,020906539       |
|           | C2 [F] | 2,151330161                           | 1,172838223       |

Table 42 Fitting results of potentiostatic-08/08/2021 evening

|                  |                   |                                       |                   |
|------------------|-------------------|---------------------------------------|-------------------|
| <b>Pressure</b>  | 0.5 bar           | T                                     | <b>80°C</b>       |
| <b>circuit</b>   | <b>LR(QR)(QR)</b> |                                       | 8even-POT         |
| <b>weighting</b> | modulus           |                                       |                   |
|                  |                   | <b>closed</b>                         |                   |
| <b>element</b>   | sub-parameters    | value                                 | error             |
| <b>L1</b>        |                   | 2,60E-06                              | 0,36728           |
| <b>R1</b>        |                   | 0,039874                              | 0,087782          |
| <b>CPE1</b>      | TDE               | 0,015361                              | 0,41233           |
|                  | PHIDE             | 1,0355                                | 0,070579          |
| <b>R2</b>        |                   | 0,077878                              | 0,10219           |
| <b>CPE2</b>      | TDE               | 1,4786                                | 0,051418          |
|                  | PHIDE             | 0,72307                               | 0,044396          |
| <b>R3</b>        |                   | 0,67932                               | 0,054731          |
|                  |                   |                                       |                   |
|                  |                   | <b>C with <math>\omega</math> max</b> | <b>C with Rct</b> |
|                  | C1 [F]            | 0,017941921                           | 0,019346391       |
|                  | C2 [F]            | 2,797568323                           | 1,481112342       |

Table 42 Fitting results of potentiostatic-09/08/2021 evening

|                  |                   |                                       |                   |
|------------------|-------------------|---------------------------------------|-------------------|
| <b>Pressure</b>  | 0.5 bar           | T                                     | <b>80°C</b>       |
| <b>circuit</b>   | <b>LR(QR)(QR)</b> |                                       | 9even-POT         |
| <b>weighting</b> | modulus           |                                       |                   |
|                  |                   | <b>closed</b>                         |                   |
| <b>element</b>   | sub-parameters    | value                                 | error             |
| <b>L1</b>        |                   | 3,25E-06                              | 0,058692          |
| <b>R1</b>        |                   | 0,023978                              | 0,028275          |
| <b>CPE1</b>      | TDE               | 0,021162                              | 0,060937          |
|                  | PHIDE             | 0,97074                               | 0,011609          |
| <b>R2</b>        |                   | 0,10482                               | 0,017531          |
| <b>CPE2</b>      | TDE               | 1,8737                                | 0,014805          |
|                  | PHIDE             | 0,73034                               | 0,014384          |
| <b>R3</b>        |                   | 0,77436                               | 0,038482          |
|                  |                   |                                       |                   |
|                  |                   | <b>C with <math>\omega</math> max</b> | <b>C with Rct</b> |
|                  | C1 [F]            | 0,018745104                           | 0,017601918       |
|                  | C2 [F]            | 3,276326076                           | 2,149724118       |

Table 42 Fitting results of potentiostatic-10/08/2021 evening

|                  |                   |                                       |                   |
|------------------|-------------------|---------------------------------------|-------------------|
| <b>Pressure</b>  | 0.5 bar           | <b>T</b>                              | <b>80°C</b>       |
| <b>circuit</b>   | <b>LR(QR)(QR)</b> |                                       | 10even-POT        |
| <b>weighting</b> | modulus           |                                       |                   |
|                  |                   | <b>closed</b>                         |                   |
| <b>element</b>   | sub-parameters    | value                                 | error             |
| <b>L1</b>        |                   | 2,87E-06                              | 0,23171           |
| <b>R1</b>        |                   | 0,033112                              | 0,062833          |
| <b>CPE1</b>      | TDE               | 0,019021                              | 0,19125           |
|                  | PHIDE             | 0,9941                                | 0,035743          |
| <b>R2</b>        |                   | 0,11336                               | 0,057423          |
| <b>CPE2</b>      | TDE               | 2,1071                                | 0,03947           |
|                  | PHIDE             | 0,66224                               | 0,046039          |
| <b>R3</b>        |                   | 0,54562                               | 0,063068          |
|                  |                   | <b>C with <math>\omega</math> max</b> | <b>C with Rct</b> |
|                  | C1 [F]            | 0,018561504                           | 0,018340399       |
|                  | C2 [F]            | 3,631921333                           | 2,262456435       |

Table 42 Fitting results of potentiostatic-11/08/2021 evening

|                  |                   |                                       |                   |
|------------------|-------------------|---------------------------------------|-------------------|
| <b>Pressure</b>  | 0.5 bar           | <b>T</b>                              | <b>80°C</b>       |
| <b>circuit</b>   | <b>LR(QR)(QR)</b> |                                       | 11even-POT        |
| <b>weighting</b> | modulus           |                                       |                   |
|                  |                   | <b>closed</b>                         |                   |
| <b>element</b>   | sub-parameters    | value                                 | error             |
| <b>L1</b>        |                   | 2,97E-06                              | 0,27196           |
| <b>R1</b>        |                   | 0,04057                               | 0,069748          |
| <b>CPE1</b>      | TDE               | 0,018007                              | 0,30389           |
|                  | PHIDE             | 1,004                                 | 0,05429           |
| <b>R2</b>        |                   | 0,10925                               | 0,085484          |
| <b>CPE2</b>      | TDE               | 1,8344                                | 0,053361          |
|                  | PHIDE             | 0,67156                               | 0,060801          |
| <b>R3</b>        |                   | 0,72652                               | 0,094672          |
|                  |                   | <b>C with <math>\omega</math> max</b> | <b>C with Rct</b> |
|                  | C1 [F]            | 0,018308024                           | 0,018459621       |
|                  | C2 [F]            | 3,359204392                           | 2,111064253       |

Table 42 Fitting results of potentiostatic-12/08/2021 evening

|                  |                   |               |             |
|------------------|-------------------|---------------|-------------|
| <b>Pressure</b>  | 0.5 bar           | <b>T</b>      | <b>80°C</b> |
| <b>circuit</b>   | <b>LR(QR)(QR)</b> |               | 12even-POT  |
| <b>weighting</b> | modulus           |               |             |
|                  |                   | <b>closed</b> |             |
| <b>element</b>   | sub-parameters    | value         | error       |

|             |        |                                       |                   |
|-------------|--------|---------------------------------------|-------------------|
| <b>L1</b>   |        | 3,25E-06                              | 0,15321           |
| <b>R1</b>   |        | 0,035123                              | 0,052113          |
| <b>CPE1</b> | TDE    | 0,021565                              | 0,17484           |
|             | PHIDE  | 0,96668                               | 0,032244          |
| <b>R2</b>   |        | 0,13205                               | 0,046953          |
| <b>CPE2</b> | TDE    | 2,1565                                | 0,040363          |
|             | PHIDE  | 0,72604                               | 0,042577          |
| <b>R3</b>   |        | 0,50414                               | 0,05463           |
|             |        | <b>C with <math>\omega</math> max</b> | <b>C with Rct</b> |
|             | C1 [F] | 0,018928016                           | 0,017620146       |
|             | C2 [F] | 3,353799577                           | 2,225599123       |

## GALVANOSTATIC

Table 42 Fitting results of galvanostatic-30/07/2021

|                  |                   |                                       |                   |
|------------------|-------------------|---------------------------------------|-------------------|
| <b>Pressure</b>  | 0.5 bar           | <b>T</b>                              | <b>60°C</b>       |
| <b>circuit</b>   | <b>LR(QR)(QR)</b> |                                       | 30-GALV           |
| <b>weighting</b> | modulus           |                                       |                   |
|                  |                   | <b>closed</b>                         |                   |
| <b>element</b>   | sub-parameters    | value                                 | error             |
| <b>L1</b>        |                   | 2,62E-06                              | 0,036062          |
| <b>R1</b>        |                   | 0,032244                              | 0,012354          |
| <b>CPE1</b>      | TDE               | 0,012495                              | 0,04052           |
|                  | PHIDE             | 1,0437                                | 0,0069558         |
| <b>R2</b>        |                   | 0,061871                              | 0,0089972         |
| <b>CPE2</b>      | TDE               | 8,6536                                | 0,021099          |
|                  | PHIDE             | 0,9683                                | 0,016646          |
| <b>R3</b>        |                   | 0,27002                               | 0,1437            |
|                  |                   | <b>C with <math>\omega</math> max</b> | <b>C with Rct</b> |
|                  | C1 [F]            | 0,015592845                           | 0,017333173       |

Table 42 Fitting results of galvanostatic-31/07/2021 morning

|                  |                   |               |             |
|------------------|-------------------|---------------|-------------|
| <b>Pressure</b>  | 0.5 bar           | <b>T</b>      | <b>60°C</b> |
| <b>circuit</b>   | <b>LR(QR)(QR)</b> |               | 31morn-GALV |
| <b>weighting</b> | modulus           |               |             |
|                  |                   | <b>closed</b> |             |
| <b>element</b>   | sub-parameters    | value         | error       |
| <b>L1</b>        |                   | 2,80E-06      | 0,30174     |
| <b>R1</b>        |                   | 0,0261        | 0,15806     |
| <b>CPE1</b>      | TDE               | 0,020851      | 0,37193     |
|                  | PHIDE             | 0,96271       | 0,068705    |
| <b>R2</b>        |                   | 0,076996      | 0,071688    |

|             |        |                                       |                   |
|-------------|--------|---------------------------------------|-------------------|
| <b>CPE2</b> | TDE    | 4,7909                                | 0,036474          |
|             | PHIDE  | 1,0729                                | 0,020718          |
| <b>R3</b>   |        | 0,81392                               | 0,034133          |
|             |        |                                       |                   |
|             |        | <b>C with <math>\omega</math> max</b> | <b>C with Rct</b> |
|             | C1 [F] | 0,017409183                           | 0,016251269       |
|             | C2 [F] | 3,852331253                           | 4,367779383       |

Table 42 Fitting results of galvanostatic-31/07/2021evening

|                  |                   |                                       |                   |
|------------------|-------------------|---------------------------------------|-------------------|
| <b>Pressure</b>  | 0.5 bar           | T                                     | <b>60°C</b>       |
| <b>circuit</b>   | <b>LR(QR)(QR)</b> |                                       | 31even-GALV       |
| <b>weighting</b> | modulus           |                                       |                   |
| <b>closed</b>    |                   |                                       |                   |
| <b>element</b>   | sub-parameters    | value                                 | error             |
| <b>L1</b>        |                   | 3,63E-06                              | 0,21875           |
| <b>R1</b>        |                   | 0,022322                              | 0,18314           |
| <b>CPE1</b>      | TDE               | 0,029739                              | 0,31717           |
|                  | PHIDE             | 0,8986                                | 0,0633            |
| <b>R2</b>        |                   | 0,10454                               | 0,059982          |
| <b>CPE2</b>      | TDE               | 4,7801                                | 0,039815          |
|                  | PHIDE             | 1,0527                                | 0,02364           |
| <b>R3</b>        |                   | 0,80277                               | 0,035897          |
|                  |                   |                                       |                   |
|                  |                   | <b>C with <math>\omega</math> max</b> | <b>C with Rct</b> |
|                  | C1 [F]            | 0,015592845                           | 0,017333173       |
|                  | C2 [F]            | 4,083027432                           | 4,468888458       |

Table 42 Fitting results of galvanostatic-01/08/2021 morning

|                  |                   |                                       |                   |
|------------------|-------------------|---------------------------------------|-------------------|
| <b>Pressure</b>  | 0.5 bar           | T                                     | <b>60°C</b>       |
| <b>circuit</b>   | <b>LR(QR)(QR)</b> |                                       | 1morn-GALV        |
| <b>weighting</b> | modulus           |                                       |                   |
| <b>closed</b>    |                   |                                       |                   |
| <b>element</b>   | sub-parameters    | value                                 | error             |
| <b>L1</b>        |                   | 2,25E-06                              | 0,30712           |
| <b>R1</b>        |                   | 0,032488                              | 0,10325           |
| <b>CPE1</b>      | TDE               | 0,01437                               | 0,36756           |
|                  | PHIDE             | 1,0297                                | 0,059683          |
| <b>R2</b>        |                   | 0,078775                              | 0,061386          |
| <b>CPE2</b>      | TDE               | 4,8384                                | 0,038853          |
|                  | PHIDE             | 1,057                                 | 0,022353          |
| <b>R3</b>        |                   | 0,80792                               | 0,035811          |
|                  |                   |                                       |                   |
|                  |                   | <b>C with <math>\omega</math> max</b> | <b>C with Rct</b> |
|                  | C1 [F]            | 0,016590452                           | 0,017475667       |

|        |             |             |
|--------|-------------|-------------|
| C2 [F] | 4,080013484 | 4,495455196 |
|--------|-------------|-------------|

Table 42 Fitting results of galvanostatic-01/08/2021 evening

|                  |                   |                                       |                   |
|------------------|-------------------|---------------------------------------|-------------------|
| <b>Pressure</b>  | 0.5 bar           | T                                     | <b>60°C</b>       |
| <b>circuit</b>   | <b>LR(QR)(QR)</b> |                                       | 1even-GALV        |
| <b>weighting</b> | modulus           |                                       |                   |
|                  |                   | <b>closed</b>                         |                   |
| <b>element</b>   | sub-parameters    | value                                 | error             |
| <b>L1</b>        |                   | 3,06E-06                              | 0,27675           |
| <b>R1</b>        |                   | 0,024485                              | 0,14191           |
| <b>CPE1</b>      | TDE               | 0,015356                              | 0,33013           |
|                  | PHIDE             | 1,003                                 | 0,057124          |
| <b>R2</b>        |                   | 0,089718                              | 0,057704          |
| <b>CPE2</b>      | TDE               | 4,9079                                | 0,039162          |
|                  | PHIDE             | 1,0471                                | 0,022406          |
| <b>R3</b>        |                   | 0,80758                               | 0,035647          |
|                  |                   | <b>C with <math>\omega</math> max</b> | <b>C with Rct</b> |
|                  | C1 [F]            | 0,015569717                           | 0,015661558       |
|                  | C2 [F]            | 4,262998137                           | 4,613103372       |

Table 42 Fitting results of galvanostatic-02/08/2021 morning

|                  |                   |                                       |                   |
|------------------|-------------------|---------------------------------------|-------------------|
| <b>Pressure</b>  | 0.5 bar           | T                                     | <b>60°C</b>       |
| <b>circuit</b>   | <b>LR(QR)(QR)</b> |                                       | 2morn-GALV        |
| <b>weighting</b> | modulus           |                                       |                   |
|                  |                   | <b>closed</b>                         |                   |
| <b>element</b>   | sub-parameters    | value                                 | error             |
| <b>L1</b>        |                   | 3,11E-06                              | 0,27679           |
| <b>R1</b>        |                   | 0,027504                              | 0,12483           |
| <b>CPE1</b>      | TDE               | 0,01489                               | 0,31543           |
|                  | PHIDE             | 1,0057                                | 0,054373          |
| <b>R2</b>        |                   | 0,095612                              | 0,054353          |
| <b>CPE2</b>      | TDE               | 4,9728                                | 0,039247          |
|                  | PHIDE             | 1,044                                 | 0,022358          |
| <b>R3</b>        |                   | 0,80509                               | 0,034857          |
|                  |                   | <b>C with <math>\omega</math> max</b> | <b>C with Rct</b> |
|                  | C1 [F]            | 0,015286204                           | 0,015453552       |
|                  | C2 [F]            | 4,359605347                           | 4,690407467       |

Table 42 Fitting results of galvanostatic-04/08/2021 evening

|                 |                   |   |             |
|-----------------|-------------------|---|-------------|
| <b>Pressure</b> | 0.5 bar           | T | <b>60°C</b> |
| <b>circuit</b>  | <b>LR(QR)(QR)</b> |   | 4even-GALV  |

|                  |                |                                       |                   |
|------------------|----------------|---------------------------------------|-------------------|
| <b>weighting</b> | modulus        |                                       |                   |
|                  |                | <b>closed</b>                         |                   |
| <b>element</b>   | sub-parameters | value                                 | error             |
| <b>L1</b>        |                | 3,47E-06                              | 0,28343           |
| <b>R1</b>        |                | 0,030916                              | 0,13683           |
| <b>CPE1</b>      | TDE            | 0,026672                              | 0,30037           |
|                  | PHIDE          | 0,9164                                | 0,060026          |
| <b>R2</b>        |                | 0,11577                               | 0,056374          |
| <b>CPE2</b>      | TDE            | 4,9533                                | 0,040281          |
|                  | PHIDE          | 1,036                                 | 0,023553          |
| <b>R3</b>        |                | 0,79792                               | 0,034431          |
|                  |                | <b>C with <math>\omega</math> max</b> | <b>C with Rct</b> |
|                  | C1 [F]         | 0,018498228                           | 0,015741466       |
|                  | C2 [F]         | 4,447668587                           | 4,722310424       |

Table 42 Fitting results of galvanostatic-05/08/2021 evening

|                  |                   |                                       |                   |
|------------------|-------------------|---------------------------------------|-------------------|
| <b>Pressure</b>  | 0.5 bar           | <b>T</b>                              | <b>60°C</b>       |
| <b>circuit</b>   | <b>LR(QR)(QR)</b> |                                       | Seven-GALV        |
| <b>weighting</b> | modulus           |                                       |                   |
|                  |                   | <b>closed</b>                         |                   |
| <b>element</b>   | sub-parameters    | value                                 | error             |
| <b>L1</b>        |                   | 2,97E-06                              | 0,20472           |
| <b>R1</b>        |                   | 0,023701                              | 0,096446          |
| <b>CPE1</b>      | TDE               | 0,011805                              | 0,23485           |
|                  | PHIDE             | 1,0369                                | 0,037313          |
| <b>R2</b>        |                   | 0,12186                               | 0,036809          |
| <b>CPE2</b>      | TDE               | 4,9402                                | 0,040098          |
|                  | PHIDE             | 1,0195                                | 0,023263          |
| <b>R3</b>        |                   | 0,80266                               | 0,034564          |
|                  |                   | <b>C with <math>\omega</math> max</b> | <b>C with Rct</b> |
|                  | C1 [F]            | 0,013992587                           | 0,014900691       |
|                  | C2 [F]            | 4,660312066                           | 4,81173044        |

Table 42 Fitting results of galvanostatic-06/08/2021 evening

|                  |                   |               |             |
|------------------|-------------------|---------------|-------------|
| <b>Pressure</b>  | 0.5 bar           | <b>T</b>      | <b>60°C</b> |
| <b>circuit</b>   | <b>LR(QR)(QR)</b> |               | 6even-GALV  |
| <b>weighting</b> | modulus           |               |             |
|                  |                   | <b>closed</b> |             |
| <b>element</b>   | sub-parameters    | value         | error       |
| <b>L1</b>        |                   | 3,05E-06      | 0,20772     |



|             |        |                                       |                   |
|-------------|--------|---------------------------------------|-------------------|
| <b>R1</b>   |        | 0,024562                              | 0,094234          |
| <b>CPE1</b> | TDE    | 0,01146                               | 0,2343            |
|             | PHIDE  | 1,0402                                | 0,036999          |
| <b>R2</b>   |        | 0,13416                               | 0,037114          |
| <b>CPE2</b> | TDE    | 4,811                                 | 0,044324          |
|             | PHIDE  | 0,99326                               | 0,026372          |
| <b>R3</b>   |        | 0,80248                               | 0,037674          |
|             |        | <b>C with <math>\omega</math> max</b> | <b>C with Rct</b> |
|             | C1 [F] | 0,013664876                           | 0,014719885       |
|             | C2 [F] | 4,908968919                           | 4,855303045       |

Table 42 Fitting results of galvanostatic-07/08/2021

|                  |                   |                                       |                   |
|------------------|-------------------|---------------------------------------|-------------------|
| <b>Pressure</b>  | 0.5 bar           | <b>T</b>                              | <b>80°C</b>       |
| <b>circuit</b>   | <b>LR(QR)(QR)</b> |                                       | 7-GALV            |
| <b>weighting</b> | modulus           |                                       |                   |
|                  |                   | <b>closed</b>                         |                   |
| <b>element</b>   | sub-parameters    | value                                 | error             |
| <b>L1</b>        |                   | 3,07E-06                              | 0,38667           |
| <b>R1</b>        |                   | 0,032592                              | 0,16695           |
| <b>CPE1</b>      | TDE               | 0,017296                              | 0,46888           |
|                  | PHIDE             | 0,98895                               | 0,086622          |
| <b>R2</b>        |                   | 0,069129                              | 0,10036           |
| <b>CPE2</b>      | TDE               | 4,4898                                | 0,039445          |
|                  | PHIDE             | 1,0268                                | 0,023638          |
| <b>R3</b>        |                   | 0,80558                               | 0,037093          |
|                  |                   | <b>C with <math>\omega</math> max</b> | <b>C with Rct</b> |
|                  | C1 [F]            | 0,016395663                           | 0,016043252       |
|                  | C2 [F]            | 4,143955907                           | 4,341643419       |

Table 42 Fitting results of galvanostatic-08/08/2021

|                  |                   |               |             |
|------------------|-------------------|---------------|-------------|
| <b>Pressure</b>  | 0.5 bar           | <b>T</b>      | <b>80°C</b> |
| <b>circuit</b>   | <b>LR(QR)(QR)</b> |               | 8-GALV      |
| <b>weighting</b> | modulus           |               |             |
|                  |                   | <b>closed</b> |             |
| <b>element</b>   | sub-parameters    | value         | error       |
| <b>L1</b>        |                   | 1,28E-06      | 0,64892     |
| <b>R1</b>        |                   | 0,044381      | 0,084298    |
| <b>CPE1</b>      | TDE               | 0,013458      | 0,39344     |
|                  | PHIDE             | 1,0485        | 0,063199    |
| <b>R2</b>        |                   | 0,080348      | 0,065932    |
| <b>CPE2</b>      | TDE               | 4,5215        | 0,040663    |
|                  | PHIDE             | 1,0172        | 0,024308    |

|           |                                       |                   |
|-----------|---------------------------------------|-------------------|
| <b>R3</b> | 0,80776                               | 0,036988          |
|           | <b>C with <math>\omega</math> max</b> | <b>C with Rct</b> |
| C1 [F]    | 0,017016957                           | 0,018457783       |
| C2 [F]    | 4,294776705                           | 4,423540769       |

Table 42 Fitting results of galvanostatic-09/08/2021

|                  |                   |                                       |                   |
|------------------|-------------------|---------------------------------------|-------------------|
| <b>Pressure</b>  | 0.5 bar           | <b>T</b>                              | <b>80°C</b>       |
| <b>circuit</b>   | <b>LR(QR)(QR)</b> |                                       | 9-GALV            |
| <b>weighting</b> | modulus           |                                       |                   |
|                  |                   | <b>closed</b>                         |                   |
| <b>element</b>   | sub-parameters    | value                                 | error             |
| <b>L1</b>        |                   | 2,79E-06                              | 0,20938           |
| <b>R1</b>        |                   | 0,025649                              | 0,10808           |
| <b>CPE1</b>      | TDE               | 0,013391                              | 0,30853           |
|                  | PHIDE             | 1,0289                                | 0,049126          |
| <b>R2</b>        |                   | 0,090237                              | 0,049842          |
| <b>CPE2</b>      | TDE               | 4,5296                                | 0,039388          |
|                  | PHIDE             | 1,0077                                | 0,023773          |
| <b>R3</b>        |                   | 0,80536                               | 0,036315          |
|                  |                   | <b>C with <math>\omega</math> max</b> | <b>C with Rct</b> |
| C1 [F]           |                   | 0,015298121                           | 0,016172195       |
| C2 [F]           |                   | 4,426474169                           | 4,485027776       |

Table 42 Fitting results of galvanostatic-10/08/2021

|                  |                   |                                       |                   |
|------------------|-------------------|---------------------------------------|-------------------|
| <b>Pressure</b>  | 0.5 bar           | <b>T</b>                              | <b>80°C</b>       |
| <b>circuit</b>   | <b>LR(QR)(QR)</b> |                                       | 10-GALV           |
| <b>weighting</b> | modulus           |                                       |                   |
|                  |                   | <b>closed</b>                         |                   |
| <b>element</b>   | sub-parameters    | value                                 | error             |
| <b>L1</b>        |                   | 7,27E-08                              | 0,033608          |
| <b>R1</b>        |                   | 0,042878                              | 0,06015           |
| <b>CPE1</b>      | TDE               | 0,0097757                             | 0,31747           |
|                  | PHIDE             | 1,1037                                | 0,045475          |
| <b>R2</b>        |                   | 0,086844                              | 0,048002          |
| <b>CPE2</b>      | TDE               | 4,7906                                | 0,040671          |
|                  | PHIDE             | 0,9923                                | 0,024642          |
| <b>R3</b>        |                   | 0,80337                               | 0,036925          |
|                  |                   | <b>C with <math>\omega</math> max</b> | <b>C with Rct</b> |
| C1 [F]           |                   | 0,015762963                           | 0,01899763        |
| C2 [F]           |                   | 4,902209057                           | 4,840962681       |

Table 42 Fitting results of galvanostatic-11/08/2021

|                  |                   |                                       |                   |
|------------------|-------------------|---------------------------------------|-------------------|
| <b>Pressure</b>  | 0.5 bar           | T                                     | <b>80°C</b>       |
| <b>circuit</b>   | <b>LR(QR)(QR)</b> |                                       | 11-GALV           |
| <b>weighting</b> | modulus           |                                       |                   |
|                  |                   | <b>closed</b>                         |                   |
| <b>element</b>   | sub-parameters    | value                                 | error             |
| <b>L1</b>        |                   | 2,97E-06                              | 0,29437           |
| <b>R1</b>        |                   | 0,042616                              | 0,087928          |
| <b>CPE1</b>      | TDE               | 0,01307                               | 0,33995           |
|                  | PHIDE             | 1,0271                                | 0,056419          |
| <b>R2</b>        |                   | 0,097232                              | 0,058762          |
| <b>CPE2</b>      | TDE               | 4,6041                                | 0,040811          |
|                  | PHIDE             | 0,98834                               | 0,025058          |
| <b>R3</b>        |                   | 0,80568                               | 0,036257          |
|                  |                   | <b>C with <math>\omega</math> max</b> | <b>C with Rct</b> |
|                  | C1 [F]            | 0,014808092                           | 0,015584189       |
|                  | C2 [F]            | 4,767497886                           | 4,675856614       |

Table 42 Fitting results of galvanostatic-12/08/2021

|                  |                   |                                       |                   |
|------------------|-------------------|---------------------------------------|-------------------|
| <b>Pressure</b>  | 0.5 bar           | T                                     | <b>80°C</b>       |
| <b>circuit</b>   | <b>LR(QR)(QR)</b> |                                       | 12-GALV           |
| <b>weighting</b> | modulus           |                                       |                   |
|                  |                   | <b>closed</b>                         |                   |
| <b>element</b>   | sub-parameters    | value                                 | error             |
| <b>L1</b>        |                   | 2,90E-06                              | 0,25835           |
| <b>R1</b>        |                   | 0,034963                              | 0,089157          |
| <b>CPE1</b>      | TDE               | 0,012491                              | 0,29927           |
|                  | PHIDE             | 1,0339                                | 0,048572          |
| <b>R2</b>        |                   | 0,10031                               | 0,049571          |
| <b>CPE2</b>      | TDE               | 4,3766                                | 0,03867           |
|                  | PHIDE             | 0,98991                               | 0,023774          |
| <b>R3</b>        |                   | 0,81117                               | 0,034787          |
|                  |                   | <b>C with <math>\omega</math> max</b> | <b>C with Rct</b> |
|                  | C1 [F]            | 0,01460248                            | 0,015550748       |
|                  | C2 [F]            | 4,510692953                           | 4,433487176       |

## Tests performed with open/closed cathode with different mass flow rates

### FIRST SERIES

Table 18 Fitting results of potentiostatic test at 60°C with recirculating pump

| circuit   | LR(QR)(QR)     | POT             |          |                 |          |
|-----------|----------------|-----------------|----------|-----------------|----------|
| weighting | modulus        |                 |          |                 |          |
|           |                | open            |          | closed          |          |
| element   | sub-parameters | value           | error    | value           | error    |
| L1        |                | 2,70E-06        | 0,27359  | 2,89E-06        | 0,50803  |
| R1        |                | <b>0,079082</b> | 0,03552  | <b>0,052069</b> | 0,088653 |
| CPE1      | TDE            | 0,015449        | 0,29533  | 0,013941        | 0,58574  |
|           | PHIDE          | 1,0392          | 0,052256 | 1,0653          | 0,10073  |
| R2        |                | <b>0,06438</b>  | 0,076091 | <b>0,089761</b> | 0,18516  |
| CPE2      | TDE            | 0,82489         | 0,025057 | 1,8797          | 0,075021 |
|           | PHIDE          | 0,79131         | 0,018029 | 0,55298         | 0,10875  |
| R3        |                | 0,88021         | 0,027784 | 1,1272          | 0,19863  |

Table 19 Parameters calculated from the fitting results of potentiostatic test at 60°C with recirculating pump

| POT    | open                  |                   | closed                |                    |
|--------|-----------------------|-------------------|-----------------------|--------------------|
|        | C with $\omega_{max}$ | C with Rct        | C with $\omega_{max}$ | C with Rct         |
| C1 [F] | 0,018505481           | <b>0,02005178</b> | 0,018274094           | <b>0,020999868</b> |
| C2 [F] | 1,048936015           | 0,758111867       |                       | 3,449006275        |

Table 20 Fitting results of galvanostatic test at 60°C with recirculating pump

| circuit   | LR(QR)(QR)     | GALV            |          |                 |          |
|-----------|----------------|-----------------|----------|-----------------|----------|
| weighting | modulus        |                 |          |                 |          |
|           |                | open            |          | closed          |          |
| element   | sub-parameters | value           | error    | value           | error    |
| L1        |                | 2,39E-06        | 0,31042  | 5,05E-07        | 0,18988  |
| R1        |                | <b>0,045802</b> | 0,090172 | <b>0,087164</b> | 0,074421 |
| CPE1      | TDE            | 0,015836        | 0,71661  | 0,12379         | 0,3544   |
|           | PHIDE          | 1,061           | 0,11439  | 0,69983         | 0,097642 |
| R2        |                | <b>0,046478</b> | 0,17595  | <b>0,12954</b>  | 0,077931 |
| CPE2      | TDE            | 2,0705          | 0,044265 | 9,982           | 0,0622   |
|           | PHIDE          | 0,56224         | 0,047414 | 0,95845         | 0,029252 |
| R3        |                | 1,1809          | 0,068365 | 0,7749          | 0,041545 |

Table 21 Parameters calculated from the fitting results of galvanostatic test at 60°C with recirculating pump

| GALV          | open                |                    | closed              |                   |
|---------------|---------------------|--------------------|---------------------|-------------------|
|               | C with $\omega$ max | C with Rct         | C with $\omega$ max | C with Rct        |
| <b>C1 [F]</b> | 0,020974829         | <b>0,023976015</b> | 0,028974141         | <b>0,02102884</b> |
| <b>C2 [F]</b> | 5,123839196         | 4,153330638        | 11,52122222         | 10,90770922       |

Table 22 Fitting results of potentiostatic test at 80°C with recirculating pump

| circuit     | LR(QR)(QR)     | POT       |          |                 |          |
|-------------|----------------|-----------|----------|-----------------|----------|
| weighting   | modulus        |           |          |                 |          |
|             |                | open      |          | closed          |          |
| element     | sub-parameters | value     | error    | value           | error    |
| <b>L1</b>   |                | 5,32E-08  | 0,12178  | 5,23E-08        | 0,11516  |
| <b>R1</b>   |                | 0,24575   | 0,031473 | 0,087554        | 0,043567 |
| <b>CPE1</b> | TDE            | 0,0081098 | 1,0378   | 0,011931        | 0,48482  |
|             | PHIDE          | 1,1791    | 0,15166  | 1,1064          | 0,075753 |
| <b>R2</b>   |                | 0,048537  | 0,22357  | <b>0,086567</b> | 0,13071  |
| <b>CPE2</b> | TDE            | 1,0022    | 0,04162  | 1,4051          | 0,059891 |
|             | PHIDE          | 0,75993   | 0,037088 | 0,64689         | 0,067438 |
| <b>R3</b>   |                | 1,2434    | 0,064994 | 0,98218         | 0,10437  |

Table 23 Parameters calculated from the fitting results of potentiostatic test at 80°C with recirculating pump

| POT           | open                |                    | closed              |                    |
|---------------|---------------------|--------------------|---------------------|--------------------|
|               | C with $\omega$ max | C with Rct         | C with $\omega$ max | C with Rct         |
| <b>C1 [F]</b> | 0,017752846         | <b>0,026680978</b> | 0,018543853         | <b>0,023111649</b> |
| <b>C2 [F]</b> | 1,559564613         | 1,074346776        | 2,288581065         | 1,675219939        |

The fitting results concerning only the high frequency impedance data are reported in table.

Table 24 Fitting results of galvanostatic test at 80°C with recirculating pump

| circuit   | LR(QR)(QR)     | GALV     |          |            |          |
|-----------|----------------|----------|----------|------------|----------|
| weighting | modulus        |          |          |            |          |
|           |                | open     |          | closed     |          |
| element   | sub-parameters | value    | error    | value      | error    |
| <b>L1</b> |                | 2,38E-07 | 0,043513 | 6,12E-07   | 0,091644 |
| <b>R1</b> |                | 0,16944  | 0,049465 | <b>0,1</b> | 0,045963 |

|             |       |          |          |                 |          |
|-------------|-------|----------|----------|-----------------|----------|
| <b>CPE1</b> | TDE   | 0,025513 | 1,1763   | 0,014122        | 0,40316  |
|             | PHIDE | 1,0092   | 0,20416  | 1,0316          | 0,065943 |
| <b>R2</b>   |       | 0,052934 | 0,25634  | <b>0,094321</b> | 0,065904 |
| <b>CPE2</b> | TDE   | 2,5521   | 0,05417  | 5,0567          | 0,038833 |
|             | PHIDE | 0,61856  | 0,05254  | 1,0126          | 0,02221  |
| <b>R3</b>   |       | 0,99303  | 0,061941 | 0,81966         | 0,031303 |

Table 25 Parameters calculated from the fitting results of galvanostatic test at 80°C with recirculating pump

| <b>GALV</b>   | <b>open</b>         | <b>closed</b>      |                     |                    |
|---------------|---------------------|--------------------|---------------------|--------------------|
|               | C with $\omega$ max | C with Rct         | C with $\omega$ max | C with Rct         |
| <b>C1 [F]</b> | 0,026617638         | <b>0,027096943</b> | 0,016335169         | <b>0,017297306</b> |
| <b>C2 [F]</b> | \                   | 4,528363073        | 4,88383015          | 4,968021787        |

## SECOND SERIES

Table 26 Fitting results of potentiostatic test at 60°C with needle valve

| <b>circuit</b>   | <b>LR(QR)(QR)</b> | <b>POT</b>      |          |                 |          |
|------------------|-------------------|-----------------|----------|-----------------|----------|
| <b>weighting</b> | modulus           | <b>open</b>     |          | <b>closed</b>   |          |
| <b>element</b>   | sub-parameters    | value           | error    | value           | error    |
| <b>L1</b>        |                   | 3,47E-06        | 0,12283  | 3,59E-06        | 0,13475  |
| <b>R1</b>        |                   | <b>0,045698</b> | 0,042345 | <b>0,072855</b> | 0,027487 |
| <b>CPE1</b>      | TDE               | 0,025478        | 0,16614  | 0,026273        | 0,12529  |
|                  | PHIDE             | 0,94029         | 0,032744 | 0,93328         | 0,0274   |
| <b>R2</b>        |                   | <b>0,085564</b> | 0,042386 | <b>0,082359</b> | 0,040258 |
| <b>CPE2</b>      | TDE               | 0,91479         | 0,021321 | 1,3443          | 0,022781 |
|                  | PHIDE             | 0,87517         | 0,014309 | 0,78353         | 0,016504 |
| <b>R3</b>        |                   | 0,59166         | 0,019583 | 5,4596          | 0,34282  |

Table 27 Parameters calculated from the fitting results of potentiostatic test at 60°C with needle valve

| <b>POT</b>    | <b>open</b>         | <b>closed</b>   |                     |                    |
|---------------|---------------------|-----------------|---------------------|--------------------|
|               | C with $\omega$ max | C with Rct      | C with $\omega$ max | C with Rct         |
| <b>C1 [F]</b> | 0,019620825         | <b>0,017264</b> | 0,019621974         | <b>0,016943578</b> |
| <b>C2 [F]</b> | 1,056187854         | 0,838096387     |                     | <b>2,33160978</b>  |

Table 28 Fitting results of galvanostatic test at 60°C with needle valve

| circuit     | LR(QR)(QR)     | GALV            |          |                 |          |
|-------------|----------------|-----------------|----------|-----------------|----------|
| weighting   | modulus        |                 |          |                 |          |
|             |                | open            |          | closed          |          |
| element     | sub-parameters | value           | error    | value           | error    |
| <b>L1</b>   |                | 1,15E-06        | 0,31627  | 9,62E-08        | 0,016459 |
| <b>R1</b>   |                | <b>0,055666</b> | 0,15659  | <b>0,081111</b> | 0,047999 |
| <b>CPE1</b> | TDE            | 0,097327        | 0,6542   | 0,044259        | 0,21937  |
|             | PHIDE          | 0,75461         | 0,15943  | 0,86441         | 0,04585  |
| <b>R2</b>   |                | <b>0,1104</b>   | 0,1607   | <b>0,21134</b>  | 0,042557 |
| <b>CPE2</b> | TDE            | 2,6301          | 0,071723 | 6,1635          | 0,066165 |
|             | PHIDE          | 0,83232         | 0,055259 | 0,90269         | 0,038047 |
| <b>R3</b>   |                | 1,0032          | 0,072777 | 0,83533         | 0,052305 |

Table 29 Parameters calculated from the fitting results of galvanostatic test at 60°C with needle valve

| GALV          | open                |                    | closed              |                 |
|---------------|---------------------|--------------------|---------------------|-----------------|
|               | C with $\omega$ max | C with Rct         | C with $\omega$ max | C with Rct      |
| <b>C1 [F]</b> | 0,033246161         | <b>0,022284572</b> | 0,027699566         | <b>0,021268</b> |
| <b>C2 [F]</b> | 4,178404029         | 3,197862712        | 8,62361429          | 7,354397664     |

Table 30 Fitting results of potentiostatic test at 70°C with needle valve

| circuit     | LR(QR)(QR)     | POT             |           |                 |          |
|-------------|----------------|-----------------|-----------|-----------------|----------|
| weighting   | modulus        |                 |           |                 |          |
|             |                | open            |           | closed          |          |
| element     | sub-parameters | value           | error     | value           | error    |
| <b>L1</b>   |                | 5,71E-08        | 0,004417  | 4,66E-06        | 0,27758  |
| <b>R1</b>   |                | <b>0,14875</b>  | 0,0099655 | <b>0,072372</b> | 0,071866 |
| <b>CPE1</b> | TDE            | 0,019597        | 0,20605   | 0,031615        | 0,25191  |
|             | PHIDE          | 1,0482          | 0,033741  | 0,88679         | 0,058036 |
| <b>R2</b>   |                | <b>0,052877</b> | 0,039782  | <b>0,11656</b>  | 0,070909 |
| <b>CPE2</b> | TDE            | 0,68435         | 0,0047127 | 1,1431          | 0,01873  |
|             | PHIDE          | 0,87613         | 0,0035897 | 0,85948         | 0,019434 |
| <b>R3</b>   |                | 11,197          | 0,020805  | 3,8713          | 0,12263  |

Table 31 Parameters calculated from the fitting results of potentiostatic test at 70°C with needle valve

| POT | open                |            | closed              |            |
|-----|---------------------|------------|---------------------|------------|
|     | C with $\omega$ max | C with Rct | C with $\omega$ max | C with Rct |

|               |             |                |             |                    |
|---------------|-------------|----------------|-------------|--------------------|
| <b>C1 [F]</b> | 0,0244675   | <b>0,02688</b> | 0,019774789 | <b>0,015460328</b> |
| <b>C2 [F]</b> | 1,111384523 | 0,912671891    |             | <b>1,457779518</b> |

Table 32 Fitting results of galvanostatic test at 70°C with needle valve

| circuit     | LR(QR)(QR)     | GALV            |          |                 |          |
|-------------|----------------|-----------------|----------|-----------------|----------|
| weighting   | modulus        |                 |          |                 |          |
|             |                | open            |          | closed          |          |
| element     | sub-parameters | value           | error    | value           | error    |
| <b>L1</b>   |                | 5,56E-07        | 0,1521   | 1,04E-07        | 0,014898 |
| <b>R1</b>   |                | <b>0,13112</b>  | 0,11575  | <b>0,097472</b> | 0,040968 |
| <b>CPE1</b> | TDE            | 0,043572        | 1,6918   | 0,034121        | 0,20719  |
|             | PHIDE          | 0,90344         | 0,3365   | 0,90412         | 0,041642 |
| <b>R2</b>   |                | <b>0,060976</b> | 0,37396  | <b>0,25033</b>  | 0,042352 |
| <b>CPE2</b> | TDE            | 2,3449          | 0,079713 | 6,3323          | 0,083536 |
|             | PHIDE          | 0,73994         | 0,06619  | 0,82666         | 0,049221 |
| <b>R3</b>   |                | 1,0496          | 0,08116  | 0,83963         | 0,06657  |

Table 33 Parameters calculated from the fitting results of galvanostatic test at 70°C with needle valve

| GALV          | open                |                   | closed              |                   |
|---------------|---------------------|-------------------|---------------------|-------------------|
|               | C with $\omega$ max | C with Rct        | C with $\omega$ max | C with Rct        |
| <b>C1 [F]</b> | 0,027925677         | <b>0,02311654</b> | 0,025043125         | <b>0,02059043</b> |
| <b>C2 [F]</b> | 2,977604503         | 3,218085796       | 11,5182863          | 8,989196224       |

Table 34 Fitting results of potentiostatic test at 80°C with needle valve

| circuit     | LR(QR)(QR)     | POT             |           |                 |          |
|-------------|----------------|-----------------|-----------|-----------------|----------|
| weighting   | modulus        |                 |           |                 |          |
|             |                | open            |           | closed          |          |
| element     | sub-parameters | value           | error     | value           | error    |
| <b>L1</b>   |                | 3,62E-06        | 0,062019  | 3,42E-06        | 0,34212  |
| <b>R1</b>   |                | <b>0,052537</b> | 0,017702  | <b>0,054939</b> | 0,08173  |
| <b>CPE1</b> | TDE            | 0,026875        | 0,073988  | 0,025963        | 0,34831  |
|             | PHIDE          | 0,92842         | 0,01465   | 0,93478         | 0,0683   |
| <b>R2</b>   |                | <b>0,11634</b>  | 0,019354  | <b>0,13143</b>  | 0,089783 |
| <b>CPE2</b> | TDE            | 1,0918          | 0,012228  | 1,2819          | 0,058869 |
|             | PHIDE          | 0,83375         | 0,0095609 | 0,80848         | 0,051418 |
| <b>R3</b>   |                | 0,53171         | 0,011152  | 0,66763         | 0,069354 |



Table 35 Parameters calculated from the fitting results of potentiostatic test at 80°C with needle valve

| POT           | open                |                 | closed              |                 |
|---------------|---------------------|-----------------|---------------------|-----------------|
|               | C with $\omega$ max | C with Rct      | C with $\omega$ max | C with Rct      |
| <b>C1 [F]</b> | 0,019975717         | <b>0,017227</b> | 0,019813307         | <b>0,017468</b> |
| <b>C2 [F]</b> | 1,322130822         | 0,979598952     | 1,67017657          | 1,23548672      |

Table 36 Fitting results of galvanostatic test at 80°C with needle valve

| circuit     | LR(QR)(QR)     | GALV           |          |                 |          |
|-------------|----------------|----------------|----------|-----------------|----------|
| weighting   | modulus        |                |          |                 |          |
|             |                | open           |          | closed          |          |
| element     | sub-parameters | value          | error    | value           | error    |
| <b>L1</b>   |                | 5,56E-07       | 0,5198   | 3,01E-06        | 0,57193  |
| <b>R1</b>   |                | <b>0,05627</b> | 0,07387  | <b>0,058067</b> | 0,10036  |
| <b>CPE1</b> | TDE            | 0,033765       | 0,44285  | 0,017941        | 0,51708  |
|             | PHIDE          | 0,93097        | 0,080201 | 1,0022          | 0,092996 |
| <b>R2</b>   |                | <b>0,11685</b> | 0,091291 | <b>0,11527</b>  | 0,12186  |
| <b>CPE2</b> | TDE            | 2,505          | 0,060081 | 2,1734          | 0,061214 |
|             | PHIDE          | 0,79252        | 0,050483 | 0,67056         | 0,062465 |
| <b>R3</b>   |                | 1,0566         | 0,071785 | 1,1685          | 0,087065 |

Table 37 Parameters calculated from the fitting results of galvanostatic test at 80°C with needle valve

| GALV          | open                |             | closed              |             |
|---------------|---------------------|-------------|---------------------|-------------|
|               | C with $\omega$ max | C with Rct  | C with $\omega$ max | C with Rct  |
| <b>C1 [F]</b> | 0,025359433         | 0,022398602 | 0,018105436         | 0,018186095 |
| <b>C2 [F]</b> | 2,626295864         | 3,232023164 | 5,82191516          | 3,435568946 |

---

# Bibliography

- [1] <https://espresso.repubblica.it/plus/articoli/2020/12/10/news/covid-cambiamento-climatico-1.356895/> .
- [2] [https://ec.europa.eu/clima/eu-action/international-action-climate-change/climate-negotiations/paris-agreement\\_en](https://ec.europa.eu/clima/eu-action/international-action-climate-change/climate-negotiations/paris-agreement_en) (cit. on p.3).
- [3] European Commission, Communication COM/2019/640: The European Green Deal, [https://knowledge4policy.ec.europa.eu/publication/communication-com2019640-european-green-deal\\_en](https://knowledge4policy.ec.europa.eu/publication/communication-com2019640-european-green-deal_en) (cit. on p.3).
- [4] European Commission, Communication COM/2020/562: Stepping up Europe's 2030 climate ambition Investing in a climate-neutral future for the benefit of our people, [https://knowledge4policy.ec.europa.eu/publication/communication-com2020562-stepping-europe%E2%80%99s-2030-climate-ambition-investing-climate\\_en](https://knowledge4policy.ec.europa.eu/publication/communication-com2020562-stepping-europe%E2%80%99s-2030-climate-ambition-investing-climate_en) (cit. on p.3).
- [5] IEA (2021), Net Zero by 2050, IEA, Paris <https://www.iea.org/reports/net-zero-by-2050> (cit. on p.3).
- [6] Robert R. Dickinson et al., Power-to-hydrogen and hydrogen-to-X pathways: Opportunities for next generation energy systems, International Conference on the European Energy Market, EEM June (2017) (cit. on p.3).
- [7] IEA (2021), Global Energy Review 2021, IEA, Paris <https://www.iea.org/reports/global-energy-review-2021> (cit. on p.4).
- [8] IEA (2021), Global Hydrogen Review 2021, IEA, Paris <https://www.iea.org/reports/global-hydrogen-review-2021> (cit. on p.5).
- [9] IEA (2021), Hydrogen, IEA, Paris <https://www.iea.org/reports/hydrogen> (cit. on pp.5-6-7).
- [10] [https://ec.europa.eu/commission/presscorner/detail/en/ip\\_21\\_6021](https://ec.europa.eu/commission/presscorner/detail/en/ip_21_6021)
- [11] <https://www.isprambiente.gov.it/it/archivio/notizie-e-novita-normative/notizie-ispra/2021/11/26a-conferenza-delle-parti-sul-cambiamento-climatico>
- [12] M. Carmo, D. L. Fritz, J. Mergel, and D. Stolen, *A comprehensive review on PEM water electrolysis*, International Journal of Hydrogen Energy, 38, 4901:4934, 2013 (cit. on pp.8-9).

- 
- [13] S. Shiva Kumar and V.Himabindu, *Hydrogen production by PEM water electrolysis – A review*, Material Science for Energy Technologies, 2, 442:454, 2019 (cit. on pp.8-9).
- [14] D. Bessarabov, H. Wang, H. Li and N. Zhao, *PEM Electrolysis for Hydrogen Production: Principles and Applications*, Taylor&Francis Group: Boca Raton, FL, USA, 2016 (cit. on p.9; pp.14-18).
- [15] F. Hegge et al., Efficient and stable low iridium loaded anodes for PEM water electrolysis made possible by nanofiber interlayers, *ACS Applied Energy Materials*, 3, 8276–8284, 2020.
- [16] S. Siracusano et al., Nanosized IrO<sub>x</sub> and IrRuO<sub>x</sub> electrocatalysts for the O<sub>2</sub> evolution reaction in PEM water electrolyzers, *Applied Catalysis B: Environmental*, 164,488-495, 2015.
- [17] A.S. Pushkarev et al., On the influence of porous transport layers parameters on the performances of polymer electrolyte membrane water electrolysis cells, *Electrochimica Acta*, 399,139436, 2021.
- [18] T. Schuler et al., Polymer Electrolyte Water Electrolysis: Correlating Porous transport layer structural properties and performance: Part I. Tomographic analysis of morphology and topology, *Journal of The Electrochemical Society*, 166 (4) F270-F281, 2019.
- [19] I. Hiroshi et al., Experimental study on porous current collectors of PEM electrolyzers, *International Journal of Hydrogen Energy*, 37, 7418-7429, 2012.
- [20] J. Parra-Restrepo et al., Influence of the porous transport layer properties on the mass and charge transfer in a segmented PEM electrolyzer, *International Journal of Hydrogen Energy*, 45 (15), 8094-8106, 2020.
- [21] IRENA (2020), *Green Hydrogen Cost Reduction: Scaling up Electrolysers to Meet the 1.5 °C Climate Goal*, International Renewable Energy Agency, Abu Dhabi.
- [22] T. Romero-Castañón, L.G. Arriaga and U. Cano-Castillo, *Impedance spectroscopy as a tool in the evaluation of MEA's*, *Journal of Power Sources*, 118, 179-182, 2003.
- [23] T. Malkow, A. Pilenga, and G. Tsotridis, «EU harmonised test procedure: electrochemical impedance spectroscopy for water electrolysis cells». In: *JRC VALIDATED METHODS, REFERENCE METHODS AND MEASUREMENT REPORTS* (2018) (cit. on p.12; pp.20-22; p.27; pp.66-68).
- [24] D. Bessarabov, P. Millet, *PEM Water Electrolysis- Volume 1*, Academic press, 2018.
- [25] A. Godula-Jopek, *Hydrogen Production by Electrolysis*, Wiley-VCH: Weinheim, Germany, 2015 (cit. on pp.16-18).

- 
- [26] J. van der Merwe, K. Uren, G. Van Schoor, D. Bessarabov, A study of the loss characteristics of a single cell PEM electrolyser for pure hydrogen production. In: Industrial Technology (ICIT), 2013 IEEE international conference on 2013, pp. 668-72.
- [27] X. Yuan, C. Song, H. Wang, J. Zhang, Electrochemical Impedance Spectroscopy in PEM Fuel Cells-Fundamentals and Applications, Springer, London, 2010 (cit. on p.22; p.27; pp.29-43; pp.66-68)
- [28] D. Vladikova. «The technique of the differential impedance analysis Part I: Basics of the impedance spectroscopy». In: *Proceedings of the International Workshop - Advanced Techniques for Energy Sources Investigation and Testing* (2004) (cit. on pp.23-25; pp.29-43; pp.77-78).
- [29] C. Gabrielli, Identification of Electrochemical Process by Frequency Response Analysis, Monograph Reference 004 /83, Solartron Instr.Group, Farnborough, England, 1980 (cit. on pp.23-26).
- [30] A. Lasia, Electrochemical Impedance Spectroscopy and its Applications, Springer, New York, 2014 (cit. on pp.25-27; p.29; pp.44-46).
- [31] M. E. Orazem, V. Tribollet, Electrochemical Impedance Spectroscopy, Wiley: Hoboken, NJ, 2008 (cit. on pp.27-28).
- [32] B. A. Boukamp, J. Electrochem. Soc., 142 (1995) 1885.
- [33] M. Schönleber, D. Klotz and E. Ivers-Tiffée, A Method for Improving the Robustness of linear Kramers-Kronig Validity Tests, *Electrochimica Acta* 131, pp. 20-27 (2014).
- [34] <http://www.iwe.kit.edu/Lin-KK.php>
- [35] M. Sluyters-Rehbach, Impedances of Electrochemical Systems: Terminology, Nomenclature and Representation Part I: Cells with Metal Electrodes and Liquid Solution, *Pure & Applied Chemistry*., 66 (9), (1994), 1831-1891.
- [36] P. Zoltowski, Non-traditional approach to measurement models for analysis of impedance spectra, *Solid State Ionics*, 176, 1979:1986, 2005 (cit. on pp.45-46).
- [37] C. Rozain and P. Millet, Electrochemical characterization of polymer electrolyte membrane water electrolysis cells, *Electrochimica Acta*, 131,160-167, 2014 (cit. on pp.47-48).

- 
- [38] J. van der Merwe, K. Uren, G. van Schoor and D. Bessarabov, *Characterization tools development for PEM electrolyzers*, International Journal of Hydrogen Energy, 39, 14212:14221, 2014.
- [39] I. Dedigama, P. Angeli, K. Ayers, J.B. Robinson, P.R. Shearing, D. Tsaoulidis and D.J.L. Brett, *In situ diagnostic techniques for characterization of polymer electrolyte membrane water electrolyzers-Flow visualisation and electrochemical impedance spectroscopy*, International Journal of Hydrogen, 39, 4458-4482, 2014.
- [40] K. Elsåe, L. Grahl-Madsen, G.G. Scherer, J. Hjelm, M.B. Morgensen, *Electrochemical Characterization of a PEMEC Using Impedance Spectroscopy*, Journal of Electrochemical Society, 164, F1419-F1426, 2017.
- [41] E. Rasten, G. Hagen, R. Tunold, *Electrocatalysis in water electrolysis with solid polymer electrolyte*, Electrochimica acta, 48,3945-3952, 2003.
- [42] C. Rozain, E. Mayousse, N. Guillet and P. Millet, *Influence of iridium oxide loadings on the performance of PEM water electrolysis cells: Part I-Pure IrO<sub>2</sub>-based anodes*, Applied Catalysis B: Environmental, 182, 153-160, 2016.
- [43] C. Rozain, E. Mayousse, N. Guillet and P. Millet., *Influence of iridium oxide loadings on the performance of PEM water electrolysis cells: Part II-Advanced oxygen electrodes*, Applied Catalysis B: Environmental,182, 123-131, 2016.
- [44] P. Lettenmeier, R. Wang, R. Abouatallah, S. Helmly, T. Morawietz, R. Hiesgen, S. Kolb, F. Burggraf, J. Kallo, A.S. Gago, K.A. Friedrich, *Durable Membrane Electrode Assemblies for Proton Exchange Membrane Electrolyzer Systems Operating at High Current Densities*, Electrochimica Acta, 210, 502-511, 2016.
- [45] P. Lettenmeier, S. Kolb, F. Burggraf, A.S. Gago, K.A. Friedrich, *Towards developing a backing layer for proton exchange membrane electrolyzers*, Journal of Power Sources, 311, 153-158, 2016.
- [46] S. Siracusano, V. Baglio, F. Lufrano, P. Staiti and A.S. Aricò, *Electrochemical characterization of PEM water electrolyzer based on a sulfonated polysulfone membrane*, Journal of Membrane Science, 448, 209-214, 2013.
- [47] S. Siracusano, V. Baglio, M.A. Navarra, S. Panero, V. Antoucci and A.S. Aricò, *Investigation of Composite Nafion/Sulfated zirconia membrane for solid polymer electrolyzer applications*, International Journal of Electrochemical Science, 7, 1532-1542, 2012.

- 
- [48] H. Su, V. Linkov and B.J. Bladergroen, *Membrane electrode assemblies with low noble metal loadings for hydrogen production from solid polymer electrolyte water electrolysis*, International Journal of Hydrogen Energy, 38, 9601-9608, 2013.
- [49] S. Siracusano, S. Trocino, N. Briguglio, V. Baglio and A.S. Aricò, *Electrochemical impedance spectroscopy as a diagnostic tool in polymer electrolyte membrane electrolysis*, Materials, 11, 1368, 2018.
- [50] M. Suermann, B. Bensmann and R. Hanke-Rauschenbach, *Degradation of proton exchange membrane water electrolysis cells: looking beyond the cell voltage increase*, Journal of the Electrochemical Society, 166, F645-F652, 2019.
- [51] Pia Aßmann, Aldo Saul Gago, Pawel Gazdzicki, Kaspar Andreas Friedrich and Michael Wark, *Toward developing accelerated stress tests for proton exchange membrane electrolyzers*, Current opinion in Electrochemistry, 21, 226-233, 2020.
- [52] S.M. Alia, S. Stariha and R.L. Borup, *Electrolyzer durability at low catalyst loading and with dynamic operation*, Journal of the Electrochemical Society, 166 (15), F11164-F1172, 2019.
- [53] C. Rakousky, U. Reimer, K. Wippermann, M. Carmo, W. Lueke and D. Stolten, *An analysis of degradation phenomena in polymer electrolyte membrane electrolysis*, Journal of Power Sources, 326, 120-128, 2016.
- [54] S. Siracusano, N. Van Dijk, R. Backhouse, L. Merlo, V. Baglio and A.S. Aricò, *Degradation issues of PEM electrolysis MEAs*, Renewable Energy, 123, 52-57, 2018.
- [55] Y. Xiaozhi, W. Haijiang, C.S. Jian, Z. Jiujun, *AC impedance technique in PEM fuel cell diagnosis- A review*, International Journal of Hydrogen Energy, 32, 4365-4380, 2007 (cit. on pp.69-70).
- [56] M. E. Orazem and B. Tribollet, *An integrated approach to electrochemical impedance spectroscopy*, Electrochimica acta, 53, 7360:7366, 2008.
- [57] J. Fleig and J. Maier, *The influence of current constriction on the impedance of polarizable electrodes*, J. Electrochem. Soc., Vol. 144, No. 11, 1997.
- [58] D.D. Macdonald, *Reflections on the history of electrochemical impedance spectroscopy*, Electrochimica Acta, 51, 1376:1388, 2006.
- [59] M. Orazem, P. Agarwal, and L.H. Garcia-Rubio, *Critical issues associated with interpretation of impedance spectra*, Journal of Electroanalytical Chemistry, 378, 54:62, 1994.

---

[60] P. Zoltowski, *A new approach to measurement modelling in electrochemical impedance spectroscopy*, Journal of Electroanalytical Chemistry, 375, 45:57, 1994.